DOE/MC/24207--2855

DE90 009666

Fluidized Bed Pressure Probes

Topical Report

April 1990

Work Performed Under Contract No.: DE-FC21-87MC24207

For
U.S. Department of Energy
Office of Fossil Energy
Morgantown Energy Technology Center
Morgantown, West Virginia

By
West Virginia University
Mechanical & Aerospace Engineering and
Department of Chemical Engineering
Morgantown, West Virginia

DISCLAIMER

DOE/MC/24207-2855
(DE90009666)
Distribution Category UC-103

Fluidized Bed Pressure Probes

Topical Report

Work Performed Under Contract No.: DE-FC21-87MC24207

For
U.S. Department of Energy
Office of Fossil Energy
Morgantown Energy Technology Center
P.O. Box 880
Morgantown, West Virginia 26507-0880

By
West Virginia University
Mechanical & Aerospace Engineering and
Department of Chemical Engineering
Morgantown, West Virginia 26506

April 1990

SUMMARY

Detailed information on local fluid bed behavior cannot be obtained using global instrumentation. However, dual static pressure probes (DSPP) which measure local axial differential pressures can be used to infer the presence of bubbles or slugs in a fluid bed. DSPP consist of two probe stems, one positioned vertically above the other, connected to a differential pressure transducer. Response of DSPP has been modeled and is fast enough to capture transient phenomena in a fluid bed provided a low dead volume transducer is used. DSPP with 0.5 inch, 0.75 inch and 1 inch stem spacings have been used to measure slugging properties of a 5.5 inch diameter air-fluidized bed filled with 0.125 inch nylon spheres. Over 500 20 second pressure traces were digitally recorded for two distributor types a variety of bed heights, air flowrates and probe positions. Slugging frequency was found from the traces using the autocorrelation function, Fourier transform and spectral density function, and was shown to decrease with bed height. Slug velocity was found using cross-correlation of signals from two DSPP, and was shown to increase with air throughput. In addition, analysis was performed to show that a distribution of bubble sizes in a fluid bed can be inferred from a distribution of chord lengths found using a probe, and pressure fields around bubble pairs were modeled. The research showed that DSPP can be used successfully to measure local phenomena in fluid beds.

TABLE OF CONTENTS

Note: All Figures and Tables are Located Before Appendices

List of Figures Page

List of Tables

1. INTRODUCTION

Understanding of bubble hydrodynamics is important in predicting the performance of fluidized bed reactors and combustors. This report addresses the progress on a project to measure and predict the pressure fields in slugging and bubbling fluidized beds. Of particular interest is the development and optimization of probes to acquire pressure data to determine whether the juxtaposition of bubbles rising in an assemblage can be inferred from probe signals. Previous work has concentrated on single bubbles or a sequence of bubbles which do not influence one another significantly.

The first year of research has addressed the measurement and modeling of pressure fields on several fronts. Firstly, the response of dual static pressure probe and transducer combinations has been modeled, and design charts for probes were produced. Secondly, probes and an experimental fluidized bed have been constructed for data acquisition of pressure fields. An extensive data set of pressure traces has been acquired and the resulting analysis of the traces has yielded information on slugging frequency and velocity over a wide range of operating conditions. Thirdly, numerical modeling of pressure fields around bubble pairs was undertaken. Fourthly, an original numerical scheme was devised for inferring bubble size from probe measurements in a fluidized bed.

2. THE LITERATURE REVIEW

In measuring the behavior of a fluidized bed several different types of probes have been employed by a great many researchers to detect and determine voidages, bubble size, frequency and rise velocity. The various types are the electrical and electronic probes such as the capacitance probe of Werther and Molerus (1973) the resistance probe of Burgess and Calderbank (1975), and the inductance probe of Cranfield (1972). Optical probes of Dutta and Wen (1979) are another type of probe used in fluidised bed research and with the advent of the optical fiber technology came the use of the optical fiber probes of Hatano and Ishida (1983). Thermal probes, strain gauge microprobes, and the electrical discharge probe have also been used in fluidized bed research (Atkinson and Clark, 1986).

Since the purpose of this study was to use the change in local pressures to determine the bed behavior, the literature search concentrated mainly on the area of direct measurements of local pressures and analysis of such measurements in the bed by means of pressure probes.

Direct measurement of pressure fluctuations in a fluidized bed can be done in two ways either by placing pressure taps at the wall of the bed or by placing pressure probes either horizontally or vertically inside the bed. Fan et al. (1981) used pressure taps installed vertically along the fluidized bed. The distance between two adjacent taps was about 0.045m. The inside openings of the taps were covered with a screen to prevent the bed material from clogging the taps. The outside of the taps were connected to one side of a differential pressure transducer with the other side open to the atmosphere. From these pressure taps the global pressure fluctuations were measured and recorded. By means of the autocorrelation function and Fourier transform techniques he came to the conclusion that the motion of the bubbles caused the pressure fluctuations and that the static bed height had a significant effect on the major frequency of the pressure fluctuations. Svoboda et al. (1983)

used a pressure probe located vertically in the bed connected to a sensitive pressure transducer. While the effect of the radial position was found to be insignificant, the pressure amplitudes were considerably influenced by the axial positioning of the probe. This showed that there was a dependence of mean amplitude on the distance of the probe above the distributor, with the maximum amplitudes occurring in the middle part of the bed. While the probe measured both static and dynamic pressures, the dynamic pressures was negligibly small in all of the experiments. Flemmer (1984) used a pneumatic probe that was capable of detecting gas voids in a fluidized bed operated at any temperature. The probe consisted of three tubes. One emits a small jet of gas to impinge upon the opening of the sensing tube, and the third compensated for the fluctuating bed pressure. The probe was connected to a differential pressure transducer for pressure measurements, and was tested in slugging bed at first and finally in a two dimensional hot bed. From the study it was concluded that bubble size and rise velocity are readily measurable. Sitnai (1982) used differential pressure records to determine bubble parameters such as bubble velocity, bubble diameter, vertical spacing of bubbles, bubbling frequency, distributions of bubble sizes and spacing, and local bubble phase fraction. He used four pairs of pressure probes to record the data which were located at various vertical as well as radial positions in the bed, with each pair of probes connected to four differential pressure transducers. The bubble parameters were found by analyzing the differential pressure recordings by means of the auto-covariance function, the cross-covariance function and the cross-correlation function. Atkinson and Clark (1988) used a dual-stem static-pressure probe (DSPP) to detect a rising bubble so that the a bubble was only sampled if it met a predescribed sampling criterion. The DSPP was connected to low dead volume differential pressure transducer and a personal computer, in which a sampling criteria program would detect the presence of a bubble passing the DSPP from the information supplied from the DSPP based on the Davidson and Harrison (1963) model for a rising bubble. The gas sampling system would then take samples at the appropriate time. The use of the unobtrusive probe in fluidized beds is of great importance and advantage because probes allow the measurement of local conditions directly, whereas normally these local features of bed behavior are inferred from global or overall measurements of the fluidized bed behavior.

3. BED AND GAS DISTRIBUTOR DESIGN AND CONSTRUCTION

3.1 Fluidized Bed Design

A bed has been designed and constructed for the experimental work. The design provides for ready access by probes and rapid change of distributor plates. See Figure 3.1.

The column consisted of three sections: the bottom section, which was the main data sampling section and two other sections that were used mainly for containment of the bed material. In the main section of the bed (lower section) there existed a total of 56 probe tapping ports, 0.25 inch NPT pipe taps, in two vertical rows of 28 ports with the ports one inch apart vertically center to center and the rows set 90 degrees apart from each other, (see Figures 3.1 and 3.2). Data could be taken from any or all of the ports.

Air was supplied to the bed from a single 0.75 inch air input into a plenum chamber with a height of 9.0 inches with an inside diameter of 5.0 inches through a porous distributor plate. Since the inside diameter of the

plenum and the column were not the same an expansion ring was inserted in between the plenum and the porous distributor in order to allow the gas to expand to gain full and even use of the distributor, (see Figure 3.3).

The fluid (air) was regulated at 40 psi. through a 0.75 inch inlet into a Dwyer flow meter (range 0-50 SCFM). The air continued through the 0.75 inch flexible inlet line until it reached the the bottom of the plenum chamber. The inlet pressure of the plenum was measured with a Marshall Town pressure tap gauge of range 0-15 psi. Air traveled through the porous distributor plate and then though the bed material creating a square nosed slug at sufficiently high air flow. The square nosed slug traveled past the pressure probes creating a variation in pressure difference between the lower and the upper stem of the probe. The difference was monitored by a differential pressure transducer. The signal from the pressure transducer was measured by an analog to digital (A/D) data acquisition board, which was located and controlled in a personal computer. The data was stored in the computer and on disk for future manipulation, computation and evaluation. The signal from the pressure transducer was simultaneously recorded on a A/D plotter in order to gain a real time plot of the raw data, which was used in trouble shooting the performance of the pressure probes in the bed and in the analysis the of the overall effectiveness of the collection system as a whole, see Figure 3.4 for overall schematic of the system.

3.2 Distributor Design

Two porous distributor plates were designed and constructed, the first was made 0.5 inch clear cast acrylic sheet with 61, 1/16 inch drilled holes. The second distributor was made of the same material and included 177, 5/64 inch drilled holes. This is similar to the plate used in the 6 Plexiglass bed at Morgantown Energy Technology Center. These plates are shown in Figures 3.5 and 3.6. Since the entire column, except for the top which is open to the atmosphere, was designed to be air tight the distributor plate was designed so that it is sandwiched between the expansion ring and the bottom of the column. With this in mind both distributors were designed with an o-ring, groove and seal in order to prevent leakage of the working fluid.

The pressure drops across the distributors were calculated according to the equations offered in Geldart and Baeyens' paper (1985), and the results are shown in Figures 3.7 and 3.8.

4. DESIGN OF PRESSURE DATA ACQUISITION EQUIPMENT

4.1 Dual Static Pressure Probes

A dual static pressure probe consists of two probe stems protruding into the bed in order to measure a local pressure gradient. The dual static (differential) pressure probe, DSPP, was selected over various other types of probes commonly used to study fluidized bed activity, because of versatility of this system to measure the local pressure fluctuations in the bed with acceptable accuracy. In order to study the local slugging phenomena within the fluidized bed the DSPP had to be constructed of a durable material in order to withstand the cyclic abrasive nature of the fluidized bed environment. The other consideration was to keep the DSPP spacing, h, constant at all times, even in the most dynamic situation, which ruled out a two piece DSPP design and greatly influenced the one piece design discussed

below. All of these factors had to be accomplished in such a manner that the DSPP would not disrupt the natural conditions of the bed and the final constraint was that the DSPP had to fit inside of the 5.5 inch inside diameter experimental fluidized bed

The final DSPP was constructed from 19 gauge stainless steel tubing which consists of an outside diameter of 0.0425 inches and inside diameter of 0.0275 inches and a wall thickness of 0.0075 inches. Since it was difficult to bend this tubing to the precise specification, the DSPP was constructed from three separate pieces of tubing. One stem was composed of one straight and one curved piece, the other of a single straight piece. The three pieces were then silver soldered together in order to achieve the proper spacing, h, (see Figure 4.1).

In all there were four dual static (differential) pressure probes (DSPP) designed and constructed, one with 1.0 inch stem spacing, one with 0.75 inch stem spacing, and two with 0.5 inch stem spacing, (see Figure 4.2). All three stem spacings were employed for pressure data acquisition, while the two DSPP with 0.5 inch spacing were used for cross-correlation work.

The DSPPs were designed in such a manner that they had to be inserted from the inside of fluidized bed and then placed through the bed wall at one or any of the 56 probe tapping ports. Once the DSPP was placed in the desired position the bed was then filled with the bed material, 0.125 inch nylon spheres, to the desired static bed height. The DSPP was then connected to the differential pressure transducer by inserting the two ends of the DSPP into separate flexible tubes, of 27.5 inches in length, and a seal was achieved at the connection by the using one hose clamp around both the tubing and the DSPP so as to not let the air escape at this point. Air leakage would distort the data: if the seal was not made satisfactorily, then very high differential pressures would be measured.

The overall design of the DSPPs turned out to be sound and the initial data was as expected except for an occasional high differential pressure. After further investigation the cause of the high pressure reading was attributed to be due to bed material clogging one stem of the DSPP, (see Figure 4.3). It was decided to make an alteration to the original DSPP design by crimping the end on the DSPP on the horizontal axis, thus making a oval opening at the end instead of a circular one. It was believed that by doing this, the end of the DSPP could not be clogged by spherical bed particles. This has been done before by Flemmer (1984). After further testing the hypothesis appeared true and all the existing DSPPs were modified to this new design parameter.

The effect of dead volume on the response time of the dual static pressure probes was taken into consideration according to the criteria established in Section 5 below. A response time was determined for 95% response to a 10% change in the bed pressure. For this calculation the tube system consisted of the DSPP stems and the flexible tubing, the dead volume was found only in the pressure transducer, 0.5 cm^3 (Atkinson, 1987). The response time was determined to be 0.187 seconds. The calculation was performed again this time using only the DSPP as the entire tube system with the dead volume consisting of the flexible tubing and the pressure transducer, a total of 6.03 cm^3. The response time was determined to be 0.217 seconds, which was the limiting time for this system. Both response times were

determined to be acceptable for use in a fluidized bed because no significant activity in the bed occurred faster than every .390 seconds, which is nearly twice the response time. Final data presented below showed that the fastest slugging rate was 2.56 slugs per second. However, it is acknowledged that any very rapid changes in the differential pressure may be smoothed by the system.

4.2 Data Acquisition System

The differential pressure transmitted by the probes was measured by means of a Validyne differential pressure transducer model P305D1-N-1-20-S-4 . The pressure transducer measures the difference in pressure of the two stems of the probe. The transducer produces an analog output ranging from (-5 to +5) volts and is converted to digital information by means of an A/D, data acquisition board in the computer. The transducer was tested in order to determine if it would react in a linear manner. In order to do this, the transducer was connected across a water manometer, and was measured on a voltmeter, and on the A/D board in the computer. The transducer was tested at pressures created by the water manometer ranging from 0.1 to 4.0 inches of water, (with an error equal to -0.1 to +0.1 inches of water), at random increments. The transducer output was simultaneously recorded on the voltmeter and the computer. From this collected data it was determined that the transducer did in fact react in an linear fashion (see Figures 4.4 and 4.5). The slope of this data was found to be 437 (computer output/ inches of water) or 2.15 (volts/ inches of water) and was used in converting the digital data in to actual pressures where it was necessary to do so.

In the case of collecting data for the cross-correlation function in order to find slug rise velocity, two pressure transducers were used with two DSPP and both were calibrated to the same output range. The graphs of the calibration of the second transducer are shown in Figures 4.6 and 4.7.

The Valydine pressure transducer operates on a (10.8 to 32) volt DC input and produces an output ranging from (-5 to +5) volts. The accuracy range of the Valydine pressure transducer is (-0.25 to +0.25%) Full Scale including linearity, hysteresis and repeatability.

The analog signal produced by the pressure transducer was recorded by means of the Analog Devices RTI-815-F A/D data acquisition board, which was located in the Zenith Z-286 PC/AT computer. The RTI-815-F board is a multifunction, data acquisition board that is capable of various analog/digital, input/output, (I/O) and time related I/O functions. The conversion resolution is 4096 counts over input signals ranging from (-5 to +5) volts. This board came with a complete directory of accessible collection routines, which were easily controlled by the means of a data acquisition program, written in Microsoft Quickbasic 3.0. The raw data was collected at 100 Hz according to the conditions stated in Table 4.1. This data was stored for further analysis, which is discussed in Section 6.

The analog pressure signal was simultaneously recorded on a Hewlett Packard 7090A measurement plotting system, which contains a built-in A/D data acquisition board used for direct plotting.

5. ANALYSIS OF PROBE RESPONSE

It is important to maintain quality of data in this research to ascertain that the pressures measured are a true reflection of the pressure in the bed. The system used in this research consists of probe tubes protruding into the bed and connected to a pressure transducer. Although it is necessary to select a pressure transducer with a high enough frequency response to account for the pressure fluctuations in the system, it is also necessary to design the whole probe system to have a sufficiently low aerodynamic response time that the signal measured by the transducer is representative of the fluctuating pressure in the fluidized bed. This section assesses the design of probes in terms of their response, and has allowed the researchers to conclude that the probes used in the experimental work have sufficiently low response time.

5.1 Theory

A typical transducer and single stem probe inserted into a pipe carrying a gas-solid mixture are shown in Figure 5.1. A differential probe can be regarded as two single stem probes for the purpose of response analysis. A one dimensional force balance for compressible laminar flow on a differential segment of the probe tube yields the equation

$$-\frac{dP\,(x,t)}{dx} = \frac{32\mu U\,(x,t)}{2D} + \frac{P\,(x,t)}{RT}\,\frac{dU\,(x,t)}{dt} \qquad (5.1)$$

where P is the pressure of the gas, x is the distance along the pipe of diameter D, μ and T are gas viscosity and temperature respectively, U is the cross-sectional average gas velocity and R is the specific gas constant. In Equation 5.1 the acceleration term, of the form $d(PU^2/RT)/dx$, is neglected since this is usually insignificant in most practical probe flow situations. For example, with a 1m long tube of 0.8mm diameter, feeding a transducer with a dead volume of 0.5 cm^3, when the pressure in the system experiences a step change from 1 to 1.1 atmospheres, the acceleration term does not exceed 5% of the total pressure gradient in the tube. In Equation 5.1 the laminar resistance term may also underestimate the frictional pressure loss when the flow is developing or unsteady. Since viscosity is weakly dependent on all variables except temperature, and since temperature varies little over the probe tube length, we may assume gas viscosity to be constant in this analysis. A mass balance on the tube segment yields the equation

$$\frac{d\,(UP)}{dx} = -\frac{dP}{dt} \qquad (5.2$$

For mutual solution of the above equations we require initial and boundary conditions. The simplest initial condition occurs at steady state when the pressure in the bed, P (t), is equal to the pressure in the transducer, $P_T(t)$, at time t = 0, in which case

$$P_b\,(0) = P_T\,(0) = P\,(x,0) \qquad (5.3)$$

and in which case

$$U(x,0) = 0 \tag{5.4}$$

Assuming no entrance or exit loss into the probe tube mouth, at x = 0,

$$P_b(t) = P(0,t) \tag{5.5}$$

and assuming entrance or exit losses and acceleration effects,

$$P_b(t) = P(0,t) + \frac{k_1 U|U|P(0,t)}{RT} + \frac{k_2 U^2 P(0,t)}{RT} \tag{5.6}$$

for constants k_1 and k_2.

At the transducer end of the probe tube the boundary condition is derived by considering that mass flow of gas into the transducer fixed volume, V, must raise the transducer pressure. Pressure P (t) is assumed constant throughout the transducer volume

$$P(L,t)\, U(L,t)\, A = V \cdot \frac{dP_T(t)}{dt} \tag{5.7}$$

where A is the tube cross-sectional area. In addition, assuming no entrance or exit losses associated with flow into or out of the transducer,

$$P(L,t) = P_T(t) \tag{5.7a}$$

or taking such losses as well as acceleration effects into account

$$P_T(t) = P(L,t) + \frac{k_1 U|U|P(L,t)}{RT} + \frac{k_2 U^2 P(L,t)}{RT} \tag{5.7b}$$

Setting,

$$x^* = x/D \quad (\text{hence } L^* = L/D)$$

$$t^* = t\frac{\sqrt{RT}}{D}$$

$$p^* = \frac{PD}{\mu\sqrt{RT}}$$

$$U^* = \frac{U}{\sqrt{RT}}$$

$$V^* = \frac{4V}{\pi D^3}$$

we may write the above equations in dimensionless form as presented below. Force balance; neglecting acceleration effects

$$-\frac{dP^*}{dx^*} = 32U^* + P^* \frac{dU^*}{dt^*} \tag{5.8}$$

Continuity equation:

$$\frac{d(P^*U^*)}{dx^*} = -\frac{dP^*}{dt^*} \tag{5.9}$$

Initial condition:

$$P_b^*(0) = P_t^*(0) = P^*(x^*, 0) \tag{5.10b}$$

$$U^*(x^*,0) = 0 \tag{5.10a}$$

Boundary conditions, neglecting entrance and exit effects:

$$P^*(0,t^*) = P_b^*(t^*) \tag{5.11}$$

$$P(L^*, t^*) = P_T^*(t^*) \tag{5.12}$$

$$U^*(L^*, t^*)\, P^*(L^*, t^*) = \frac{dP_T^*(t^*)}{dt^*} \tag{5.13}$$

One can also perform this analysis for turbulent flow in the probe tube, in which case Eqn. 5.8 is substituted with

$$\frac{-dP^*}{dx^*} = \frac{P^*(U^*)^2 f(P^*U^*, \varepsilon/D)}{2} + P^* \frac{dU^*}{dt^*} \tag{5.14}$$

where P^*U^* is equal to the Reynolds number of the flow and f is the friction factor which is available as a function of Reynolds number and tube relative roughness, ε/D. Only the laminar flow case is analyzed below since this is applicable to most small probe systems.

5.2 SOLUTION PROCEDURE

The above equations can be solved numerically for a given bed pressure function $P_b^*(t^*)$ using the following scheme. At a small time interval Δt^*, after the initial condition, a value for $U^*(0, \Delta t^*)$ is assumed. Working from the boundary condition at $x^* = 0$ (Eqn. 5.11), Equations 8 and 9 are solved mutually along the length of the pipe, making use of the initial condition. At the transducer end of the tube, $x^* = L^*$, both boundary conditions, Eqns. 5.12 and 5.13 must be met. If they are not, a new value for $U^*(0, \Delta t^*)$ must be selected and the process repeated. Once the distribution of P^* and U^* along the tube has been found by trial and error at time Δt^*, one may proceed

to solve for time $2\Delta t^*$, and so on.

5.3 DISCUSSION

Computer solution of the equations of laminar flow, neglecting exit and entrance effects at the tube ends, has provided data on the response of probes and transducer combinations to step changes in bed pressure. Figure 5.2 shows the response of a probe with $L^* = 1250$ and $V^* = 1250$ to a sudden rise in pressure from 100 kPa in the bed. Such a probe, for example, might have a length of 1m, a diameter of 0.8mm, and be connected to a transducer with a dead volume of $0.5cm^3$. Figure 5.3 illustrates the dimensionless time t^* required for the change in transducer pressure to reach 63% (one "time constant") of the step change in pressure in the bed from 100 to 110 kPa, for a wide range of L^* and V^*. Reliability of the numerical solution was tested by varying the size of time and space increments used, and noting that this had little influence on the result.

Since the response to a step change is not exponential, data are also presented in Figure 5.4 for the time taken for the transducer to read 95% of the step change in pressure. Figures 5.3 and 5.4 provide useful response criteria for those selecting probes to monitor pressure fluctuations. It is recommended that the user selects a system with a time constant considerably smaller than that of the pressure event which he wishes to measure. In a fluidized bed without strong circulation, 0.01 seconds should be used as an absolute maximum for the time taken to reach 63% of the pressure rise, while in pneumatic conveyors, fast fluidized beds and strongly circulating systems, pressure events may be one or two orders of magnitude more rapid. In some instances it will prove imprudent to assume that the transducer pressure is a fair representation of the bed pressure even when a low dead volume transducer is used.

The results presented above are for laminar systems ($Re = P^*U^* < 2000$) only. Response times will be slower for turbulent systems, which may merit attention with some larger probes for industrial combustor application.

A previous analytic model for laminar flow probe response (Clark and Atkinson, 1988) was also compared with the present computer solution. In this model it was assumed that all dead volume, of both the tube and transducer, could be lumped at the transducer end of the tube. This simplification had also been used previously by Flemmer et al. (1984). Clark and Atkinson also assumed incompressible flow, at a mean density, in the tube. They found that

$$P_b(t) - P_t(t) = \left(\frac{k}{M}\right)\frac{dP_t}{dt} + \left(\frac{\alpha}{M}\right)\frac{d^2P_t}{2} \qquad (5.15)$$

where $k = \dfrac{128\,\mu L}{\pi D^4}$ is the resistance to flow and where $\alpha = \dfrac{\rho L}{\pi D^2}$ is the inertial term and where $M = P / V$ accounts for the total dead volume, V, of the system, with P an average pressure at the transducer. Practical solution shows that this is an overdamped (non-oscillatory) second order

system. Response of this model to a step change in bed pressure of ΔP is given by the equation

$$\Delta P_t = \Delta P_b \left(1-e^{-kt/2\alpha}\right) \left[\cosh \sqrt{\frac{k^2}{4\alpha M} - 1}\ \frac{t\sqrt{M}}{\sqrt{\alpha}} + \frac{k}{2\sqrt{\alpha M}\left(\sqrt{\frac{k^2}{4\alpha M} - 1}\right)} \sin h \sqrt{\frac{k^2}{4\alpha M} - 1}\ \frac{t\sqrt{M}}{\sqrt{\alpha}} \right] \tag{5.16}$$

If inertia of the air in the tube is neglected, the resulting approximate solution to Equation 5.15 is far simpler

$$\Delta P_t = \Delta P_b \left(1 - e^{-kt/M}\right) \tag{5.17}$$

Figure 5.5 compares the probe response to a step rise in bed pressure from 100 to 110 kPa as predicted by Equations 5.16 and 5.17 and by the numerical solution developed earlier. This response is for a probe of 0.8mm internal diameter and 1m length, with a transducer volume of $0.5cm^3$. Total dead volume of the transducer and tube is thus $1m^3$. The value of P was 105 kPa.

Response predicted by the numerical scheme is sigmoidal and differs noticeably from the exponential response predicted by the simplest analytic models. This is readily explained by the fact that compressibility of air in the tube is neglected in the simpler models so that an immediate influx of air into the transducer is predicted as soon as the bed pressure changes. When compressibility of air in the tube is considered, initial air flow into the transducer is far lower than the air flow into the tube mouth. Thus the simple model overpredicts initial response, but underpredicts later response. However, Figure 5.5 shows that for a typical probe geometry the simplified models (Equations 5.16 and 5.17) do provide a fair estimate of the system's response time.

In this section a differential equation has been presented to predict the response times of probe and transducer combinations. Numerical solution of the equation for laminar flow has yielded graphs to provide the response time as a function of dimensionless probe tube length and dimensionless transducer dead volume. Furthermore these new results have shown that simpler analytic models (Clark and Atkinson, 1988) can err in lumping all dead volume at the transducer end of the probe, although they still provide a good estimate of response time.

6. THEORY OF DATA ANALYSIS

6.1 Davidson Model For A Rising Bubble

The main thrust of this work concerns the analysis of data coming from a slugging fluidized bed. However, the effect of bubble interactions in bubbling fluidized beds is of importance in understanding and analyzing

pressure fluctuations from pressure probes immersed in such beds. As a consequence of the importance of bubbling beds, the data obtained from them and theoretical analysis presented in this report a brief review of Davidson's model of a rising bubble in a fluidized bed is presented here.

The Davidson model for a rising bubble in an incipiently fluidized medium is based on the existence of high static pressure gradients in the fluid medium immediately above and below the bubble, with the pressure gradient within the bubble being negligible (zero). The following assumptions were made by Davidson and Harrison (1963) in order to create an easily manageable mathematic formulation of the problem at hand.

ASSUMPTIONS

a) The fluidized bed must consist of two separate and very distinct phases, the particulate phase, (the solid phase consisting of particles with minute separations), and the fluid phase.

b) The solid phase, (particulate phase), is considered to be an incompressible, inviscid fluid with the same bulk density as the whole bed would exhibit while being incipiently fluidized. This is considered true under the assumption that all excess fluid passes through the bed as bubbles, where the excess fluid is defined as the fluid above that which was needed to induce incipient fluidization. In a two dimensional bed the continuity equation for the particles is

$$\frac{dv_y}{dy} + \frac{dv_x}{dx} = 0 \qquad (6.1)$$

where (x,y) being the orthogonal coordinates and v_x and v_y the velocity components of the particles in the horizontal and vertical directions.

c) In looking at the fluidizing fluid the continuity equation is based on the assumption that the fluid is incompressible, inviscid and that the voidage everywhere in the bed corresponds to minimum fluidizing conditions.

$$\frac{du_y}{dy} + \frac{du_x}{dx} = 0 \qquad (6.2)$$

d) The relative velocity between the fluidizing fluid and particles is assumed to be proportional to the pressure gradient within the fluidizing fluid and the absolute components of the fluid velocity are therefore:

$$u_x = v_x - K\frac{dP_f}{dx} \qquad (6.3a)$$

$$u_y = v_y - K\frac{dP_f}{dy} \qquad (6.3b)$$

where K is a permeability constant characteristic of the particles and of the fluidizing fluid, and P_f is the pressure within the fluid. The assumed proportionality between the relative velocity and the pressure gradient is the same as D'Arcy's law, which is a well established relation for percolation through fixed beds of fine sand and filters. D'Arcy's law as well as this analysis holds true only for systems with low Reynolds numbers. By eliminating the velocities from Equations (6.1), (6.2), and (6.3a,b) an equation can be derived in terms of pressures.

$$\frac{d^2 P_f}{dx^2} + \frac{d^2 P_f}{dy^2} = 0 \qquad (6.4)$$

This equation is then solved for the pressure distribution around a single rising bubble by means of the boundary conditions (i) the pressure gradient within the fluid far above and far below the bubble is equal to the static pressure gradient in the fluid as if the bubble did not exist, (ii) the pressure throughout the bubble is constant meaning that the pressure gradient within the bubble is zero, (negligible).

Assuming that the pressure field is influenced by the vertical component of Equation 6.4 and that the axial component is negligible, then pressure gradient in the fluid far above the bubble and far below the bubble is related to the permeability K by the equation

$$\frac{dP_f}{dy} = 0 \qquad (6.5)$$

Equation 6.5 would give the relationship for the pressure gradient in the dense phase

$$\frac{dP_f}{dy} = K = \rho_s \, g \, (1 - \varepsilon_{mf}) \qquad (6.6)$$

This completes the necessary theory of pressure fields by Davidson, and results in the creation of the simplified Davidson model for a rising square nosed slug Section 6.2.

6.2 Analysis of Square Nosed Slugs

In order to arrive at the pressure field associated with a single rising square nosed slug, the Davidson model for a single rising bubble can be simplified, into an ideal fluidized bed model, by using the following assumptions. That, there exists a constant pressure gradient in the dense phase with height and no pressure gradient within the slug itself. Clear physical boundaries between the dense phase and the slug exist. The pressure gradient in the dense phase is constant, and there are no very high gradients immediately above or below the slug.

By considering the DSPP immersed in the dense phase and neglecting the density of the gas phase of the bed, the differential pressure between the two probe stems with a vertical separation of h is given by Equation 6.7 (see Figures 6.1 and 6.2):

$$P_f = h\ \rho_s\ g\ (1-\varepsilon_{mf}) \tag{6.7}$$

where ρ_s is the density of the solid particles, g is the gravitational acceleration constant and ε_{mf} is the void fraction of the dense phase.

As Atkinson (1987) showed in his simplified model for bubbles, when the slug passes the DSPP the measured differential pressure is decreased by some fraction of the probe spacing h, now occupied by the slug, which has an assumed pressure gradient of zero. The measured pressure is then given by the equation

$$P_f = \rho_s\ g\ (h-h_b)\ (1-\varepsilon_{mf}) \tag{6.8}$$

where h_b is the height between the probes which is occupied by some part of the slug. For slugs which are smaller than the DSPP height h, the maximum value of h_b is the height of the slug itself, Y, this is referred to as a small slug. This will result in the differential pressure given by Equation (6.8) with h_b=Y, will persist from the time when the base of the slug leaves the lower stem of the pressure probe until the crown, or top, of the slug touches the upper stem of the probe, (see Figure 6.3). This means, that when chordal height of the slug Y is less than the probe spacing h the differential pressure reaches minimum value and holds this value for a short period of time, then rises into the dense phase value.

The time that it takes the slug to travel from the lower to upper stem can be determined from

$$t_{crown} = t_3 - t_1 \tag{6.9}$$

similarly the time for the base of the slug to travel the same distance is

$$t_{base} = t_4 - t_2 \tag{6.10}$$

If the slug is indeed square then the time it takes the bubble to rise past both stems will be the same, (see Figure 6.4), or

$$t_{crown} = t_{base} \tag{6.11}$$

Therefore the rise velocity of the slug is

$$U_b = \frac{h}{t_{crown}} \text{ , or } \frac{h}{t_{base}} \qquad (6.12)$$

It is also known that the time it takes the slug to rise past the lower stem is

$$t_{lower} = t_2 - t_1 \qquad (6.13)$$

and the time it takes the slug to rise past the upper stem is

$$t_{upper} = t_4 - t_3 \qquad (6.14)$$

Thus the height of the slug D that passes the DSPP is

$$D = U_b\, t_{lower} \text{ , or } U_b\, t_{upper} \qquad (6.15)$$

There also exists a case where the chordal height of the slug is greater than the height of the DSPP spacing h, referred to as a large slug. In this case the equations remain the same but the provided that the events at t_2 and t_3 are interchanged, (see Figures 6.5 and 6.6).

The slug rise velocity can also be determined by the slope of the pressure trace in Figures 6.4 and 6.6 in the manner that follows

if dx, then $dP = -(1-\varepsilon)\rho_s g\, dx$

if $\frac{dx}{dt}$, then $\frac{d(\Delta P)}{dt} = -(1-\varepsilon)\rho_s g \frac{dx}{dt}$

therefore the slug rise velocity is

$$V_s = \frac{d(\Delta P)}{dt} * \frac{1}{\pm\rho_s(1-\varepsilon)g} \qquad (6.16)$$

6.3 Digital Signal Analysis

A variety of data reduction techniques are available to analyze pressure fluctuation measurements in fluidized beds. In this study the dominant

frequency of pressure fluctuations was determined using the autocorrelation function, the fast Fourier transform, and the power spectral density function. The velocity of a rising slug was found by using the cross-correlation function.

6.3.1 The Autocorrelation Function

The autocorrelation function seeks to find the "best fit" time delay between similar events in the bed, from a single recorded signal. In this case, we may interpret these events to be square nosed slugs If the instantaneous probe pressure signal at time t is $R_x(t)$, then results are best represented as a plot of

$$R_{xx} = \frac{1}{\tau} \int_0^{\tau} R_x(t)\, R_x(\tau + t)\, d\tau \qquad (6.17)$$

versus τ. The time lag τ at which the maximum value of the autocorrelation function occurs is an indication of the dominating slugging frequency. According to Fan et al. (1986), the dominating frequency f_d of pressure events corresponds to the frequency of the first peak after $\tau = 0$ of the autocorrelation function. The autocorrelation program is listed in Appendix B.

6.3.2 The Fast Fourier Transform

Another approach to finding the slugging frequency of the signal, and examining the amplitudes of the frequencies is the Fast Fourier Transform (FFT). The FFT is used on a data set of 2^n samples taken at equal intervals to find and compute the discrete Fourier transform. The dominate frequency is assumed to be the slugging frequency in the bed. If the differential pressure trace has a time length t_1, and is composed of n intervals Δt such that $n\,\Delta t = t$, then the Fourier series returned will have the form

$$\Delta P(t) = A_0 + \sum_{i=1}^{n} A_i \left[\sin\left(\frac{\pi i t}{t_1} + \Phi \right) \right] \qquad (6.18)$$

Where A_0 is the average value of the pressure differential Δp, A_i are the Fourier coefficients (amplitudes) and Φ_i are the phase angles. A_i represents the amplitude of a sine wave with period $i^{th}2i\Delta t$, so that frequency of an harmonic number is found readily from the n^{th} harmonic number and the total time of the trace. The dominant frequency is thus visually identified from a plot of A_i versus i.

The computer program that was used to find the dominating frequencies of the data set was obtained from Chapter 8 of Quin-Curtis Science and Engineering Graphic Tools for Microsoft Quick Basic (model IPC-QB-006). This program used the discrete Fourier transform Equation 6.19

$$W_k = \sum_{j=0}^{N-1} c_j \, e^{2\pi i jk/N} \qquad k = 0,, \quad ,N-1 \tag{6.19}$$

where the $|c_j|$'s are the discrete fourier coefficients and the dominating frequency can be found from a plot of c_j versus j. The FFT program is listed in Appendix C.

6.3.3 The Power Spectral Density Function (PSD)

The method of power spectrum estimation used is a simple version of an estimator called, the periodogram. For a N-point sample of a function c(t) taken at equal intervals the FFT (Equation 6.19) is used to compute its discrete Fourier transform. To complete the power spectral density of a the function c(t) the modulus-squared of the found discrete Fourier function of some finite sample N must be taken. There are several different descriptions of the total power: sum squared amplitude, the mean squared amplitude, and the time integral squared amplitude. The program used to find the PSD of the data set was obtained again from Quin-Curtis, which chose to use the mean squared amplitude description which is

$$\frac{1}{T} \int_0^T |c(t)|^2 \, dt \simeq \frac{1}{N} \sum_{j=0}^{N-1} |c_j|^2 \tag{6.20}$$

The power spectral density function gives an estimate at discrete values of frequency f_i, where i ranges over integer values. Thus the periodogram estimate of the power spectrum is defined at (N/2 + 1) frequencies as

$$P(0) = P(f0) = \frac{1}{N^2} |W0|^2 \tag{6.21}$$

$$P(fk) = \frac{1}{N^2} \left[|Wk|^2 + |WN-k|^2) \right] \qquad k = 1,2,..,(N/2 -1) \tag{6.22}$$

$$P(fc) = P(fN/2) = \frac{1}{N^2} |Wn/2|^2 \tag{6.23}$$

where fk is defined for the zero and positive frequencies. The PSD program is listed in Appendix D.

6.3.4 The Cross-Correlation Function

Data collection for the cross-correlation function required the use of two separate DSPPs located directly above one another. The two probes were located in the radial center of the bed, 2.75 inches from the inside bed wall.

The bottom probe was located one inch below the middle of the static bed height and the top probe was located one inch above the middle of the static bed height, for static bed heights 6, 12, and 24 inches. The vertical separation of the two probes was two inches. Each DSPP required its own pressure transducer in order to produce two separate signals, one from each DSPP. These signals were recorded at 100 Hz per channel in the same manner as stated in Section 4.

The cross-correlation function is similar to the autocorrelation function in that they both seek to find the "best fit" time delay between similar events in the bed, but differ in the fact that the autocorrelation function uses only one signal R_x, where the cross-correlation function uses two signals R_x and R_y and compares the first (R_x) to the second (R_y). If the instantaneous probe pressure signal at time t is $R_x(t)$, and the instantaneous probe pressure initial at time t is $R_y(t)$ then results are best represented as a plot of

$$R_{xy} = \frac{1}{\tau} \int_0^{\tau} R_x(t)\, R_y(\tau + t)\, d\tau \qquad (6.24)$$

versus τ. The time lag τ at which the maximum value of the cross-correlation function occurs is an indication of the dominate slug rise velocity, the time it takes the slug to rise past the two DSPP a distance of two inches. The cross-correlation program is listed in Appendix E.

7. RESULTS AND DISCUSSION OF PRESSURE TRACES

Throughout this study over 500 digital recordings were collected, and these are all presented in Appendix A. Each recording was a 20 second trace from a dual static pressure probe. The experimental matrix explored both distributor types described in Section 3, probe stem spacings of 0.5, 0.75 and 1.0 inches, two gas flowrates, three heights, within the bed (near the grid, halfway up the bed, and near the free surface) and at two radial positions (at the bed center and near the wall). The bed was operated at three different static heights (6, 12 and 24 inches). It was possible to concentrate only on a small selected portion of the data taken. The data selected were collected under combinations of the following conditions: a DSPP probe stem spacing of 0.5 inches, located at the center of the bed (2.75 inches from the bed wall) and at half the height of the bed material during static conditions with various bed heights, one of 6 inches, one of 12 inches, and one of 24 inches, using air flow rates of 39 and 52 SCFM with distributor #2. The data was recorded at a rate of 100 Hz over a 20 second time interval collecting a total of 2000 points of data for each data set. All six sets of data were analyzed and reported in the following text.

The data collection for the cross-correlation function to find slug velocity required the use of two separate DSPPs each having a probe stem spacing of 0.5 inches. The two DSPP were located directly above one another in the radial center of the bed, 2.75 inches from the inside bed wall. The bottom probe was located one inch below the middle of the static bed height and the top probe was located one inch above the middle of the static bed

height, for static bed heights 6, 12 and 24 inches. The vertical separation of the two probes was two inches. Each DSPP required a single differential pressure transducer in order to produce two separate signals, one from each DSPP (see Figure 7.0). These signals were recorded at 100 Hz per channel per DSPP (200 Hz between both DSPP). The data was collected over a 20 second time interval collecting 2000 points of data per each DSPP for a total of 4000 points of data for each data set. Each set of data was collected in the same manner as when one DSPP was used.

7.2 Slugging Frequencies

It was apparent from the initial digital plot of the data sampling that there was a constant and clear frequency in the occurrence of the square nosed slugs during the low air flow rate of 39 scfm. This did not hold true for the higher air flow rate of 52 scfm, where the signal was very noisy and showed no initial signs of having a clear frequency. The raw data was analyzed using three methods i.e. autocorrelation, Fourier transform, and power spectral density function, as discussed above in this report. From this analysis the frequency of the data collected at 39 scfm correlated well with the frequency from the direct digital plot as was expected. The frequency from the data collected at 52 scfm which was not attainable from the direct digital plot was explicitly clear after the extensive analysis. Table 7.1 provides information of the figures relevant for determining slugging frequency.

The dominating frequency for the data set G7 Figure 7.1 which had a static bed height of six inches and a gas flow rate of 39 SCFM was determined to be 1.72 pressure events per second using the autocorrelation function, (Figure 7.2) and 1.75 pressure events per second according to the fast Fourier transform and the power spectral density function, (Figures 7.3 and 7.4 respectively). (In all six cases examined there was good agreement between the three methods for determining slugging frequency, see Figure 7.5 and the results are shown in Table 7.1.)

7.3 Slug Velocities

Six sets of data were collected according to the criteria in Table 7.2. For example the dominating velocity for the data set HA which had a static bed height of 6.0 inches and a gas flow rate of 39 SCFM was found to be 1.27 ft/sec using the cross-correlation function as shown in Figure 7.26. The velocity of the rising square nosed slugs was best determined from the cross-correlation method, for which the program is listed in Appendix E. From all six locations in the bed the dominating velocity was determined and listed in Table 7.3. Slug rise velocity was also determined from the analysis of single probe traces, by finding the slope of ΔP versus time as the slug rose past the probe stems. This consistently yielded values which were lower than (but varied in sympathy with) the values found from cross-correlation of two DSPP signals. This was ascribed to the finite response time of the probes, so that the data using cross-correlation are to be favored.

7.4 Discussion of Probe Traces

A question addressed in this work was whether the square-nosed gas slugs arising in the column were formed at the distributor plate or some distance above it. Visual observation determined that at low gas flow-rates the slugs (which appear incipiently as concentration waves rising through the medium) were formed about 2 to 3 inches above the plate. Bed material in the lower

zone moved very little, so that the fluidization was quiescent. This was confirmed through pressure measurements near the distributor, and at a height half way up the bed. Figure 7.32 shows a 10-second trace of pressure difference between two points on the column center axis, 6 7/8 inches and 7 7/8 inches respectively above the distributor plate. Gas flow-rates was 34 scfm, with 32 scfm being the minimum fluidizing condition for this bed. It is evident in Figure 7.32 that regular pressure events (the gas slugs passing the probe) are occurring. High differential pressure (about 1.7 volts) indicates that dense phase is surrounding the probes, whereas the low values correspond to passage of a gas slug. The fact that the pressure difference never drops to zero is indicative of the fact that the slugs are not as high as the 1 inch probe stem spacing, so that the two stems are never simultaneously enveloped by the same gas slug. This agrees with visual observation: slugs appeared to be 1/4 to 1/2 inch high at 34 scfm. Near the distributor, the pressure signal is quite different from that in the bulk of the bed. Figure 7.33 shows a 10 second trace of the pressure difference between two points on the bed axis, respectively 1 5/8 and 2 3/4 inches above the distributor plate. Pressure fluctuations are more frequent and of lower amplitude than in the slugging zone higher in the bed, although the presence of the fluctuations does imply void variations and solids movement in this lower zone. It is interesting to note a change in the signal in the last 4 seconds in Figure 7.33. The major fluctuations suddenly become less frequent and larger, suggestive of incipient slug formation, having a frequency of about 1 Hz, similar to those of slugs higher in the bed (Figure 7.32). It is of interest to know whether these conditions prevail over the whole bed diameter. Figure 7.34 was taken at the wall, at 34 scfm, between heights 6 7/8 and 7 7/8 inches above the plate, and should thus be compared with Figure 7.32. It shows that the gas slugs do persist from the center to the wall, with pressure fluctuations having the same frequency but slightly lower amplitude than at the column center. We may conclude, in agreement with observation, that the bed operates in a one-dimensional fashion above the grid zone.

Figure 7.34 shows a pressure trace taken at the bed wall in the grid zone (two stems, 1 5/8 and 2 3/4 inches above the distributor) at 34 scfm. This may be compared with the center trace shown in Figure 7.33 The trace in Figure 7.35 is remarkably regular, and the frequency of the major fluctuations appears to be unrelated to the bed slugging frequency. Amplitude of the fluctuations is also smaller than amplitude at the column center. A possible explanation is that more air is being introduced near the column center than near the wall by the distributor (See Figure 7.36), so that gas voids are generated preferentially near the center. These then spread to form square nosed slugs higher in the column. Figures 7.36 through 7.39 provide pressure traces of the bed operating at a gas throughput of 40 scfm. The upper part of the bed is still in slugging mode, with gas slugs having greater height. Figures 7.36 and 7.37 provide traces of differential pressure between 6 7/8 and 7 7/8 inches above the distributor, at the bed center and wall respectively. Wider valleys in the pressure trace confirm the increased height of the slugs: note that pressure difference is very close to zero during slug passage, suggesting slug heights of over one inch. Amplitude of the fluctuations is lower at the wall, as is the mean differential pressure. This appears to be the case throughout the column, and is attributed to a net circulation (up at the center, down at the wall) occurring in the bed. Such circulation patterns are documented in the literature.

Just above the distributor at a flow-rate of 40 scfm the pressure traces are atypical of slugging and the bed merely appears disordered. Traces at the center (Figure 7.38) and at the wall (Figure 7.39), taken between 1 5/8 and 2 3/4 inches above the plate are very similar to one another. Both traces have the characteristic of a moderate frequency signal of 4 or 4 Hz, which seems to change significantly in amplitude every 5 to 10 seconds. Figure 7.40, a longer trace taken for the same conditions as Figure 7.39, shows this "beating" phenomenon. Bursts of high amplitude activity occur, separated by periods of lower amplitude fluctuations. The higher amplitude activity is indicative of incipient slug production, so that these traces are well explained by a time-varying height above the grid at which the slugs develop.

At very high throughputs, 50 scfm, the bed appears far more disordered. The slugs are no longer square, there is some circulation, and the grid zone is in turmoil. Differential pressure traces have been acquired in this regime:

Figure 7.41 is a trace from just above the distributor on the bed axis.

Figure 7.42 is a trace from just above the distributor at the bed wall.

Figure 7.43 is a trace from the upper bed zone, on the axis.

Figure 7.44 is a trace from the upper bed zone, near the wall.

It is evident from these Figures that a clear slugging trace can be seen only in the upper section on the bed centerline, and that the other traces are corrupted with higher frequency components, probably associated with local solids movements. For example, the negative differential pressures seen just above the distributor at the wall correlate well with the visual observation of periodic downward movement of solids at the wall in the grid zone. Again this would be caused by the distributor which favored central gas introduction.

8. PRESSURE FIELD MODELING

A finite element method was developed initially to model the pressure field around a single bubble, so that more complex bubble assemblages could be modeled with confidence later in the research program. A finite element approach was selected because of the bubble geometry, which is illustrated in Figure 8.1. Due to symmetry, we needed only model one-quarter of the problem. The method used linear interpolation over triangular elements, with the finite element mesh shown in Figure 8.2. The method can be easily extended to multiple bubble problems by changing the geometry and boundary conditions.

The model assumes incompressible flow, with uniform vertical flow velocity W in the dense phase far from a spherical bubble, so that the vertical pressure gradient in the far field is

$$\frac{dP}{dy} = -\frac{W}{k} \qquad (8.1)$$

where k is a flow resistance term (Davidson & Harrison, 1963). Laplace's equation is used to generate the pressure field

$$\frac{d^2P}{dx} + \frac{d^2P}{dy} = 0 \qquad (8.2)$$

with the boundary conditions given by the fact that

(1) the pressure in the bubble is constant and equal to the pressure in the far field at the height of its center in the bed.
(2) the pressure field is known far from the bubble, say due to atmospheric pressure at the top of the bed and the known gradient given by Equation 7.1.

Figure 8.3 shows preliminary results from the program as a plot of dimensionless pressure, $P^* = P/P_{atmospheric}$ around a bubble of 1cm radius in a bed with the vertical pressure gradient at one bubble radius equal to 10 kPa/m. The field agrees in trends with the analytical solution of Davidson and Harrison (1963).

The numerical modeling technique was extended to predict the pressure field around two bubbles on the same horizontal plane. It was known that the pressure in these bubbles would be the same if their centers were at the same height in an idealized fluidized bed. Figures 8.4 through 8.6 show the fields around a pair of bubbles, with different spacings, side by side in the bed, modeled in two dimensions. Currently modeling is proceeding for the case where one bubble is vertically above the other. The permeability of the bed is an added factor in this latter case, since it will determine the pressure difference between the two bubbles.

It is evident from the results obtained so far in the modeling that the pressure field is significantly distorted from the single bubble case when two bubbles are separated by one radius (i.e. their centers are 1.5 radii apart). Closer spacing distorts the field further and it is evident from qualitative examination of the results that two close bubbles tend to have a rather one-dimensional pressure gradient immediately above them. Clearly this may cause probes to misinterpret hydrodynamic events if a single bubble pressure field is assumed.

9. BUBBLE SIZE INFERENCE

The presence of a bubble at a point in a fluidized bed can be determined using optical, capacitance or pressure probes. However, as Werther (1974a, 1974b) observes, the bubble will not necessarily cut the probe along its central axis so that probe signals cannot be converted directly to bubble size distribution, even if the bubble velocity is known. Differential pressure probes which resemble and "over and under" shotgun type (Oka, 1983) which differ slightly from the widely spaced probes used so far in this study are likely to be most suited to measuring bubble size because they require the simplest data interpretation. As with capacitance probes, both optical and pressure probes can produce data which may be transformed into a binary signal, denoting the presence or absence of a bubble at each moment in time.

Werther (1974a) has argued that bubble velocities are erratic and difficult to characterize and has used a single value of bubble rise velocity to transform the distribution of time intervals during which the bubble surrounds the probe to a distribution of "pierced lengths" representing the cutting of the bubble by the probe. It is from this distribution of pierced lengths that Werther (1974a, 1974b) deduced the bubble size distribution, by assuming that the bubble shape could be approximated by a distorted ellipsoid. This analysis will show that such a transformation is also possible using a more accurate approximation of fluidized bed bubble shape, viz. the top greater section of an ellipsoid or sphere (See Figure 9.1). In addition, it is possible to account for the dependence of bubble rise velocity on bubble size, rather than assume a constant rise velocity. However, it is acknowledged that in a strongly circulating bed, bubble rise velocity will be difficult to determine without the use of pairs of probes with cross-correlation of their signals.

9.1 Theory

Consider that we have, at our disposal, a distribution of pierced lengths, y, given by the probability density function P(y). We wish to transform this into a bubble size distribution, given by P(R) where 2R = D is the largest horizontal dimension of a bubble, as shown in Figure 9.1. This figure also shows that a truncated ellipsoid is a good representation of the spherical cap bubble which is most common in fluidized beds (Werther, 1974a). Note also that at any radius, r, from the bubble center, the pierced length, y, is uniquely defined. If, within the region of the probe, no bubble channeling occurs and bubbles rise with an even density throughout this region, the conditional distribution of the radii at which bubbles of a given size D intersect the probe is given by

$$P(r|R) = 8r/D^2 = 2r/R^2 \qquad (9.1)$$

Since y is known for each value of r and R, one can derive the conditional probability density function for finding a pierced length y from a bubble of size R. This analysis has been conducted previously by Clark and Turton (1988) who showed that for $0 \leq y < 2\alpha QR$

$$P(y|R) = \frac{y}{2\alpha^2 R^2} \qquad (9.2a)$$

and for $2\alpha QR \leq y \leq \alpha R(1+Q)$

$$P(y|R) = \frac{2}{\alpha^2 R^2} (y - \alpha RQ) \qquad (9.2b)$$

else $P(y|R) = 0$. The vertical height of the bubble at the circle of truncation is $2\alpha RQ$ and the maximum bubble height is $\alpha R(1+Q)$. (See Figure 9.1).

Using Equation 9.2, for a given distribution of bubble sizes, which are pierced by the probe, P(R), the distribution of pierced lengths is readily found by

$$P(y) = \int_0^{\infty} P(y|R)\, P(R)\, dR \qquad (9.3)$$

To illustrate Equation 9.3, Figure 9.2 shows the distribution of pierced lengths which can be expected for a uniform distribution of bubble sizes touching the probe. However, it is the back transform, finding P(R) from P(y), that is usually of interest. Moreover, P(R) would be the distribution of bubble sizes touching the probe, and we must transform this further to the distribution of bubble sizes in the bed, $P_B(R)$, using a weighting factor of R^2 to account for the higher likelihood of larger bubbles touching the probe. Since the form of P(R) is unknown, Clark and Turton (1988) have solved for P(R) using a numerical approach, similar to that of Werther (1974a). Consider a set of data consisting of n observations of chord lengths y. Let us divide the chord lengths into m equal length partitions such that

$$y_i = y_{max} - (i + 1/2) \quad 0 \le i \le m - 1 \quad \text{where} \quad \Delta y = \frac{y_{max}}{m}$$

Then an approximation to the probability of finding a chord length y between y_i and y_{i+1} is defined as

$$W\,(y_i < y \le y_{i+1}) = \frac{\text{Number of chord lengths between } y_i \text{ and } y_{i+1}}{\text{Total number of chord lengths, n}}$$

The matrix solution has the following triangular form:

$$W_o = C_{o,o}\, P(R_o)\, \Delta R$$

$$W_1 = C_{1,o}\, P(R_o)\, \Delta R + C_{1,1}\, P(R_1)\, \Delta R$$

$$\vdots$$

$$W_{m-1} = C_{m-1,o}\, P(R_o)\Delta R + C_{m-1,1}\, P(R_1)\Delta R + \ldots + C_{m-1,m-1}\, P(R_{m-1})\, \Delta R \qquad (9.4)$$

where

$$C_{i,j} = \int_{y_i}^{y_{i+1}} P(y|R_j)\, dy$$

and

$$R_j = R_{max} - j\, \Delta R \qquad 0 \le j \le m-1$$

with

$$\Delta R = \frac{R_{max}}{m} = \frac{y_{max}}{\alpha\ (1+Q)m} \qquad (9.5)$$

Note that $C_{i,j}$ is zero for $i < j$, essentially because there is an upper limit to the pierced length that can be yielded by a bubble of a particular size.

A numerical example of this approach is given below. Using a uniform bubble size distribution (as used in Figure 9.2) and shape given in Figure 9.1, 5000 pierced lengths were synthesized using a Monte Carlo simulation. The back transform matrix was applied, using 10 intervals of bubble size to yield a bubble size distribution in good agreement with that used to produce the chord lengths (see Figure 9.3). However, the back transform can become unstable if too many size divisions or too few pierced length observations are used. Figures (9.4a) and (9.4b) show the results of the back transform when only 1000 and 100 pierced lengths are used. In extreme cases, even negative probabilities may result. These instabilities arise from the fact that a representative number by bubbles must be present in each sub-division of chord lengths (i.e. in each Δy). Thus stability will be favored for a large sample data set with a few sub-divisions.

It was assumed above that the pierced length was known from the time interval during piercing, t. This is simply determined if one assumes a constant bubble rise velocity as a first approximation (Werther, 1974a). This approach will be valid if the bubbles are themselves rising in a fast-moving fluidized stream. On the other hand one may use pairs of probes vertically above one another with cross-correlation of the signals to measure directly the bubble rise velocity, u, so that $y = u.t$

If we choose to adopt an accepted model to predict bubble rise velocity as a function of bubble size, such as

$$u = c'\sqrt{gD} = c\sqrt{gR} \qquad (9.6)$$

then

$$P(tR) = P(r|R)\left|\frac{dr}{dt}\right|$$

$$= P(y|R)\left|\frac{dy}{dt}\right|$$

$$= P(y|R)\ c\sqrt{gR} \qquad (9.7)$$

Combining this with equation (9.2), we find that for $0 \leq c\sqrt{gR}\ t \leq 2\alpha QR$, that is for $0 \leq t \leq \frac{2\alpha QR}{c\sqrt{gR}}$

$$P(t|R) = \frac{c\sqrt{gr}\ t}{2\alpha^2 R^2} \cdot c\sqrt{gR}$$

$$= \frac{c^2 gt}{2\alpha^2 R} \qquad (9.8a)$$

and for $2\alpha QR < c\sqrt{gR}\ t \leq \alpha R(1+Q)$

that is, for $\frac{2\alpha QR}{c\sqrt{gR}} < t \leq \frac{\alpha R(1+Q)}{c\sqrt{gR}}$

$$P(t|R) = \frac{2}{\alpha^2 R^2} (c\sqrt{gR}\ t - \alpha RQ)\ c\sqrt{gR}$$

$$= \frac{2c}{\alpha^2 R} (cgt - \alpha Q\sqrt{gR}) \qquad (9.8b)$$

else $P(t|R) = 0$. For a given size distribution of bubbles touching the probe, $P(t)$, the distribution of time intervals would be

$$P(t) = \int_0^\infty P(t|R)\ P(R)\ dR \qquad (9.9)$$

Once again we are more interested in the back transform. Following the logic and notation used previously in this paper, with $W_i = W(t_i < t \leq t_{i+1})$ and with

$$E_{i,j} = \int_{t_i}^{t_{i+1}} P(t|R_j)dt \qquad (9.10)$$

the matrix for back transformation

10. CONCLUSIONS

This research has demonstrated conclusively that DSPP can be used successfully to measure void properties in fluidized beds. DSPP response is adequate for recording local differential pressures in fluid beds provided that the probe system is properly sized using the charts developed for this purpose. A data bank of pressure traces from a slugging bed is now available, and analysis of this data has provided the slugging frequency and velocity in the bed. Slugging frequency decreased with bed height, while slug velocity increased with air superficial velocity. It is evident that DSPP will prove a robust and reliable means for monitoring performance of large beds or obtaining further experimental data during research. However, in the benefit of probes with three or four stems should also be assesed in the future.

Furthermore, analysis has shown that one can infer a bubble size distribution in a fluidized bed provided that a distribution of chord length can be obtained from a probe. However, instabilities in this back-transform technique merit further investigation.

11. REFERENCES

Atkinson, C.M., "The Development of a Gas Sampling System For Fluidized Beds", M.S. Thesis, West Virginia University, Dept. of Mechanical and Aerospace Engineering 1987.

Atkinson, C.M., and Clark, N.N., 1986, "Analysis of Fluidized Bed Behavior using Probes", Proc. 11th Powder and Bulk Solids Conf., Rosemont, Illinois, pp. 437-443.

Atkinson, C.M. and Clark, N.N., 1988, "Gas Sampling from Fluidized Beds: A Novel Probe System", Powder Technology, Vol. 54, pp. 59-70.

Burgess J. M., Calderbank, P.H., "The Measurement of Bubble Parameters in Two-Phase Dispersions-I", Chemical Engineering Science, 1975, Vol. 30., pp. 743-750.

Cheremisinoff, N.P., 1986, "Review of Experimental Methods for Studying Hydrodynamics of Gas-Solid Fluidized Bed", I & EC Process Design and Development, Vol. 25, pp. 329-351.

Clark, N.N. and Atkinson, C.M., "Amplitude Reduction and Phase Lag in Fluidized Bed Pressure Measurements," Chemical Engineering Science, 1988, Vol. 43, pp. 1547-1557.

Clark, N.N. and Turton, R., 1987, "Chord Length Distributions Related to Bubble Size Distributions in Multiphase Systems", Int. Jour. Multiphase Flow, Vol.14, 1988, pp. 413-424.

Cranfield, R., "A Probe for Bubble Detection and Measurment in Large Particale Fluidized Beds", Chem. Eng. Sci., Vol. 27, 1972, pp. 239.

Davidson, J.F. and Harrison, D., Fluidized Particles, Cambridge University Press, Cambridge, 1963.

Dutta, S., Wen, C. Y., "A Simple Probe for Fluidized Bed Measurements", The Canadian Journal of Chemical Engineering, Vol. 57, February, 1979, pp. 115-119.

Fan L. T., Ho C. T., Hiraoka S., Walawender W. P., "Pressure Fluctuations ia a Fluidized Bed", AIChE Journal, Vol. 27, 1981, pp. 388-395.

Fan, L.T., Huang, Y.W. and Yutani, N., "Determination of the Lower Bound of Minimum Fluidization Velocity: Application at Elevated Temperatures," Chemical Engineering Science, Vol. 41, 1986, pp. 189-192.

Fan, L.T., Huang, Y.W., Neogi, D. and Yutani, N., "Statistical Analysis of Temperature Effects on Pressure Fluctuations in a Gas-Solid Fluidized Bed", Fluidization '85, Science Press, Beijing, 1985.

Fitzgerald, T.J., 1979, "Review of Instrumentation for Fluidized Beds", Workshop Rensselaer Polytechnic Institute, Troy, New York, Oct. 1979.

Flemmer, R.L.C., "A Pneumatic Probe to Detect Gas Bubbles in Fluidized Beds 1: Method of Operation", Ind. Eng. Chem. Fundam., Vol. 23, 1984, pp. 113-115.

Flemmer, R.L.C., Swart, H.C. and Mori, H., "A Pneumatic Probe to Detect Gas Bubbles in Fluidized Beds 2: Response of the Probe," Ind. Eng. Chem. Fundam., Vol. 23, 1984, pp. 116-119.

Geldart, D., and Baeyens, J., "The Design of Distributors for Gas-Fluidized Beds", Powder Technology, Vol. 42, 1985, pp. 67.

Goldstein, R.J., Fluid Mechanics Measurements, Hemisphere, Washington, 1983.

Ho, T.C., Yutani, N., Fan, L. T. and Walawender, W. P., "The Onset of Slugging in Gas-Solid Fluidized Beds with Large Particles", Department of Chemical Engineering, Kansas State University, Manhattan, KS 66506 (U.S.A.), (Received April 12, 1982; in revised form December 16, 1982).

Hatano H., Ishida, M., "The Continuous Measurement of Local Concentration with a Optical-Fiber Probe", International Chemical Engineering, 1983, Vol.23, No. 4, pp. 682-688.

Oka, Y., 1983, "Fluidization Characteristics in Fluidized Beds Connected Vertically by the Riser and Downcomer Pipers", M.S. Thesis, Illinois Institute of Technology.

Sitnai, O., "Utilization of Pressure Differential Records from Gas Fluidized Beds with Internals for Bubble Parameter Determination," Chemical Engineering Science, Vol. 37, 1982, pp. 1059-1066.

Svoboda, K., Cermak, J., Hartman, M., Drahos, J. and Selucky, K., "Pressure Fluctuations in Gas-Fluidized Beds at Elevated Temperatures", Ind. fEng. Chem. Proc. Des. Dev., Vol. 22, 1983, pp. 514-520.

Werther, J., 1974a, "Bubbles in Gas Fluidized Beds - Part 1", Trans. Inst. Chem. Engrs., Vol. 52, pp. 149-159.

Werther, J., 1974b, "Bubbles in Gas Fluidized Beds - Part 2", Trans. Inst. Chem. Engr., Vol. 52, pp. 160-169.

Werther, J. and Molerus, O., 1973, "The Local Structure of Gas Fluidized Beds", Int. Jour. Multiphase Flow, Vol. 1, pp. 103-122.

Yutani, N., Ototake, N. and Fan, L.T., "Stochastic Analysis of Fluctuations in the Local Void Fraction of a Gas-Solids Fluidized Bed", Powder Technology, Vol. 48, 1986, pp. 31-38.

12. PUBLICATIONS ARISING FROM CONTRACT

Turton, R. and Clark, N.N., "Interpreting Probe Signals from Fluidized Beds", Powder Technology, Accepted for publication.

Turton, R. and Clark, N.N., "Predicting the Response of Pressure Probes in Pneumatic Conveying and Fluidized Beds", Powder and Bulk Solids Conf., Rosemont, Ill., May 1988, Proceedings, pp. 341-350. To appear in Journal of Powder and Bulk Solids Technology.

Clark, N.N., Turton, R., McKenzie, E.A., Jr., and Wang, Y-Z., "Fluidized Bed Pressure Probes", Dept. of Energy Advanced Research and Technology Development Contractors Review Meeting, Pittsburgh, Sept. 1988 (Poster Presentation and Published in Proceedings).

Clark, N.N., Wang, Y-Z., McKenzie, E.A., Jr., and Turton, R., "Fluidized Bed Instrumentation Using Pressure Probes", ASME 10th Conf. on Fluidized Bed Combustion, May 1989.

McKenzie, E. A.,Jr., Clark, N. N., Gautam, M. E., Turton, R. A., "Slug Frequency, Rise Velocity, and Size with Air-Fluidized Nylon Spheres", Powder and Bulk Solids Conf., Rosemont Ill., 1990.

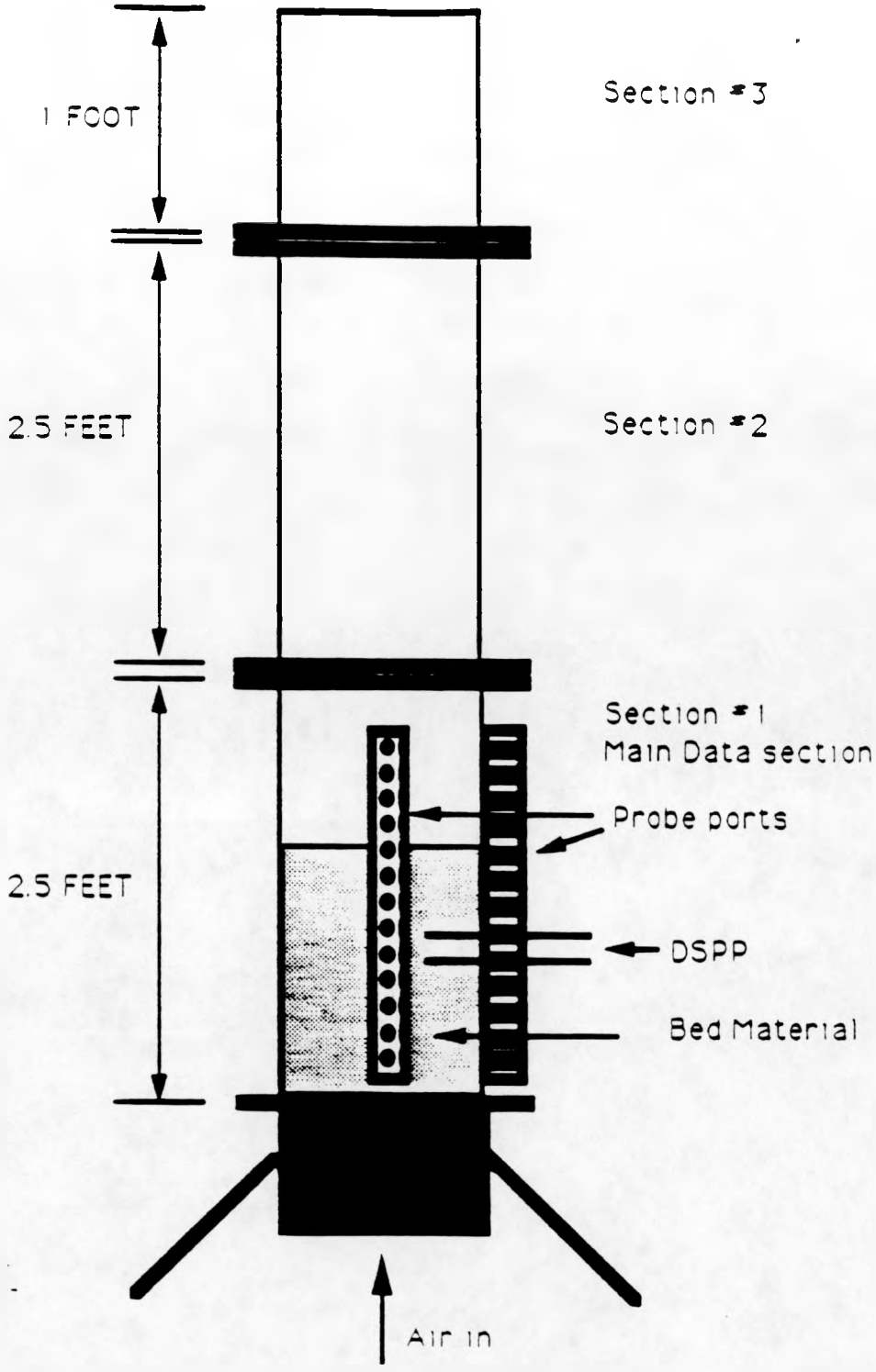

Figure 3.1 **The Fluidized bed**

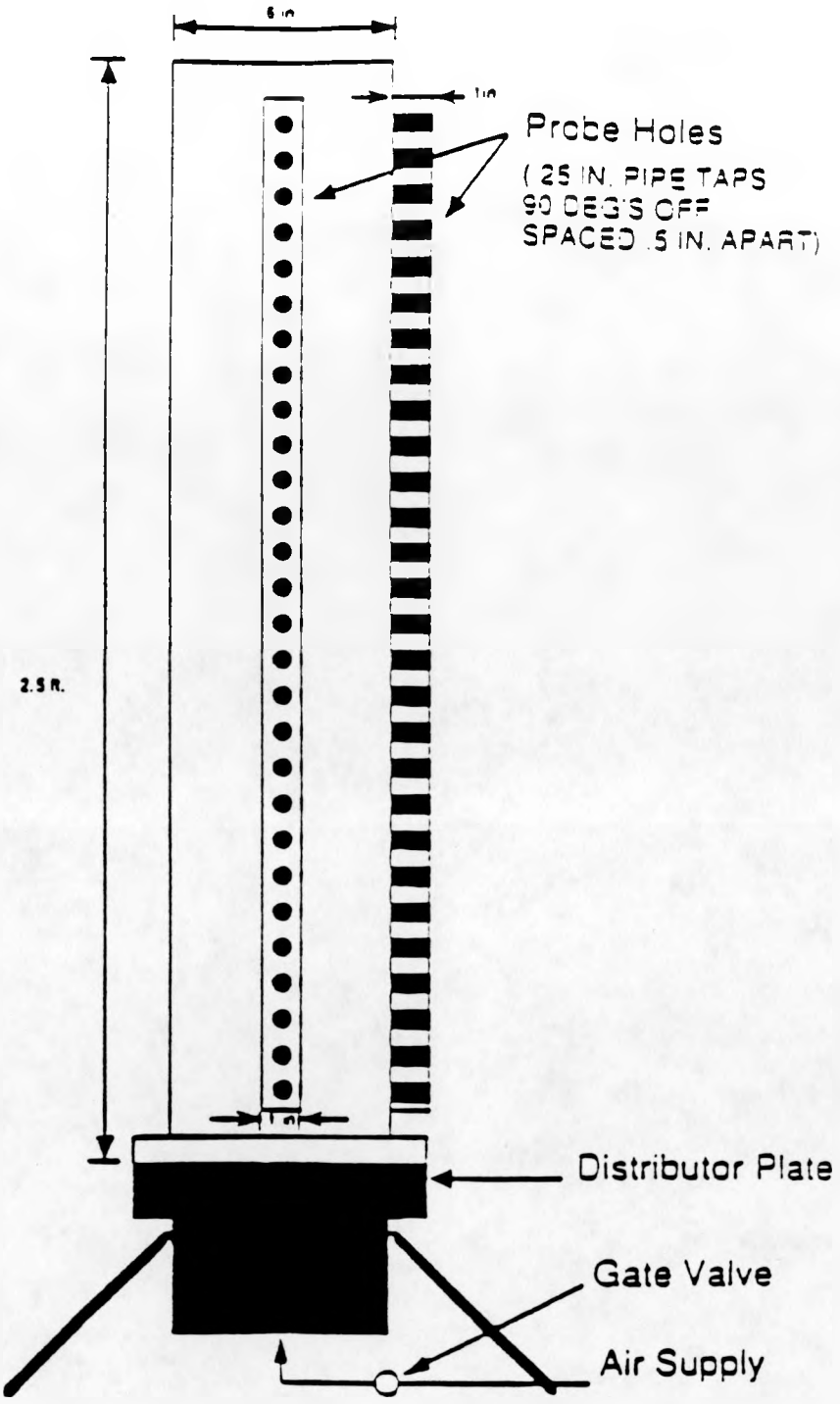

Figure 3.2 Main Data Sampling Section (lower section)

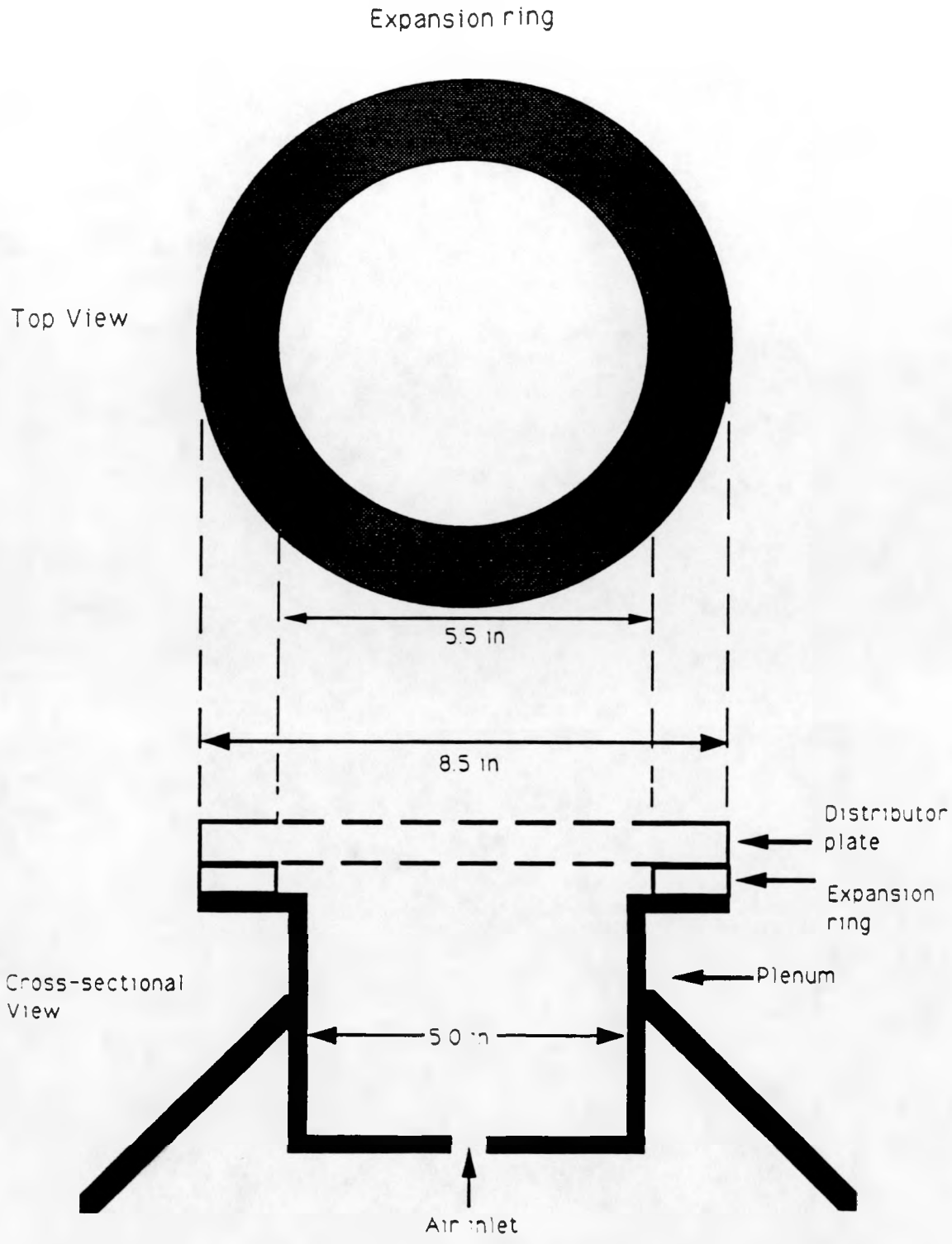

Figure 3.3 Expansion Ring and Plenum

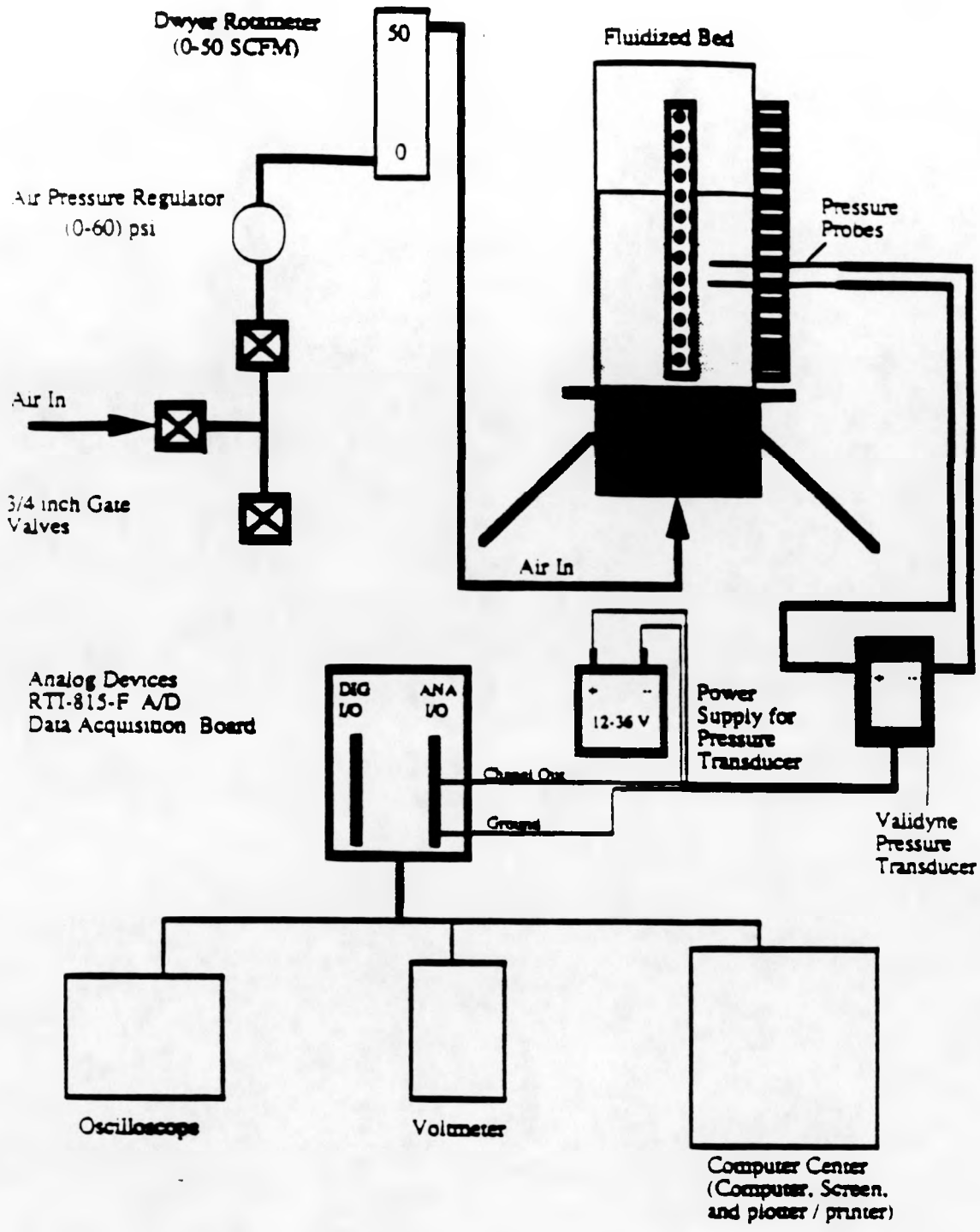

Figure 3.4 Schematic of Experimental Work Station

DISTRIBUTOR PLATE # 1

1/2 INCH THICK FLAT CAST ACRYLIC SHEET

CONSISTING OF:

→ 61 1/16 INCH DRILLED HOLES

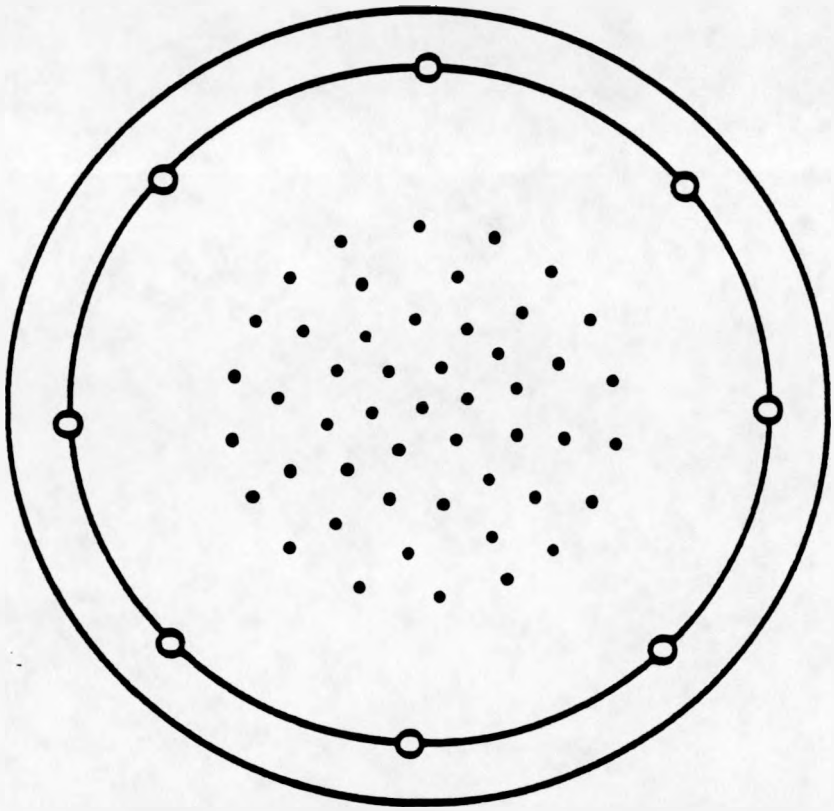

Figure 3.5 Distributor Plate #1 61 1/16 Inch Holes

DISTRIBUTOR PLATE #2

1/2 INCH THICK FLAT CAST ACRYLIC SHEET

CONSISTING OF:

→ 177 5/64 INCH DRILLED HOLES

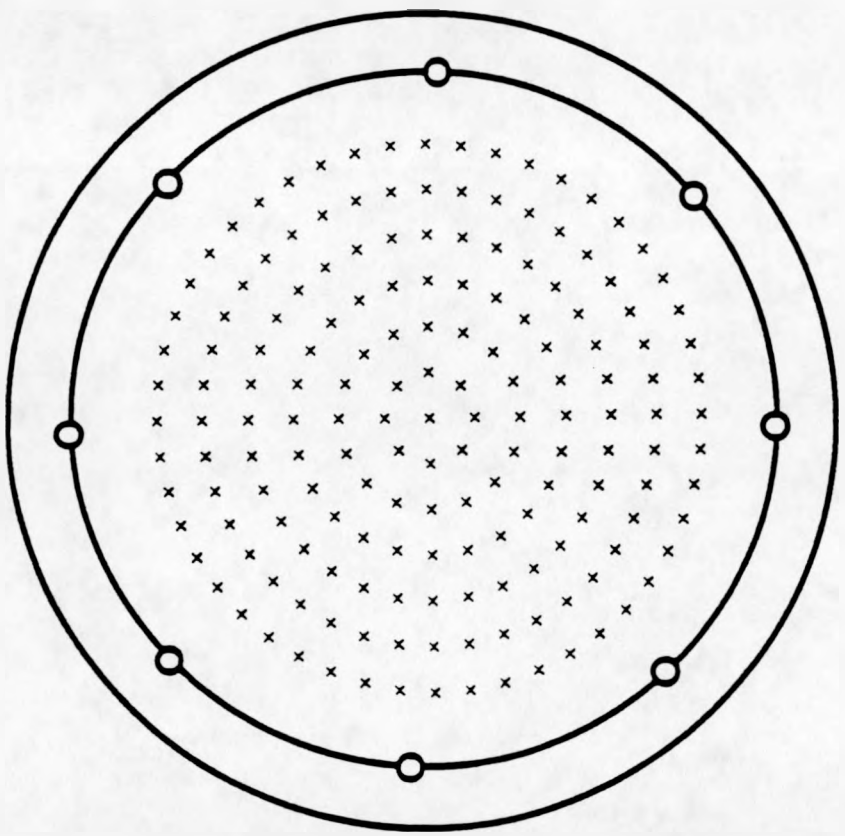

Figure 3.6 Distributor Plate #2 5/64 inch Holes

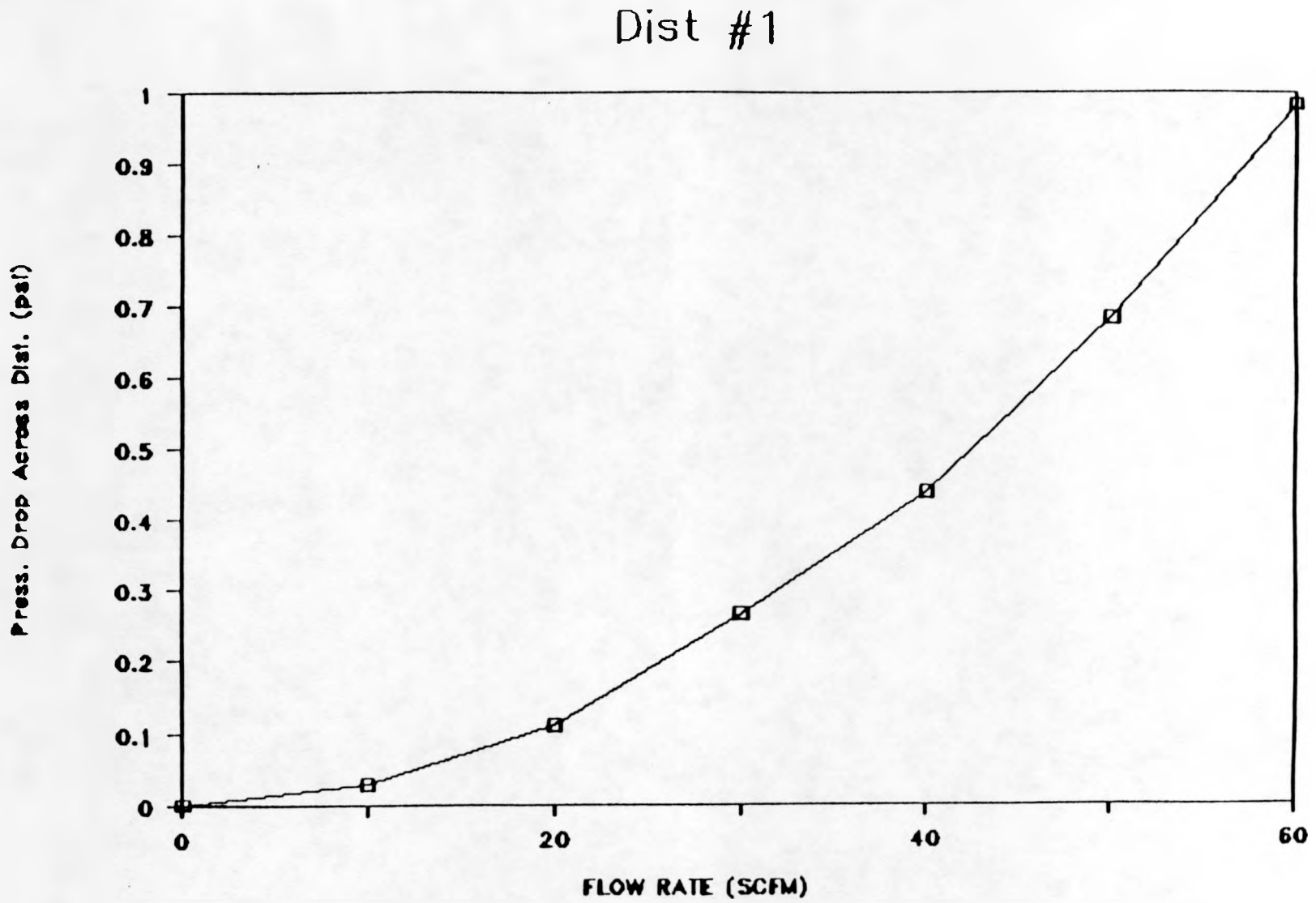

Figure 3.7 Pressure Drop Across Distributor #1 (psi vs SCFM)

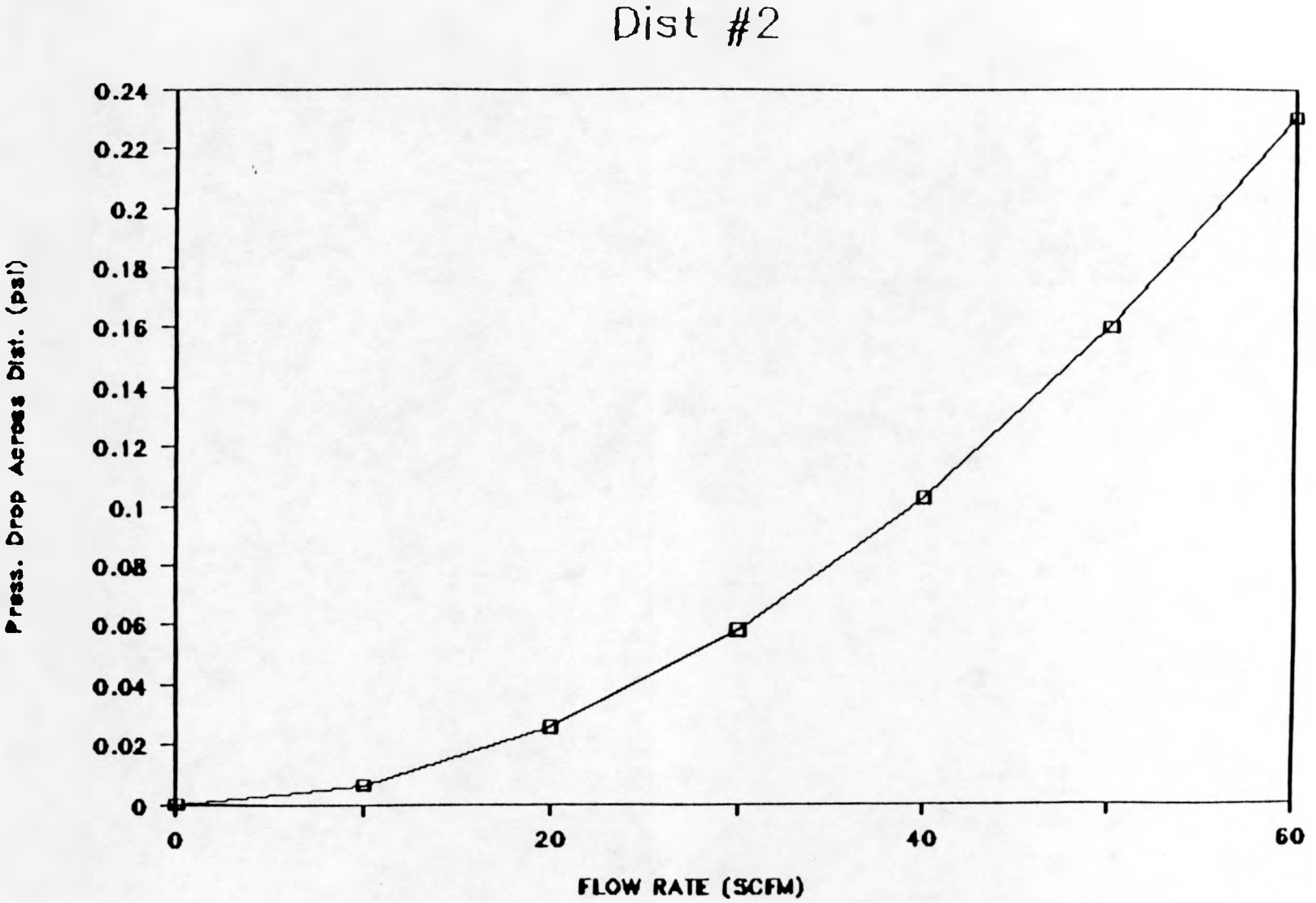

Figure 3.8 Pressure Drop Across Distributor #2 (psi vs SCFM)

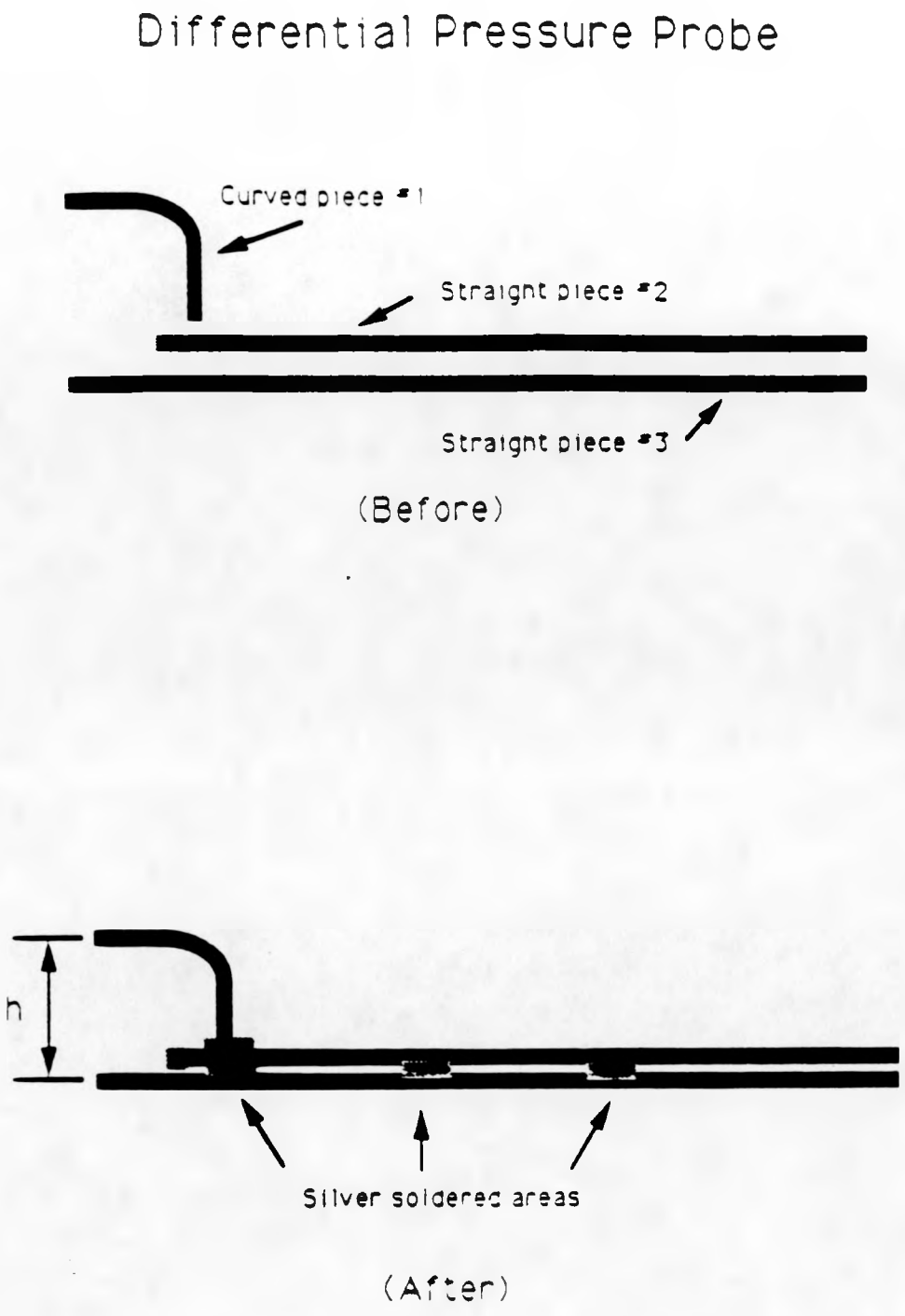

Figure 4.1 Construction of Differential Pressure Probe

Dual Static Pressure Probes

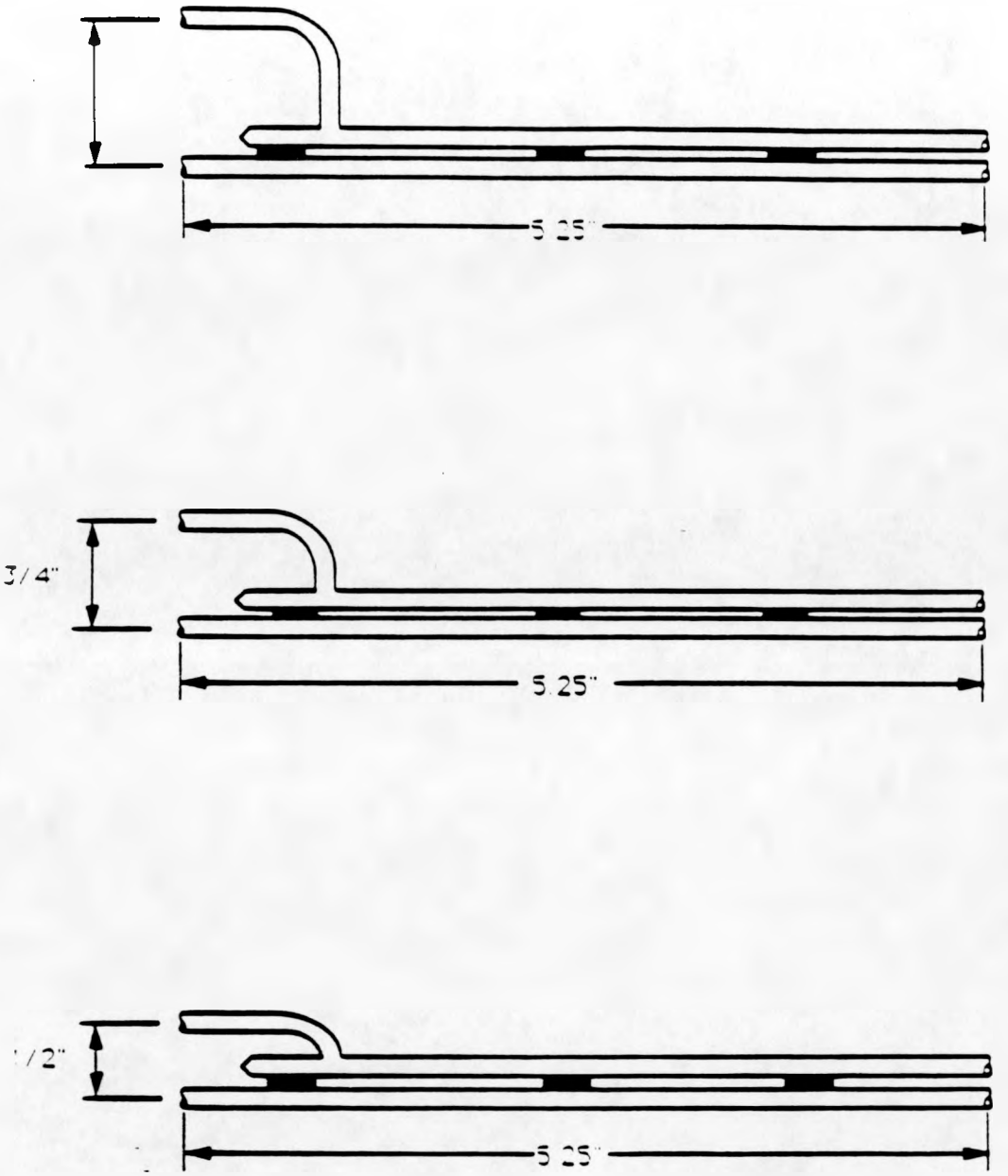

Figure 4.2 Three Different Probe Spacing of the Dual Static Pressure Probes

DSPP Modification

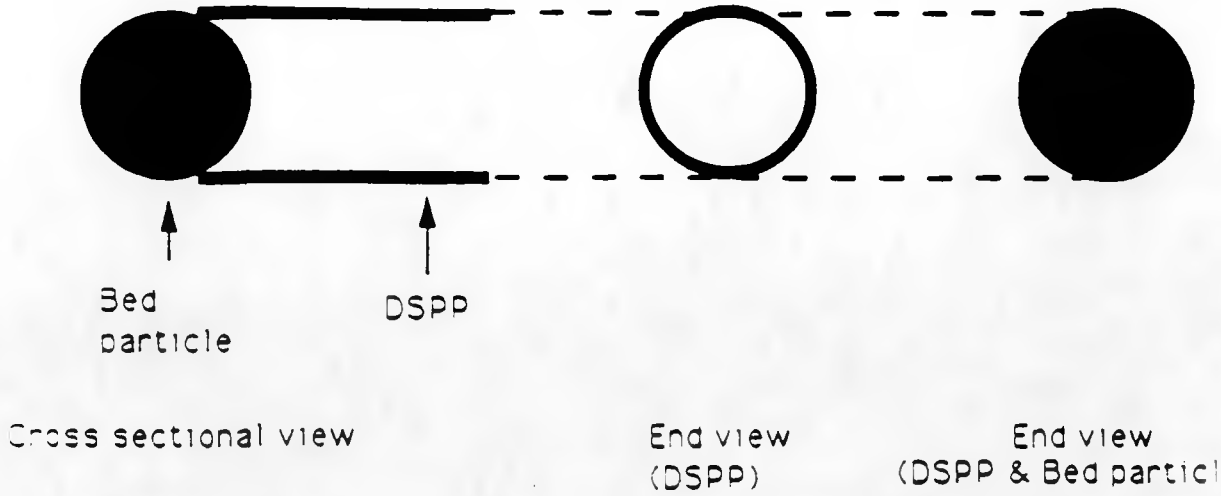

(BEFORE)

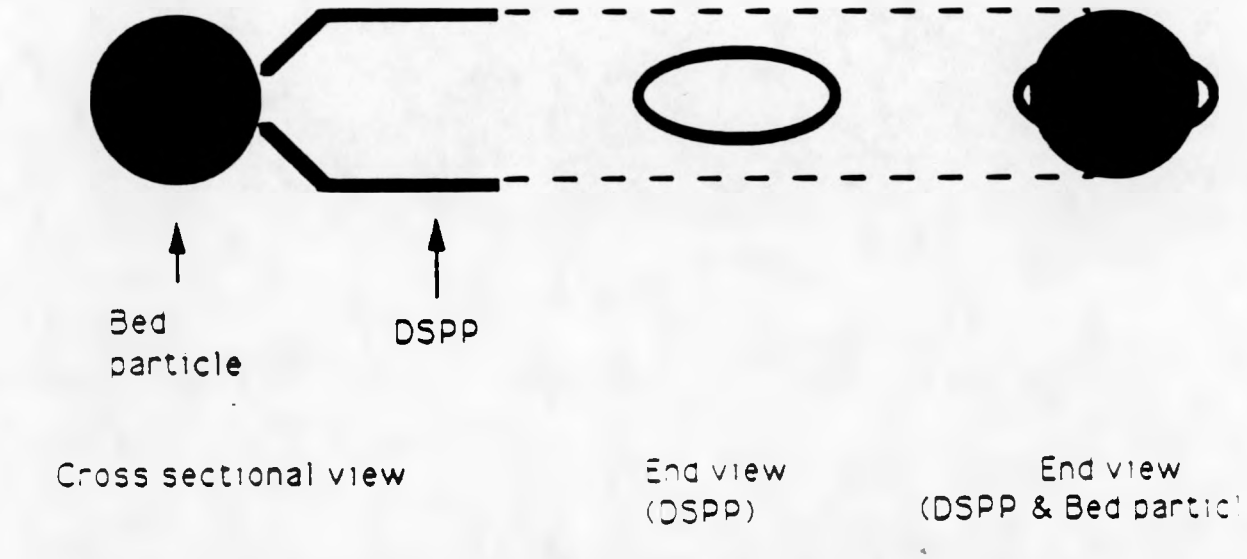

(AFTER)

Figure 4.3 Modification of Dual Static Pressure Probe

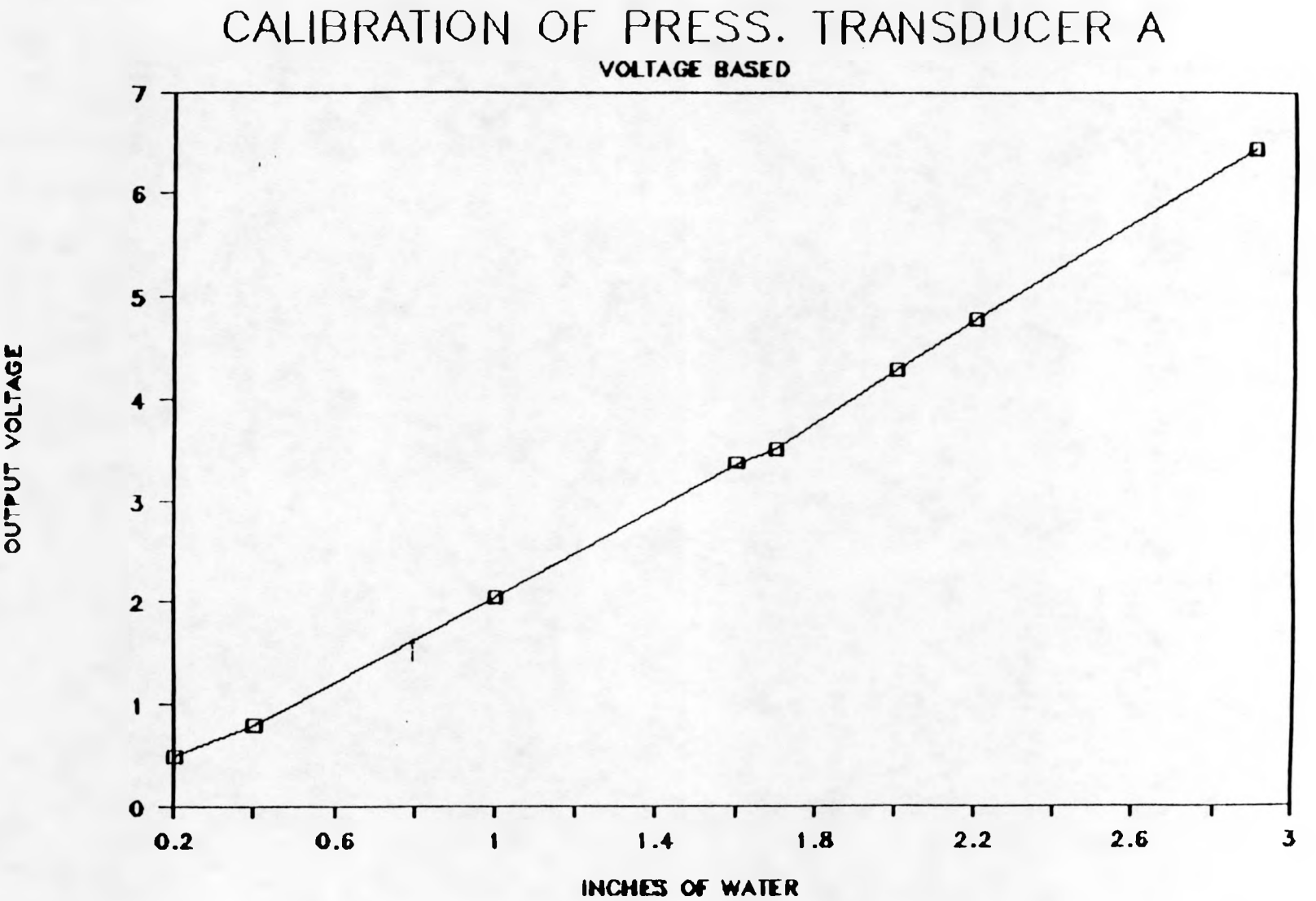

Figure 4.4 Calibration Curve of Validyne Pressure Transducer A (output voltage vs inches of water)

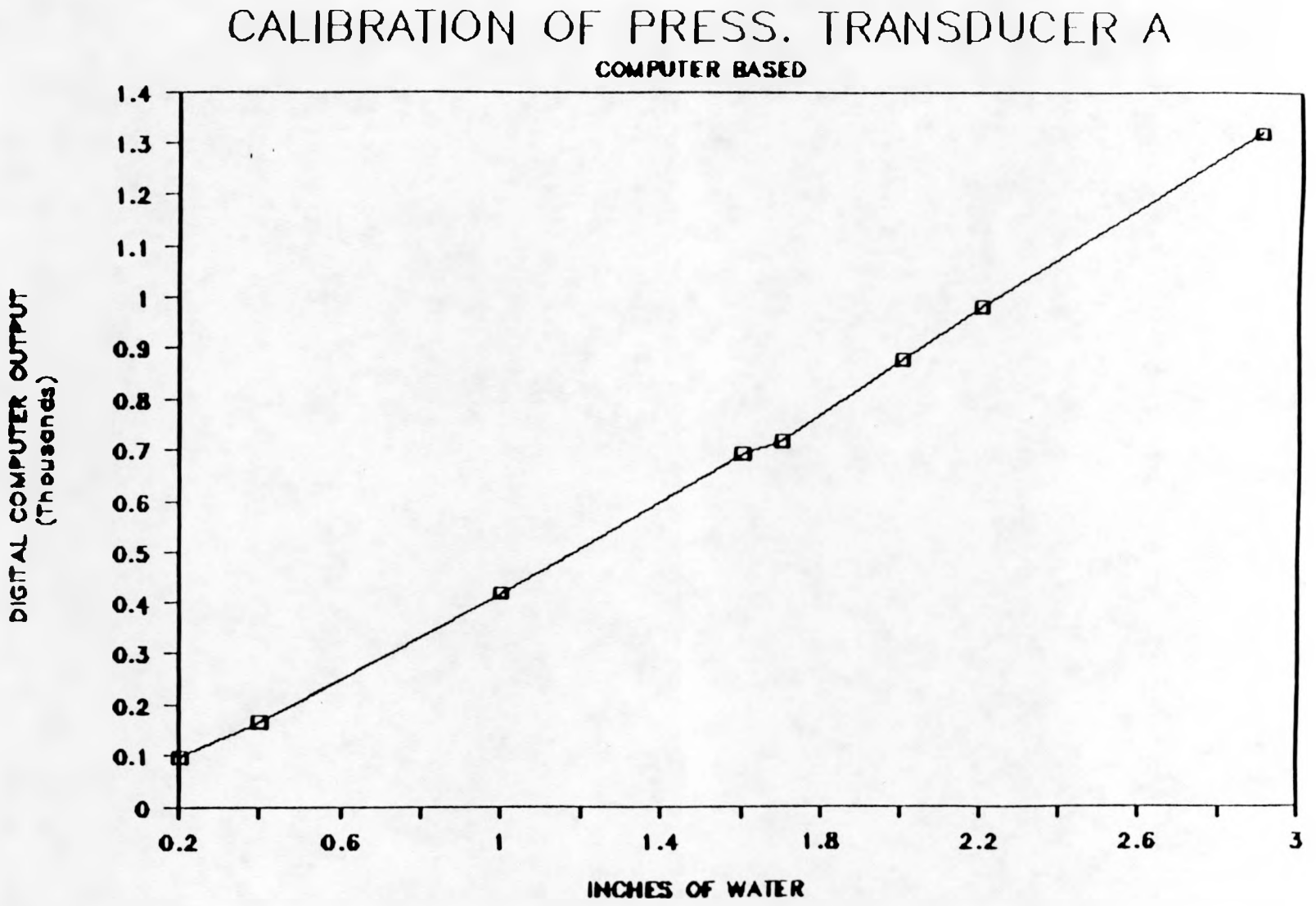

Figure 4.5 Calibration Curve of Validyne Pressure Transducer A (digital computer output vs inches of water)

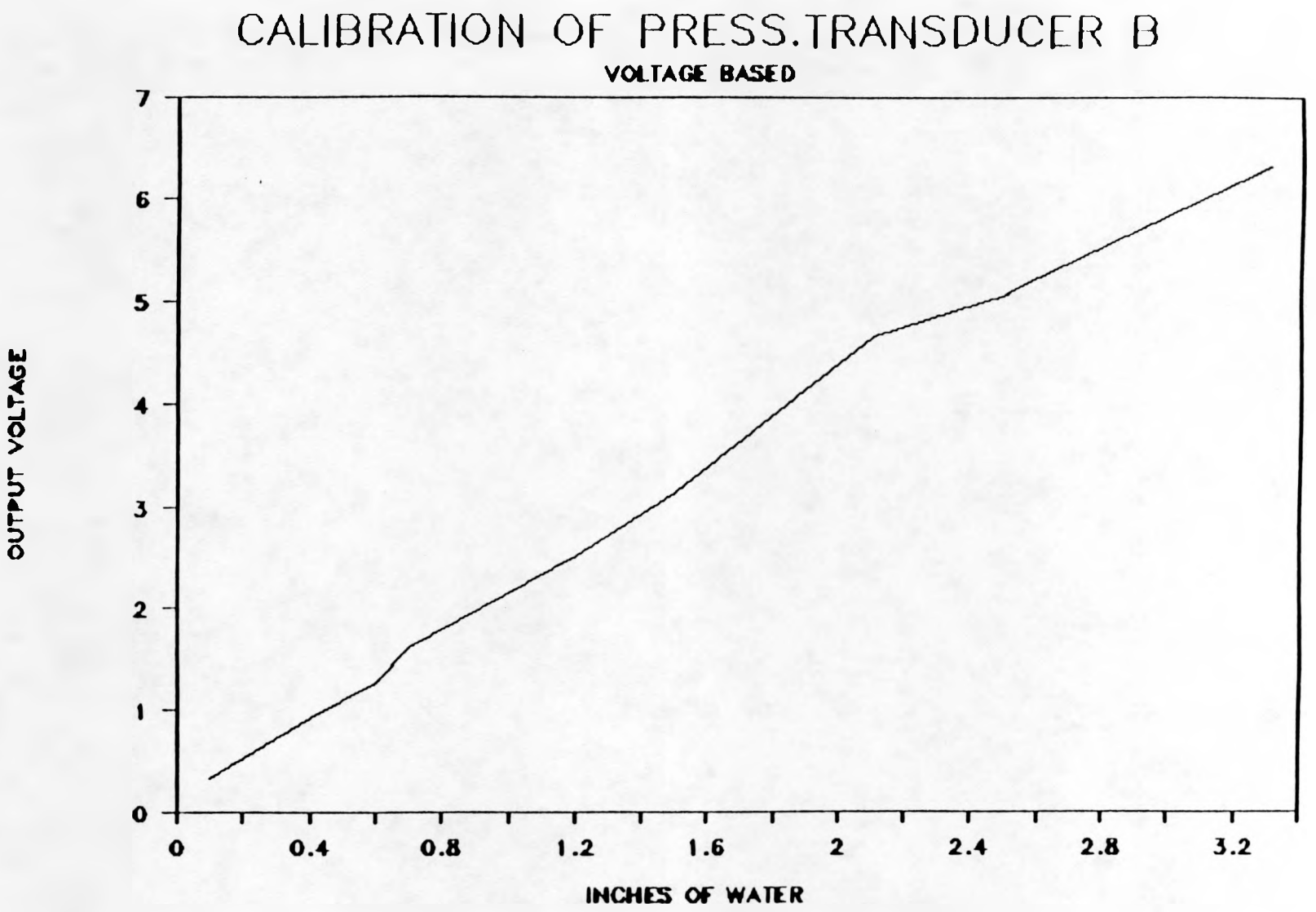

Figure 4.6 Calibration Curve of Validyne Pressure Transducer B (output voltage vs inches of water)

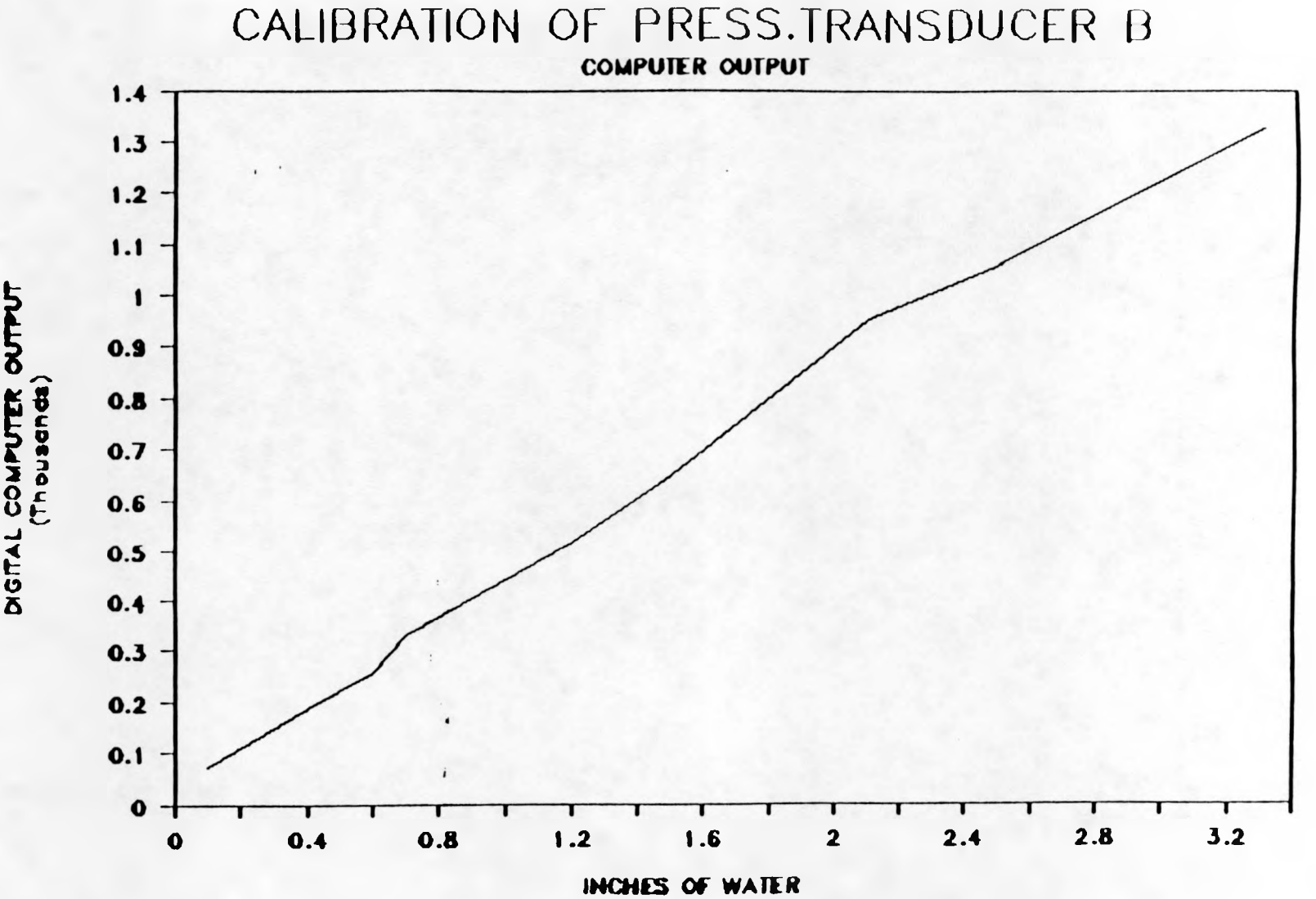

Figure 4.7 Calibration Curve of Validyne Pressure Transducer B (digital computer output vs inches of water)

Table 4.1 Experimental Conditions for Data Collection for a Single DSPP

DATA RUN NUMBER	BED HEIGHT (INCHES)	PROBE SPACING (INCHES)	PROBE HEIGHT (INCHES)	FLOW RATE (SCFM)
G7	6	0.5	3.625	39
G8	6	0.5	3.625	52
G25	12	0.5	6.75	39
G26	12	0.5	6.75	52
G43	24	0.5	11.5	39
G44	24	0.5	11.5	52

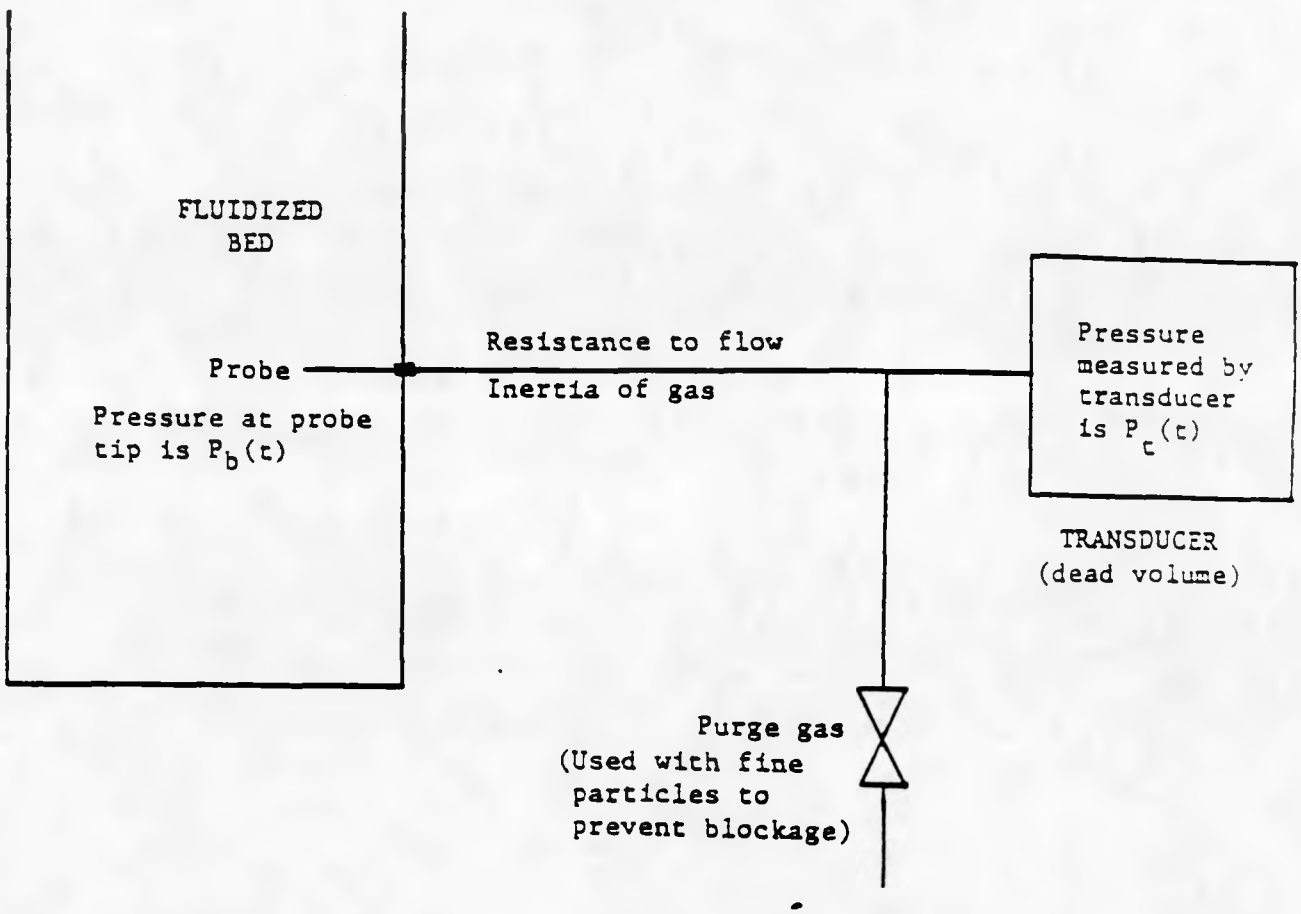

Figure 5-1: Transducer and single stem probe combination: no purge gas is necessary for large particle work.

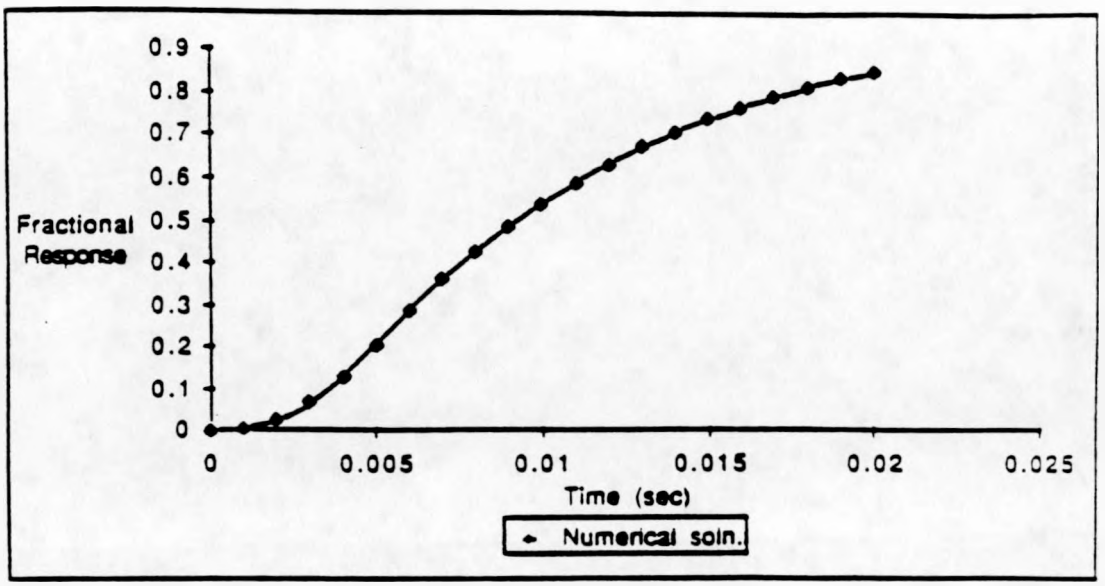

Figure 5-2: Response of a probe and transducer to a step change in bed pressure (simulated)

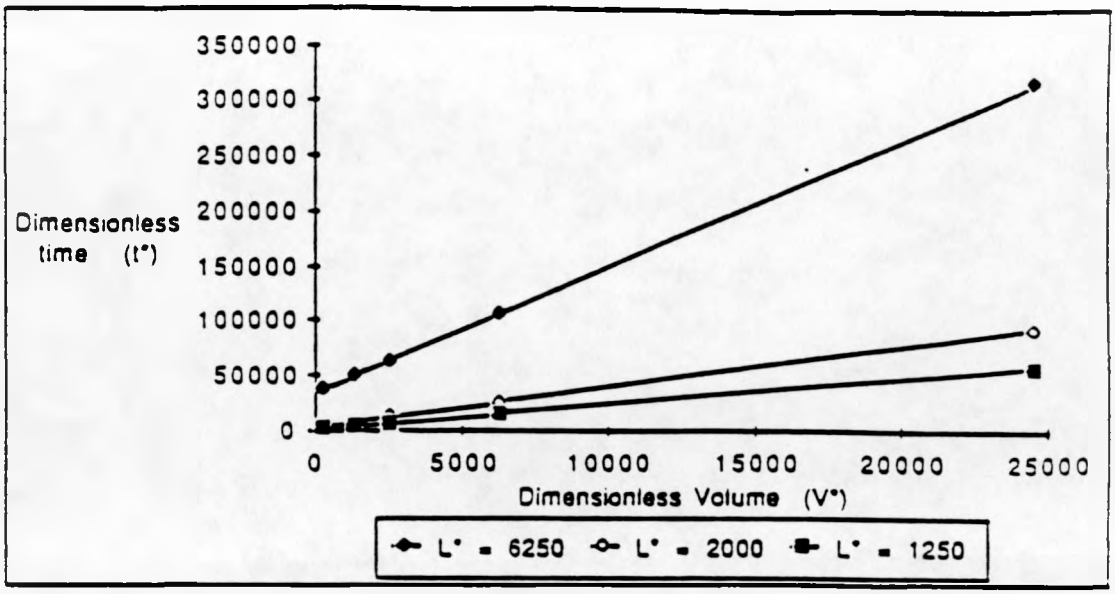

Figure 5-3: Response time of probes of different geometries to a step change in bed pressure (time to respond to 63% of the step).

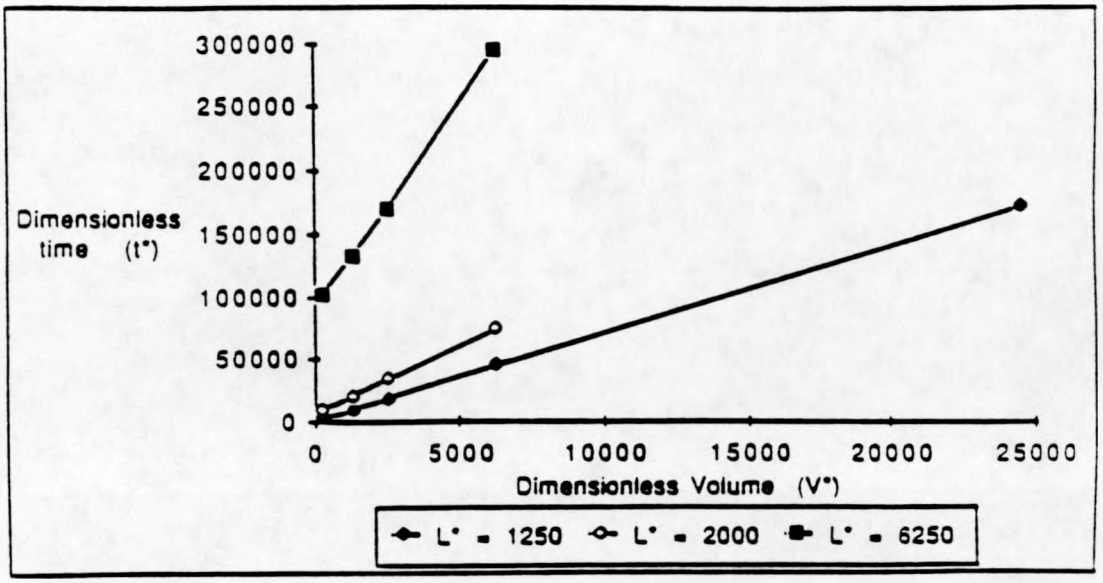

Figure 5-4: Response time of probes of different geometries to a step change in bed pressure (time to respond to 95% of the step).

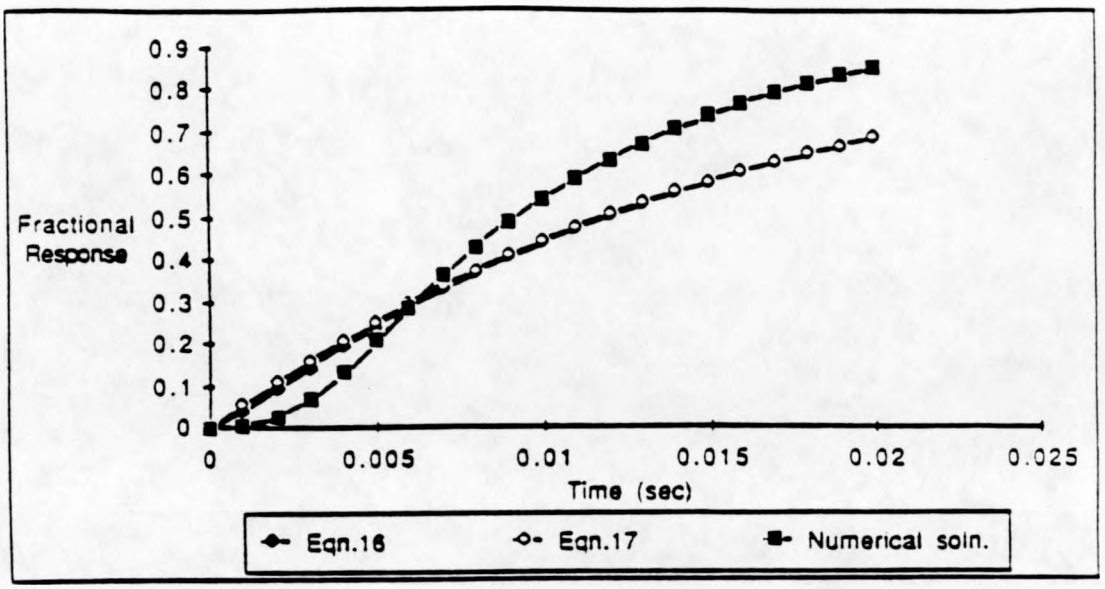

Figure 5-5: Comparison of a recent numerical model of probe response with previous simplified models.

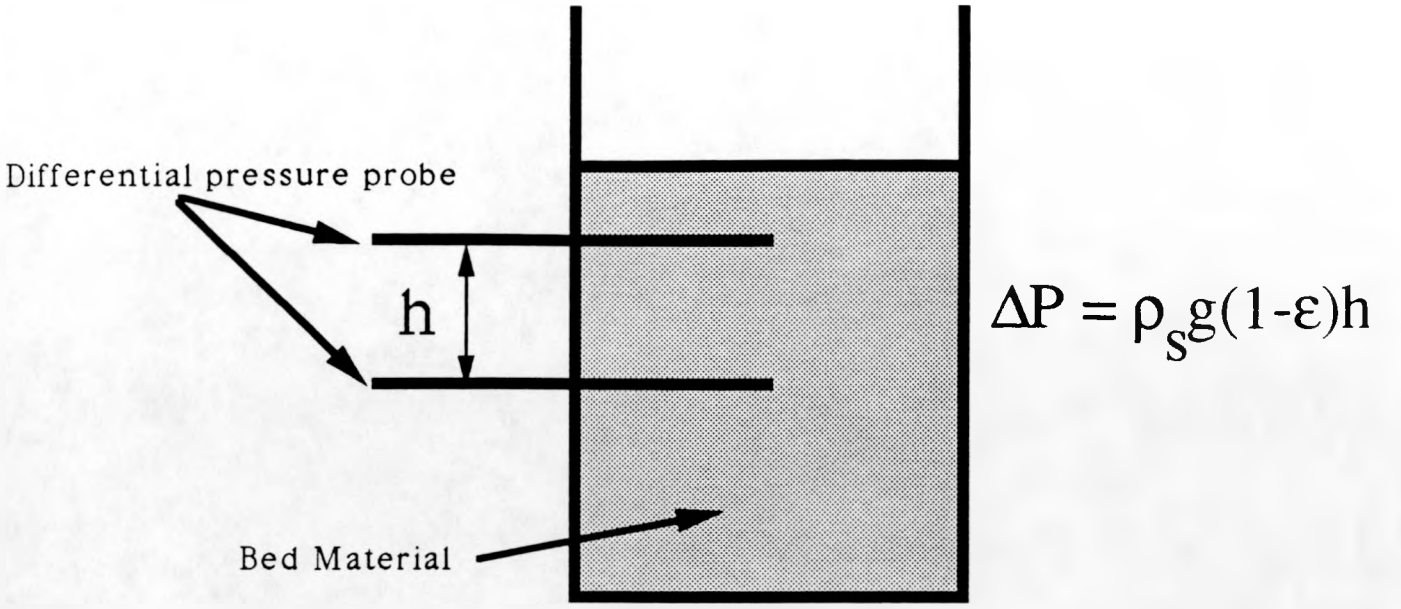

Figure 6.1 Fluidized Bed Steady State

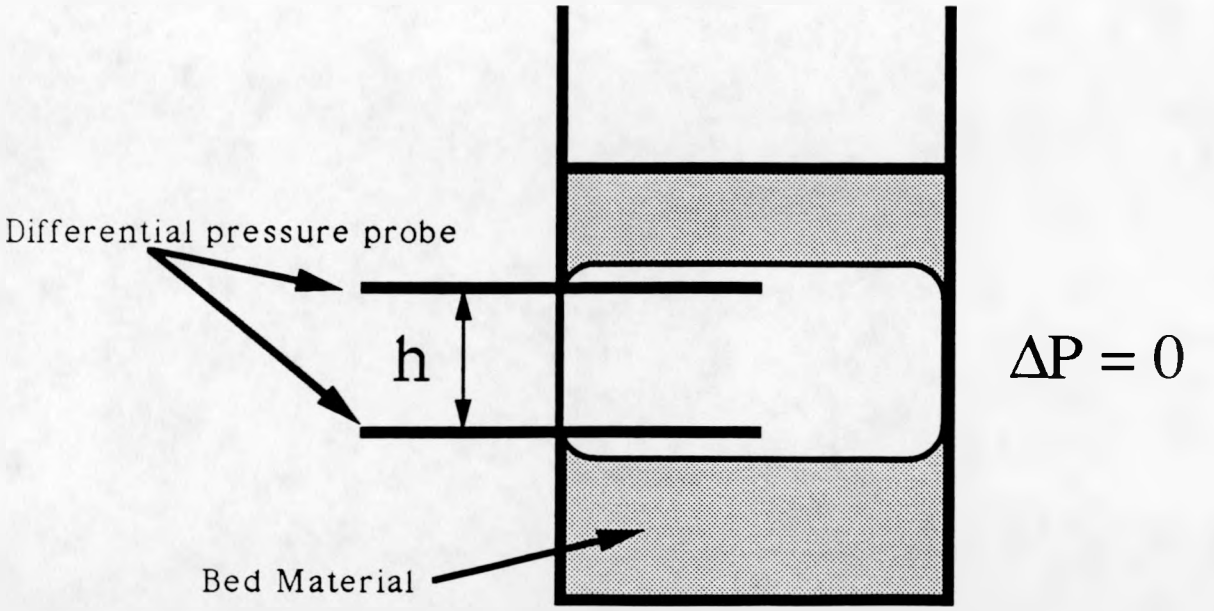

Figure 6.2 Fluidized Bed Unsteady State

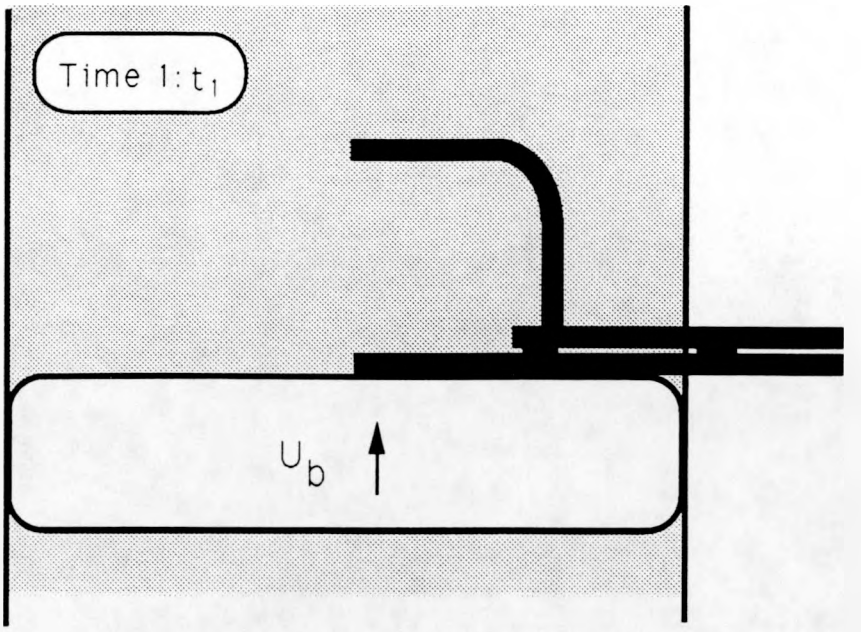

Crown of bubble touches lower stem

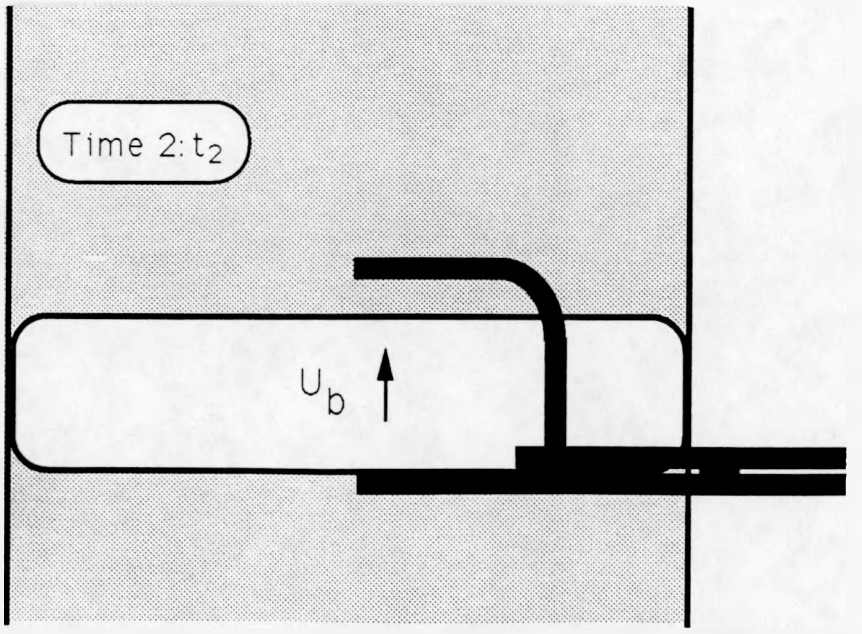

Base of bubble leaves lower stem

Figure 6.3 Detection Of A Small Slug Using The DSPP System

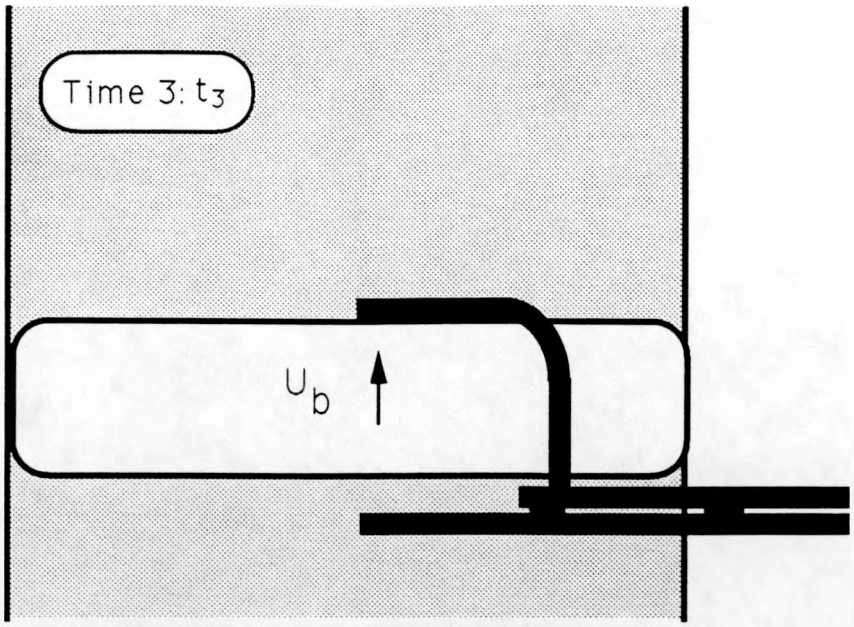

Crown of bubble touches upper stem

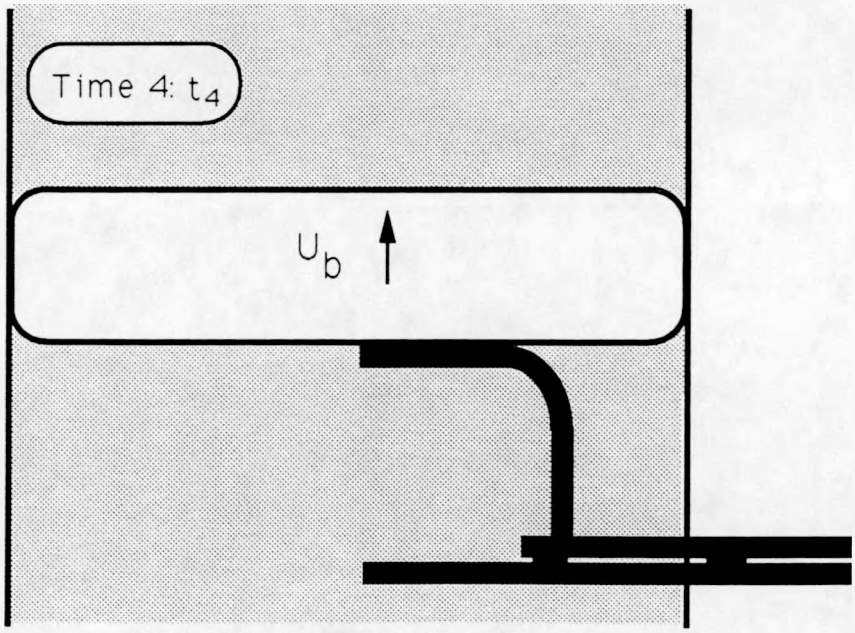

Base of bubble leaves upper stem

Figure 6.3 : Continued

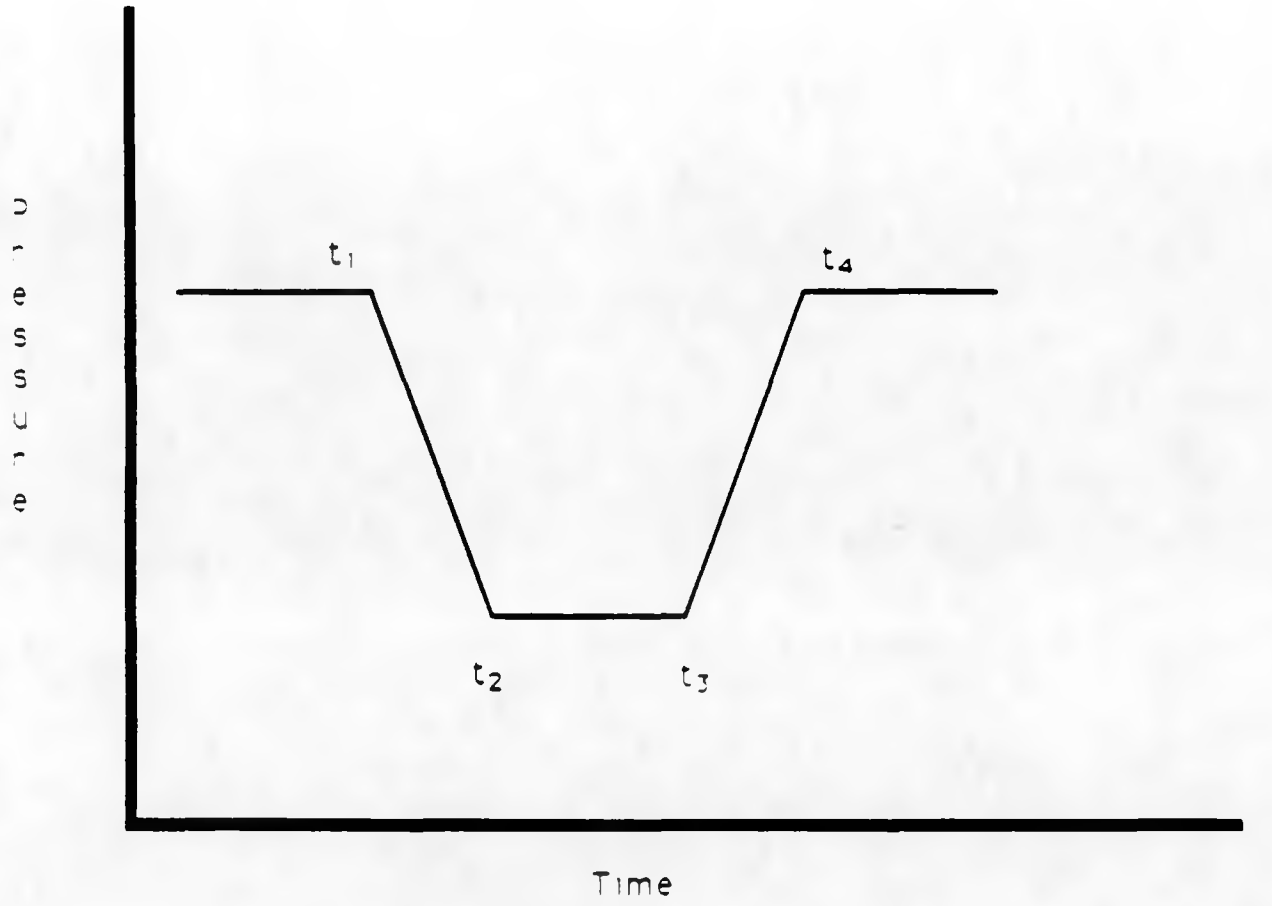

Figure 6.4 Pressure Trace of Small Slug as Detected by the DSPP System (Pressure vs Time)

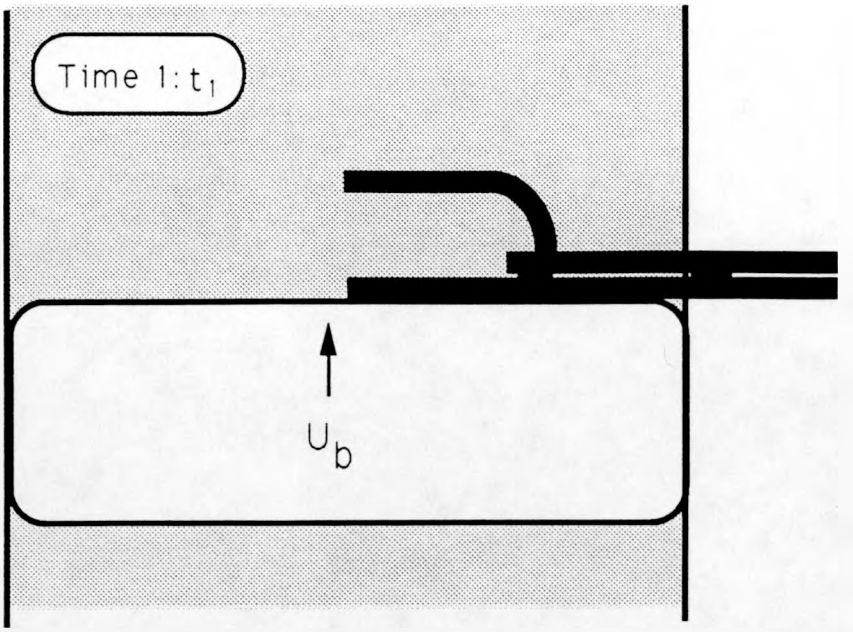

Crown of bubble touches lower stem

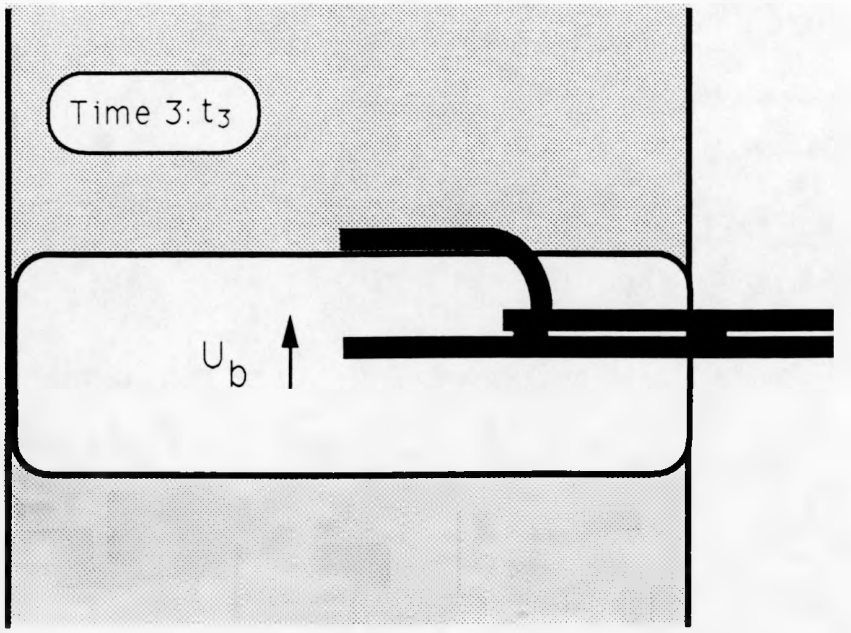

Crown of bubble touches upper stem

Figure 6.5 Detection Of A Large Slug Using DSPP System

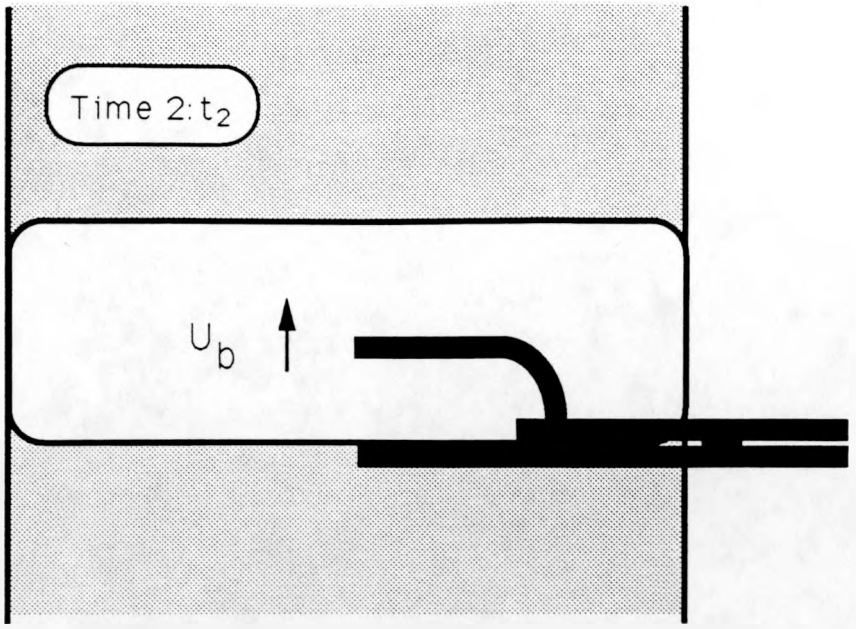

Base of bubble leaves lower stem

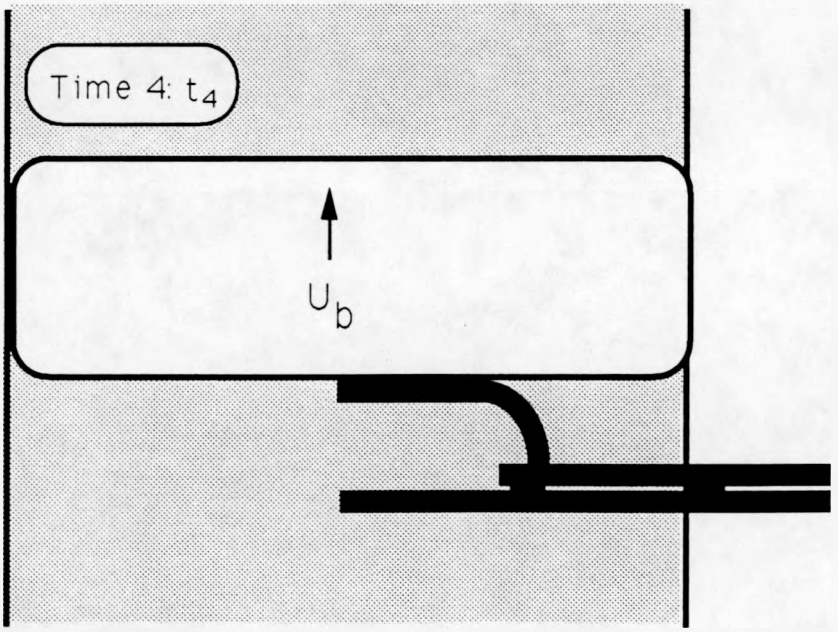

Base of bubble leaves upper stem

Figure 6.5 : Continued

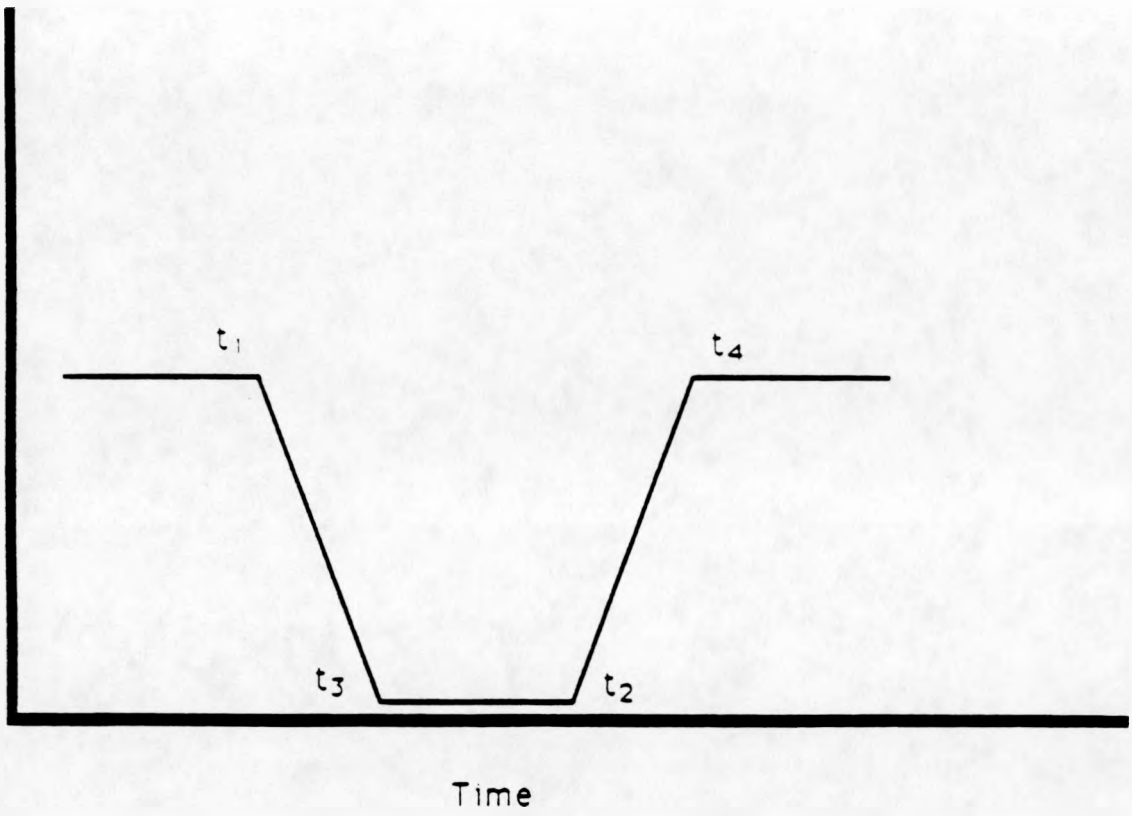

Figure 6.6 Pressure Trace of Large Slug as Detected by the DSPT System (Pressure vs Time)

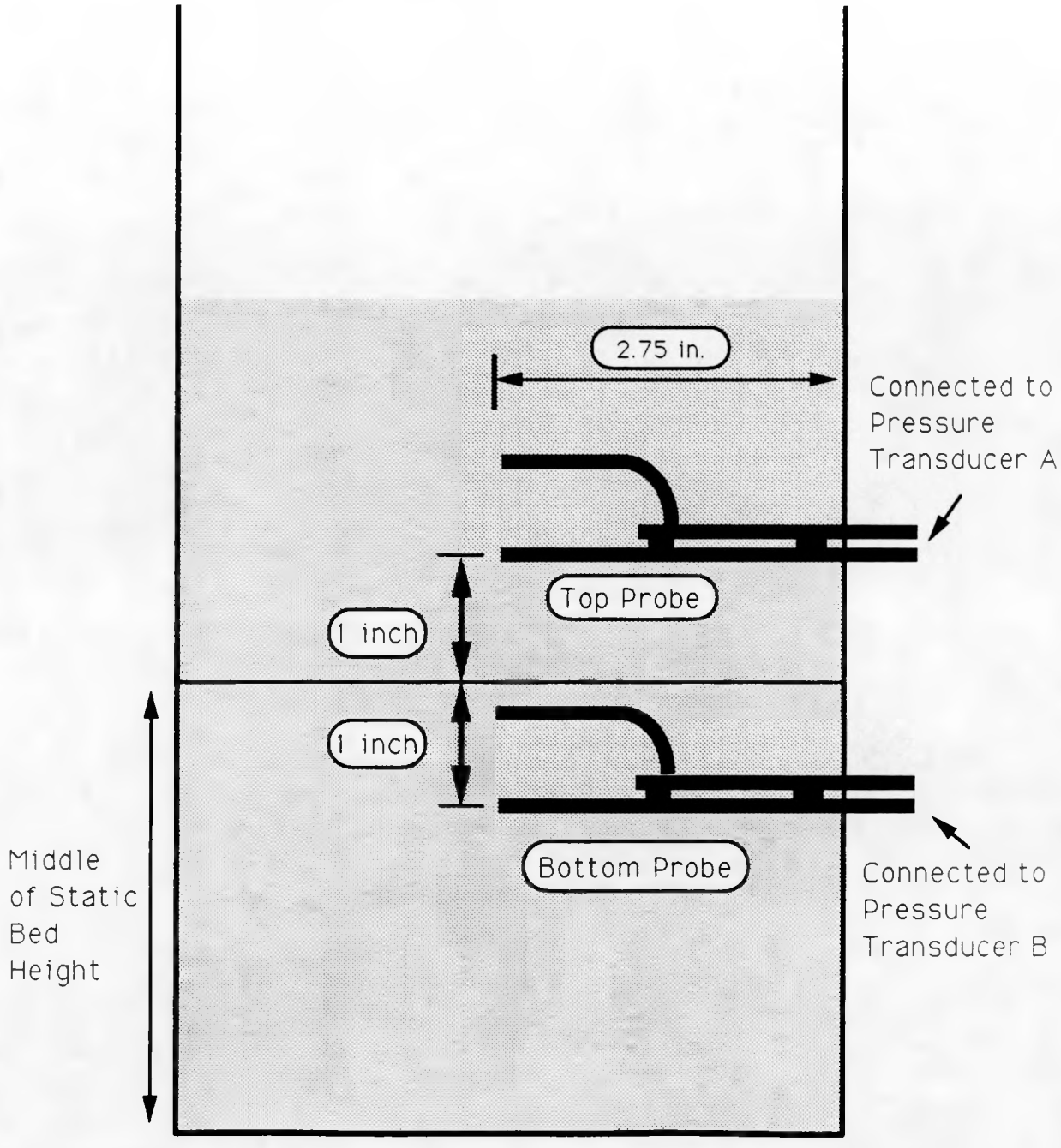

FIGURE 7.0 Location Of DSPP In Fluidized Bed For The Collection Of Data For Cross-correlation

Table 7.1 Frequency Results

		Frequency (Pressure events per seceond)					
DATA RUN NUMBER	Figure Number	Autocorrelation Function	Figure Number	Fast Fourier Transform	Figure Number	Spectral Density Function	Figure Number
G7	7.1b	1.72	7.2	1.75	7.3	1.75	7.4
G8	7.6	2.56	7.7	2.5	7.8	2.5	7.9
G25	7.10	1.2	7.11	1.25	7.12	1.25	7.13
G26	7.14	1.37	7.15	1.4	7.16	1.4	7.17
G43	7.18	0.63	7.19	0.65	7.20	0.6	7.21
G44	7.22	0.74	7.23	0.78	7.24	0.75	7.25

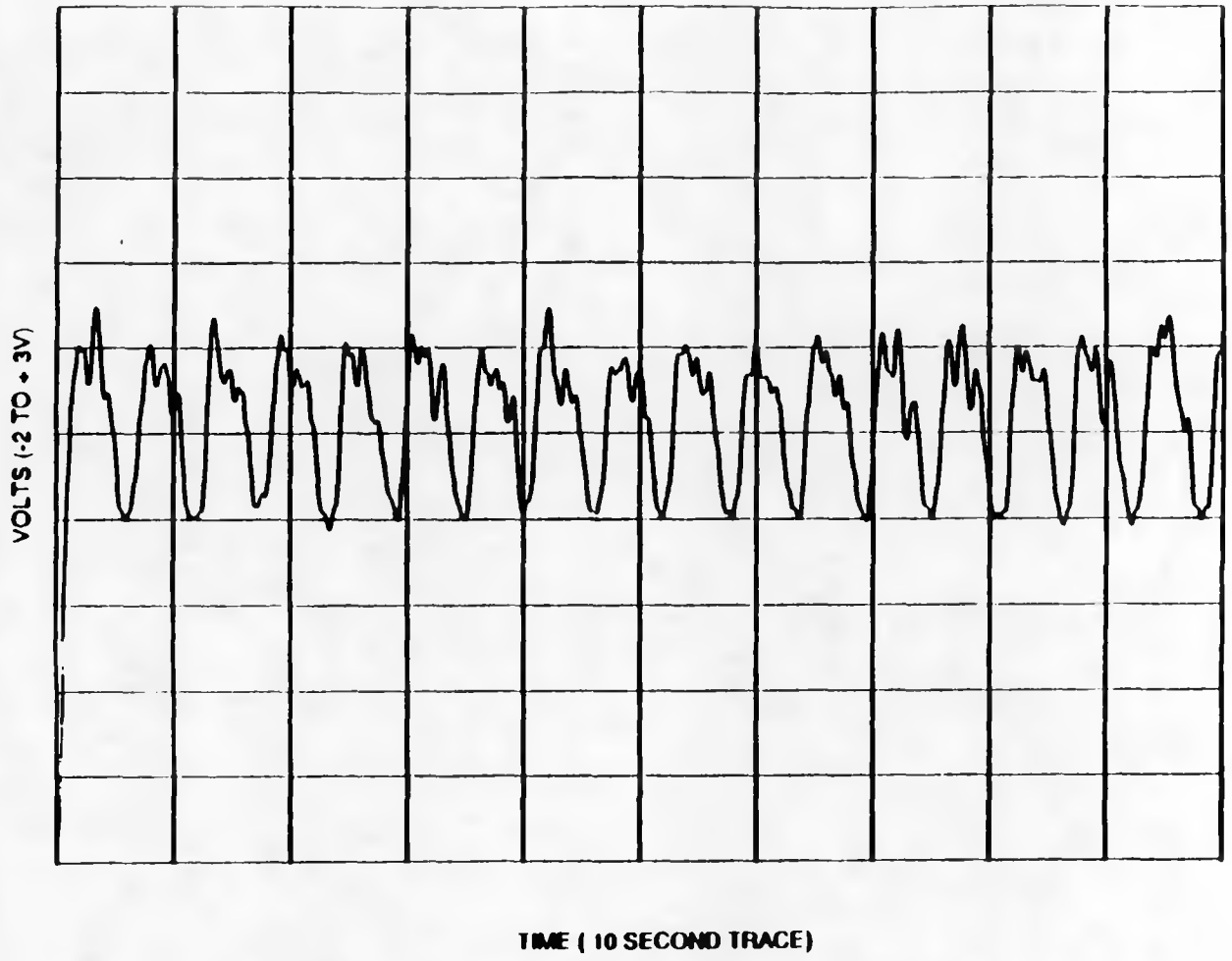

Figure 7.1 Plot of Raw Data Recorded on the Hewlett Packard Plotter (Voltage Output vs Time) of Data Set G7 (Bed Height 6 inches, Height of Probe in Bed 3.625 inches, Horizontal Distance from bed wall 2.75 inches, and Flow Rate 39 SCFM, Distributor #2)

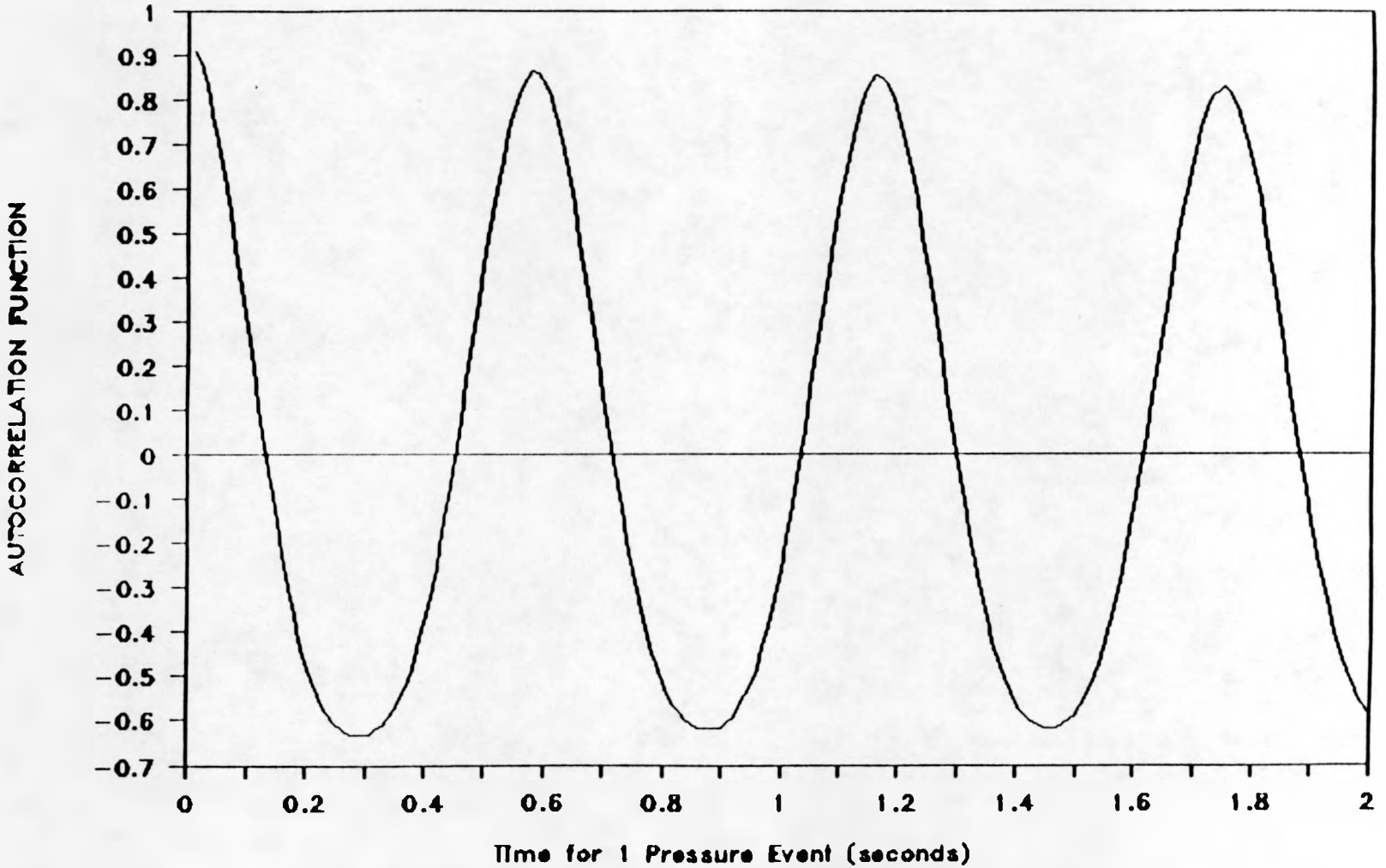

Figure 7.2 Plot of Autocorrelation Function vs Time to Determine the Time for One Pressure Event to Occur (Period) of Data set G7

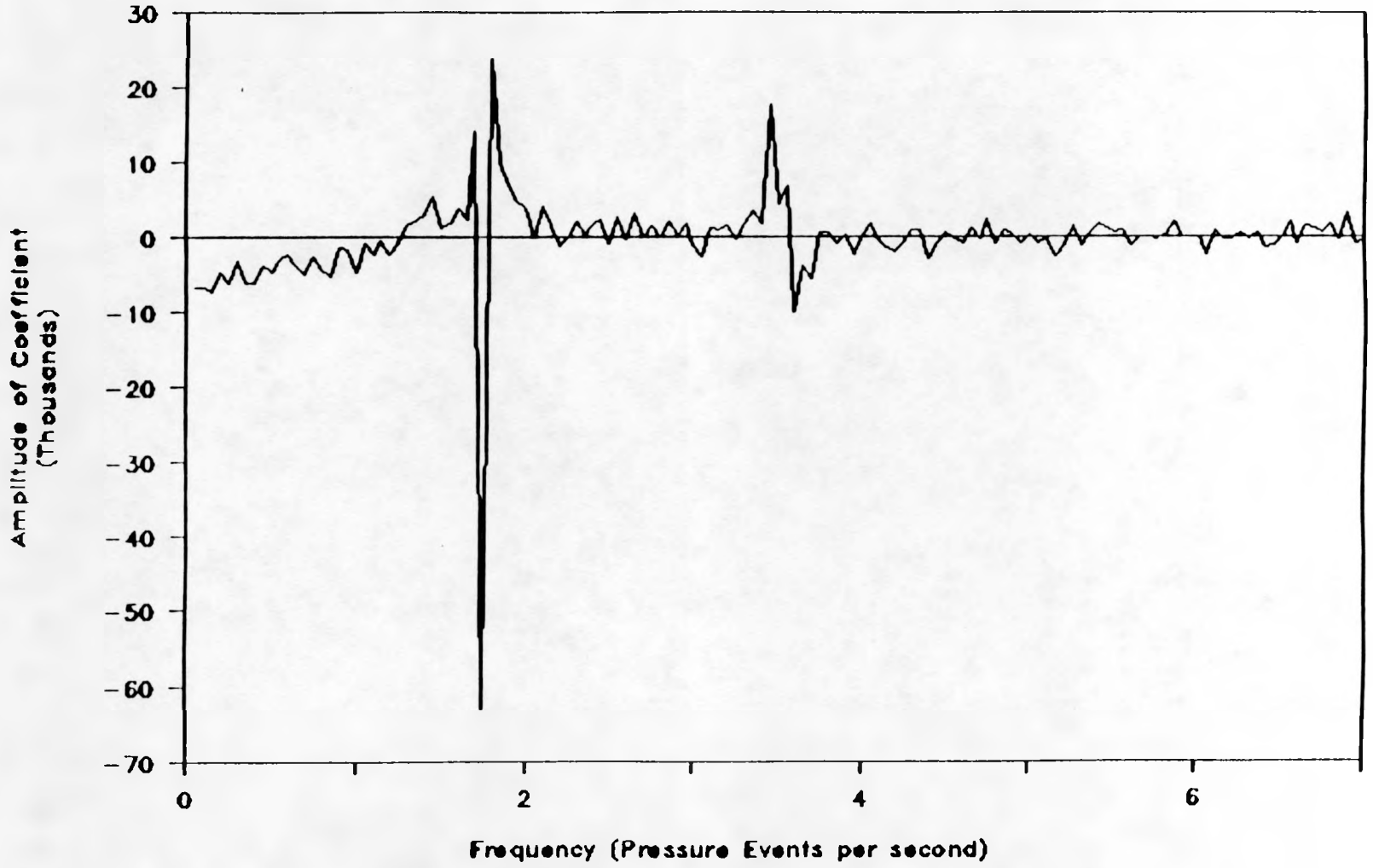

Figure 7.3 Plot of The Fast Fourier Transform Function, Amplitude of Coefficient vs Frequency (Pressure Events per Second) of Data Set G7

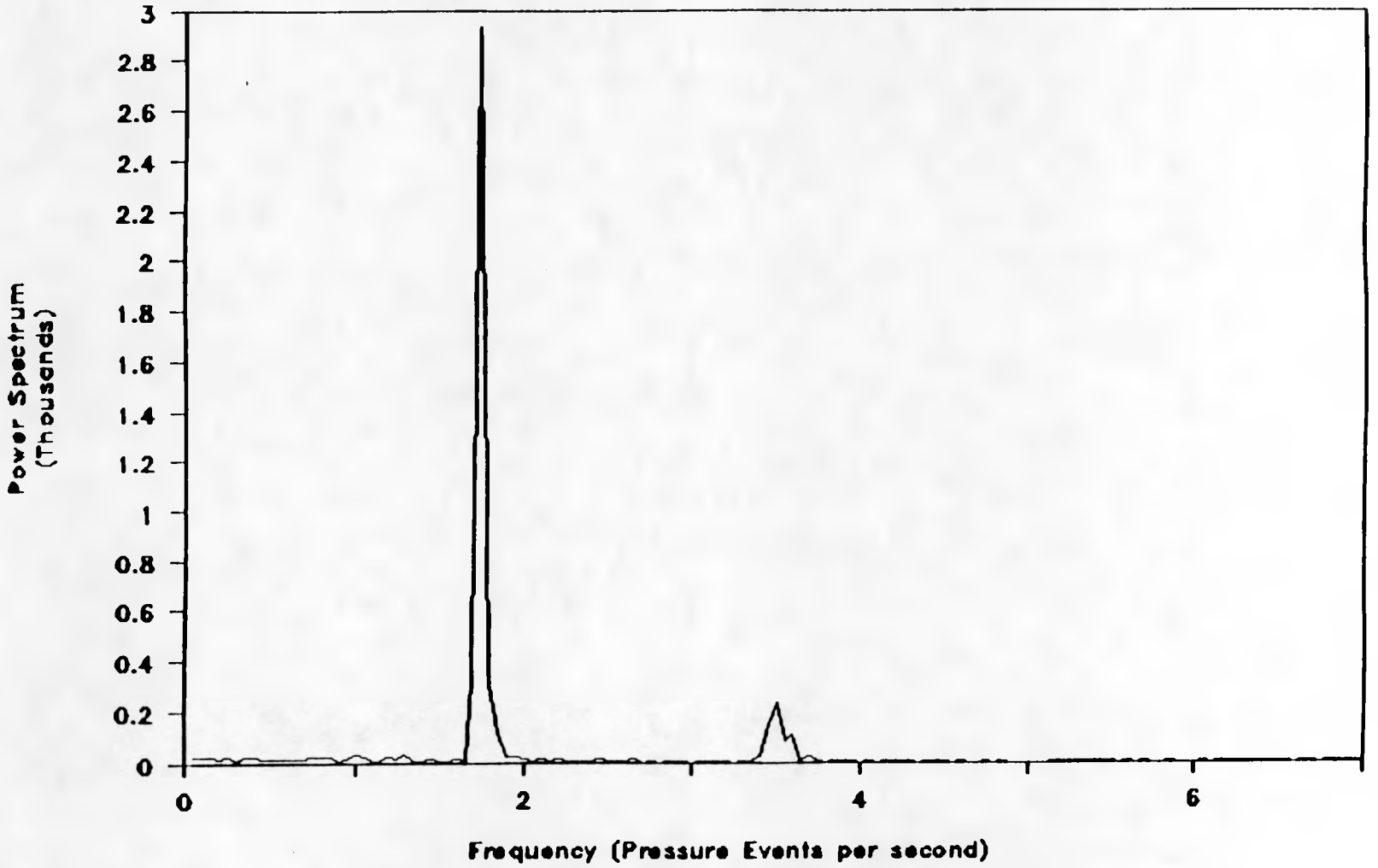

Figure 7.4 Plot of the Power Spectral Density Function, Power Spectrum vs Frequency (Pressure Events per Second) of Data Set G7

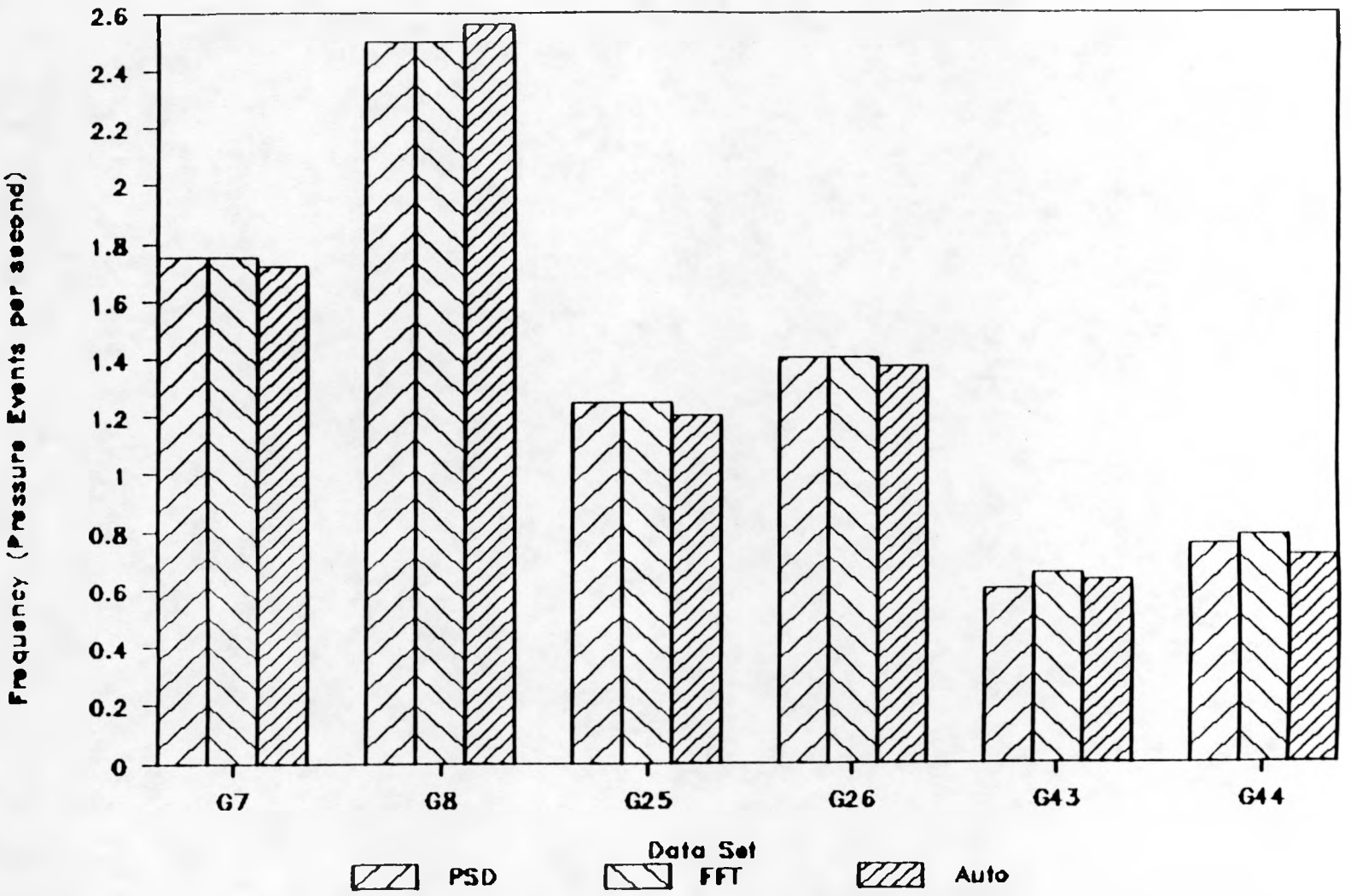

Figure 7.5 Comparison of Frequency Determination Spectral Density Function, Fast Fourier Transform, and Autocorrelation Function

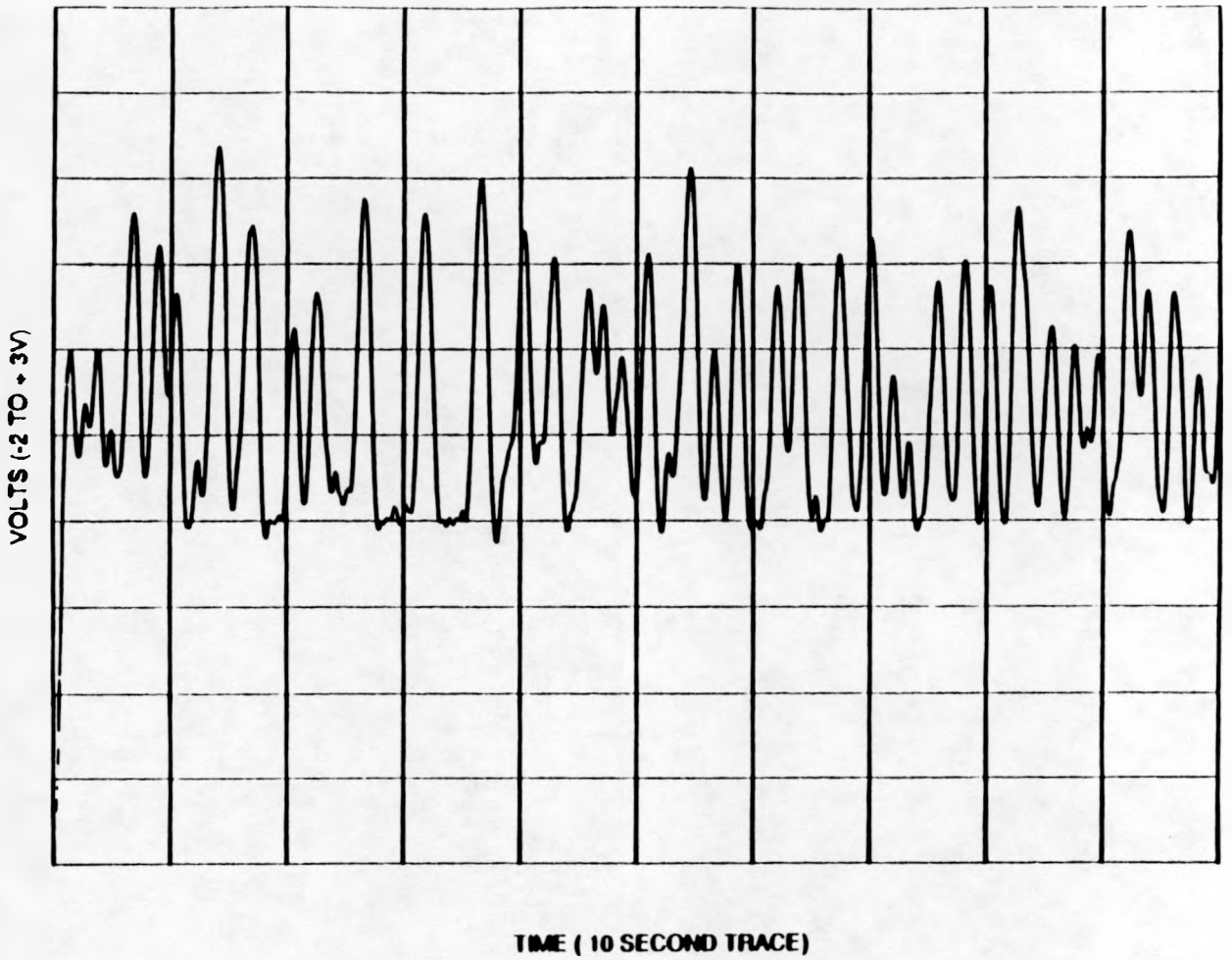

Figure 7.6 Plot of Raw Data Recorded on the Hewlett Packard Plotter (Voltage Output vs Time) of Data Set G8 (Bed Height 6 inches, Height of Probe in Bed 3.625 inches, Horizontal Distance from bed wall 2.75 inches, and Flow Rate 52 SCFM, Distributor #2)

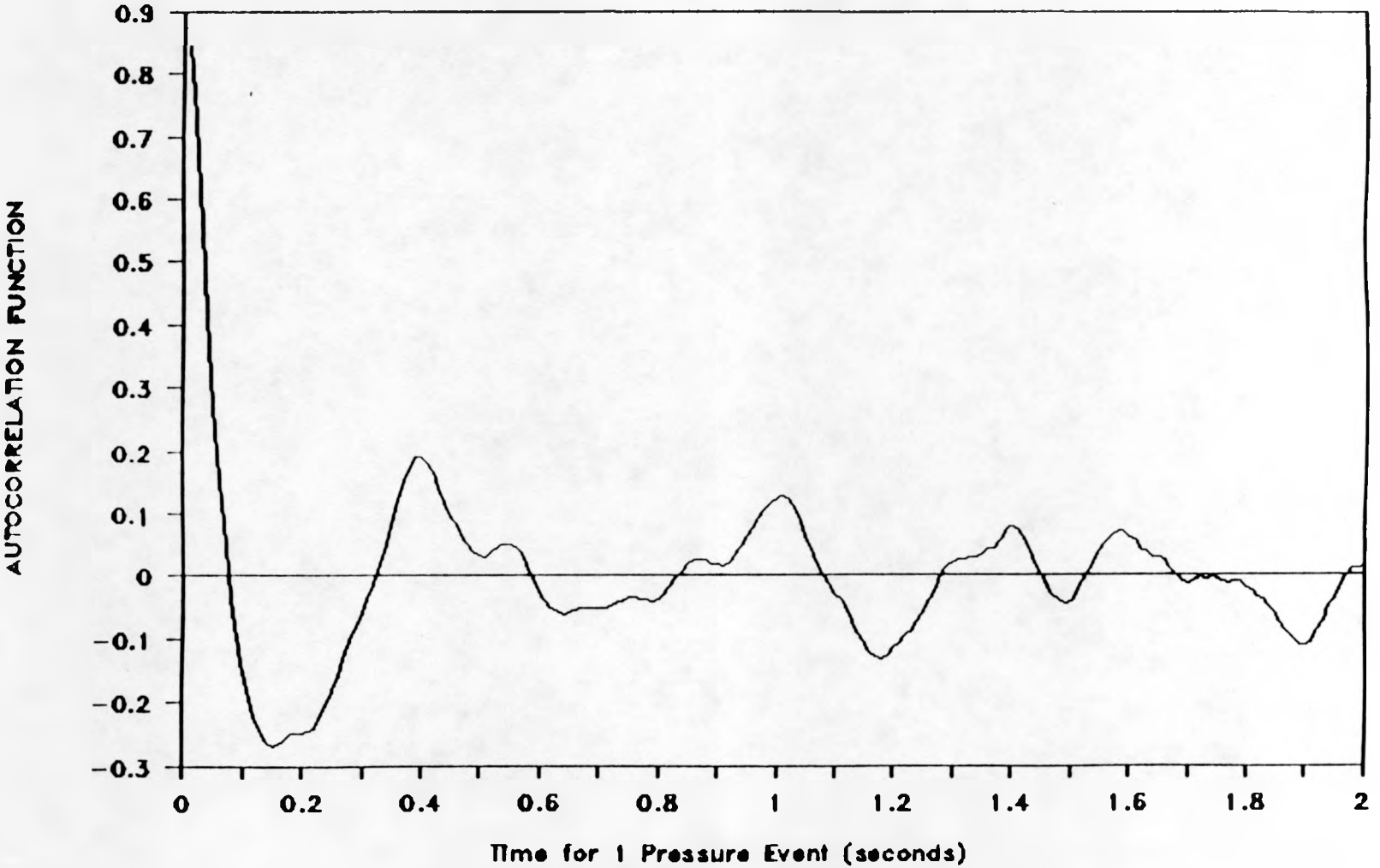

Figure 7.7 Plot of Autocorrelation Function vs Time to Determine the Time for One Pressure Event to Occur (Period) of Data set G8

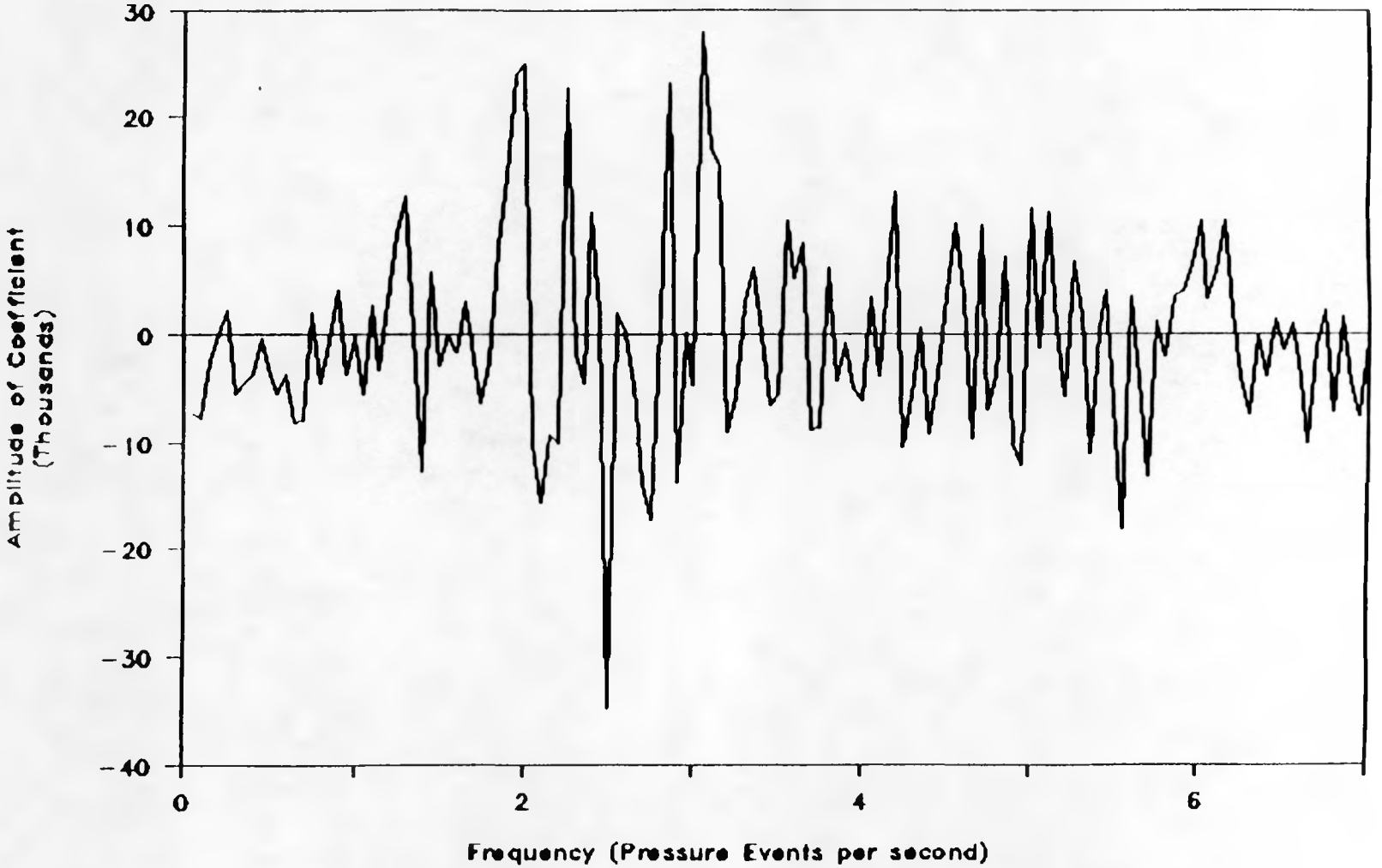

Figure 7.8 Plot of The Fast Fourier Transform Function, Amplitude of Coefficient vs Frequency (Pressure Events per Second) of Data Set C8

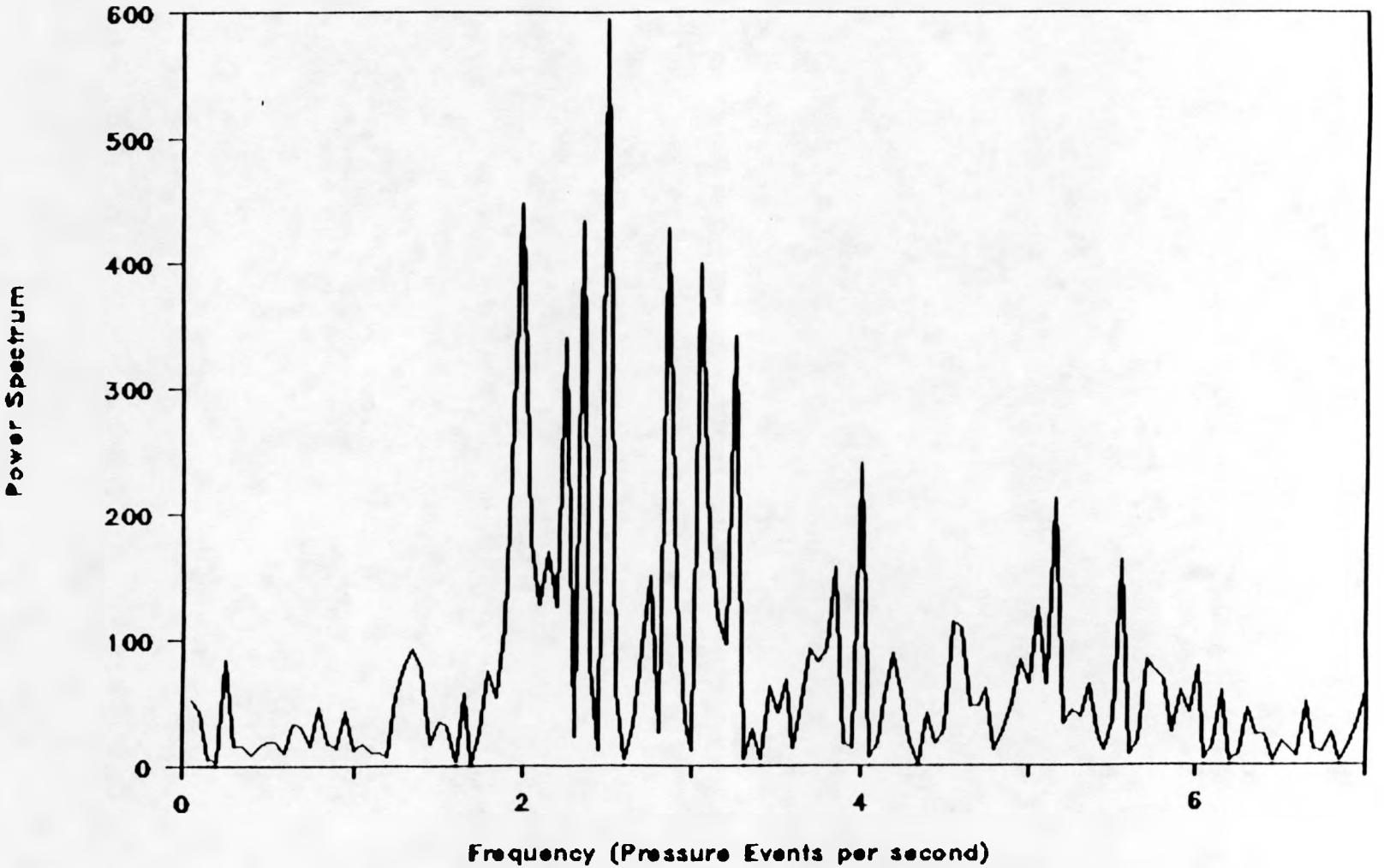

Figure 7.9 Plot of the Power Spectral Density Function, Power Spectrum vs Frequency (Pressure Events per Second) of Data Set G8

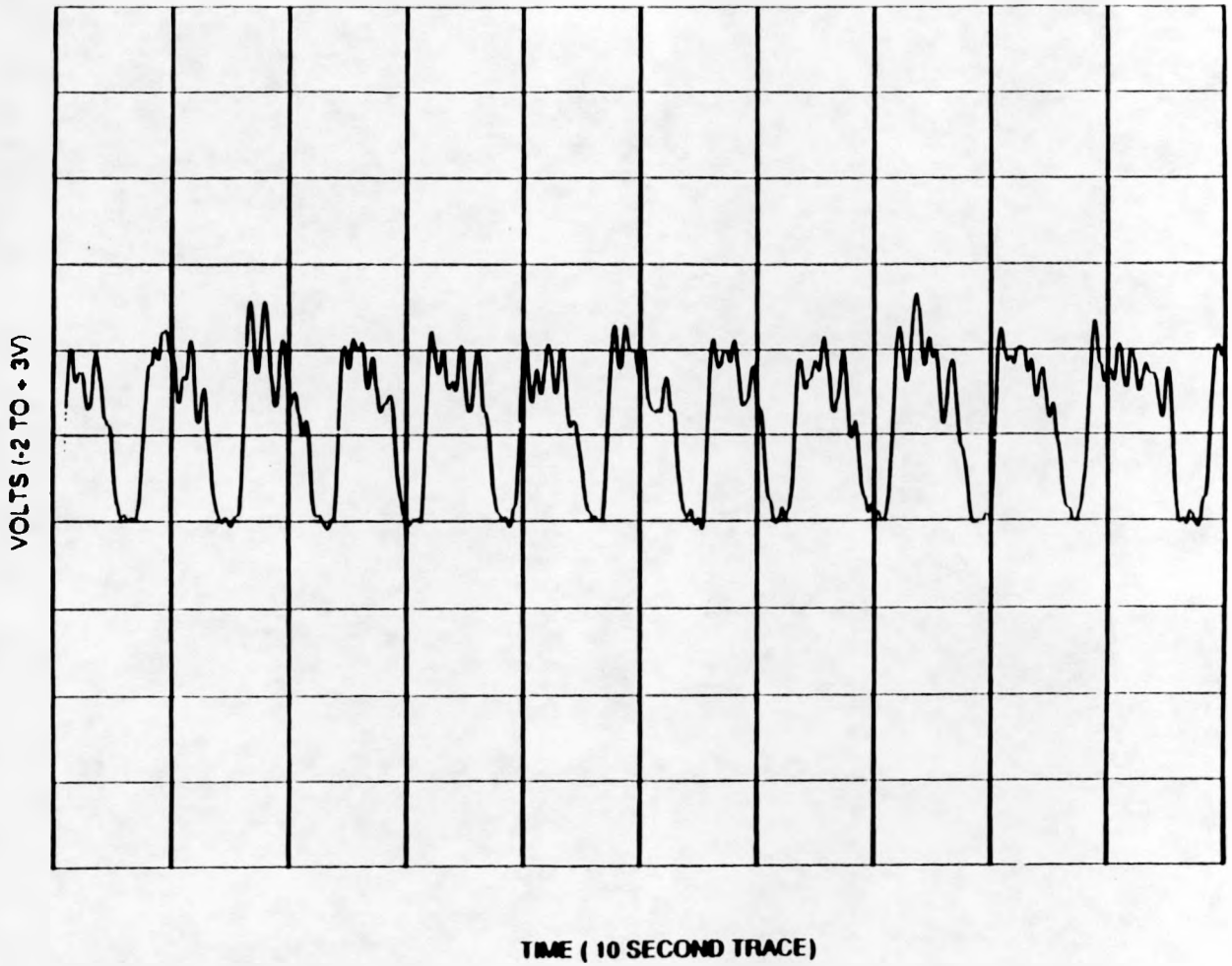

Figure 7.10 Plot of Raw Data Recorded on the Hewlett Packard Plotter (Voltage Output vs Time) of Data Set G25 (Bed Height 12 inches, Height of Probe in Bed 6.75 inches, Horizontal Distance from bed wall 2.75 inches, and Flow Rate 39 SCFM, Distributor #2)

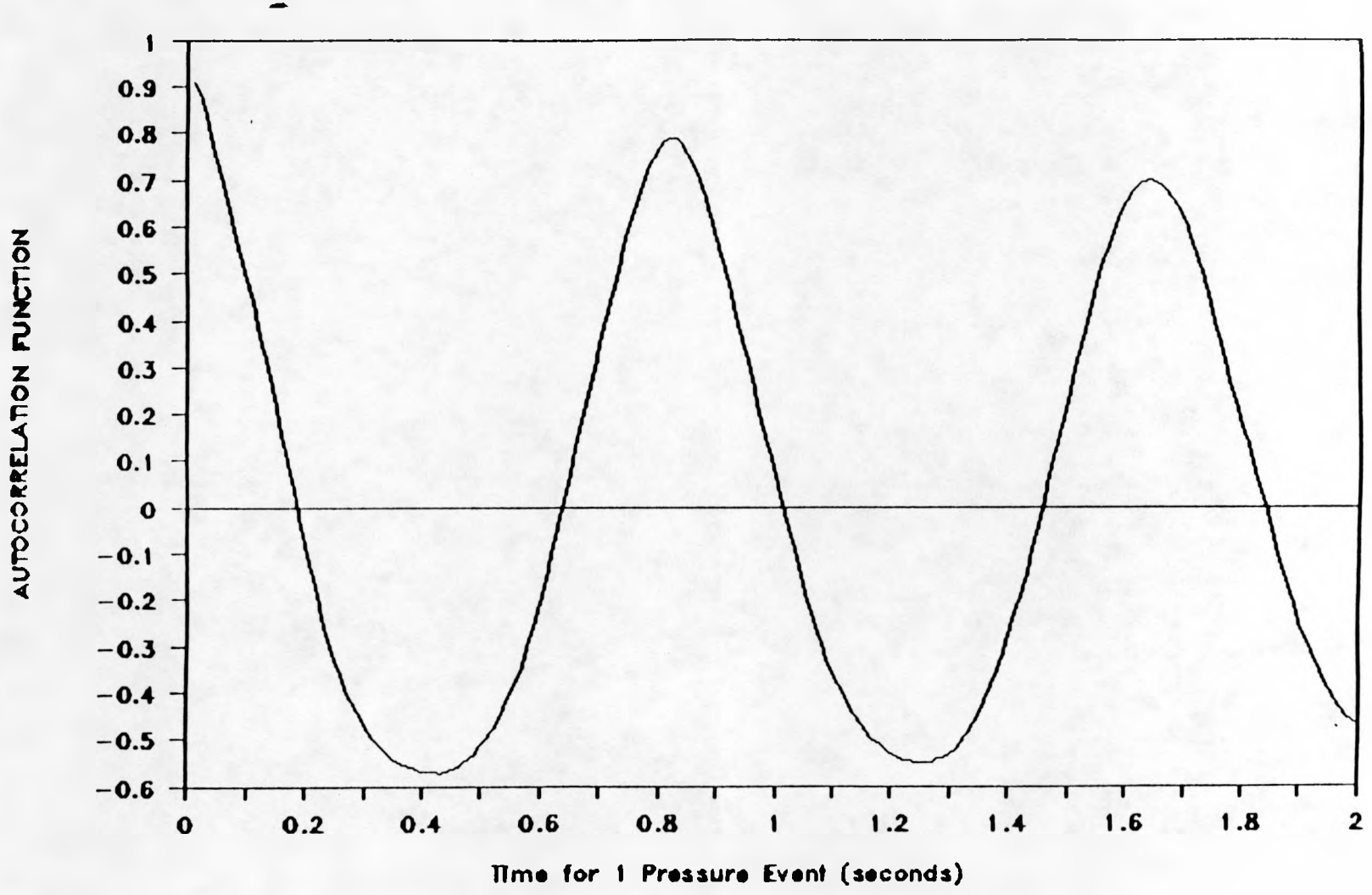

Figure 7.11 Plot of Autocorrelation Function vs Time to Determine the Time for One Pressure Event to Occur (Period) of Data set G25

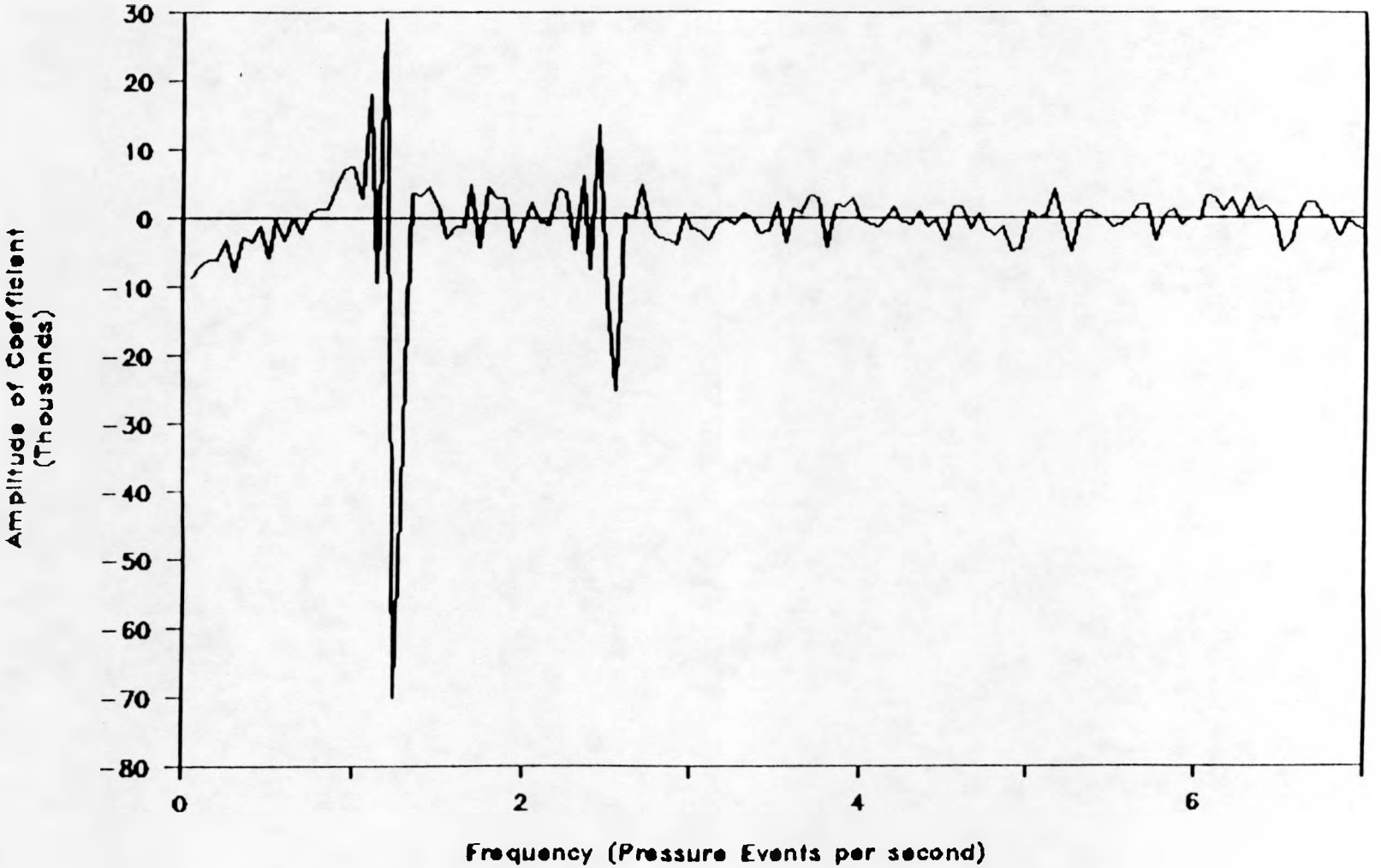

Figure 7.12 Plot of The Fast Fourier Transform Function, Amplitude of Coefficient vs Frequency (Pressure Events per Second) of Data Set G25

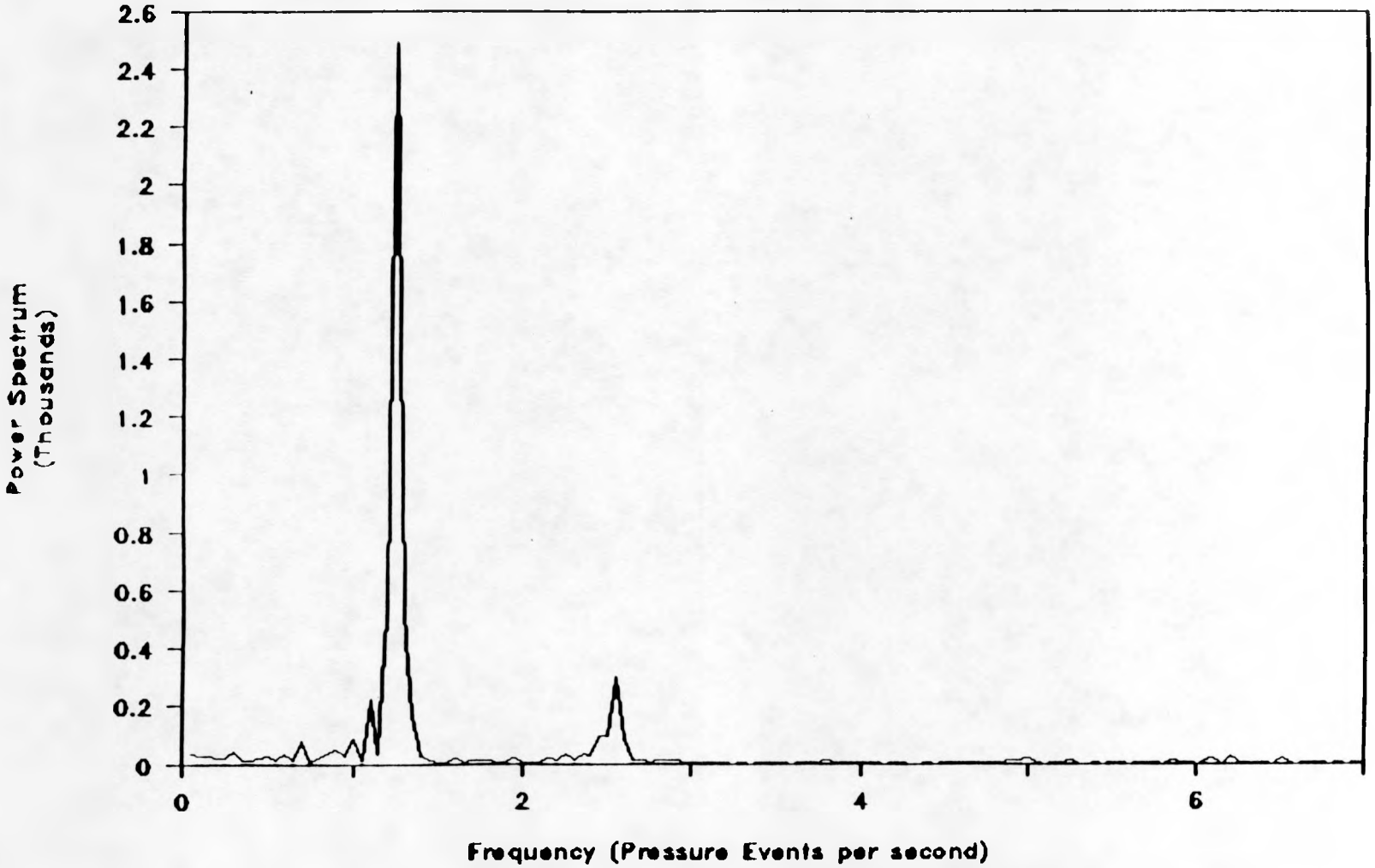

Figure 7.13 Plot of the Power Spectral Density Function, Power Spectrum vs Frequency (Pressure Events per Second) of Data Set G25

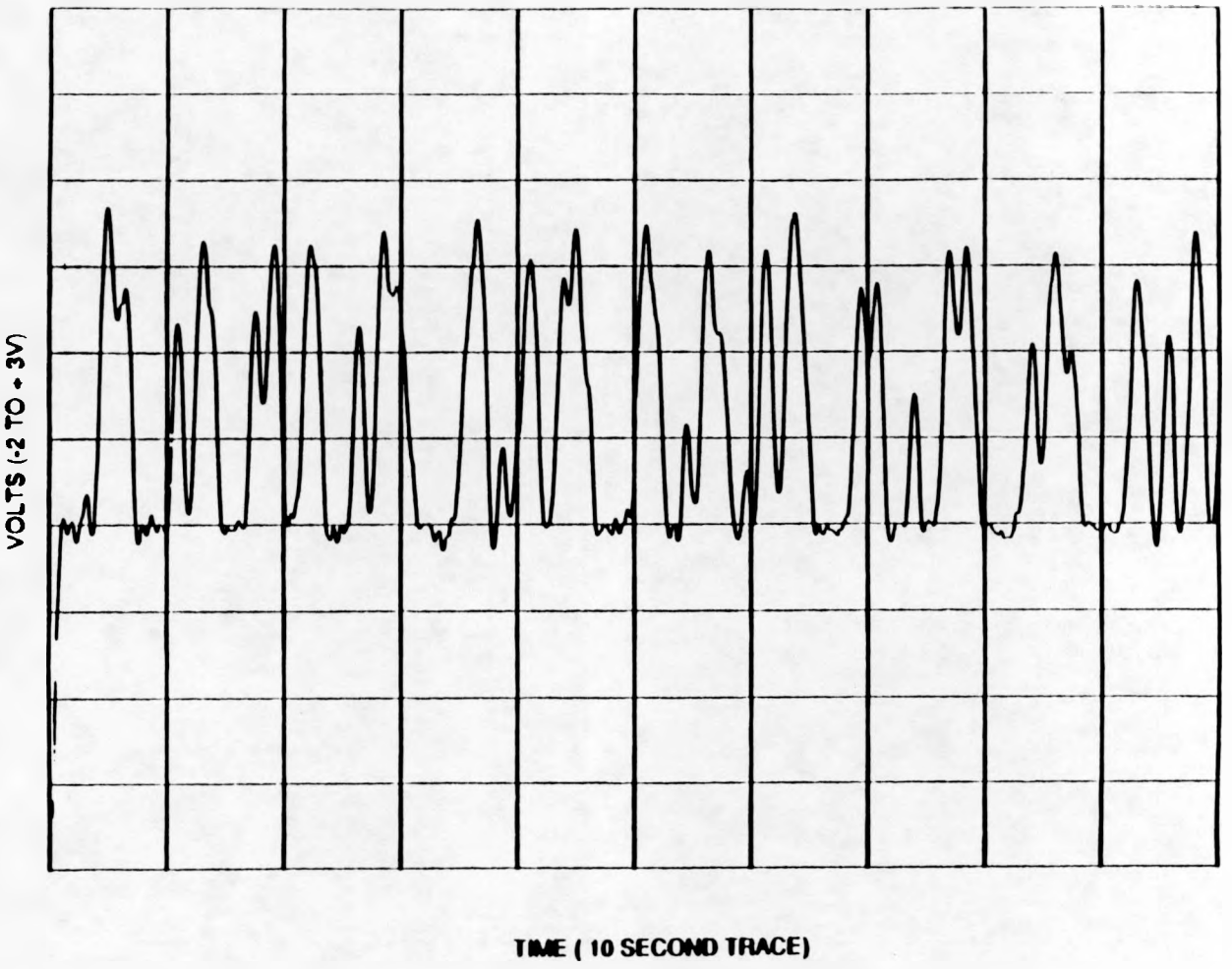

Figure 7.14 Plot of Raw Data Recorded on the Hewlett Packard Plotter (Voltage Output vs Time) of Data Set G26 (Bed Height 12 inches, Height of Probe in Bed 6.75 inches, Horizontal Distance from bed wall 2.76 inches, and Flow Rate 52 SCFM, Distributor #2)

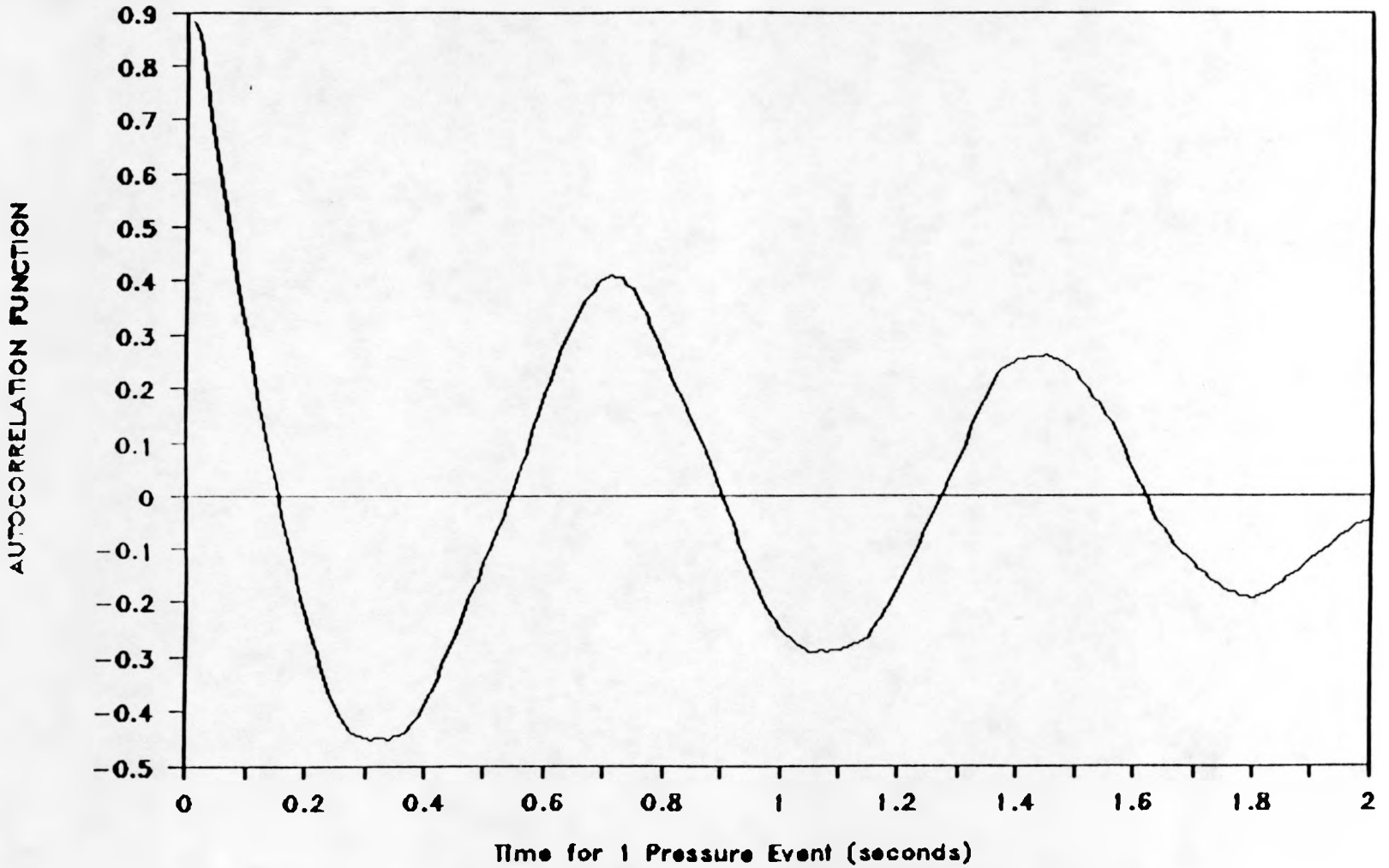

Figure 7.15 Plot of Autocorrelation Function vs Time to Determine the Time for One Pressure Event to Occur (Period) of Data set G26

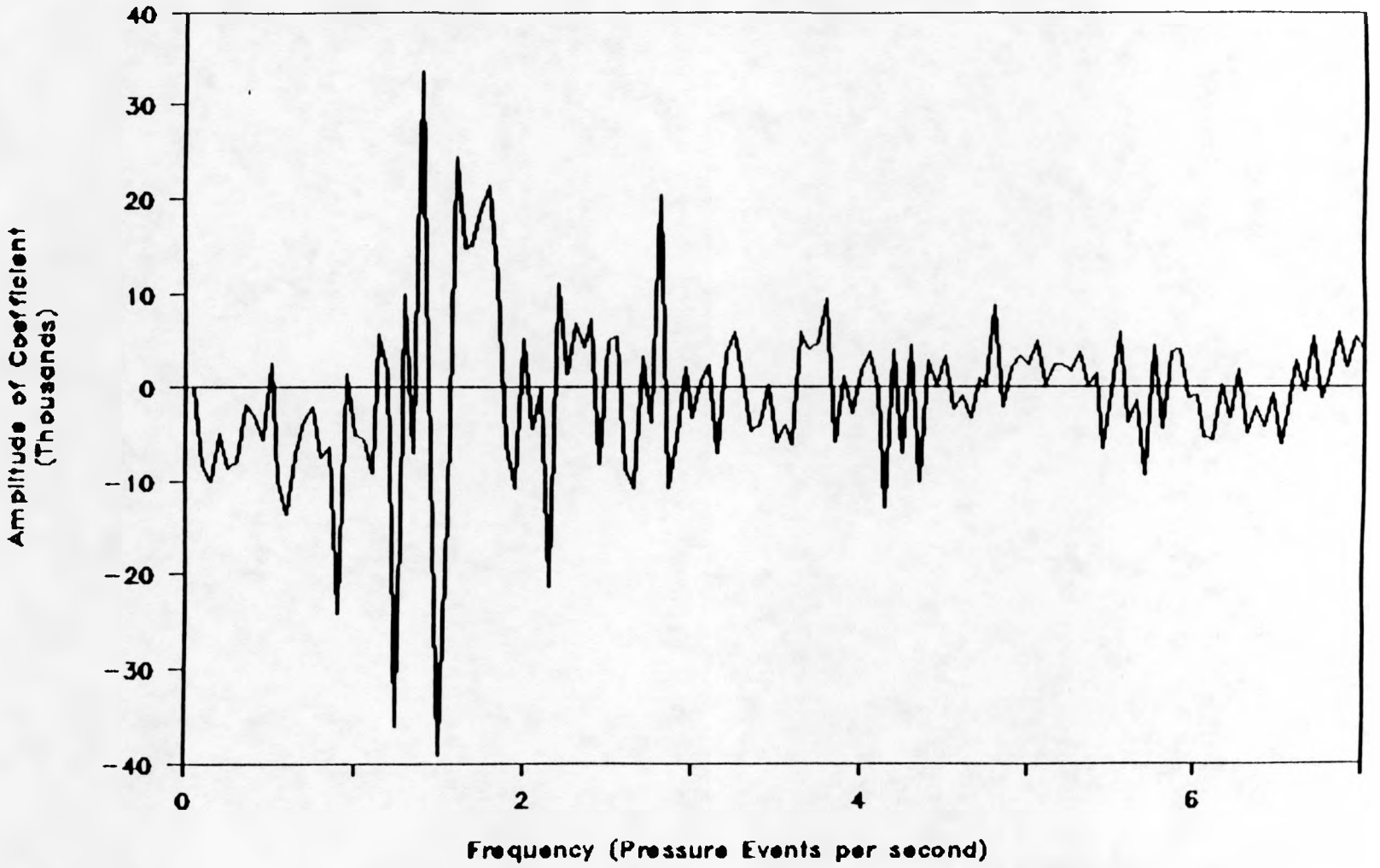

Figure 7.16 Plot of The Fast Fourier Transform Function, Amplitude of Coefficient vs Frequency (Pressure Events per Second) of Data Set G26

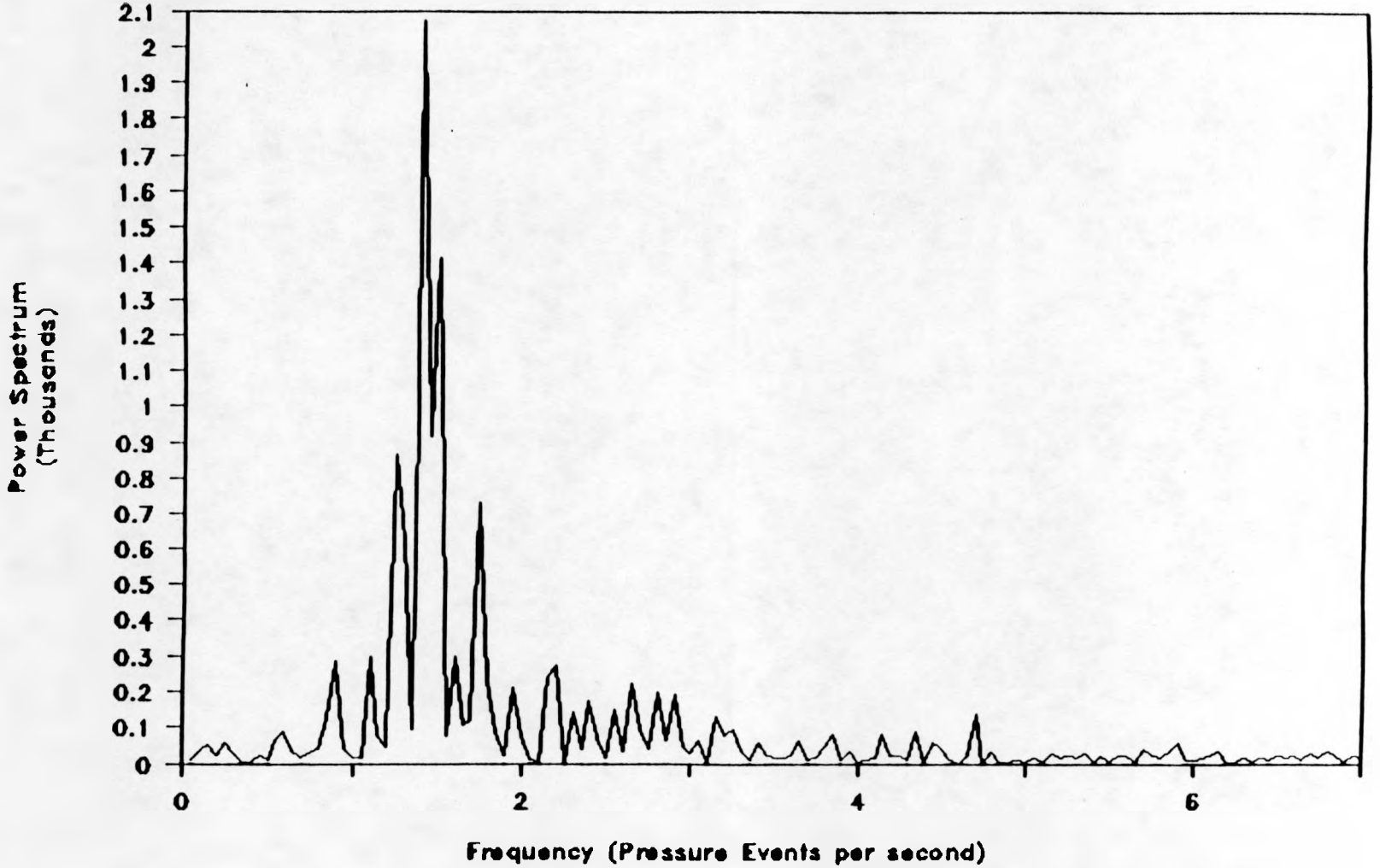

Figure 7.17 Plot of the Power Spectral Density Function, Power Spectrum vs Frequency (Pressure Events per Second) of Data Set G26

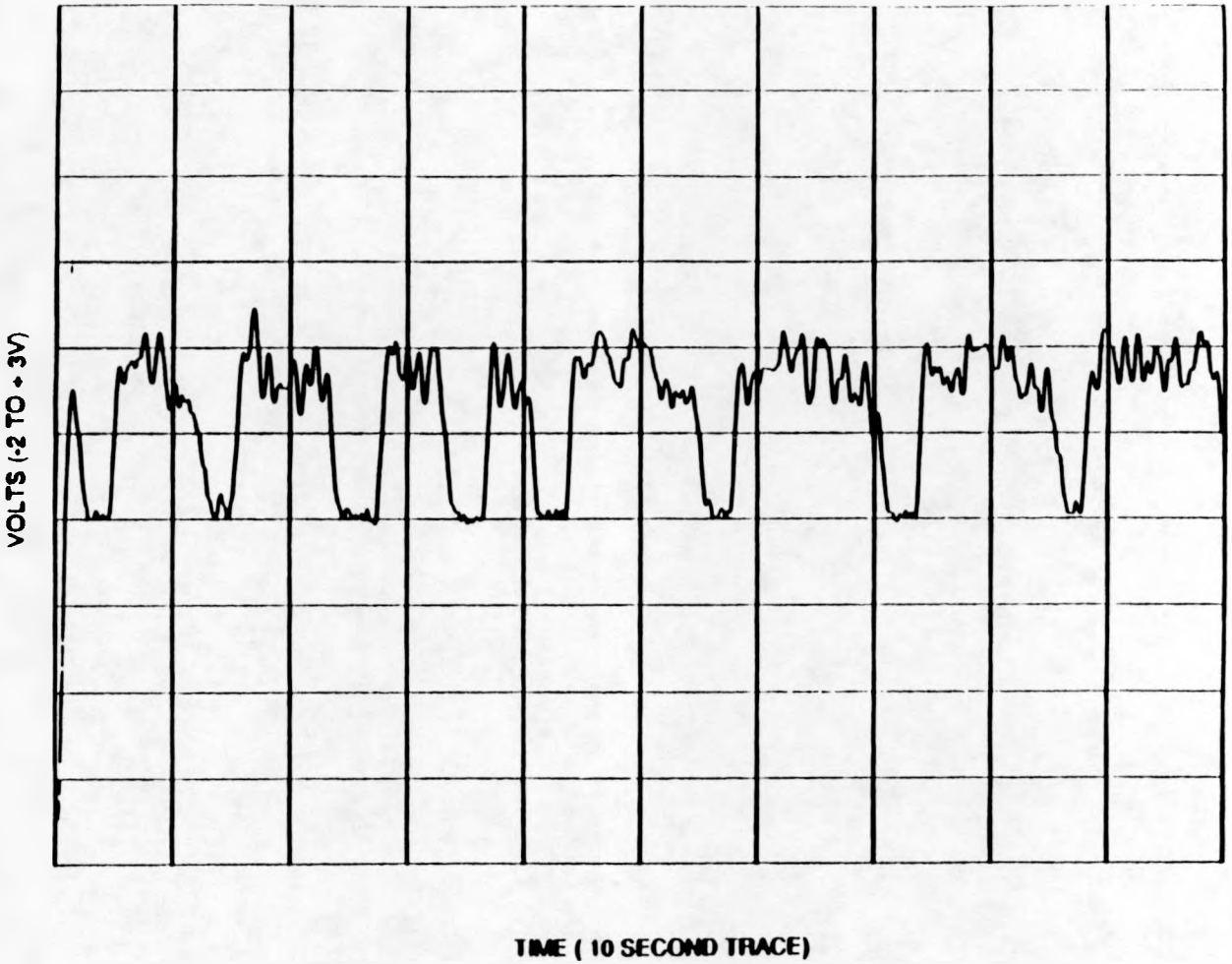

Figure 7.18 Plot of Raw Data Recorded on the Hewlett Packard Plotter (Voltage Output vs Time) of Data Set G43 (Bed Height 24 Inches, Height of Probe in Bed 11.5 Inches, Horizontal Distance from bed wall 2.75 Inches, and Flow Rate 39 SCFM, Distributor #2)

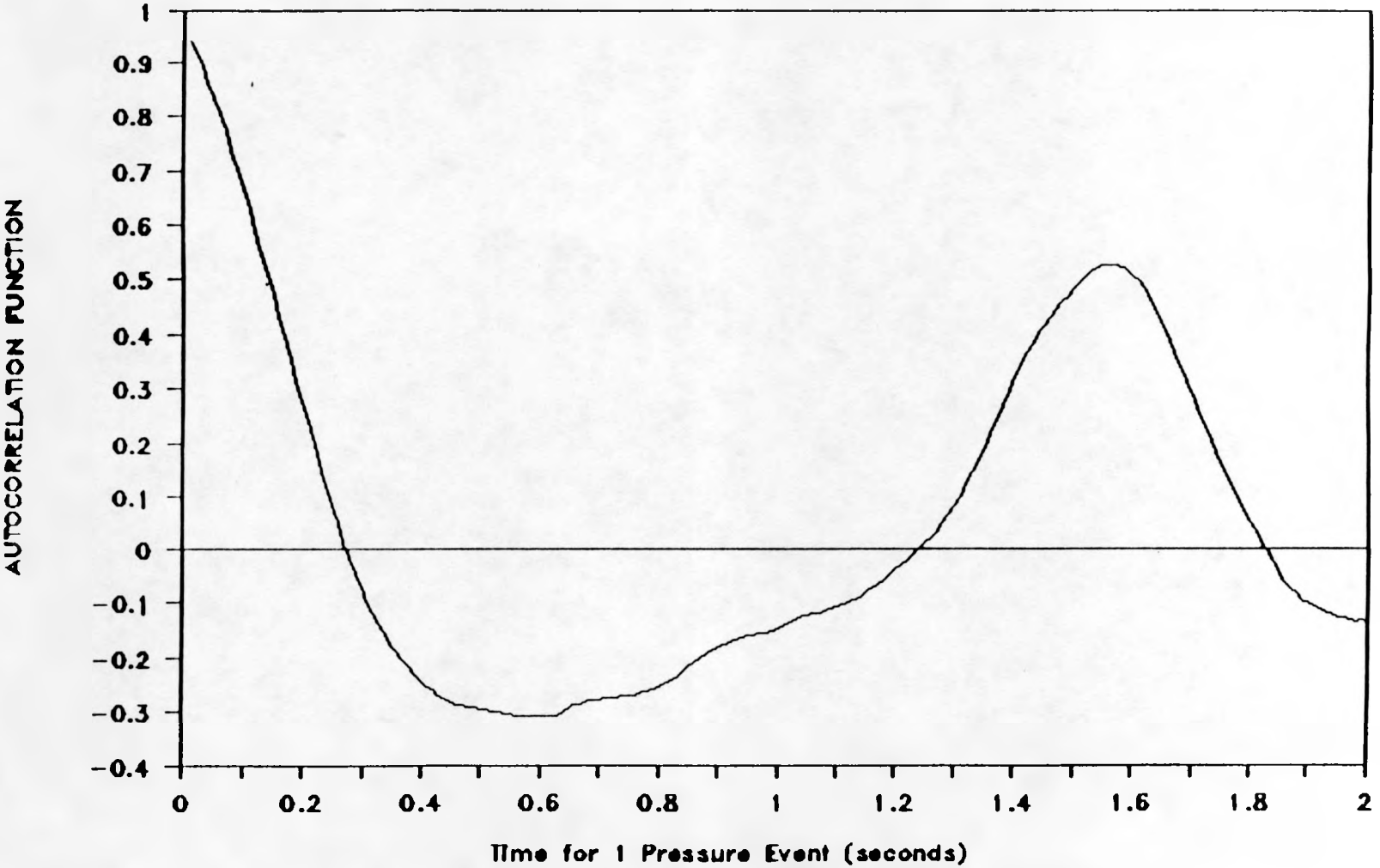

Figure 7.19 Plot of Autocorrelation Function vs Time to Determine the Time for One Pressure Event to Occur (Period) of Data set G43

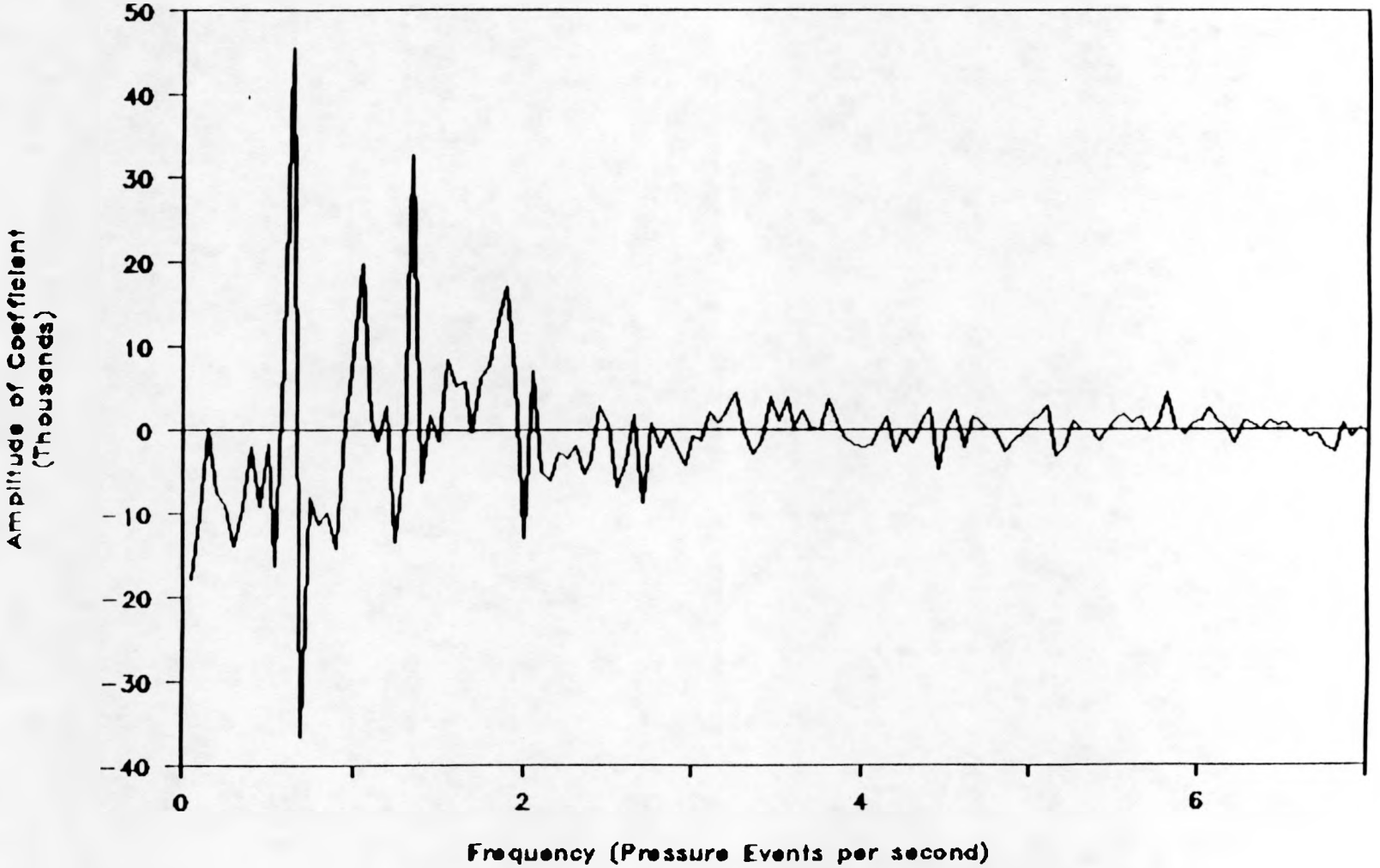

Figure 7.20 Plot of The Fast Fourier Transform Function, Amplitude of Coefficient vs Frequency (Pressure Events per Second) of Data Set G43

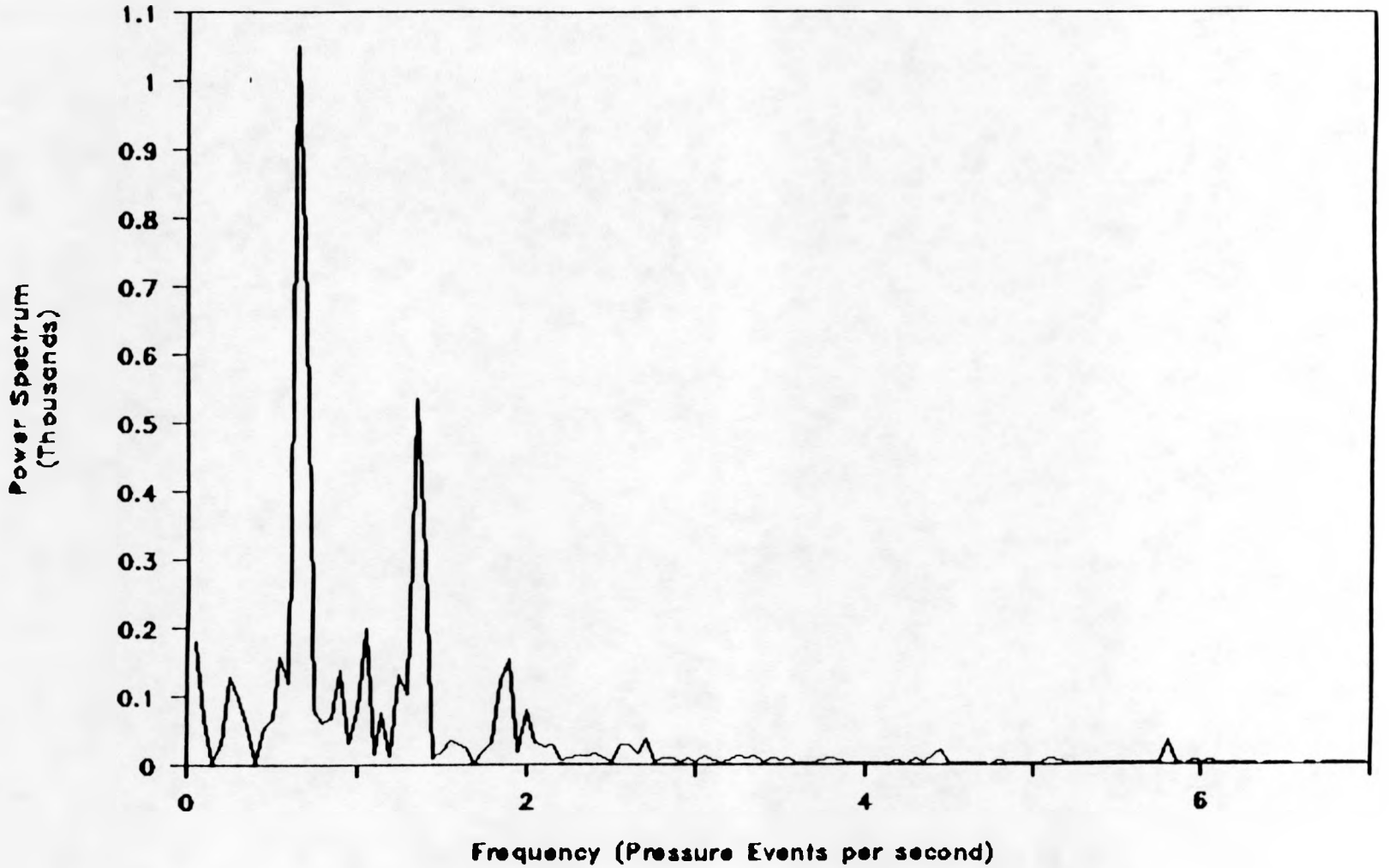

Figure 7.21 Plot of the Power Spectral Density Function, Power Spectrum vs Frequency (Pressure Events per Second) of Data Set G43

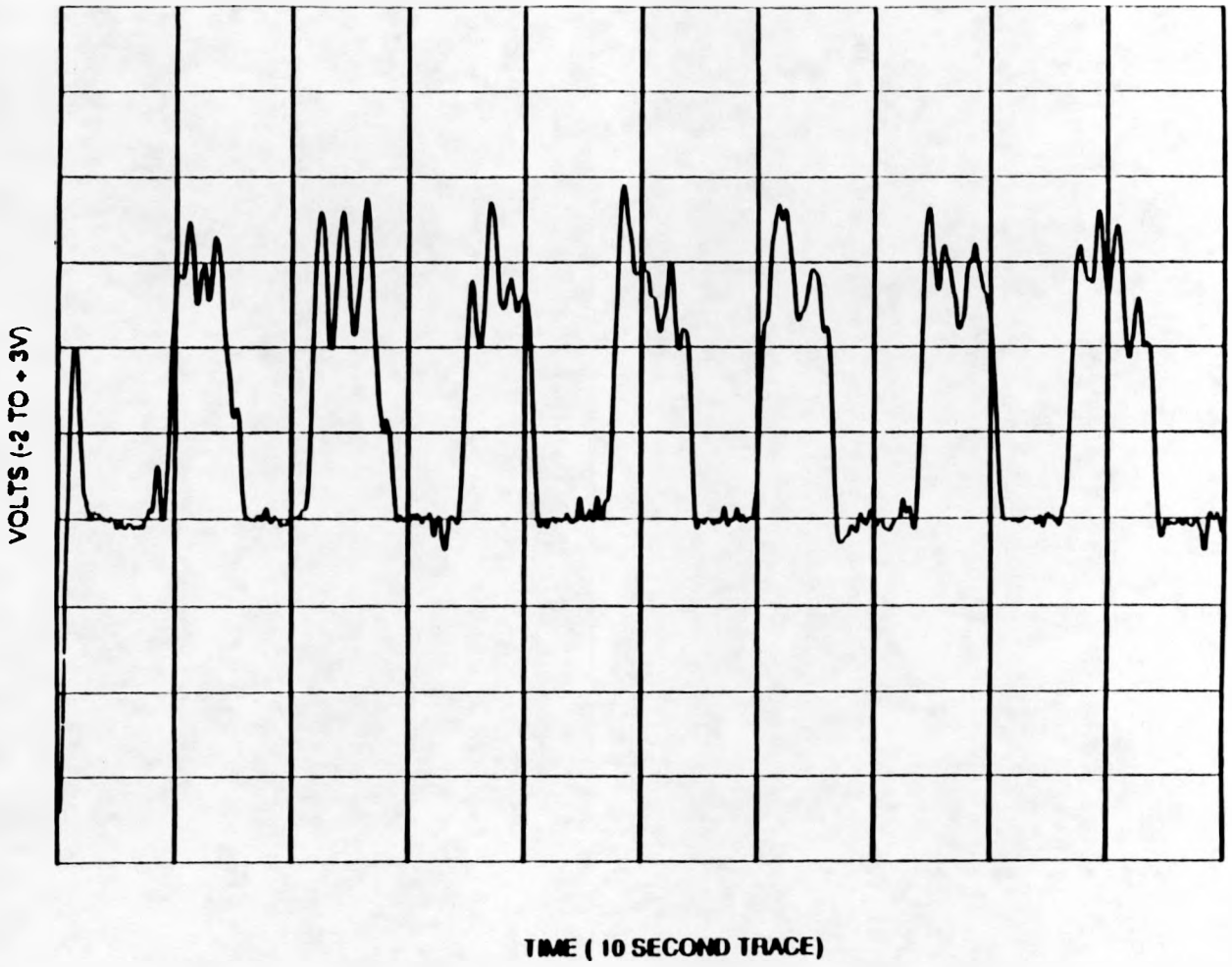

Figure 7.22 Plot of Raw Data Recorded on the Hewlett Packard Plotter (Voltage Output vs Time) of Data Set G44 (Bed Height 24 inches, Height of Probe in Bed 11.5 inches, Horizontal Distance from bed wall 2.75 inches, and Flow Rate 52 SCFM, Distributor #2)

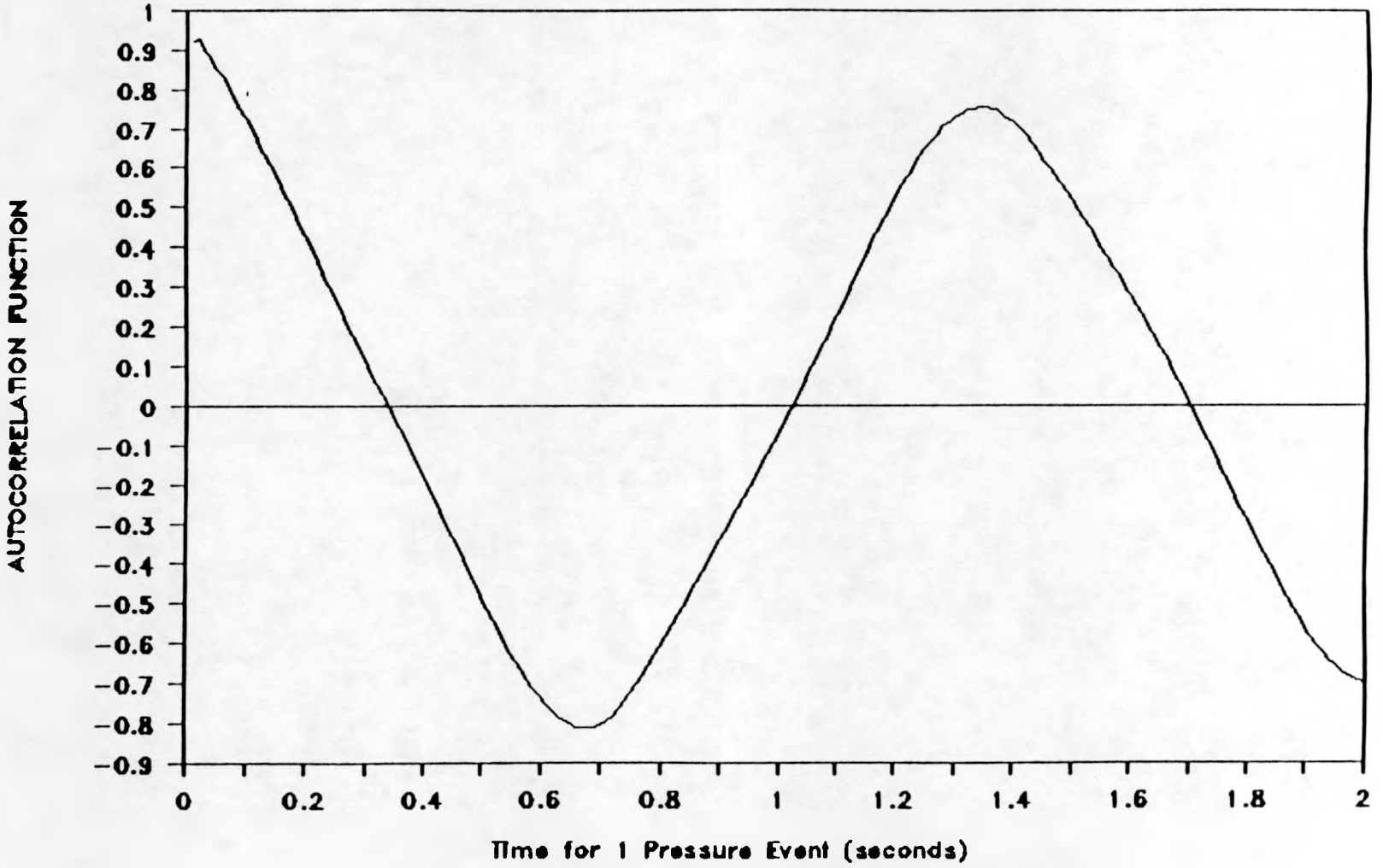

Figure 7.23 Plot of Autocorrelation Function vs Time to Determine the Time for One Pressure Event to Occur (Period) of Data set G44

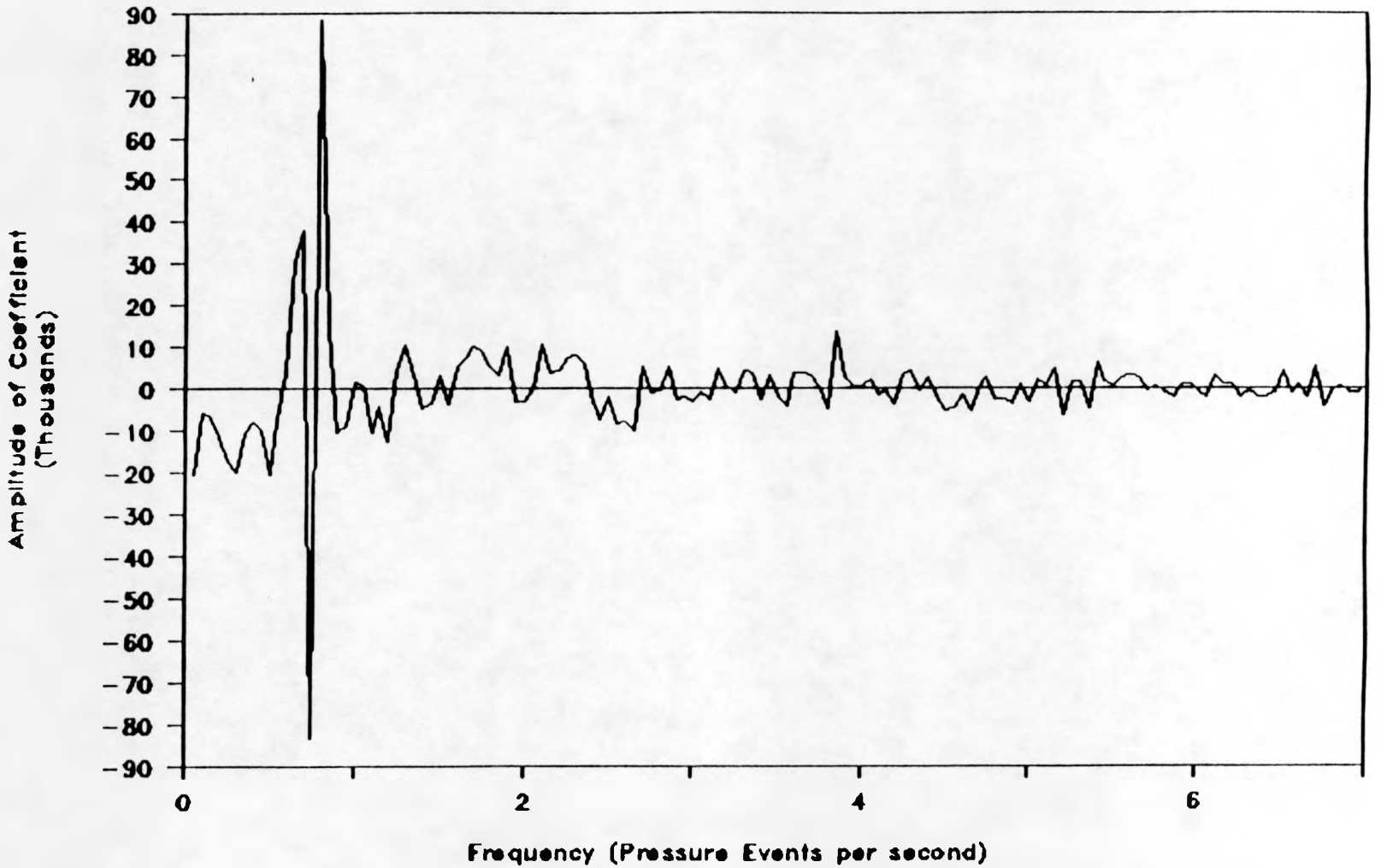

Figure 7.24 Plot of The Fast Fourier Transform Function, Amplitude of Coefficient vs Frequency (Pressure Events per Second) of Data Set G44

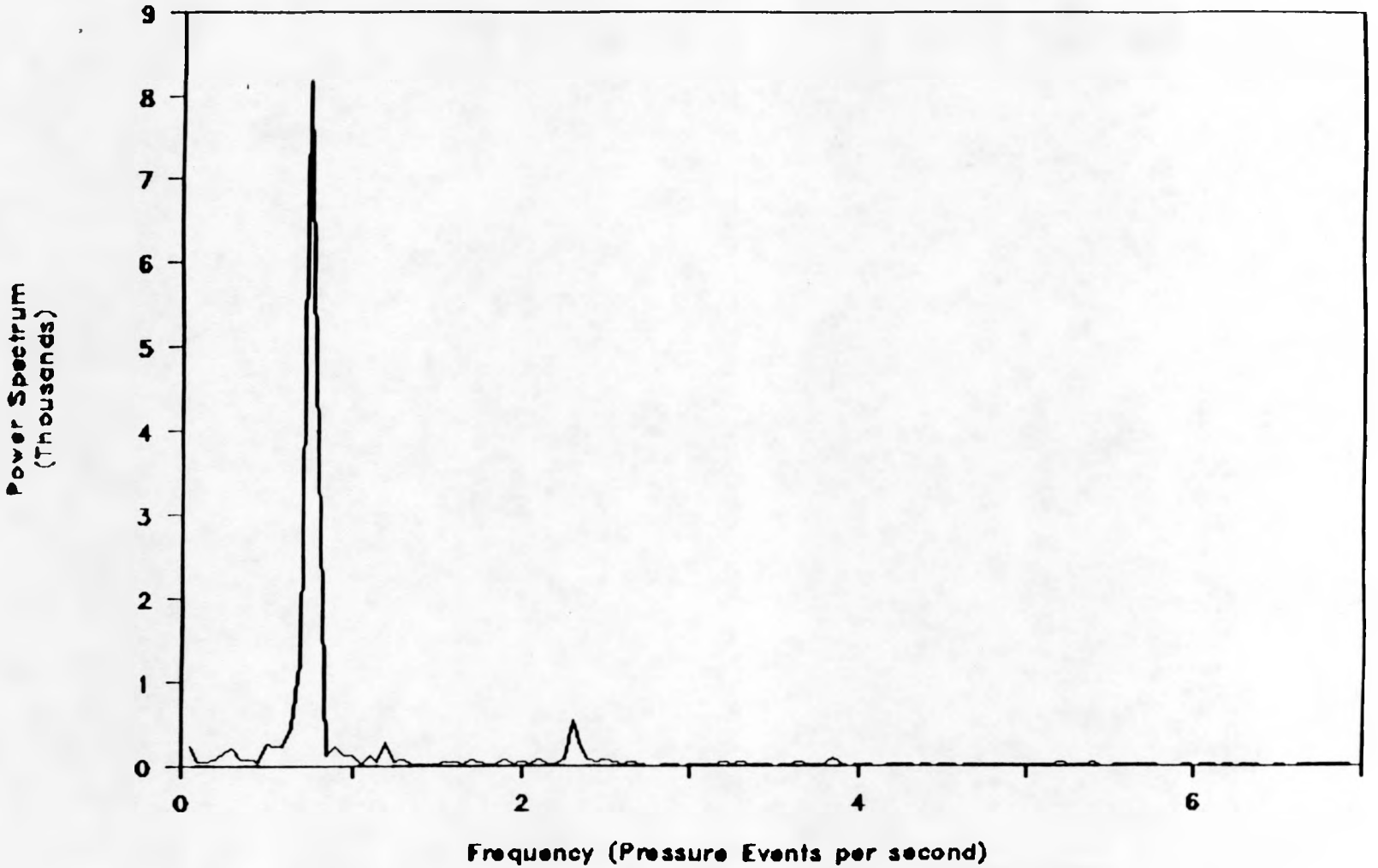

Figure 7.25 Plot of the Power Spectral Density Function, Power Spectrum vs Frequency (Pressure Events per Second) of Data Set G44

Table 7.2 Experimental Conditions For Data Collection for 2 DSPPs

DATA RUN NUMBER	BED HEIGHT (INCHES)	PROBE STEM SPACING (INCHES)	TOP PROBE HEIGHT (INCHES)	BOTTOM PROBE HEIGHT (INCHES)	PROBE SEPERATION (INCHES)	PROBE INTRUSION (INCHES)	FLOW RATE (SCFM)
HA	6	0.5	4.625	2.625	2	2.75	39
HB	6	0.5	4.625	2.625	2	2.75	52
HC	12	0.5	7.75	5.75	2	2.75	39
HD	12	0.5	7.75	5.75	2	2.75	52
HE	24	0.5	12.5	10.5	2	2.75	39
HF	24	0.5	12.5	10.5	2	2.75	52

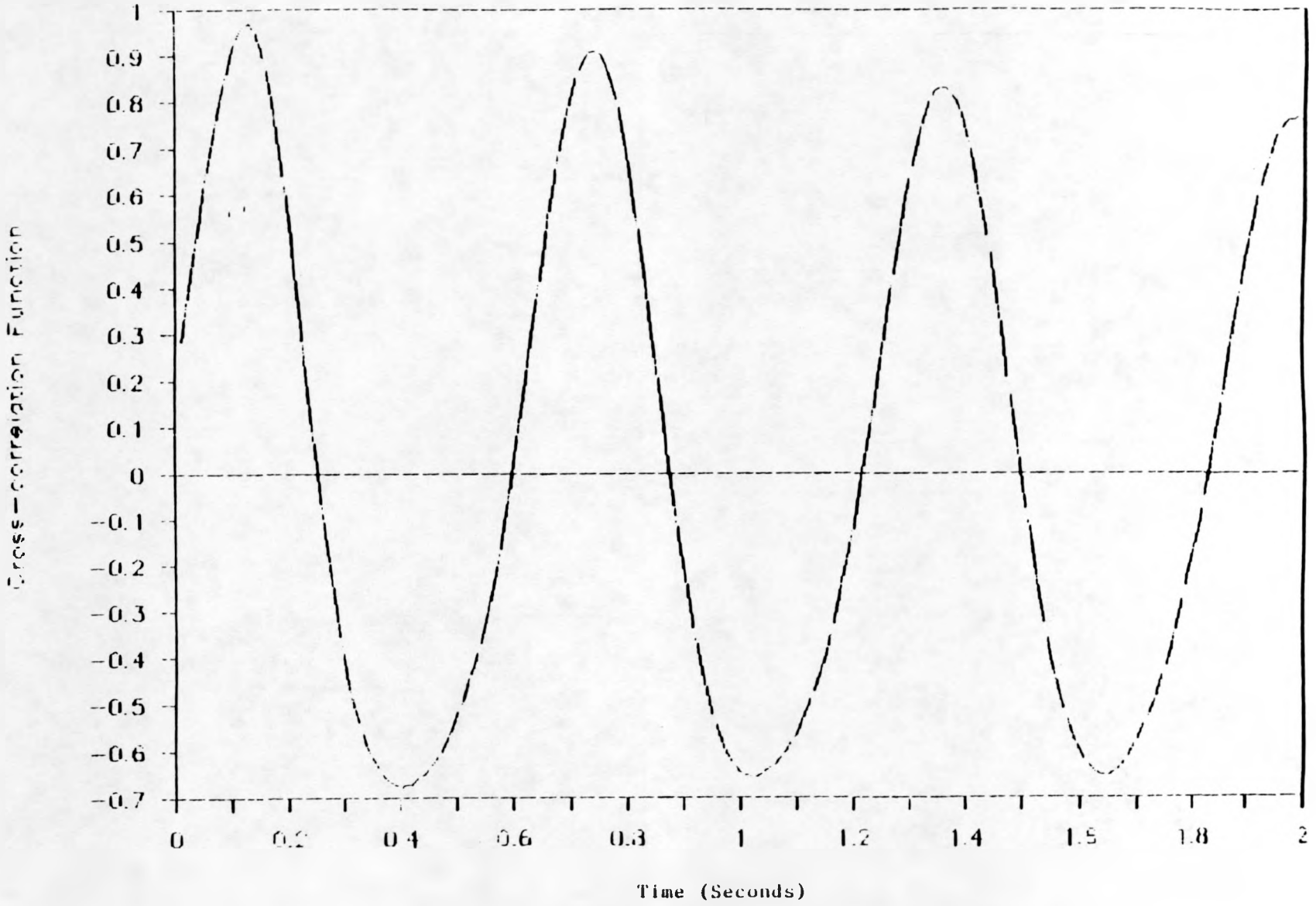

Figure 7.26 Plot of Cross-correlation Function vs Time to Determine the Time for one Pressure Event to Rise Passed a Vertical Probe Spacing of 2 inches of Data set IIA

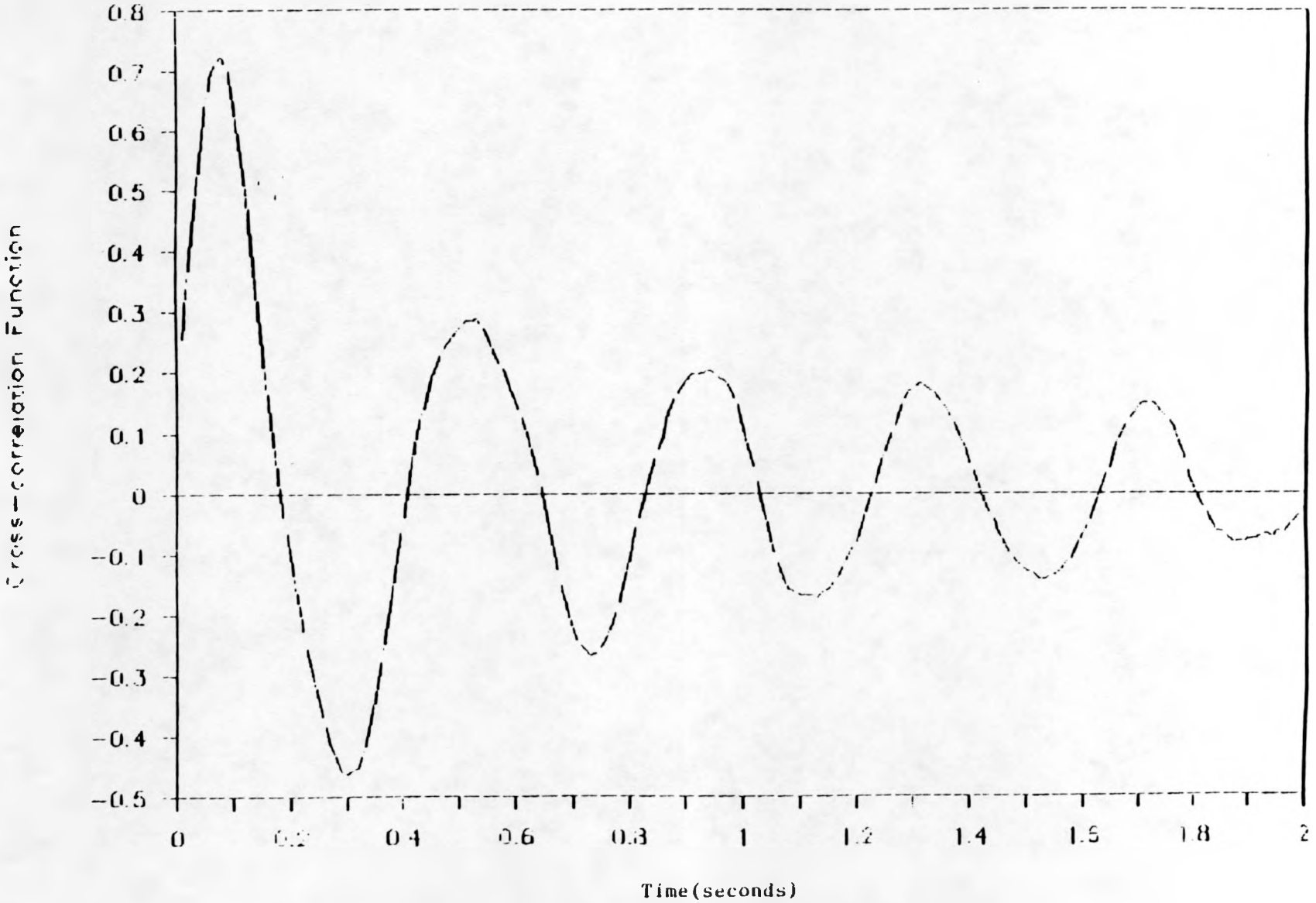

Figure 7.27 Plot of Cross-correlation Function vs Time to Determine the Time for one Pressure Event to Rise Passed a Vertical Probe Spacing of 2 inches of Data set HB

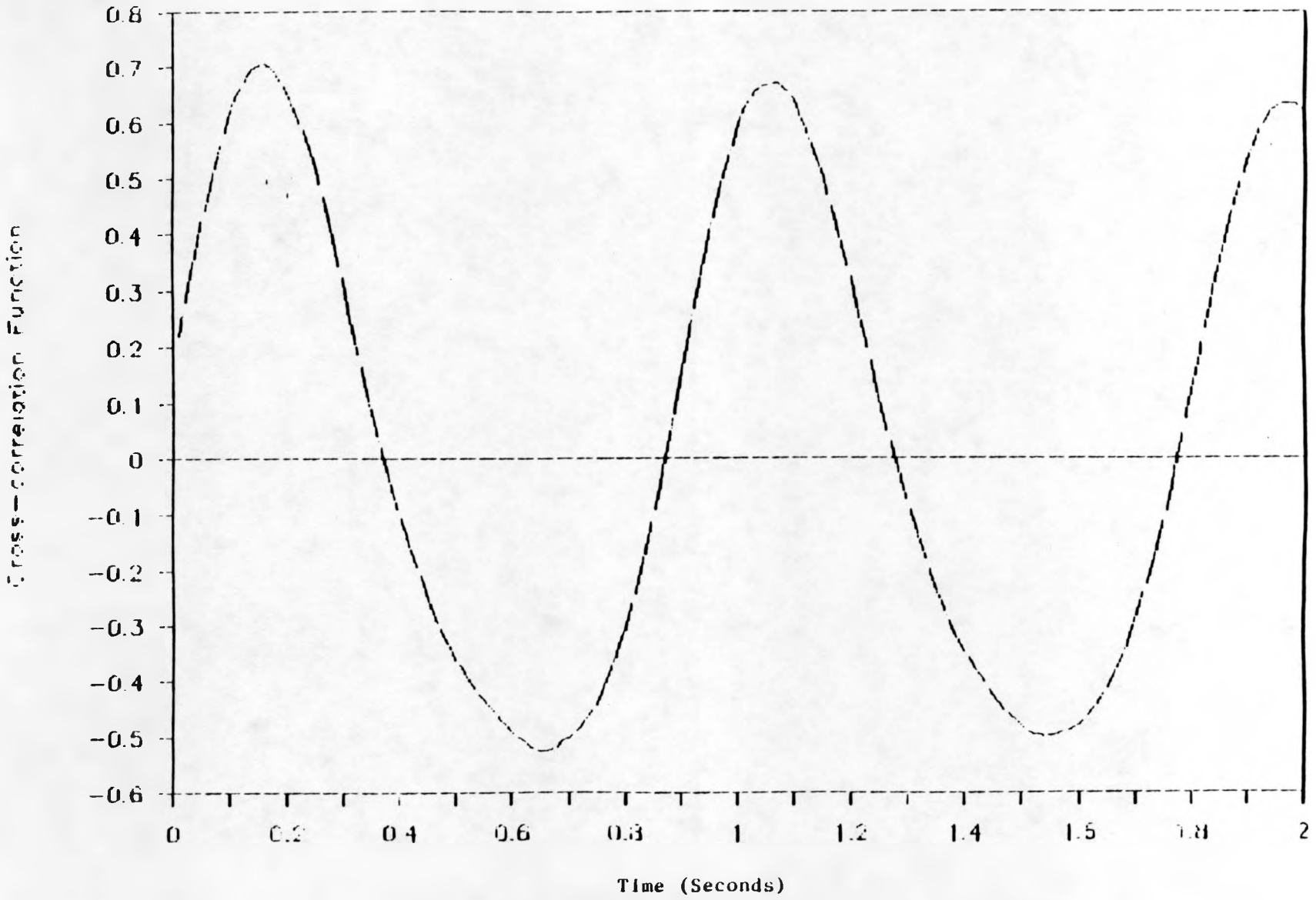

Figure 7.28 Plot of Cross-correlation Function vs Time to Determine the Time for one Pressure Event to Rise Passed a Vertical Probe Spacing of 2 inches of Data set HC

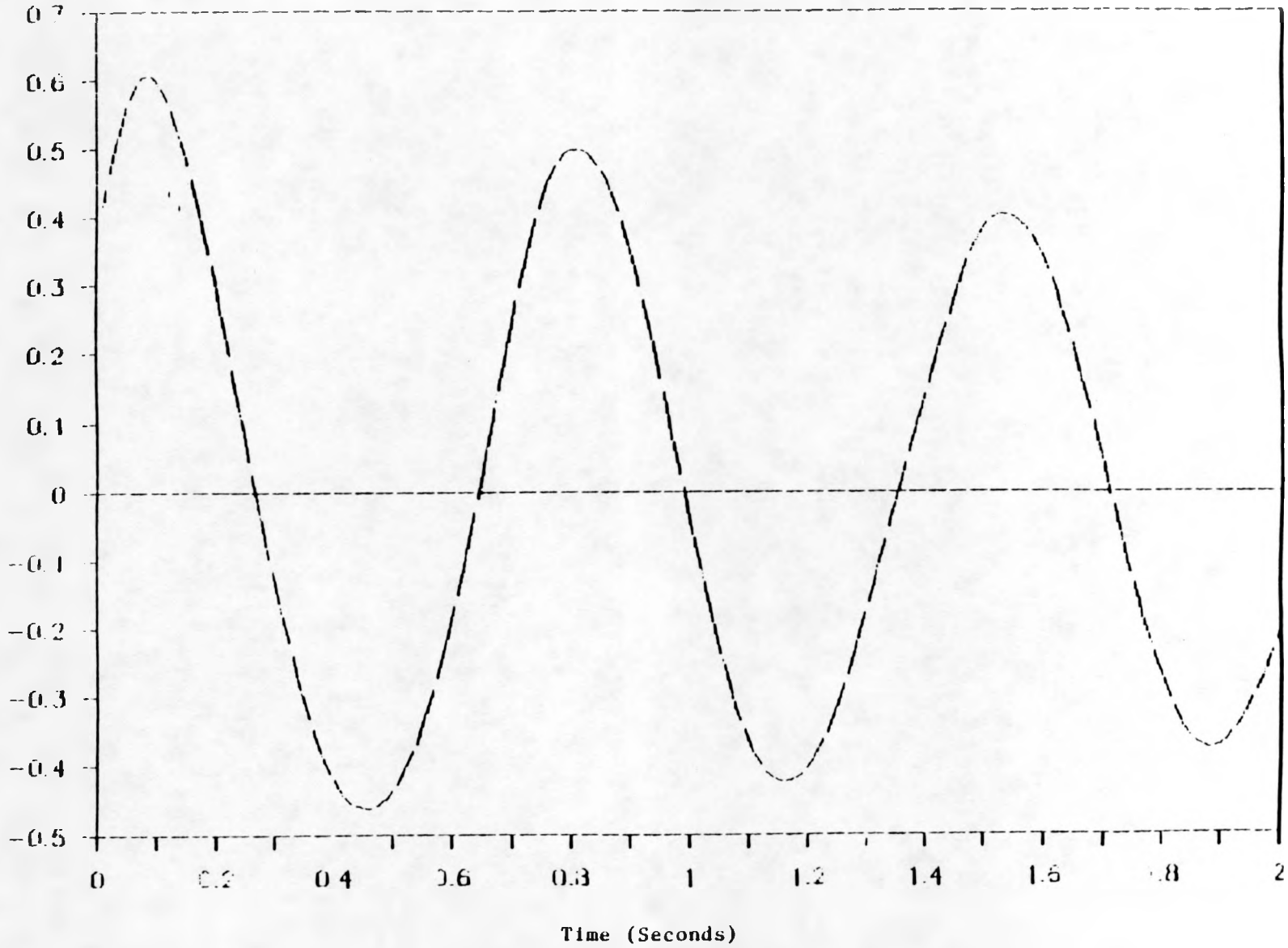

Figure 7.29 Plot of Cross-correlation Function vs Time to Determine the Time for one Pressure Event to Rise Passed a Vertical Probe Spacing of 2 inches of Data set HD

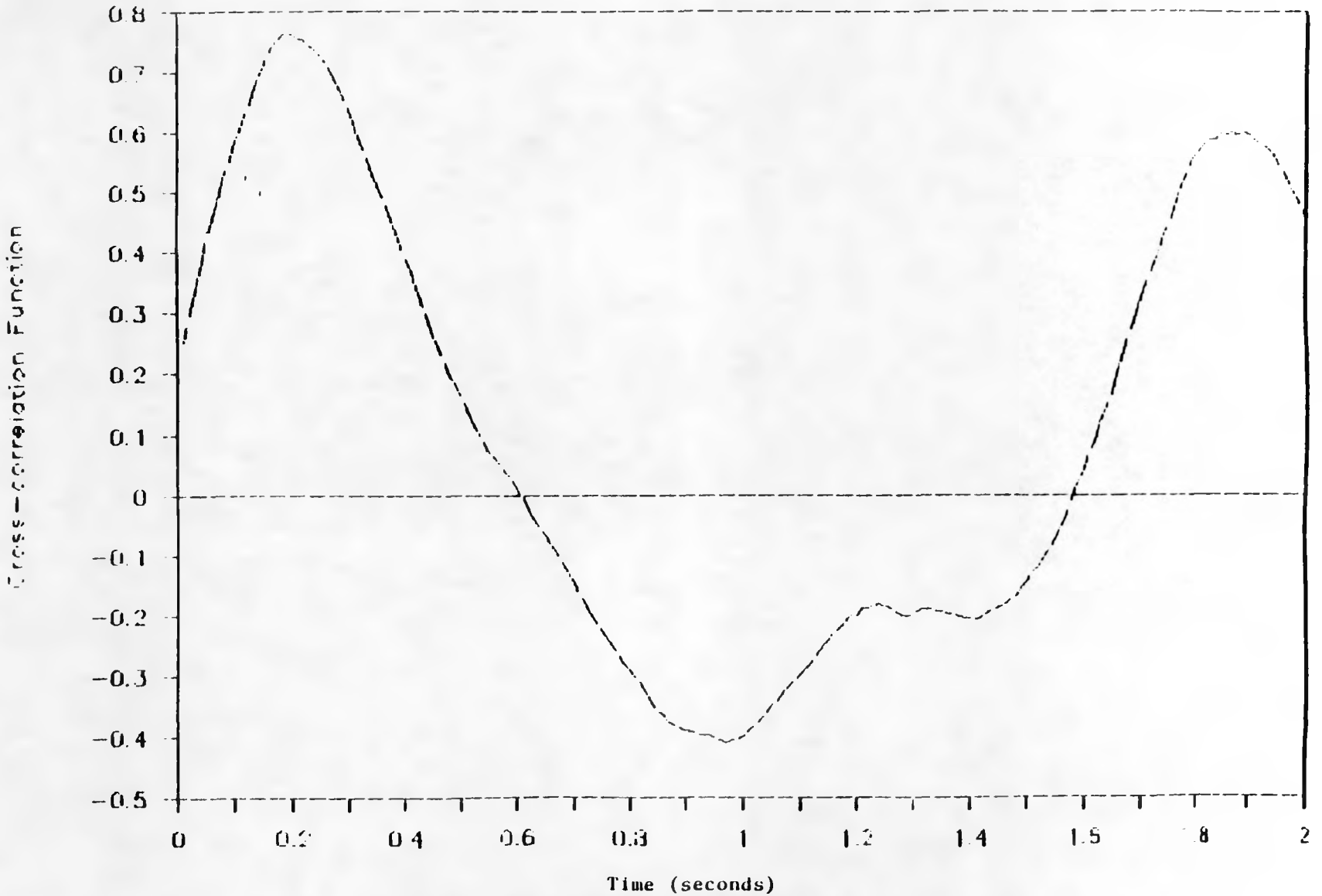

Figure 7.30 Plot of Cross-correlation Function vs Time to Determine the Time for one Pressure Event to Rise Passed a Vertical Probe Spacing of 2 inches of Data set HE

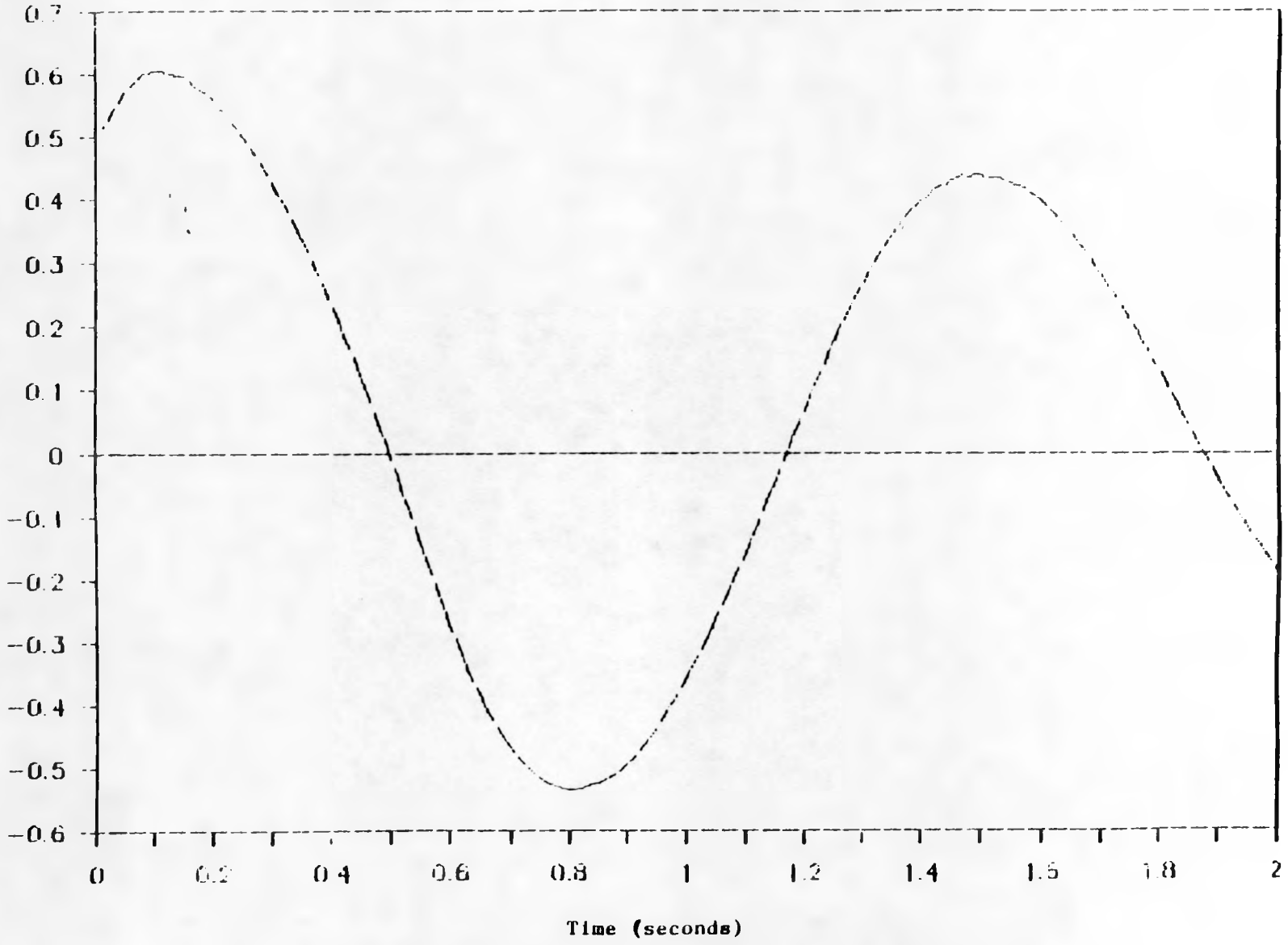

Figure 7.31 Plot of Cross-correlation Function vs Time to Determine the Time for one Pressure Event to Rise Passed a Vertical Probe Spacing of 2 inches of Data set HF

Table 7.3 Slug Rise Velocity Results from Cross-correlation, Pressure Trace Analysis, and Video Analysis

DATA RUN NUMBER	Cross-correlation Function Velocity (ft/sec)	Figure Number	Pressure Trace Analysis			Video Anlysis
			Average Velocity (ft/sec)	Number of Velocities Averaged	Range (min to max) (ft/sec)	Velocity (ft/sec)
HA	1.27	7.26	0.698	13	0.371 to 1.23	NA
HB	2.075	7.27	1.3	17	0.398 to 1.92	NA
HC	1.037	7.28	0.708	14	0.193 to 1.30	NA
HD	1.84	7.29	1.43	9	1.13 to 2.20	NA
HE	0.874	7.30	0.479	12	0.181 to 0 .949	0.555
HF	1.51	7.31	1.34	6	1.02 to 1.94	0.833

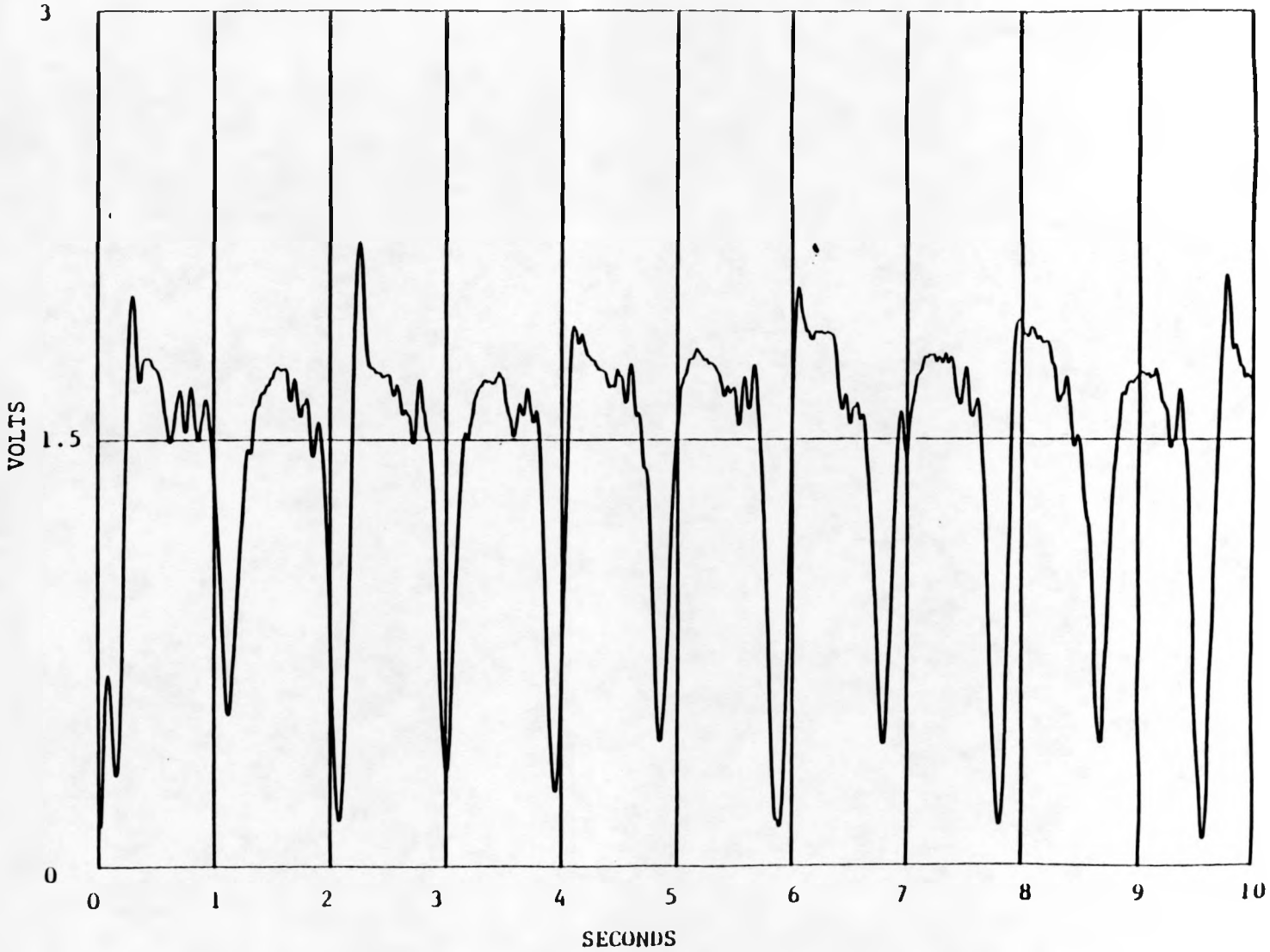

Figure 7.32 Pressure Trace, Stems at 6 7/8 and 7 7/8 Inches Above Distributor, on Bed Axis at Flowrate of 34 scfm

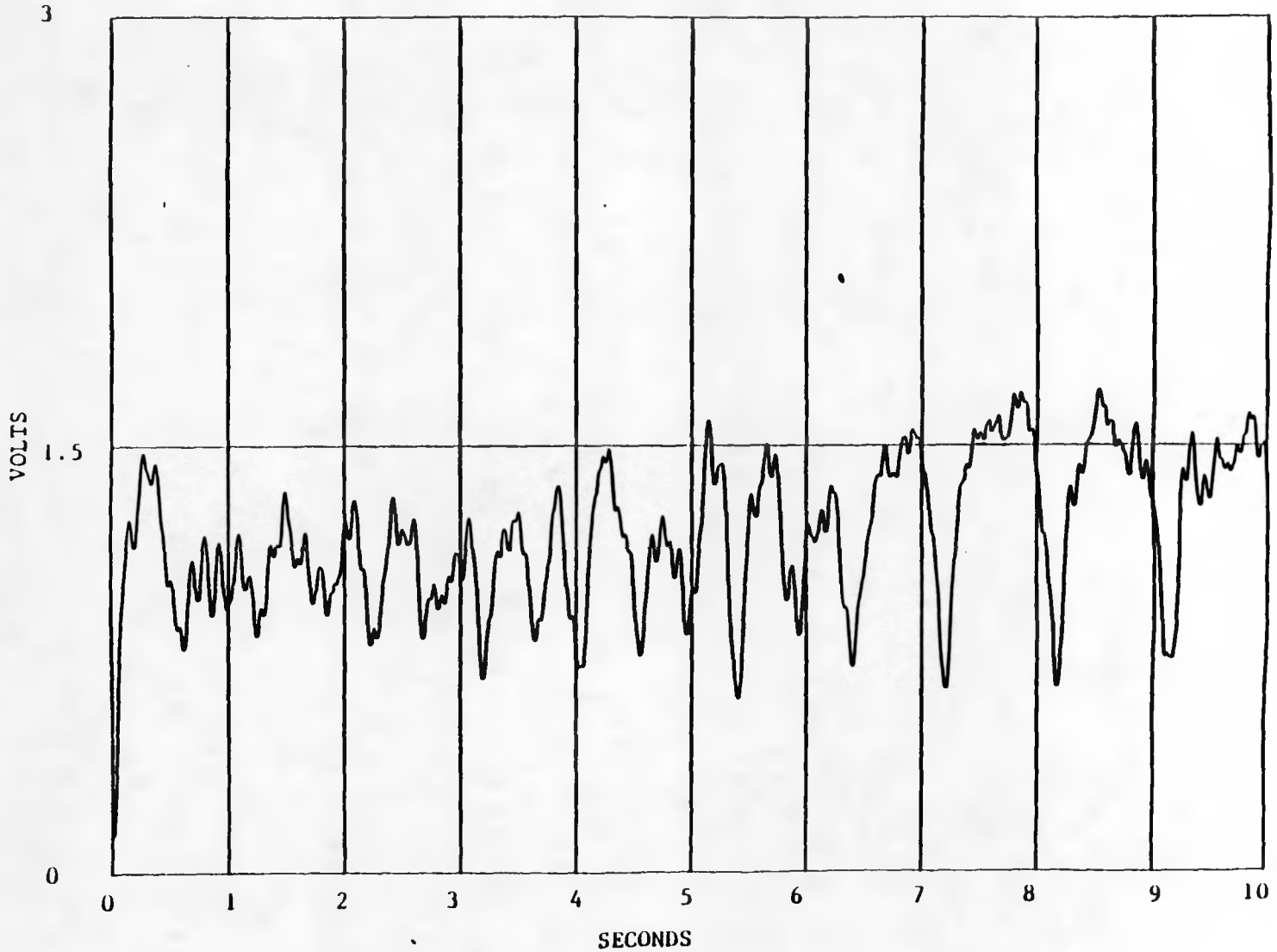

Figure 7.33 Pressure Trace, Stems 1 5/8 and 2 3/4 Inches Above Distributor, on Bed Axis, at Flowrate of 34 scfm

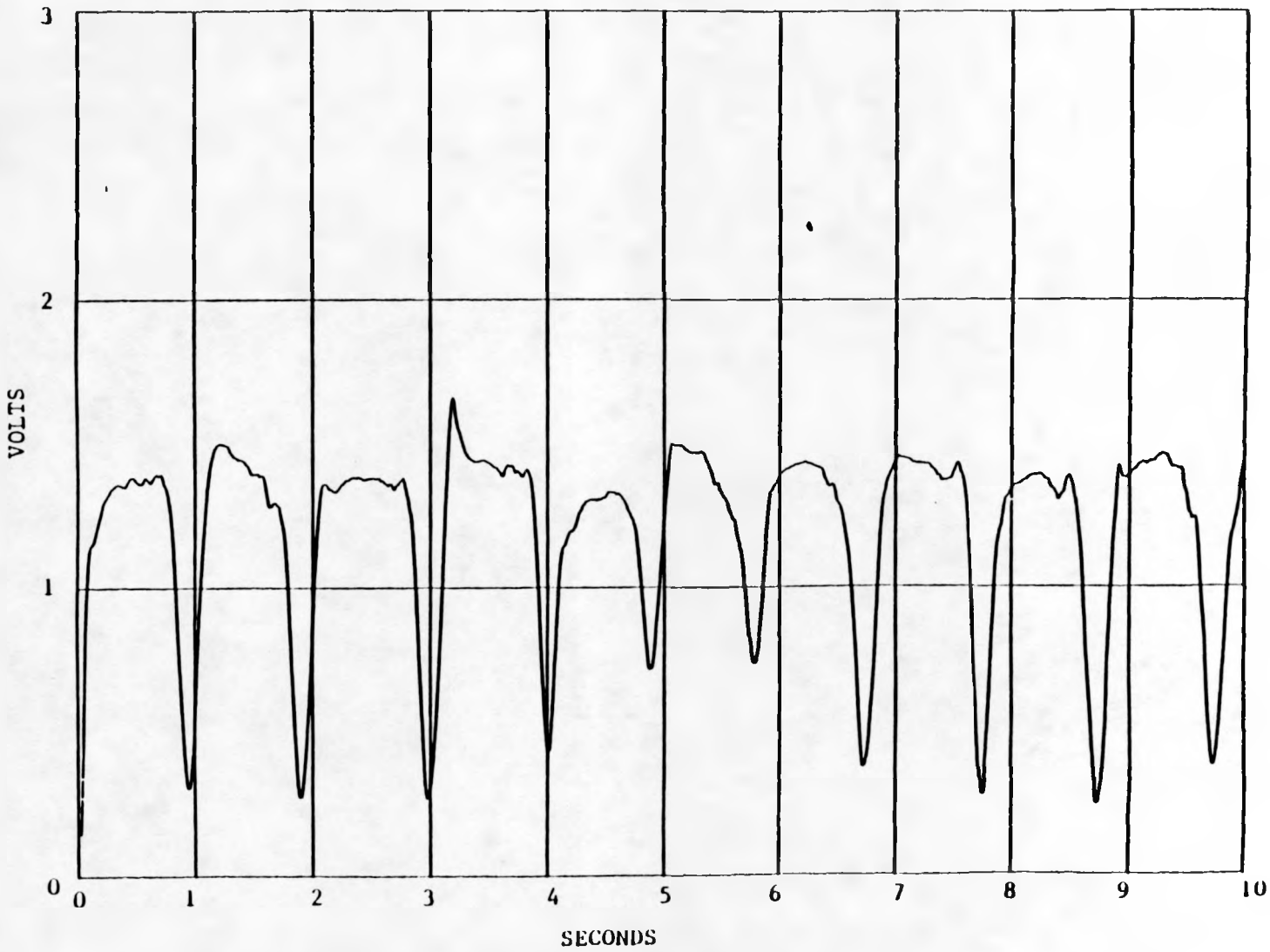

Figure 7.34 Pressure Trace, Stems 6 7/8 and 7 7/8 Above Distributor, at Bed Wall, Flowrate 34 scfm

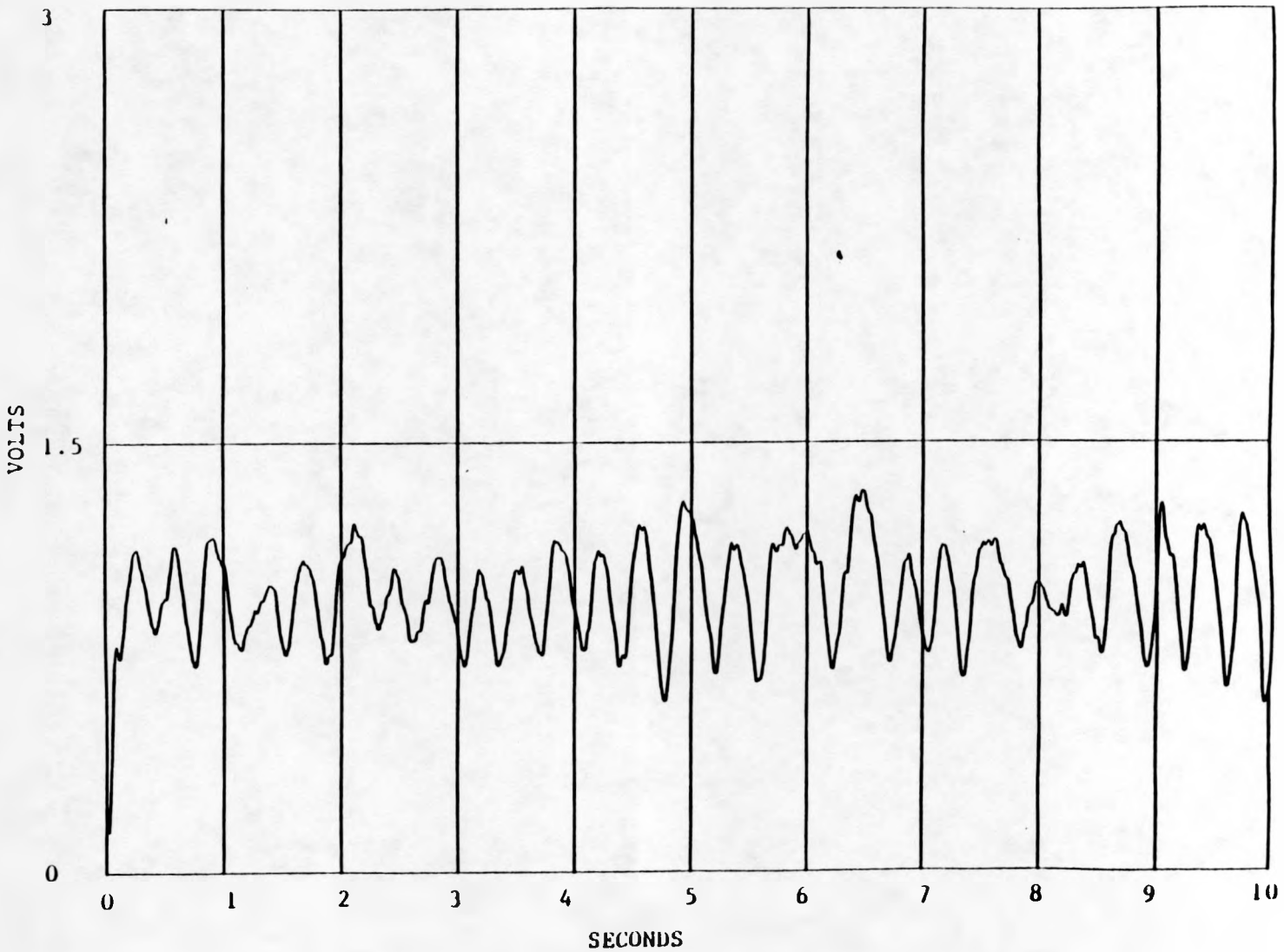

Figure 7.35 Pressure Trace, Stems 1 5/8 and 2 3/4 Inches Above Distributor Plate, at Bed Wall, Flowrate 34 scfm

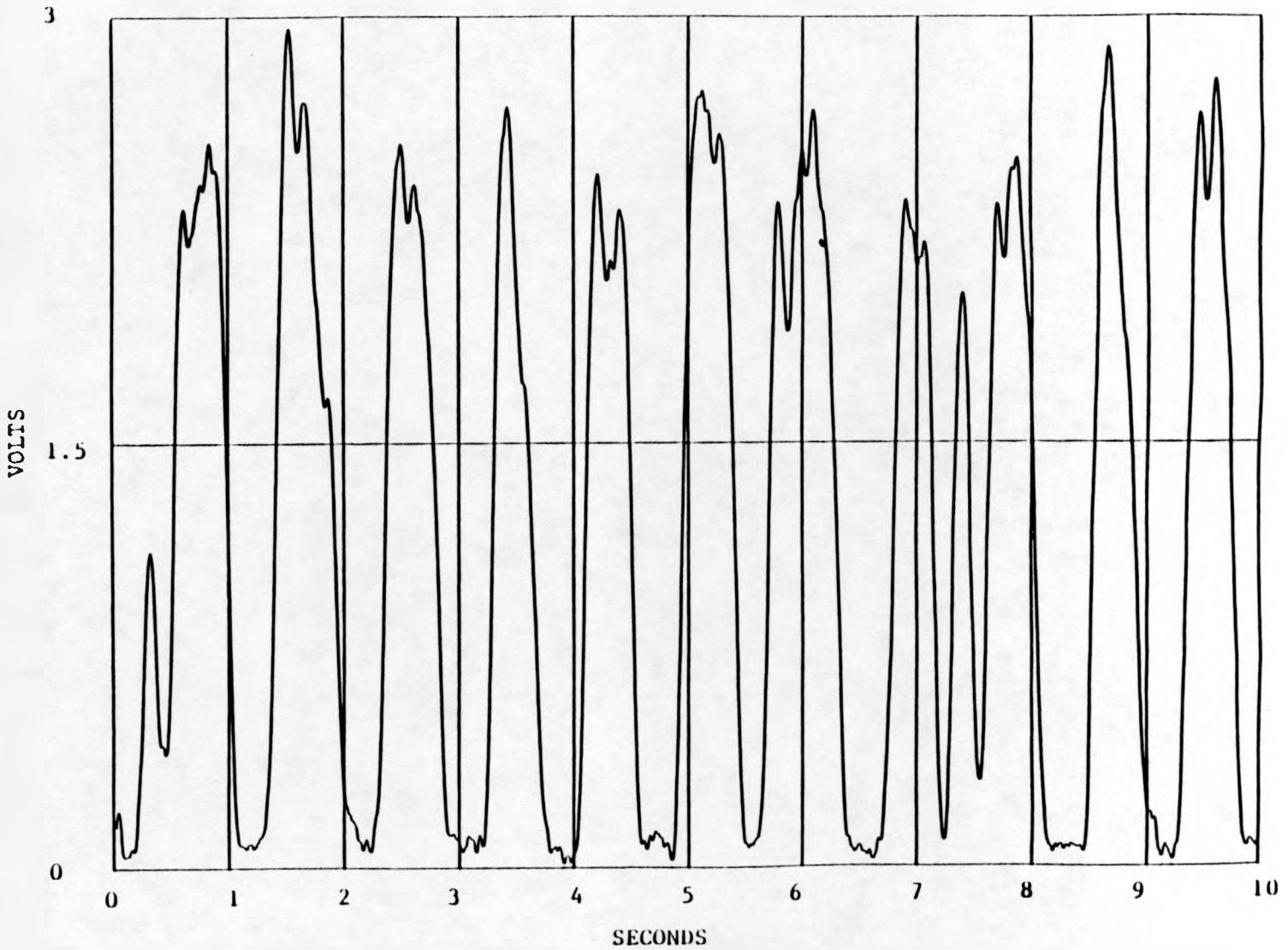

Figure 7.36 Pressure Trace, Stems 6 7/8 and 7 7/8 Inches Above Distributor, at Bed Center, Flowrate 40 scfm

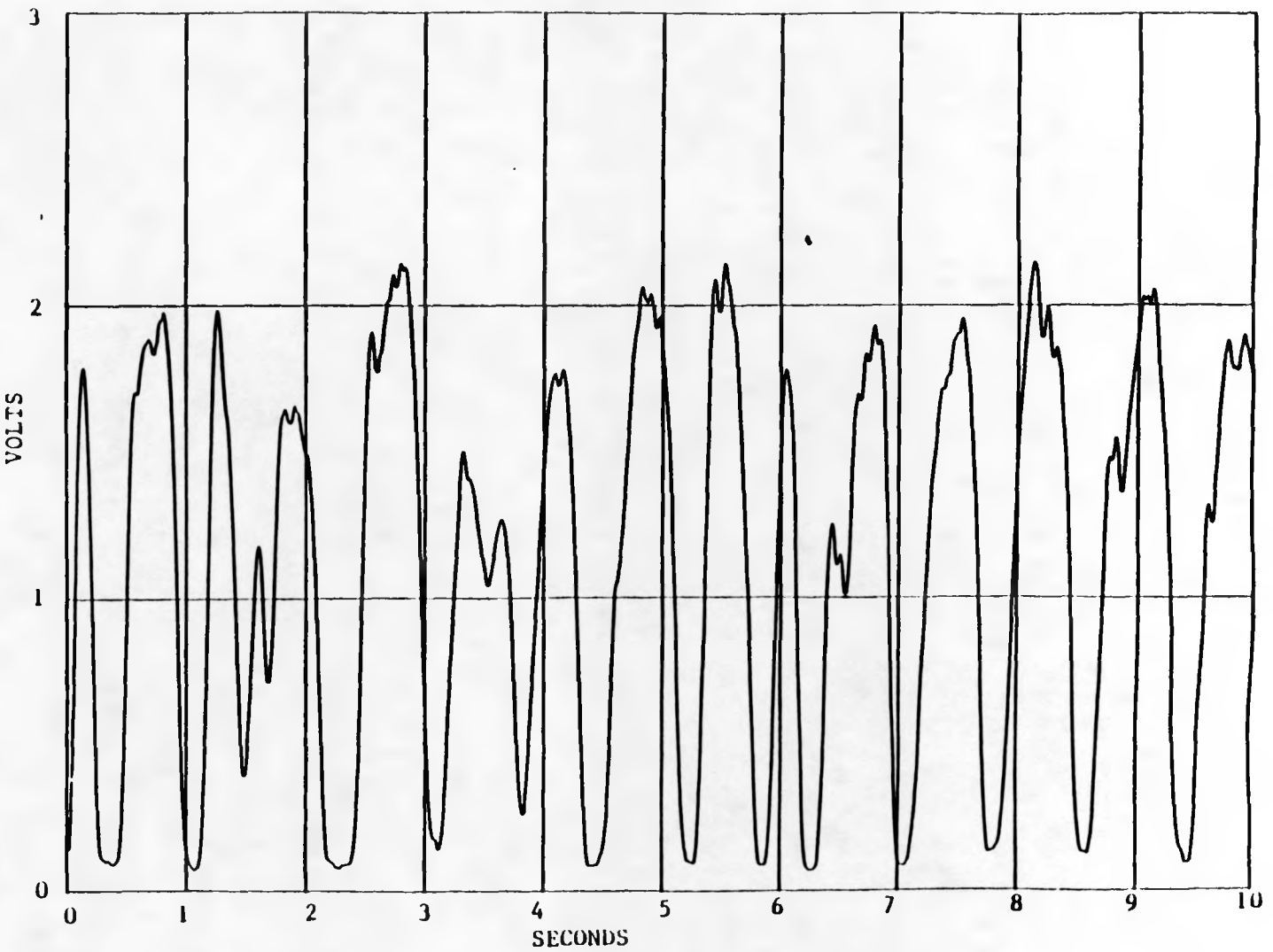

Figure 7.37 Pressure Trace, Stems 6 7/8 and 7 7/8 Inches Above Distributor, at Bed Wall, Flowrate 40 scfm

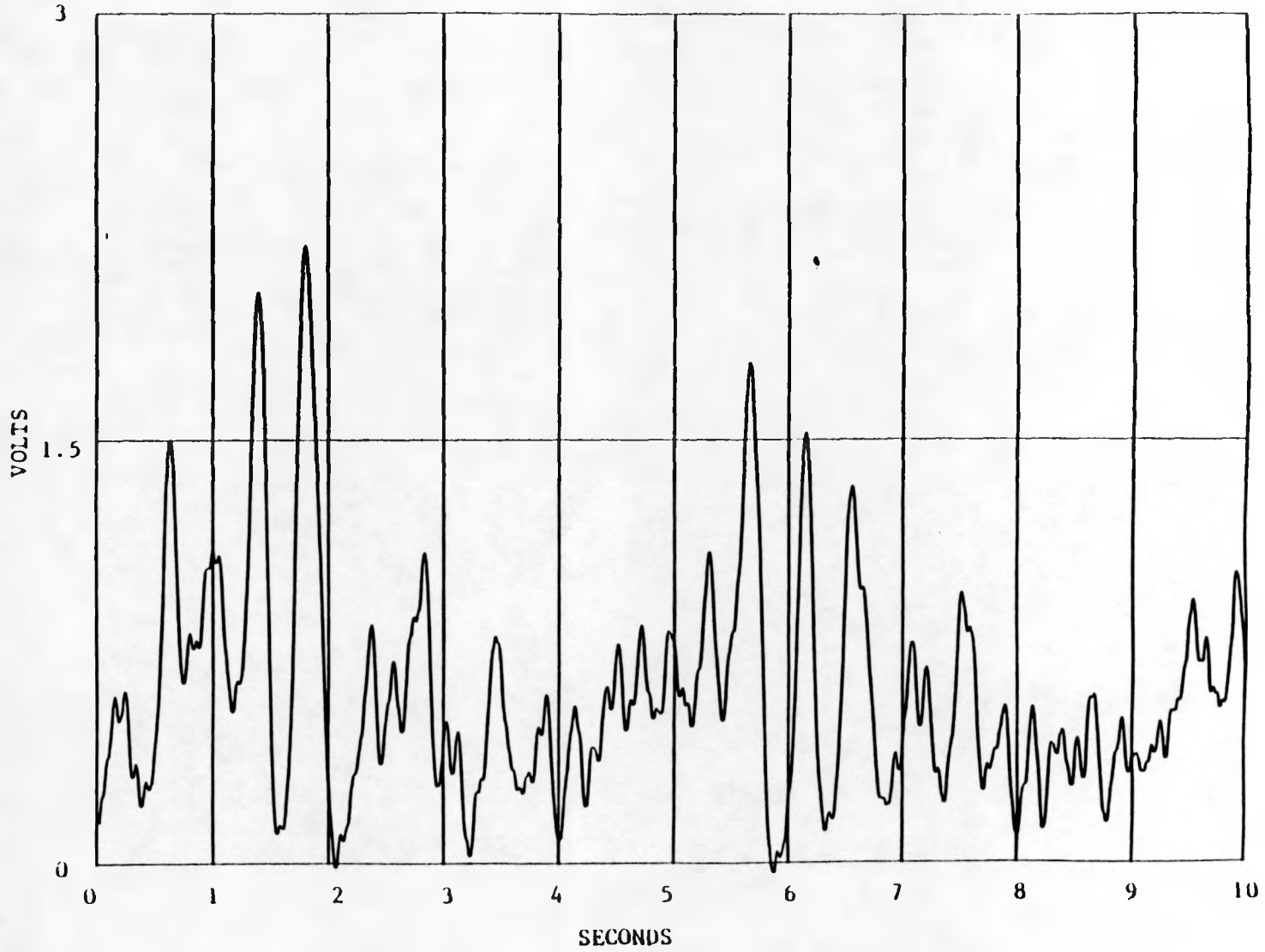

Figure 7.38 Pressure Trace, Stems 1 5/8 and 2 3/4 Inches Above Distributor, at Bed Center, Flowrate 40 scfm

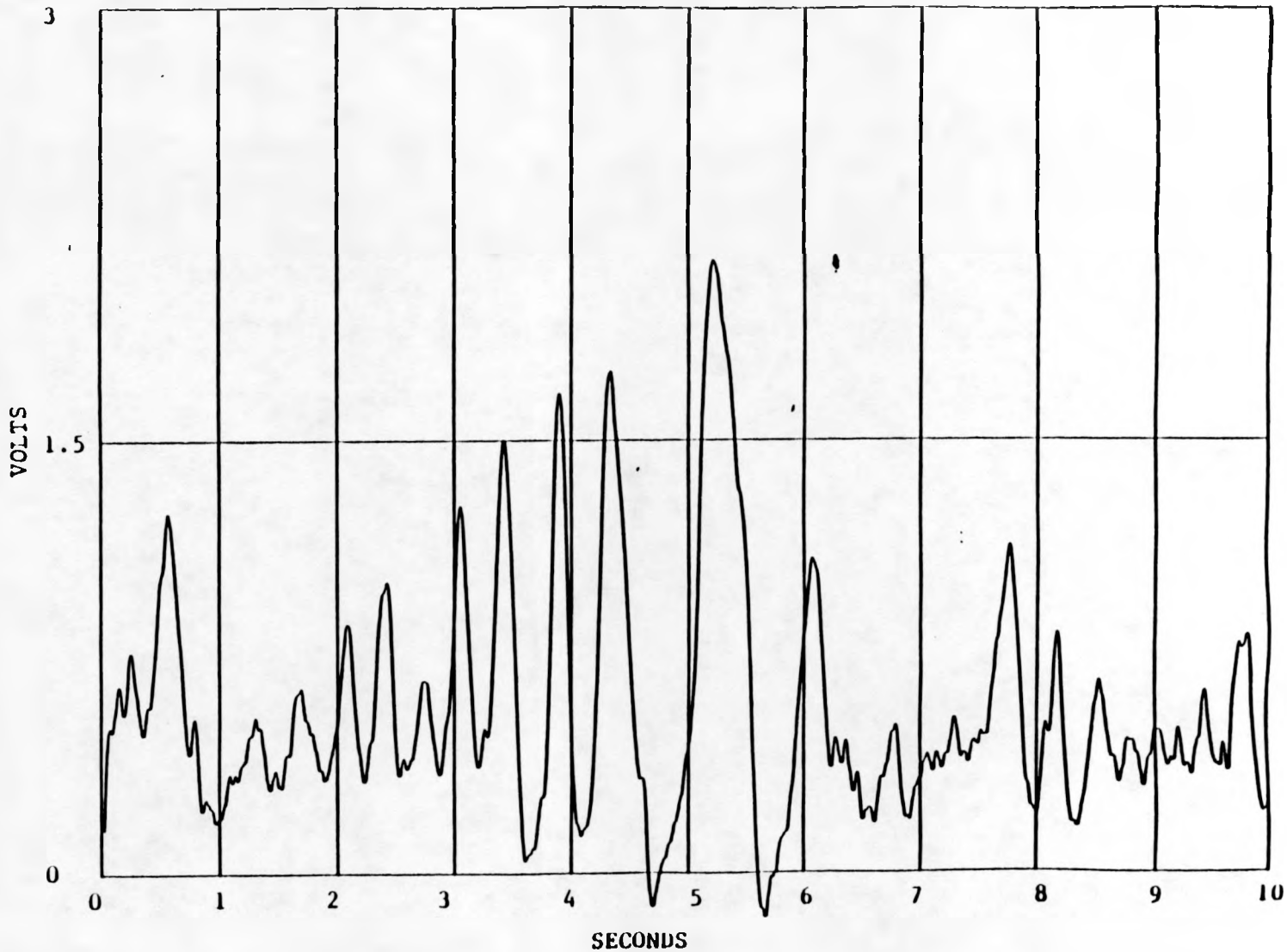

Figure 7.39 Pressure Trace, Stems 1 5/8 and 2 3/4 Inches Above Distributor, at Bed Wall, Flowrate 40 scfm

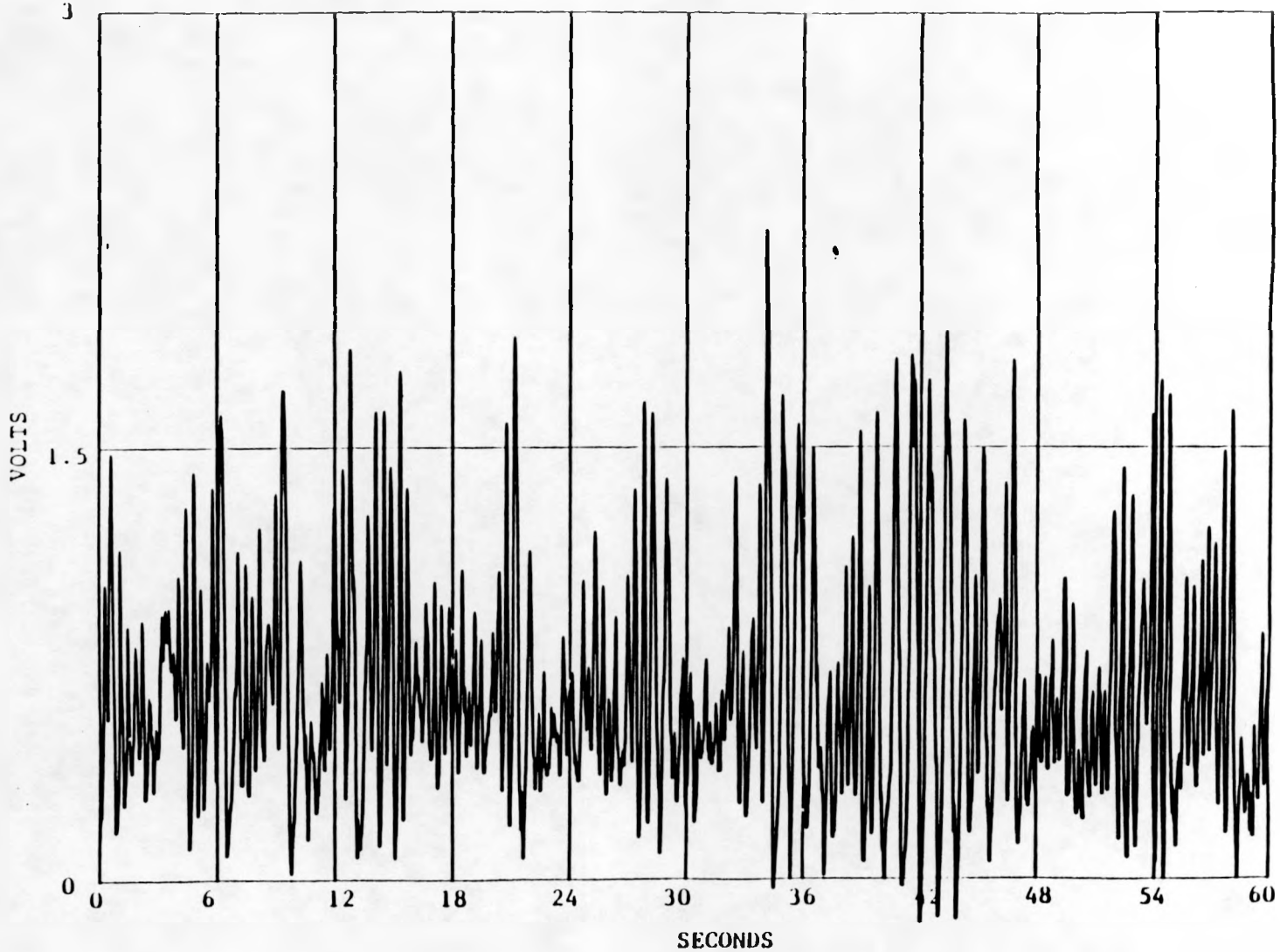

Figure 7.40 A Longer Differential Pressure Trace at the Same Position and Conditions as Fig. 11

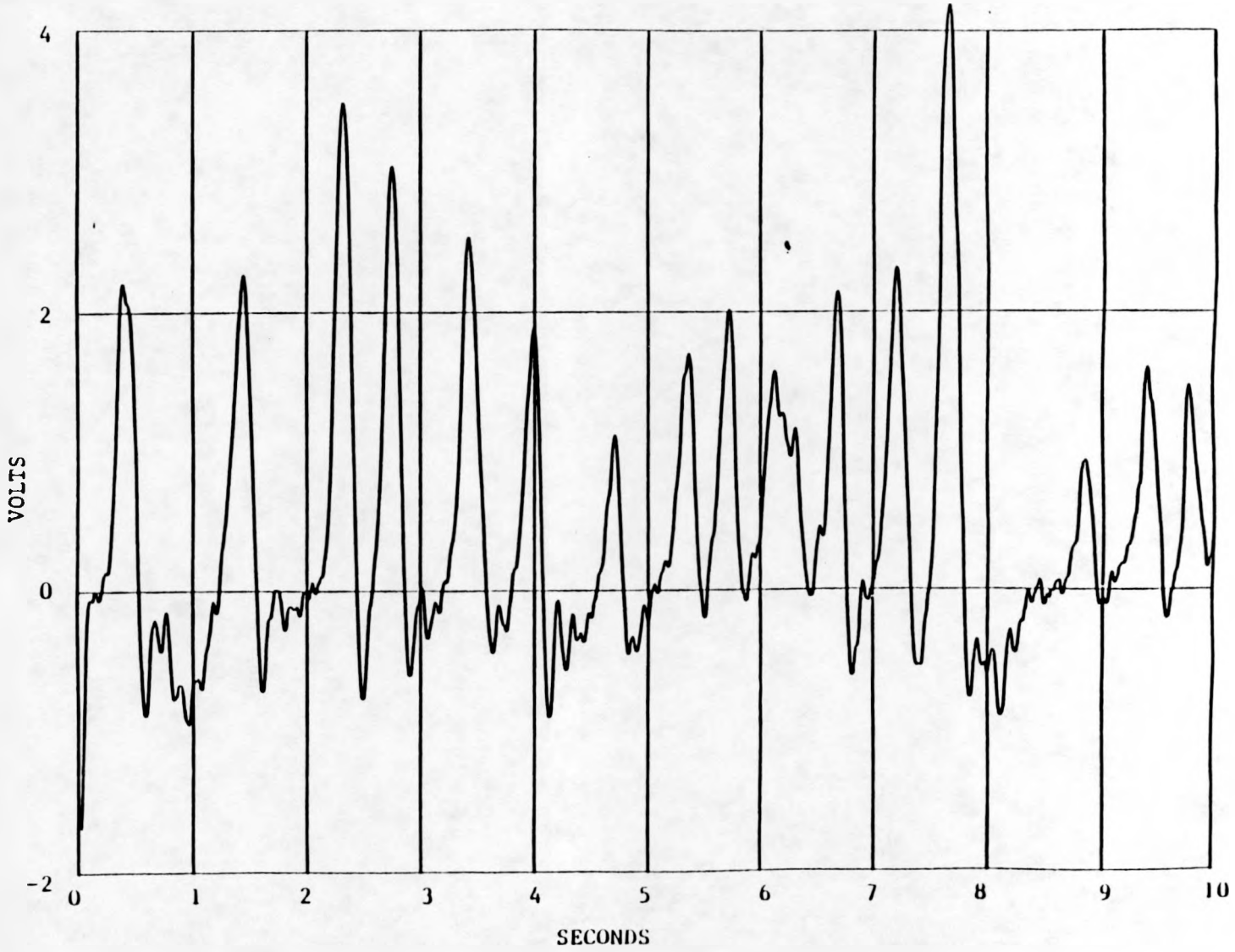

Figure 7.41 Pressure Trace, Stems 1 5/8 and 2 3/4 Inches Above Distributor, on Bed Axis, Flowrate 50 scfm

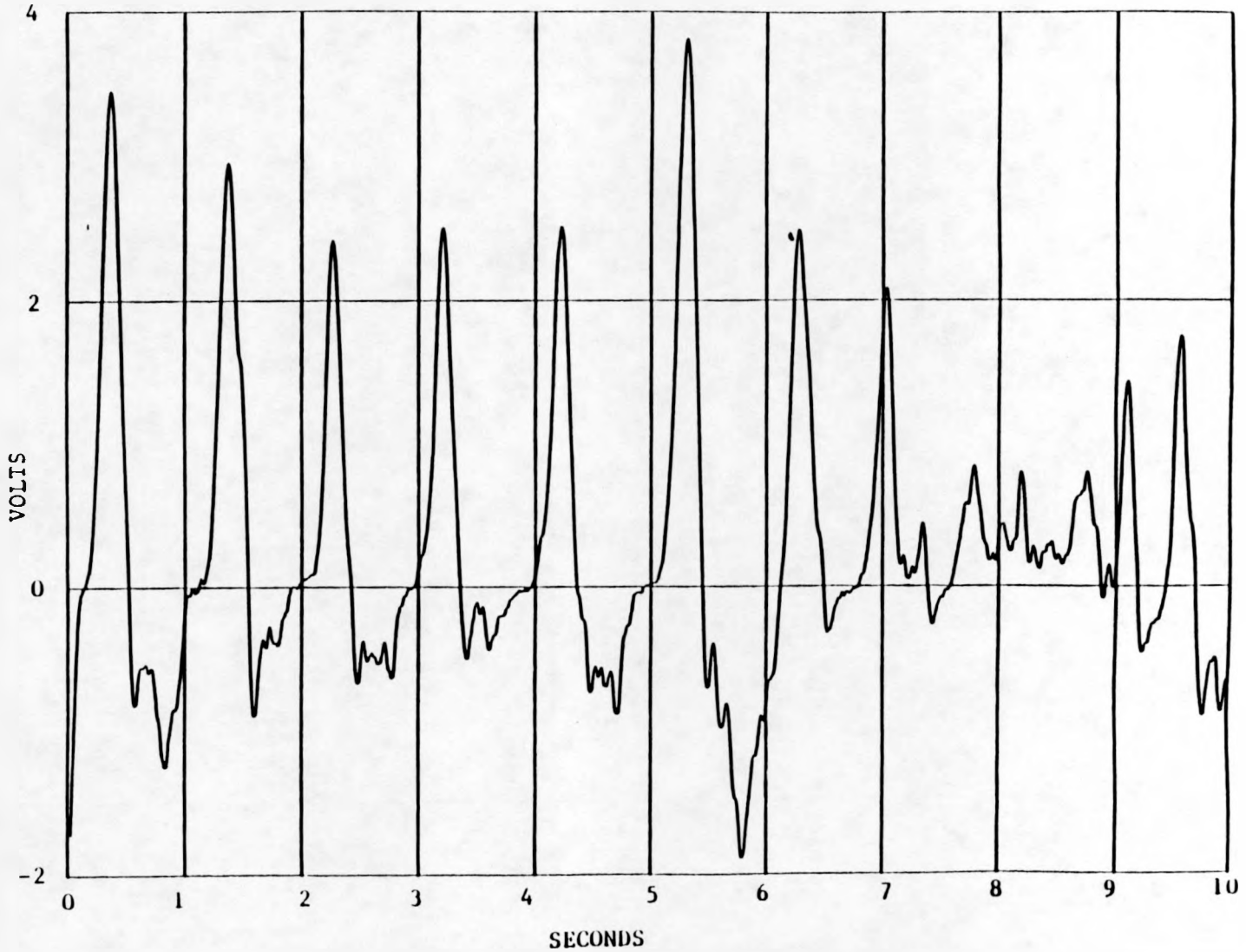

Figure 7.42 Pressure Trace, Stems 1 5/8 and 2 3/4 Inches Above Distributor, at Bed Wall, Flowrate 50 scfm

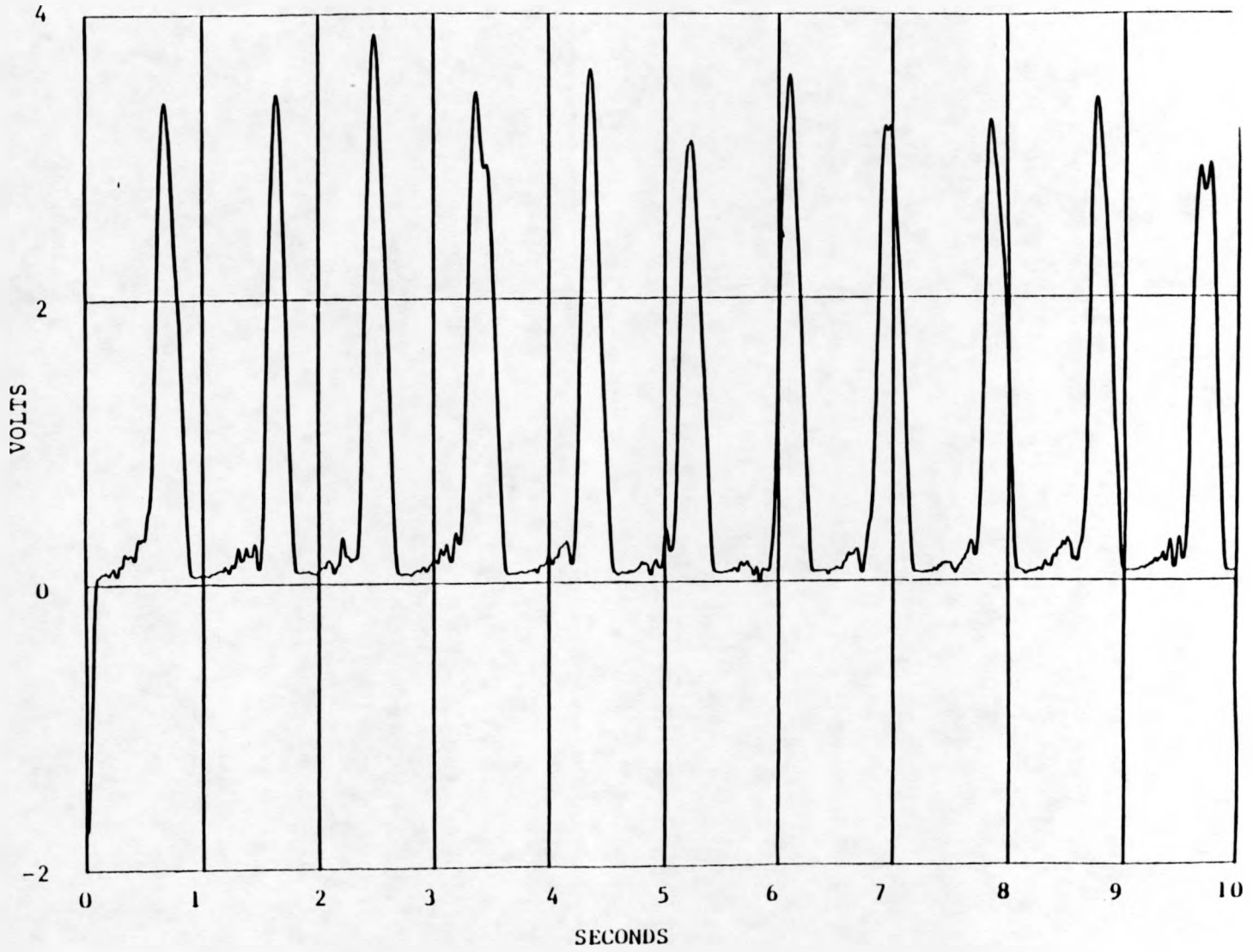

Figure 7.43 Pressure Trace, Stems 6 7/8 and 7 7/8 Above Distributor, on Bed Axis, Flowrate 50 scfm

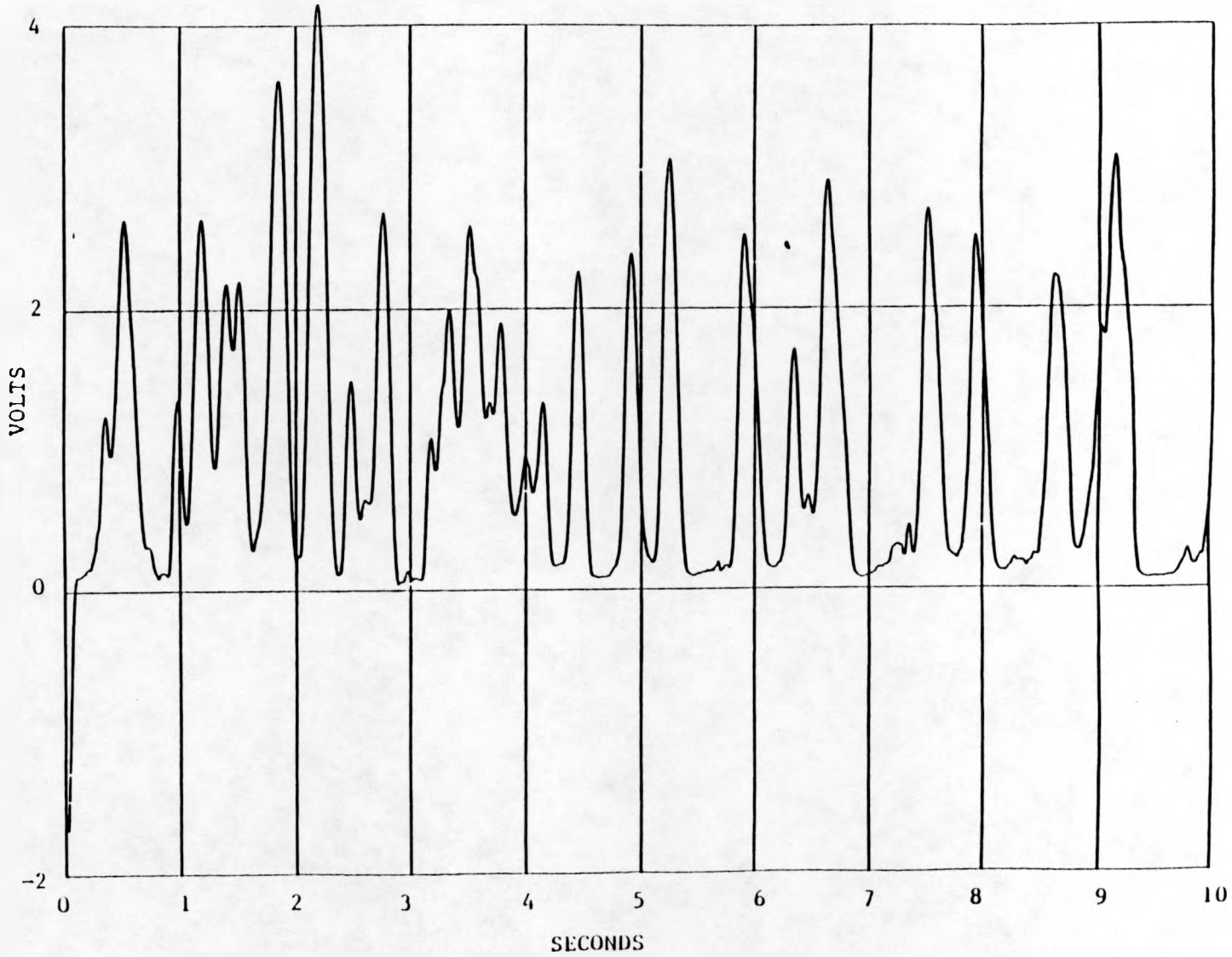

Figure 7.44 Pressure Trace, Stems 6 7/8 and 7 7/8 Inches Above Distributor, at Bed Wall, Flowrate 50 scfm

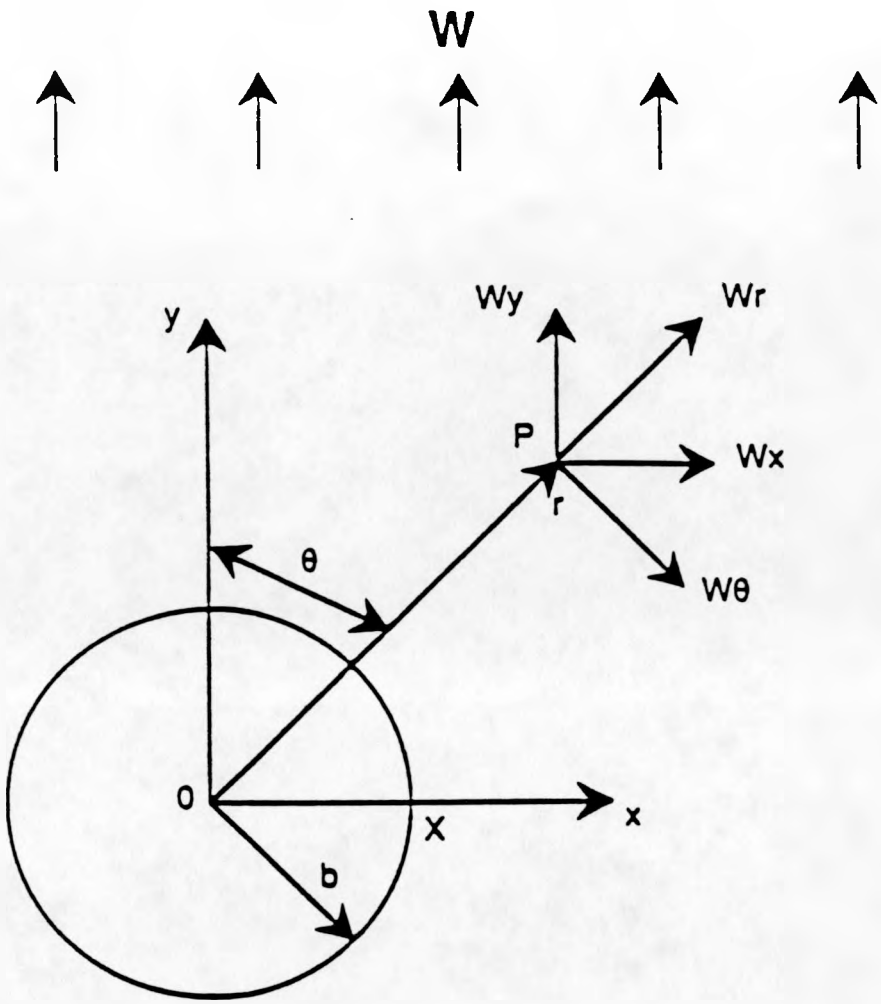

Figure 8.1 **Two dimensional model selected for predicting pressure fields.**

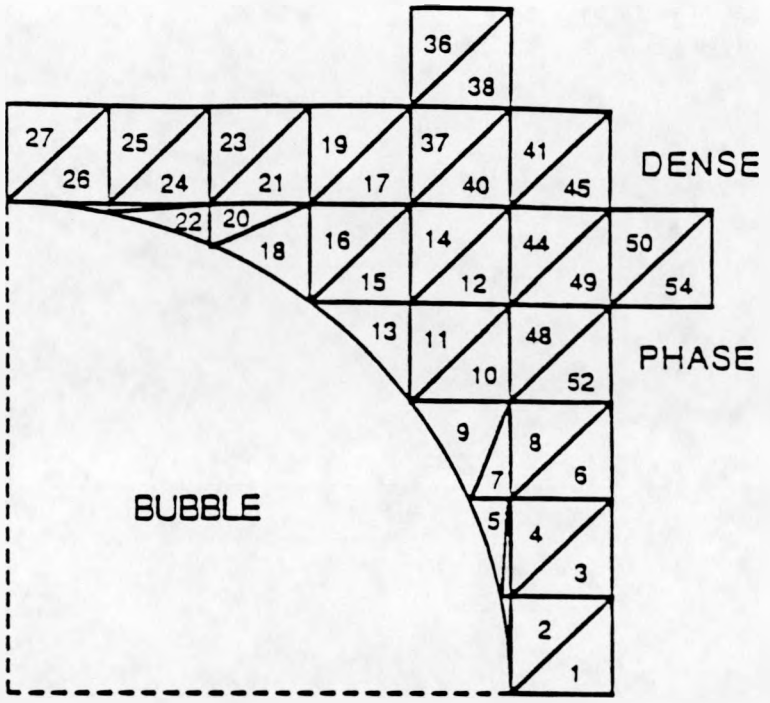

Figure 8.2 Part of the finite element mesh surrounding the bubble.

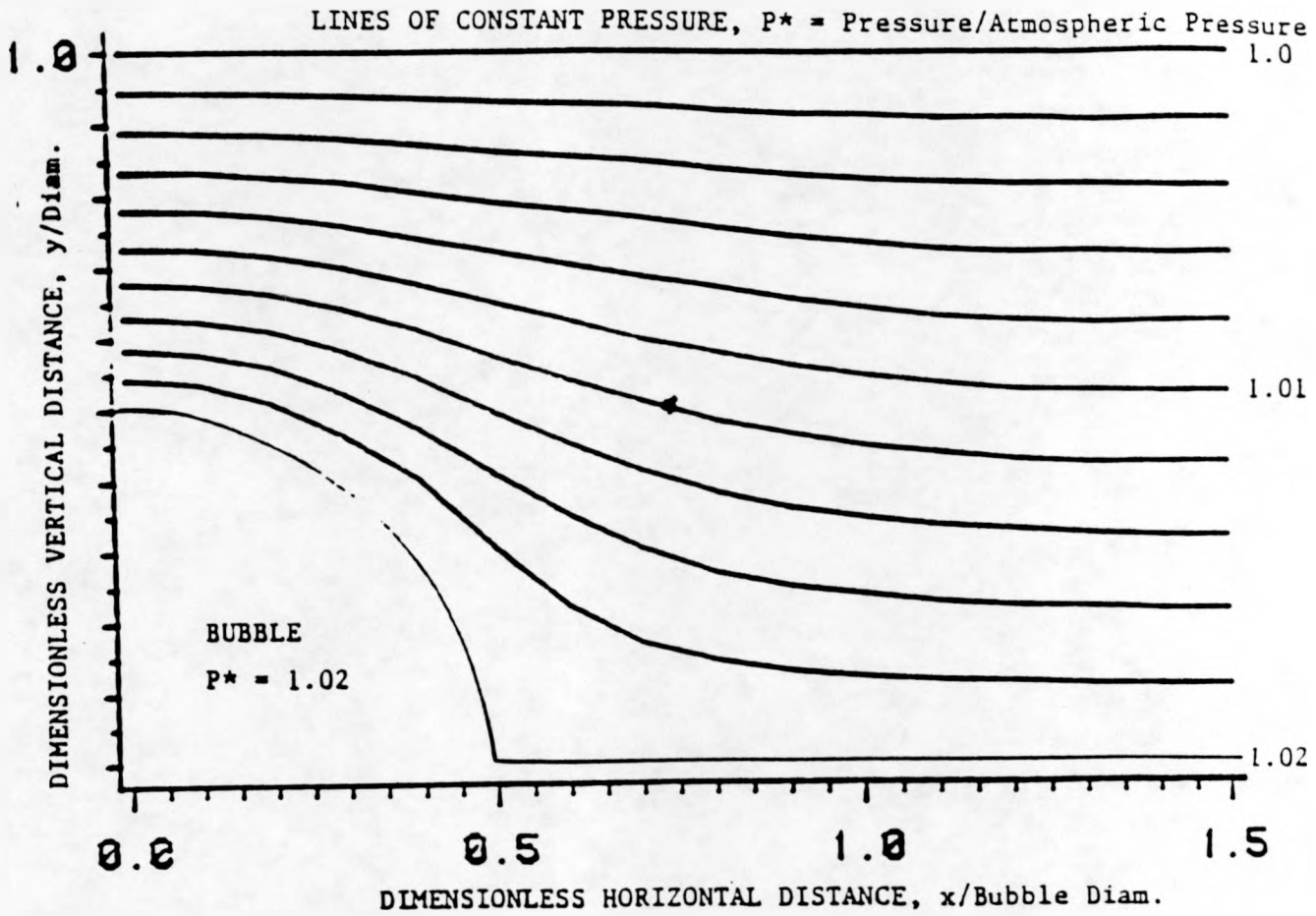

Figure 8.3 Preliminary Results From Finite Element Model

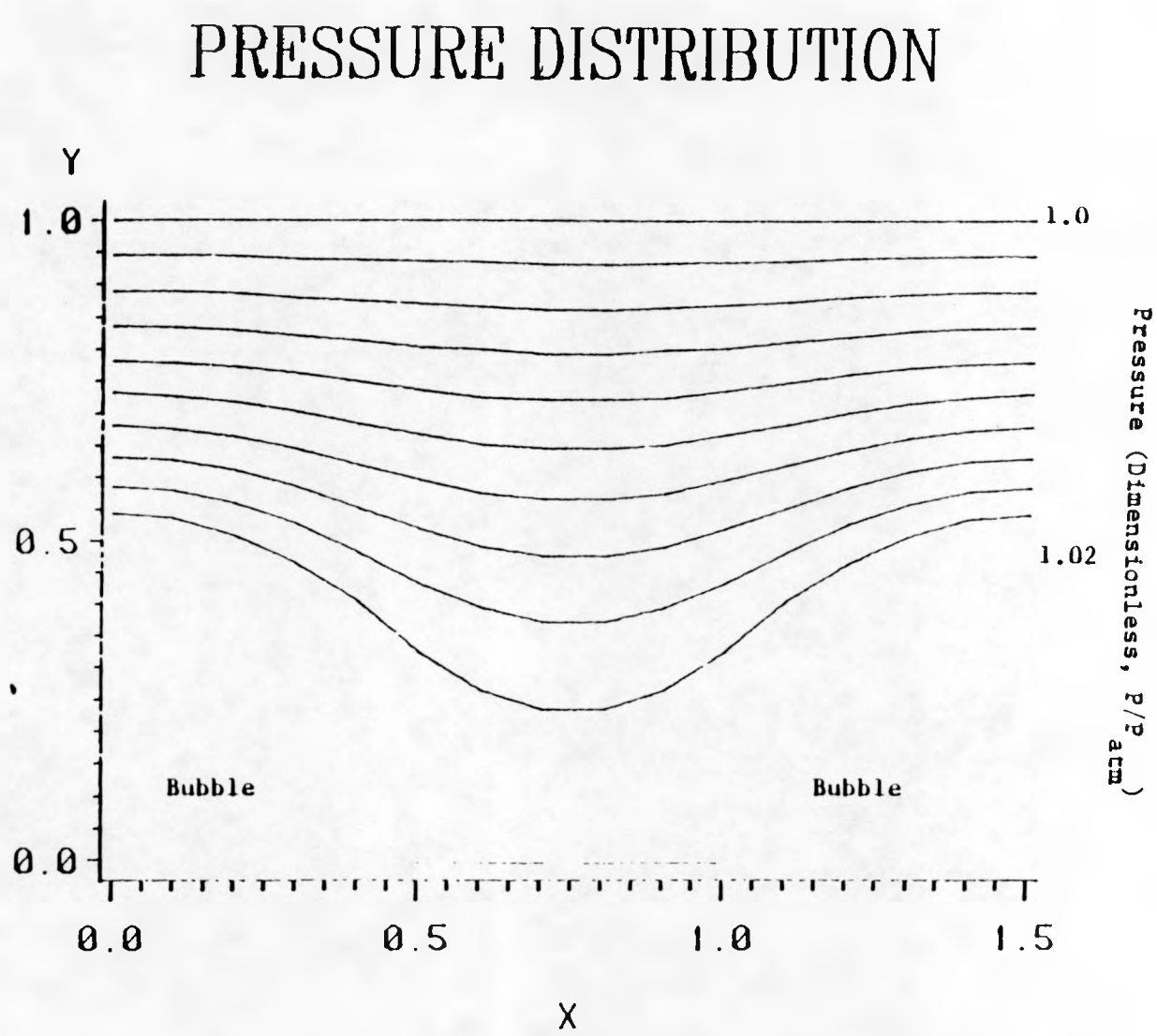

Figure 8.4 Lines of constant pressure surrounding two bubbles with their centers 1-5 bubble radii horizontally apart.

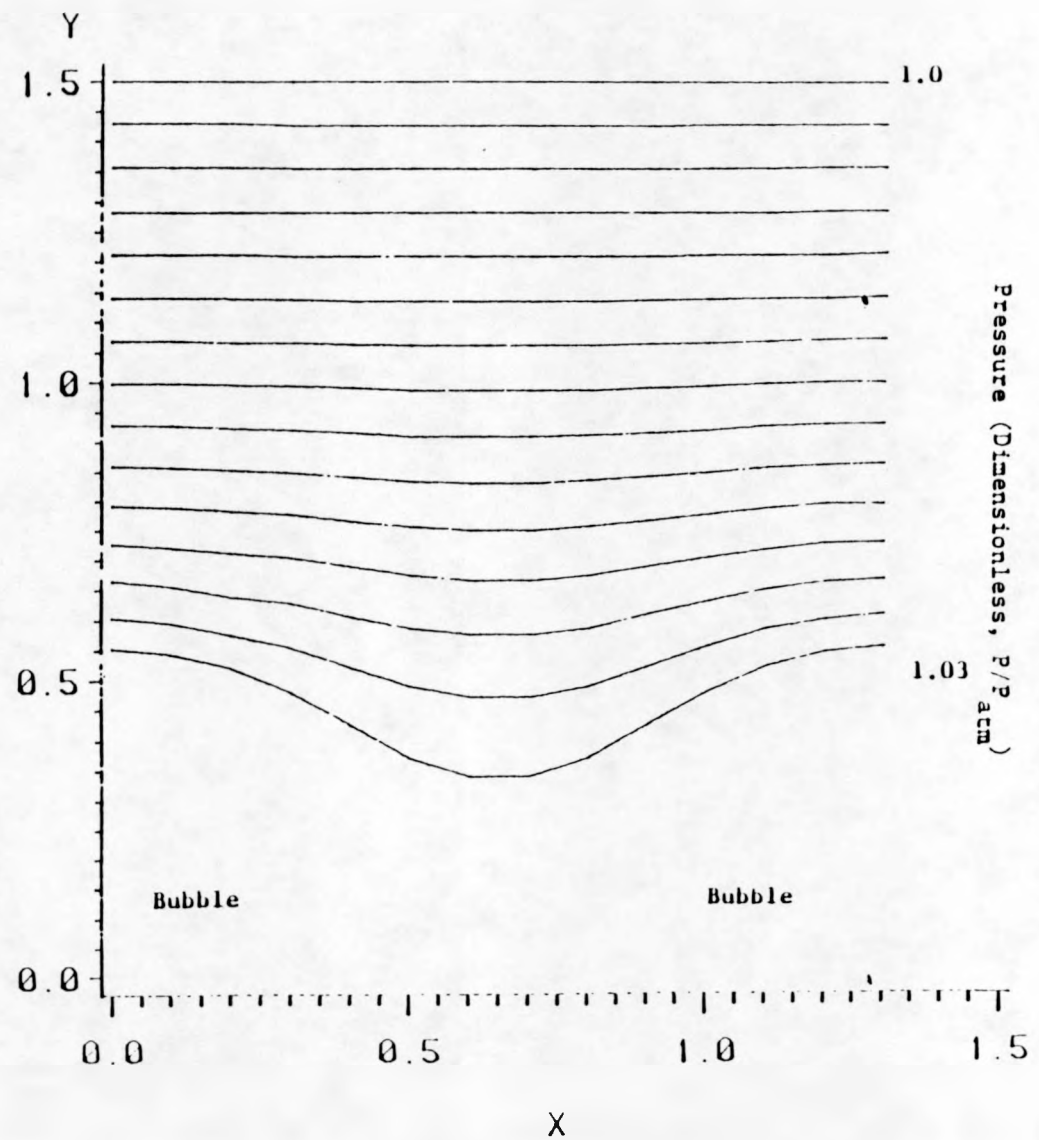

Figure 8.5 Lines of Constant Pressure Surrounding Two Bubbles

PRESSURE DISTRIBUTION

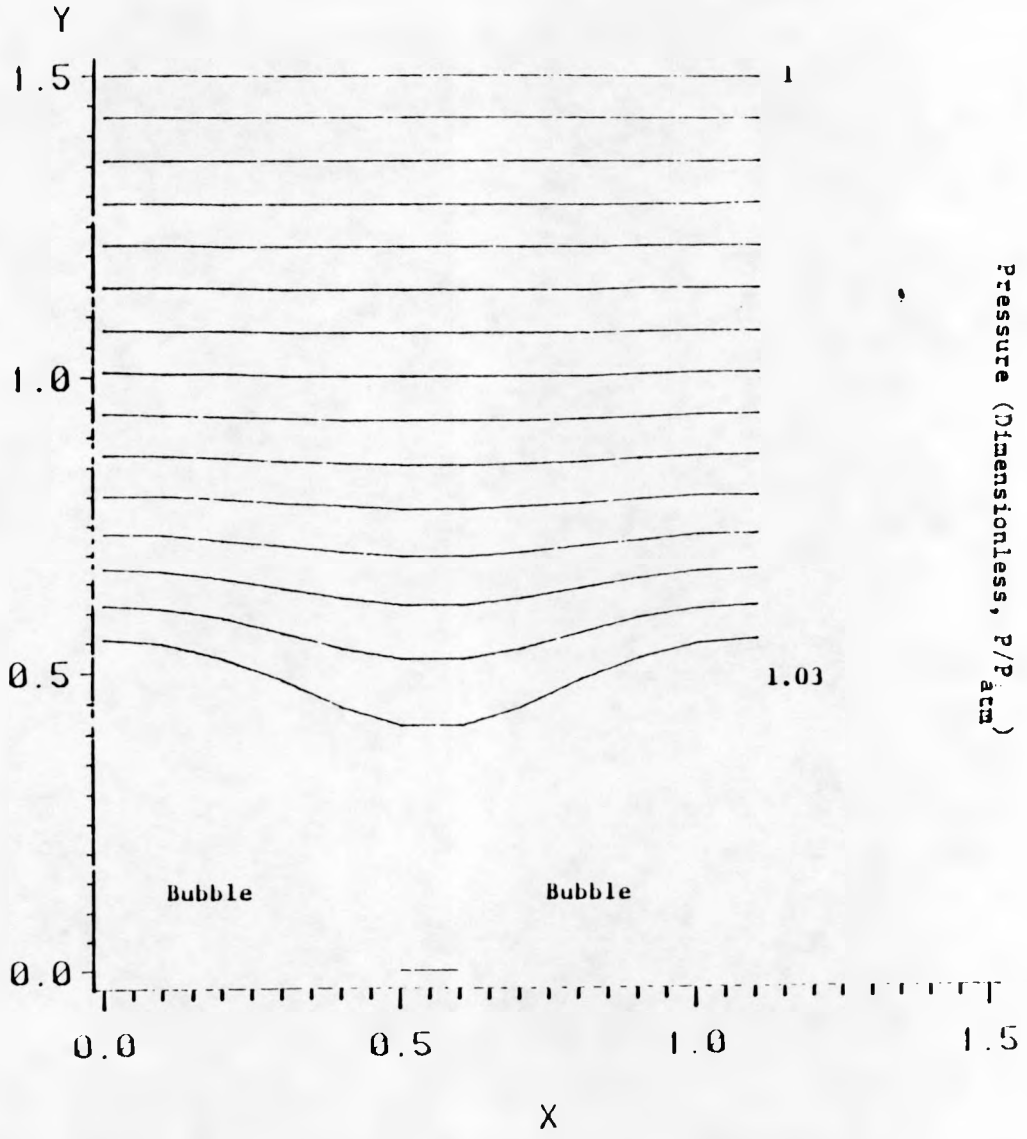

Figure 8.6 Lines of Constant Pressure Surrounding Two Bubbles

$$Q = \sqrt{1-k^2}$$

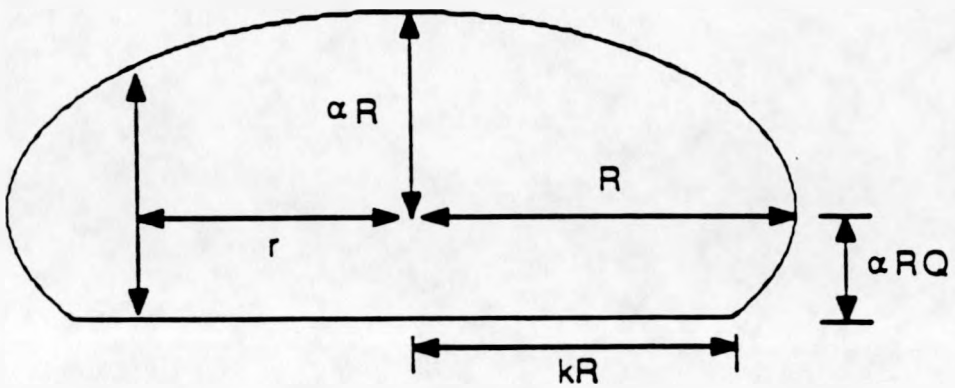

Figure 9.1 Ellipsoidal bubble used to approximate true bubble shape in a fluidized bed.

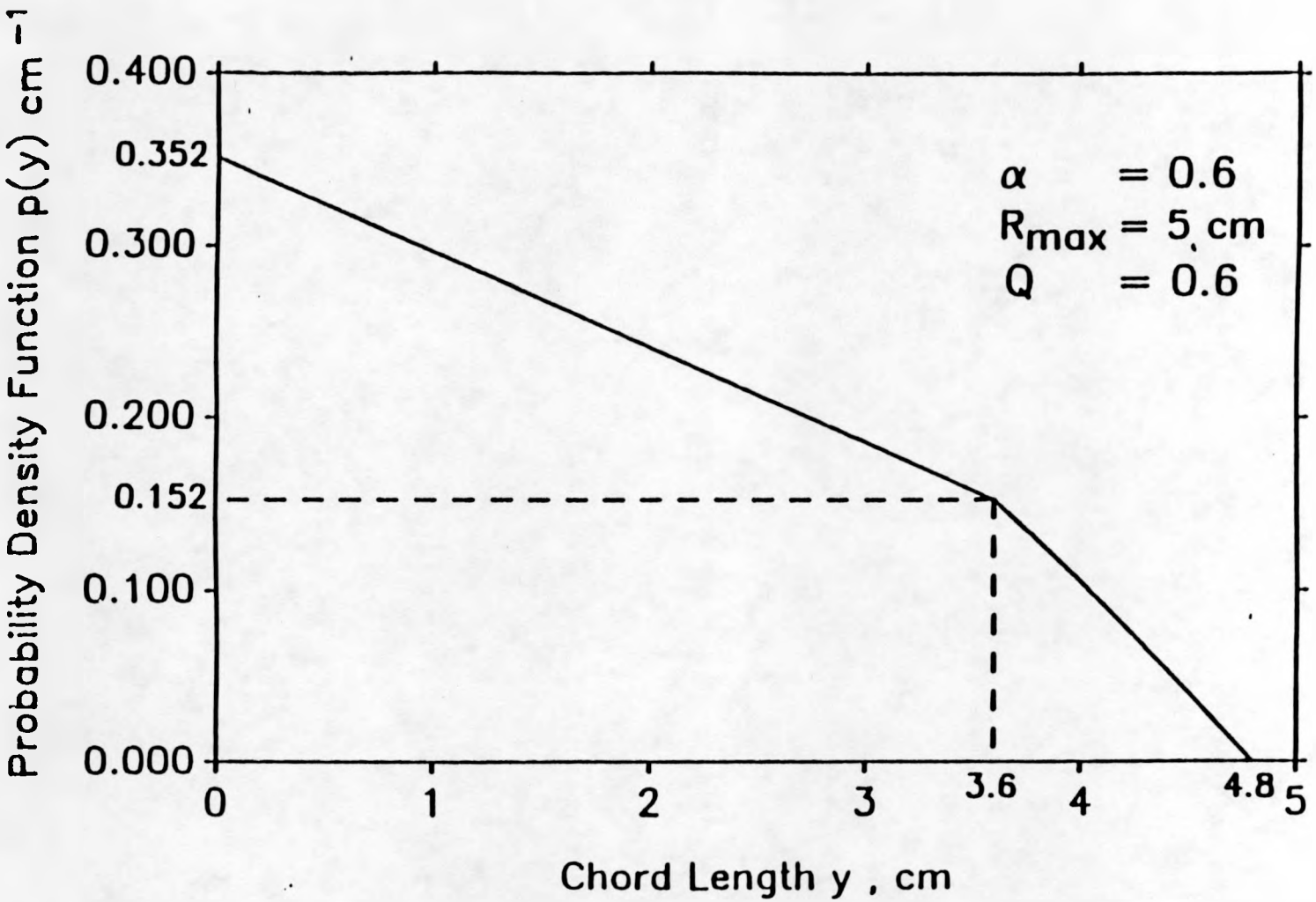

Figure 9.2 Distribution of pierced lengths obtained for a uniform distribution of bubble sizes touching the probe.

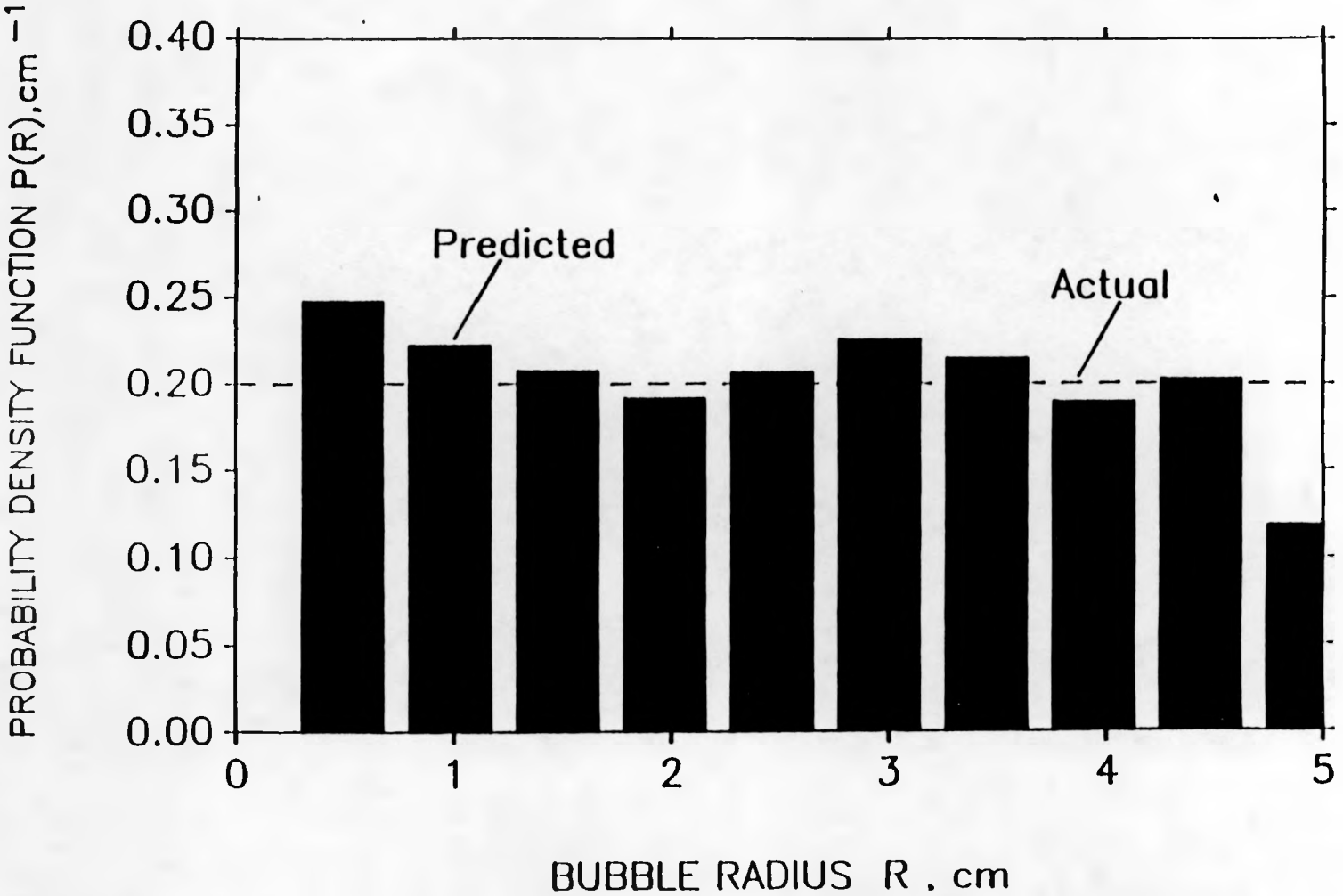

Figure 9.3 Comparison of Back Transformed Bubble Distribution with the True Distribution From Which the Chord Length Data was Obtained. (5000 chord lengths and 10 size intervals)

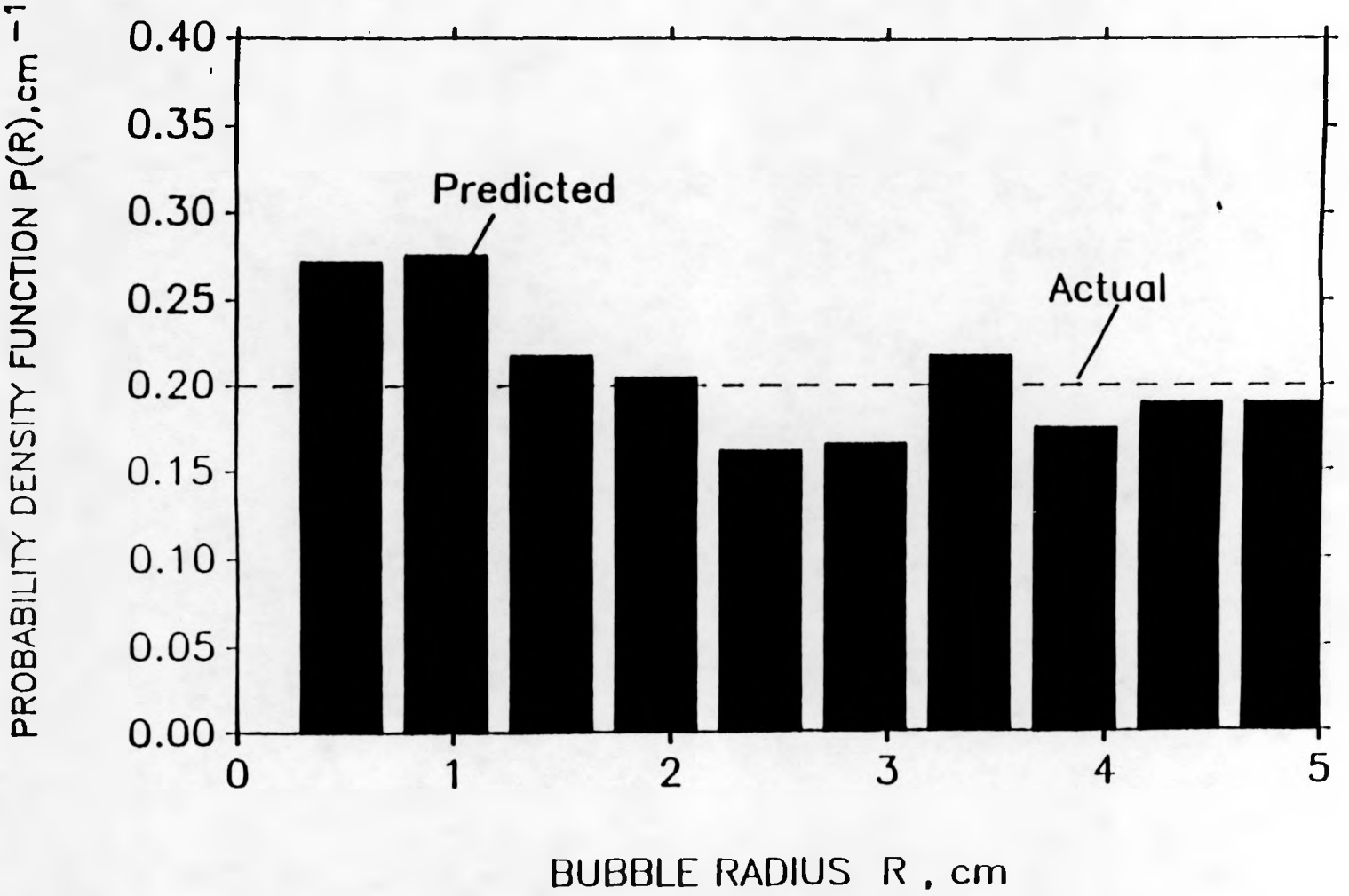

Figure 9.4a Comparison of Back Transformed Bubble Distribution with the True Bubble Distribution

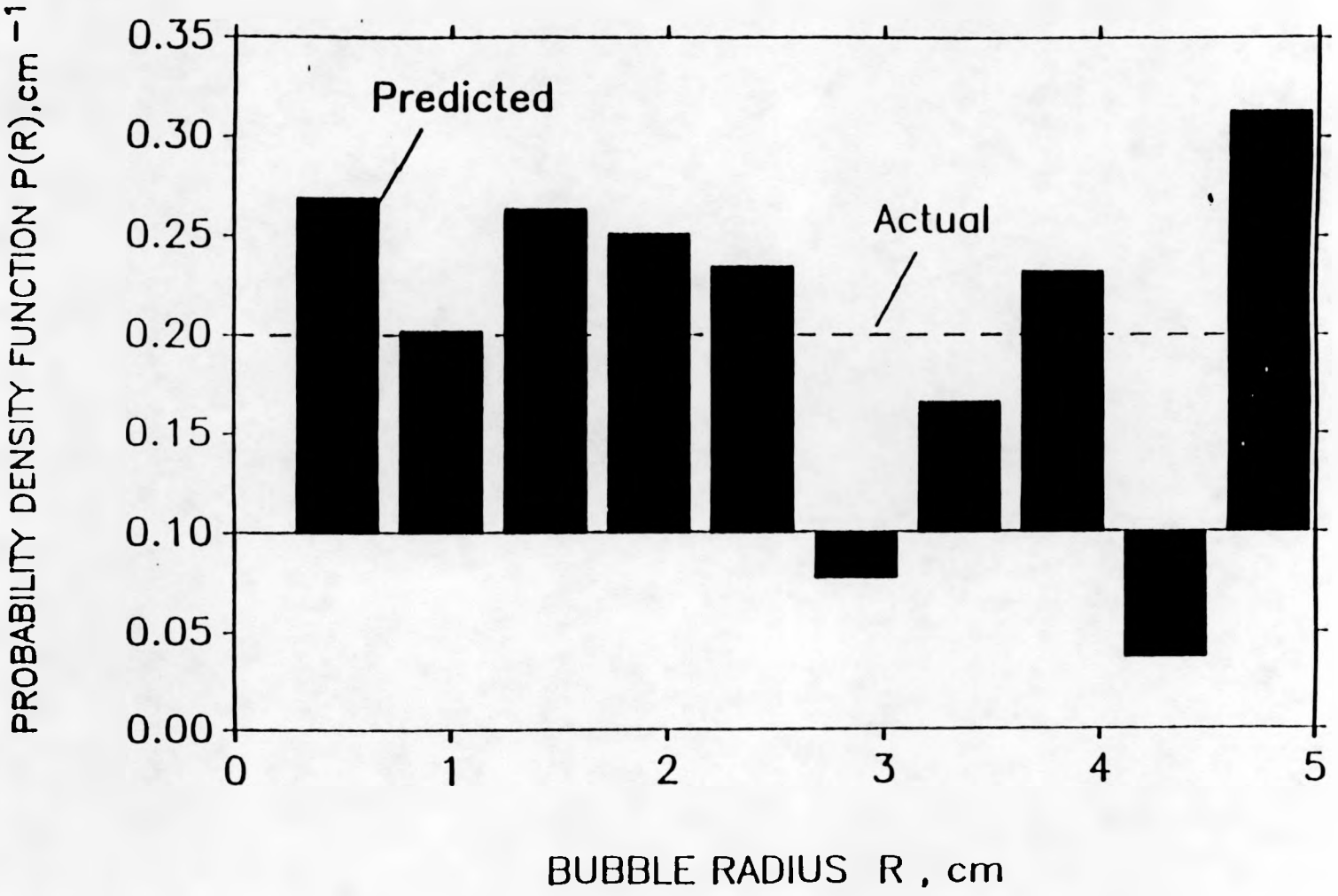

Figure 9.4b Severe instability in back transform: 100 pierced lengths.

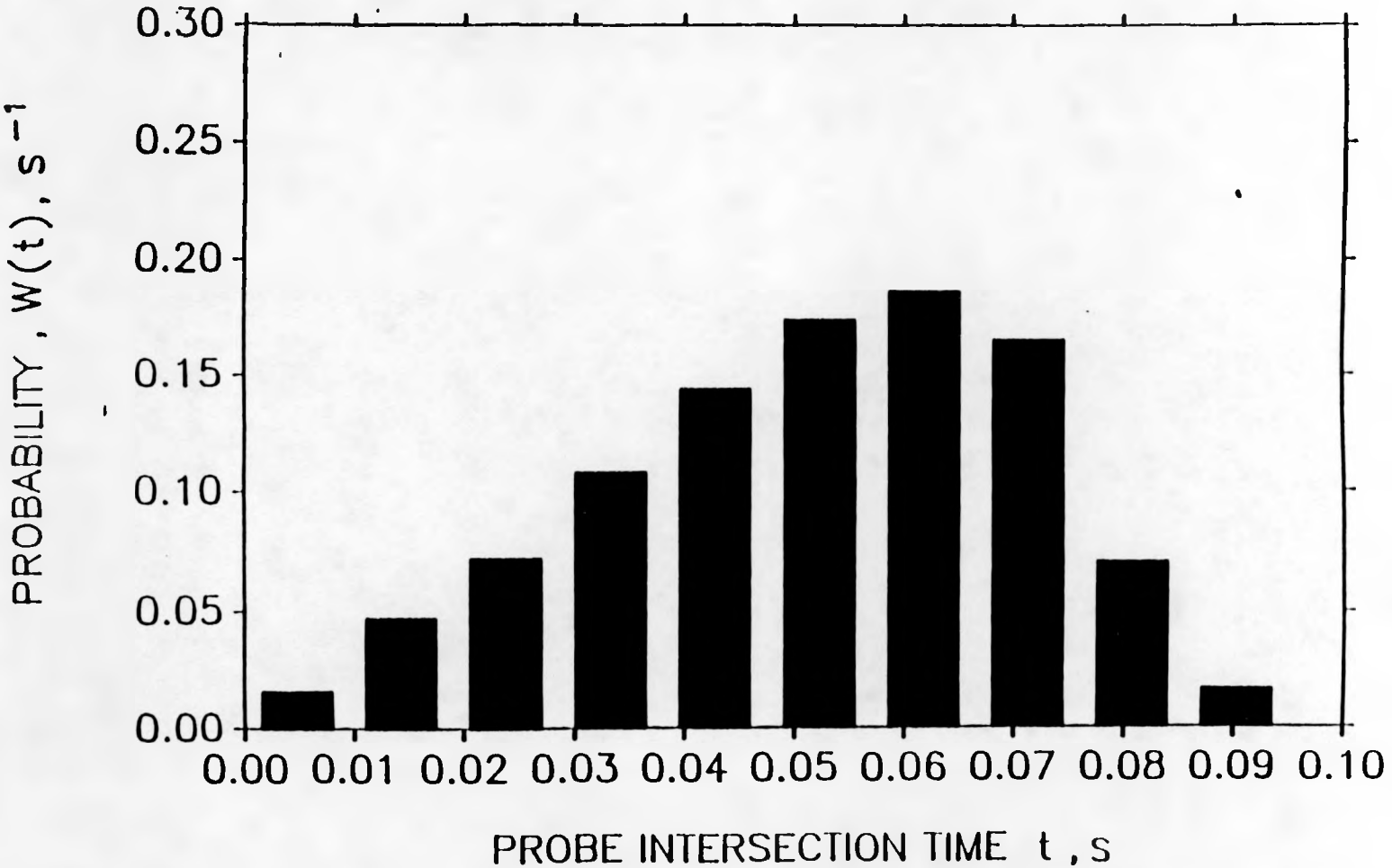

Figure 9.5a Triangular distribution of bubble sizes used in the study of the back transformation method. Distribution of time intervals obtained by Monte Carlo simulation from the distribution of bubble sizes shown by the broken line in (b) [5000 bubbles were used]

Figure 9.5b Comparison of the back transformed distribution of bubble sizes with the true distribution.

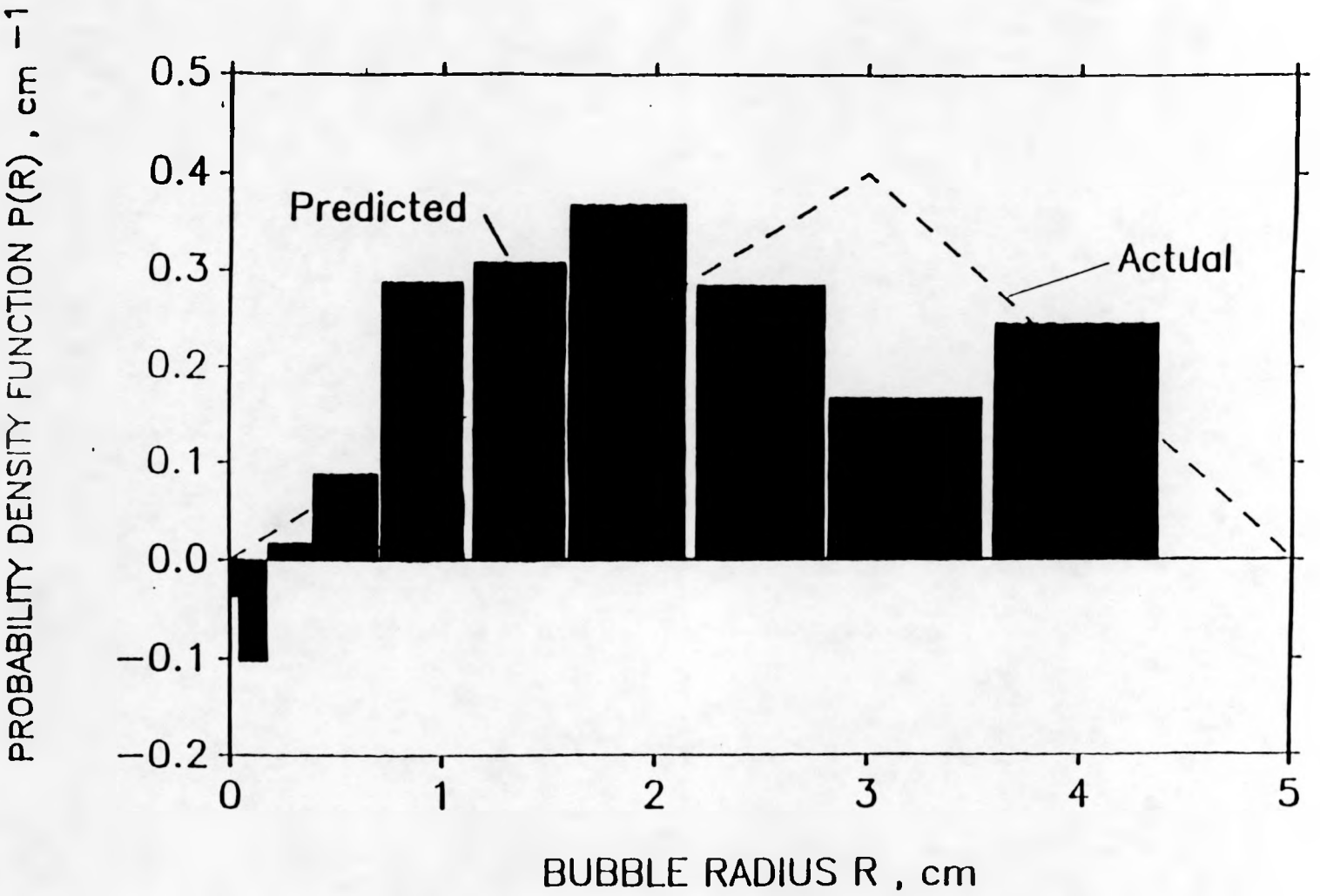

Figure 9.6a Comparison of the back transformed bubble size distribution from the distribution of time intervals with the true bubble size distribution a) 100 bubbles and 10 intervals. Instabilities demonstrate that there are too many intervals used for the number of measurements taken.

Figure 9.6b Instability increases when the number of intervals is doubled to 20, even when there are 1000 bubbles used in the simulation.

APPENDIX A

Direct pressure traces recorded on the Hewlett Packard Measurements Plotting System model 7090A using distributor #2 and pressure transducer A and DSPP with h = 0.5 inches the traces represent a the output voltage from the pressure transducer versus time where 1V ≅ .465 inches of water

DISTRIBUTOR NUMBER 2 .5 INCH PROBE
6 INCH BED

DATA FILE NUMBER	PROBE HEIGHT (INCHES)	PROBE INTRUSION (INCHES)	GAS FLOW RATE (CFM)	INLET PRESSURE (PSI)	GAS FLOW RATE (SCFM)
G1	1.5	2.75	39	0	39
G2	1.5	2.75	50	1	52
G3	1.5	1.875	39	0	39
G4	1.5	1.875	50	1	52
G5	1.5	1.125	39	0	39
G6	1.5	1.125	50	1	52
G7	3.625	2.75	39	0	39
G8	3.625	2.75	50	1	52
G9	3.625	1.875	39	0	39
G10	3.625	1.875	50	1	52
G11	3.625	1.125	39	0	39
G12	3.625	1.125	50	1	52
G13	5.5	2.75	39	0	39
G14	5.5	2.75	50	1	52
G15	5.5	1.875	39	0	39
G16	5.5	1.875	50	1	52
G17	5.5	1.125	39	0	39
G18	5.5	1.125	50	1	52

DISTRIBUTOR NUMBER 2 .5 INCH PROBE
12 INCH BED

DATA FILE NUMBER	PROBE HEIGHT (INCHES)	PROBE INTRUSION (INCHES)	GAS FLOW RATE (CFM)	INLET PRESSURE (PSI)	GAS FLOW RATE (SCFM)
G19	1.5	2.75	39	0	39
G20	1.5	2.75	50	1.5	52
G21	1.5	1.875	39	0	39
G22	1.5	1.875	50	1.5	52
G23	1.5	1.125	39	0	39
G24	1.5	1.125	50	1.5	52
G25	6.75	2.75	39	0	39
G26	6.75	2.75	50	1.5	52
G27	6.75	1.875	39	0	39
G28	6.75	1.875	50	1.5	52
G29	6.75	1.125	39	0	39
G30	6.75	1.125	50	1.5	52
G31	10.75	2.75	39	0	39
G32	10.75	2.75	50	1.5	52
G33	10.75	1.875	39	0	39
G34	10.75	1.875	50	1.5	52
G35	10.75	1.125	39	0	39
G36	10.75	1.125	50	1.5	52

DISTRIBUTOR NUMBER 2 .5 INCH PROBE
24 INCH BED

DATA FILE NUMBER	PROBE HEIGHT (INCHES)	PROBE INTRUSION (INCHES)	GAS FLOW RATE (CFM)	INLET PRESSURE (PSI)	ADJUSTED GAS FLOW RATE SCFM
G37	1.5	2.75	39	1	40
G38	1.5	2.75	50	2	53
G39	1.5	1.875	39	1	40
G40	1.5	1.875	50	2	53
G41	1.5	1.125	39	1	40
G42	1.5	1.125	50	2	53
G43	11.5	2.75	39	1	40
G44	11.5	2.75	50	2	53
G45	11.5	1.875	39	1	40
G46	11.5	1.875	50	2	53
G47	11.5	1.125	39	1	40
G48	11.5	1.125	50	2	53
G49	22.75	2.75	39	1	40
G50	22.75	2.75	50	2	53
G51	22.75	1.875	39	1	40
G52	22.75	1.875	50	2	53
G53	22.75	1.125	39	1	40
G54	22.75	1.125	50	2	53

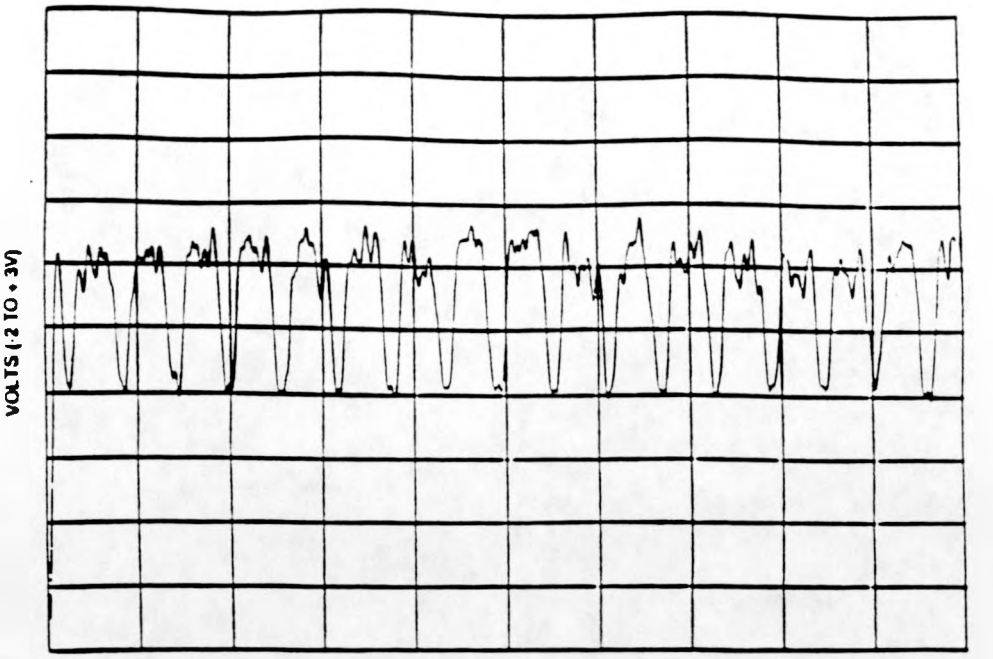

TIME (10 SECOND TRACE)

RUN NO. G1

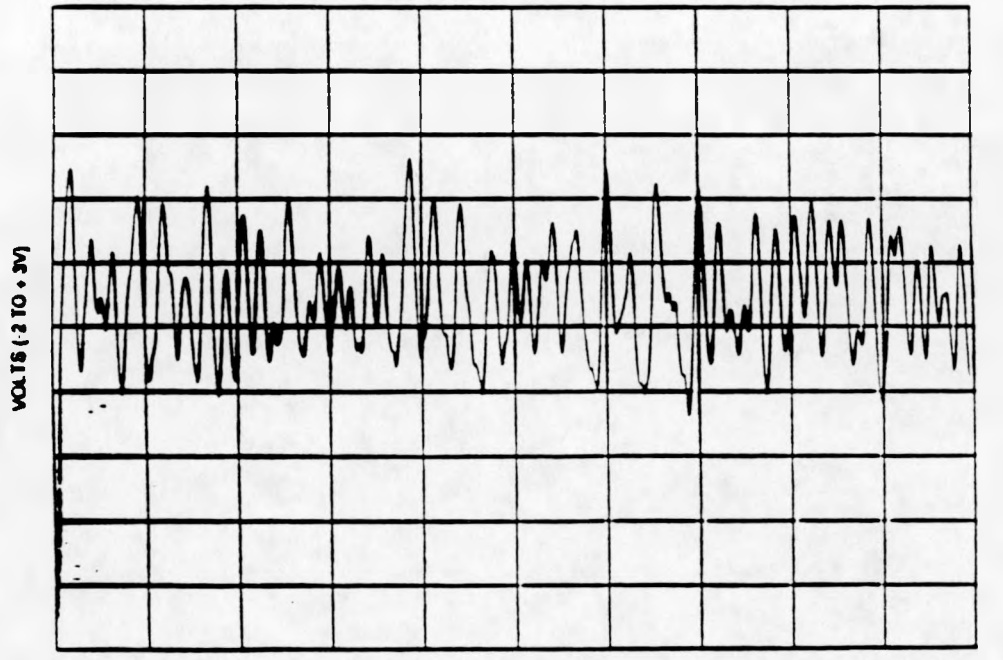

TIME (10 SECOND TRACE)

RUN NO. G2

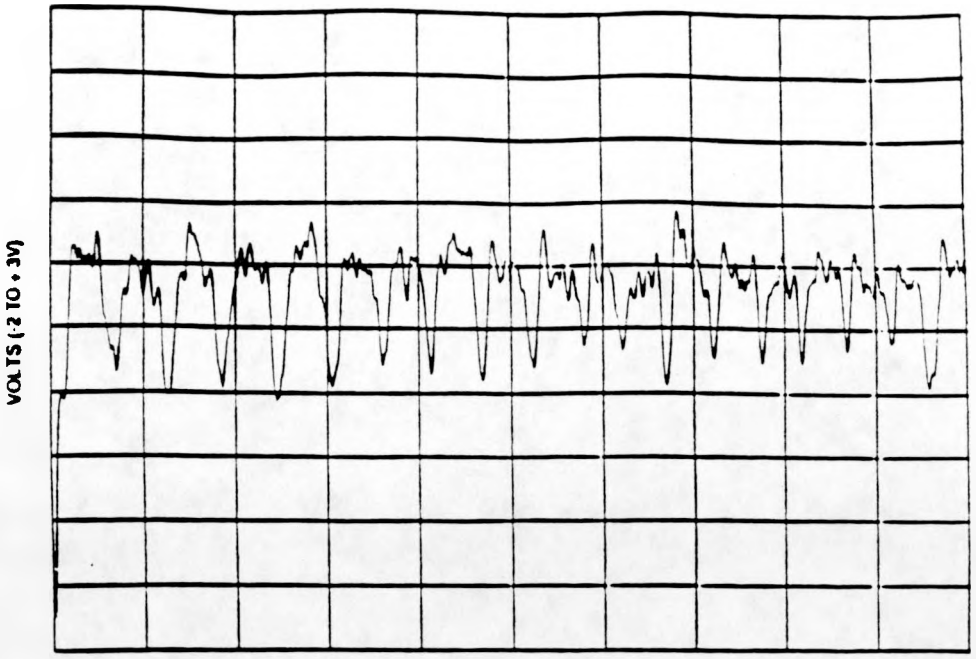

TIME (10 SECOND TRACE)

RUN NO. [illegible]

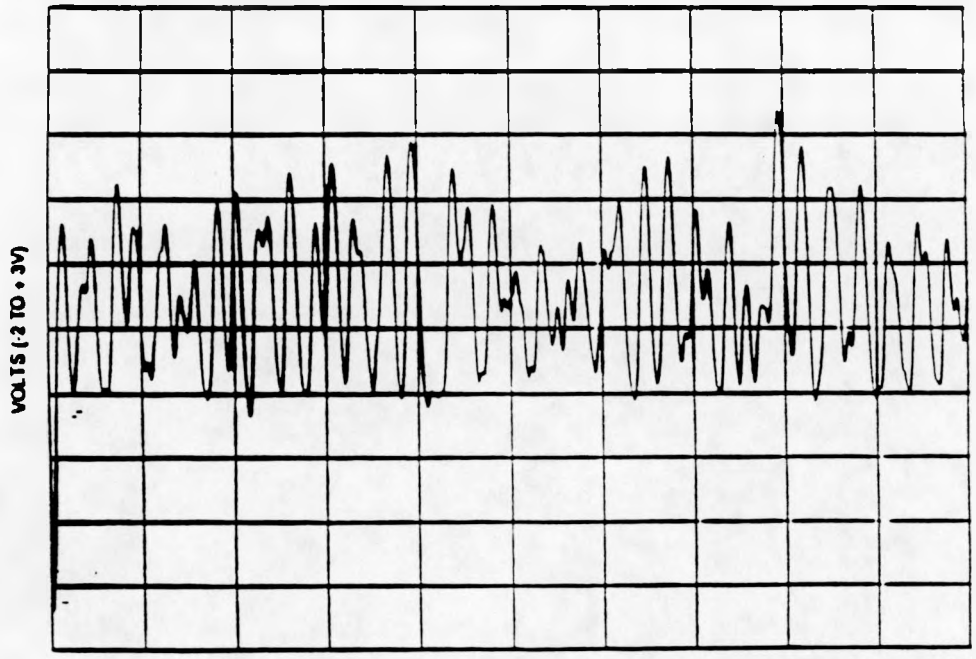

TIME (10 SECOND TRACE)

RUN NO. [illegible]

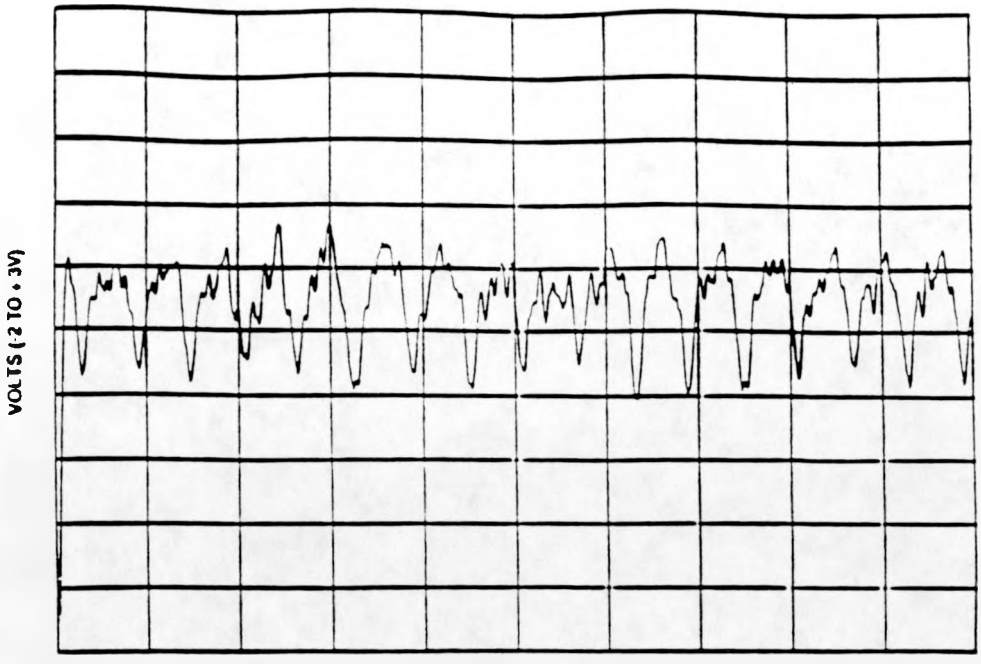

TIME (10 SECOND TRACE)

RUN NO. [illegible]

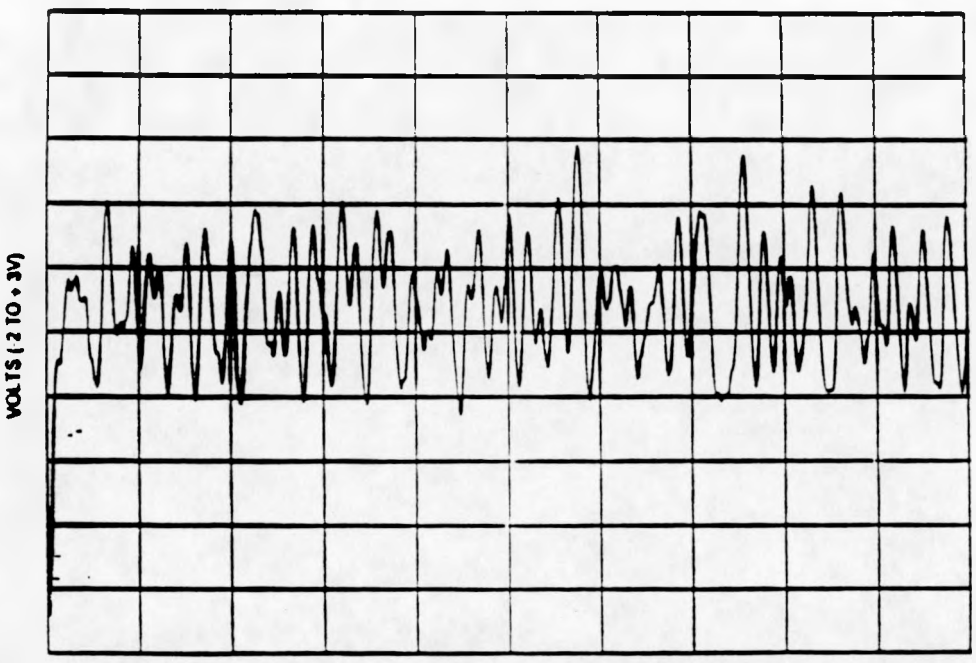

TIME (10 SECOND TRACE)

RUN NO. [illegible]

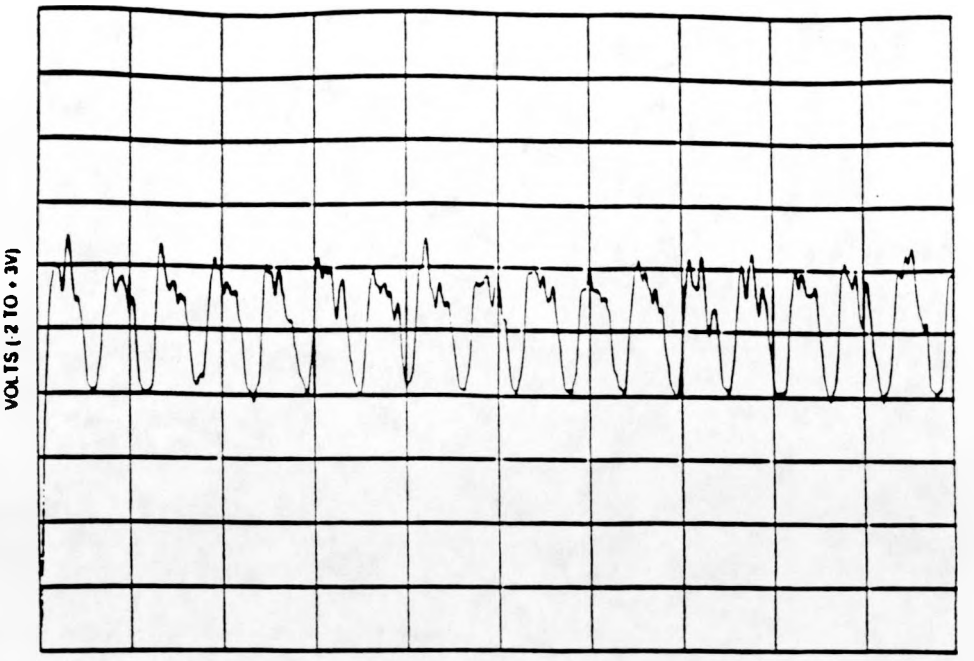
VOLTS (-2 TO +3V)
TIME (10 SECOND TRACE)
RUN NO.

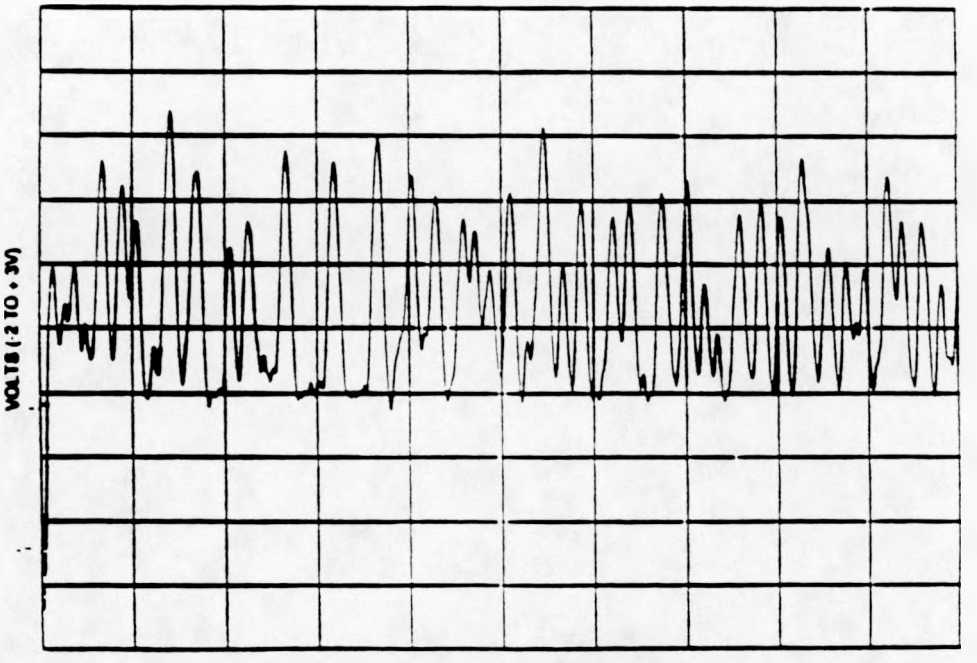
VOLTS (-2 TO +3V)
TIME (10 SECOND TRACE)
RUN NO

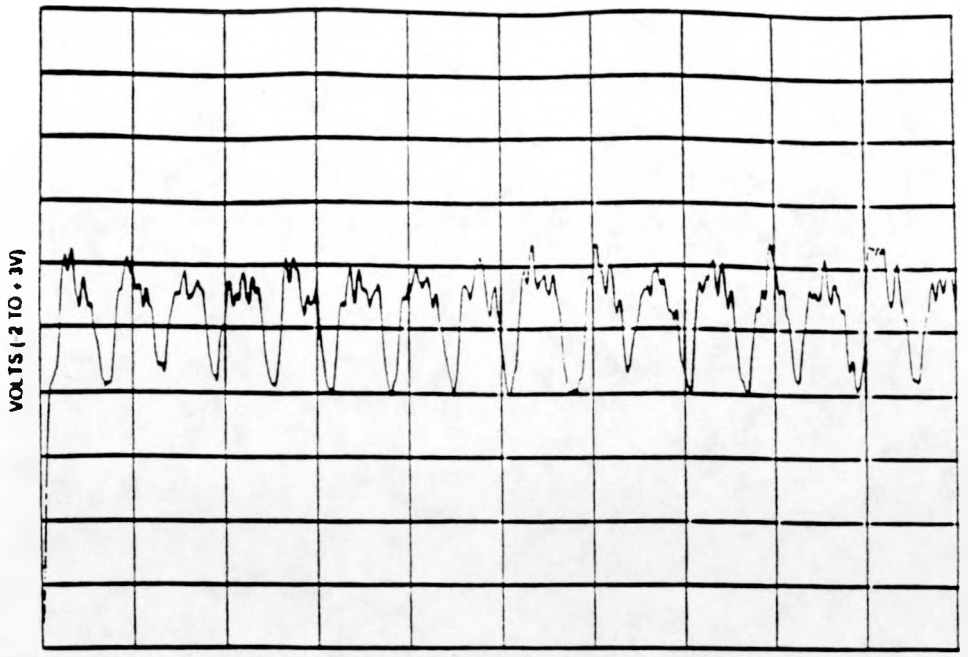

TIME (10 SECOND TRACE)

RUN NO 42

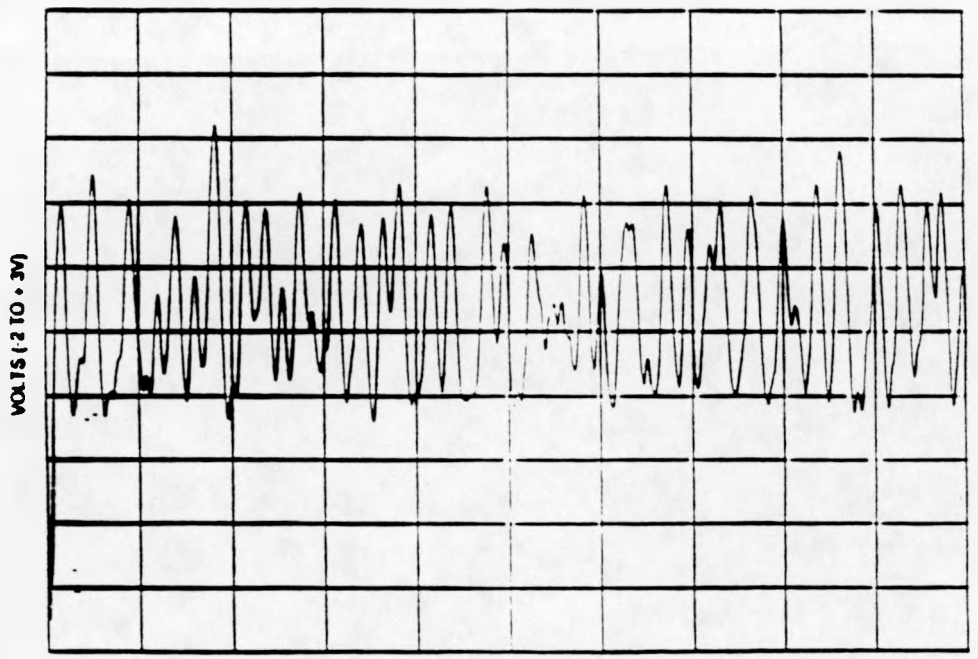

TIME (10 SECOND TRACE)

RUN NO 41

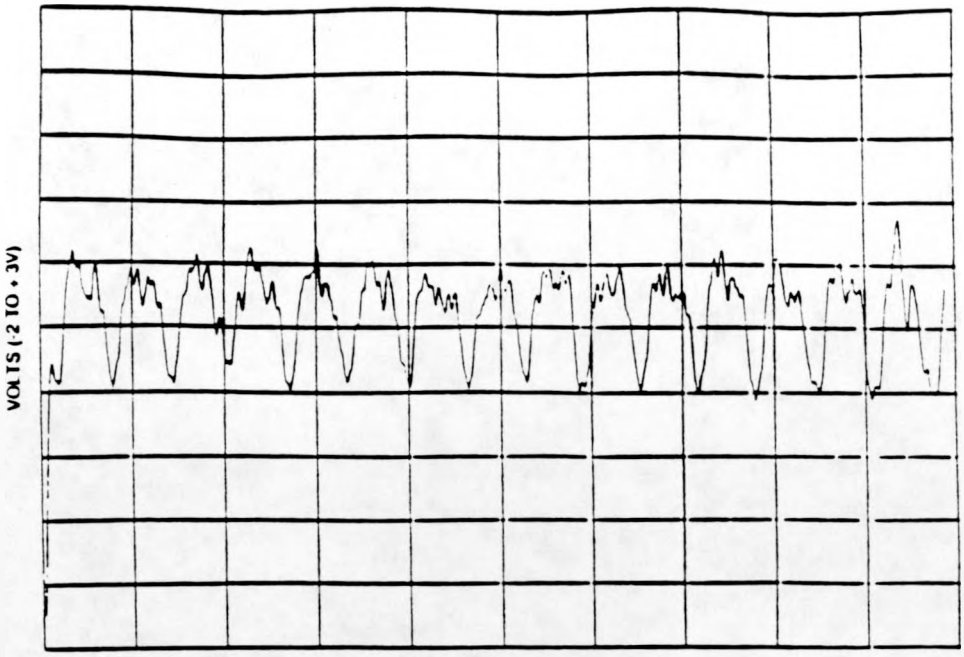
VOLTS (-2 TO +3V)
TIME (10 SECOND TRACE)
RUN NO

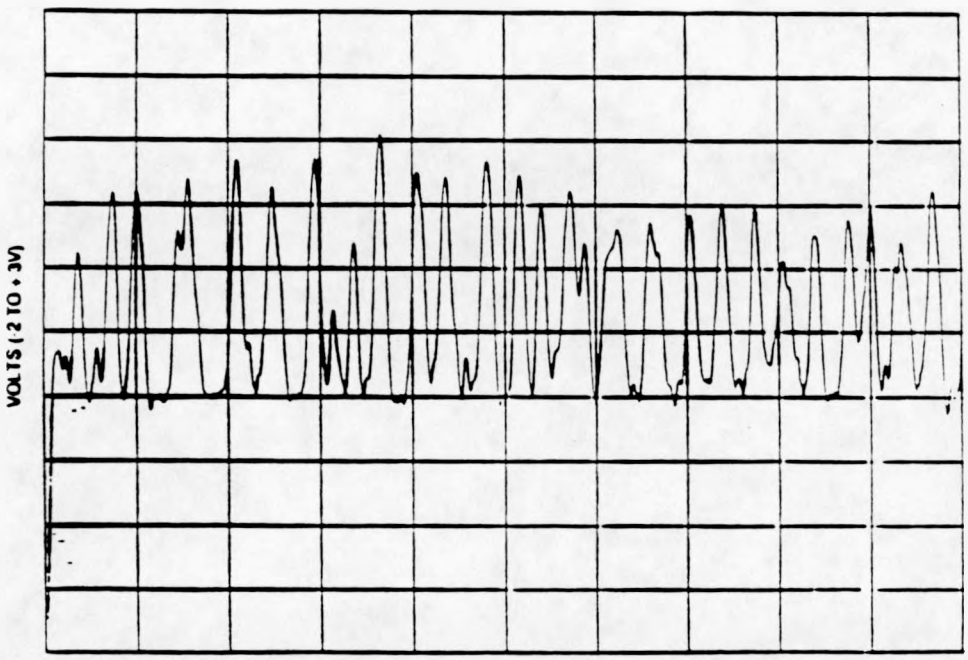
VOLTS (-2 TO +3V)
TIME (10 SECOND TRACE)
RUN NO

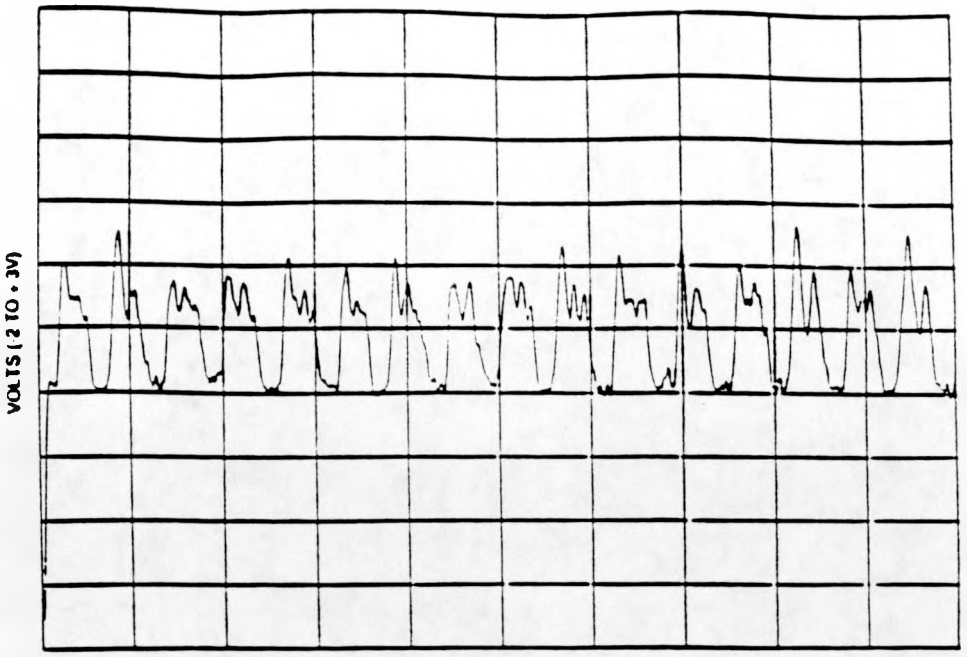

TIME (10 SECOND TRACE)

RUN NO 11

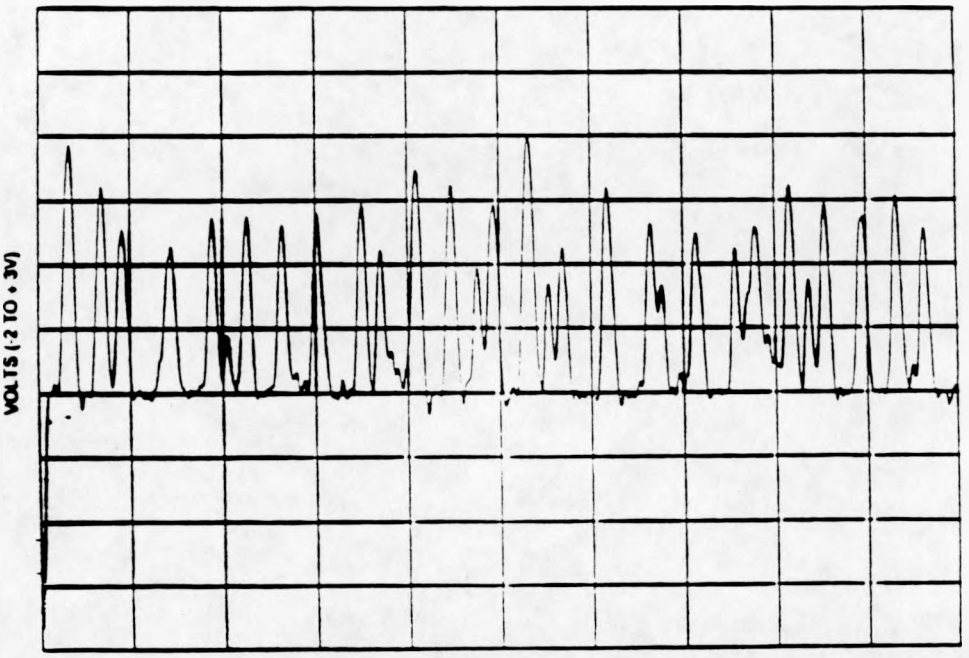

TIME (10 SECOND TRACE)

RUN NO 11.

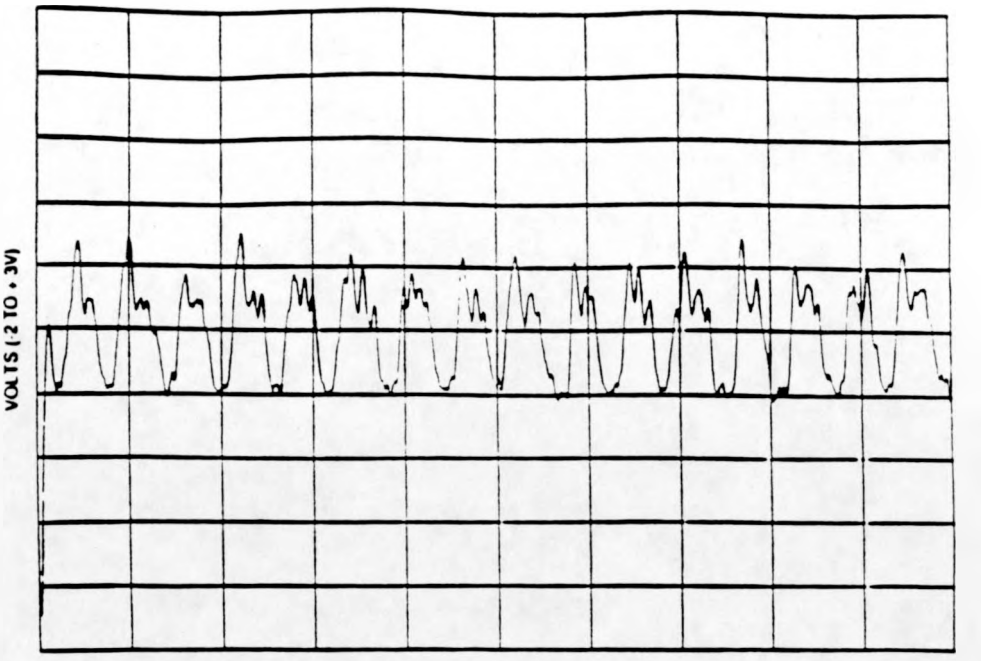

TIME (10 SECOND TRACE)

RUN NO [illegible]

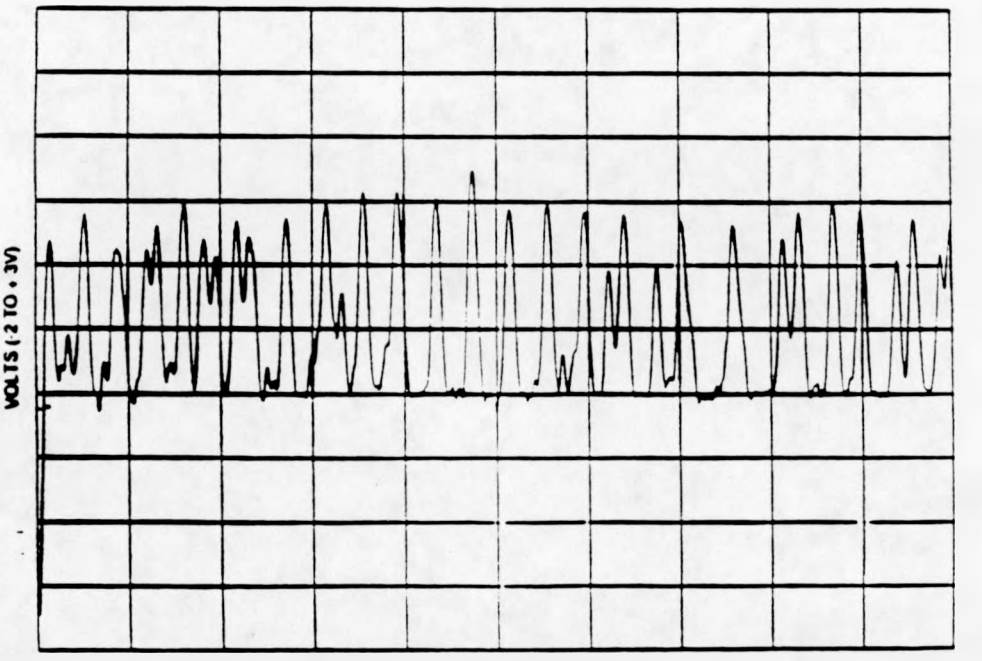

TIME (10 SECOND TRACE)

RUN NO [illegible]

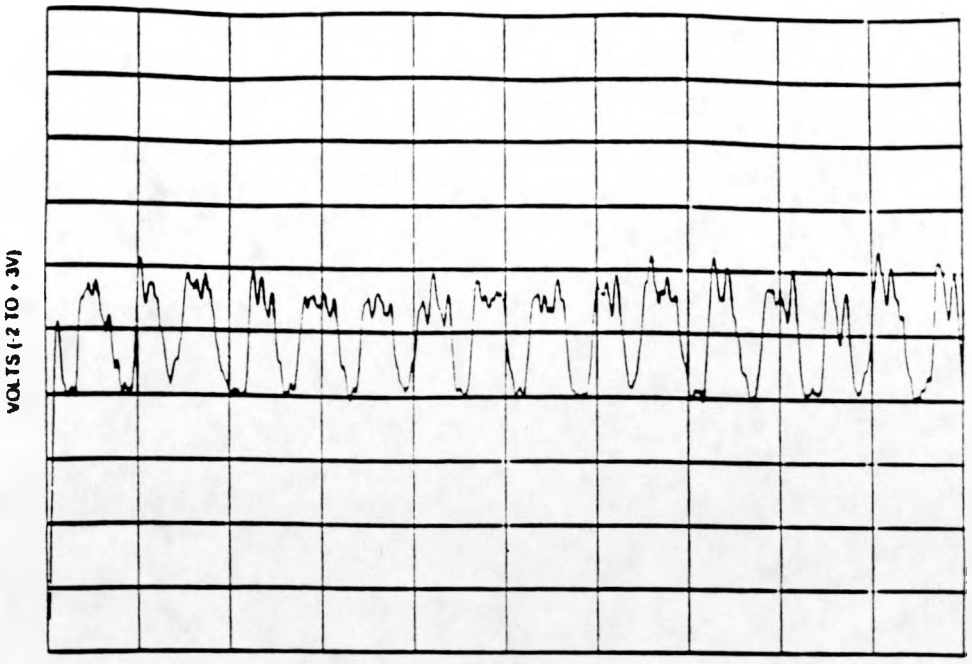

RUN NO 617

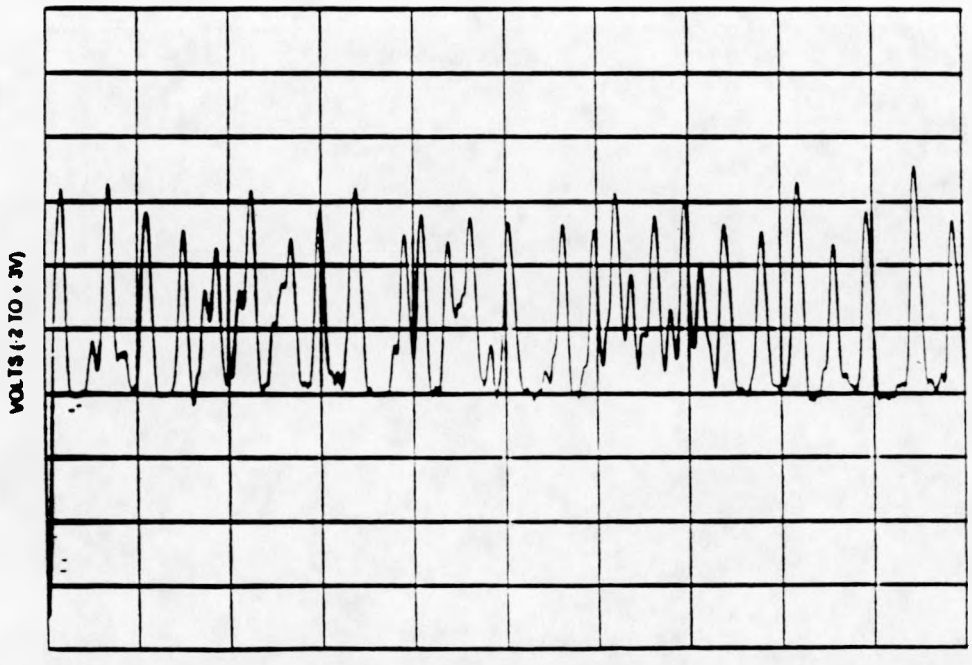

RUN NO 618

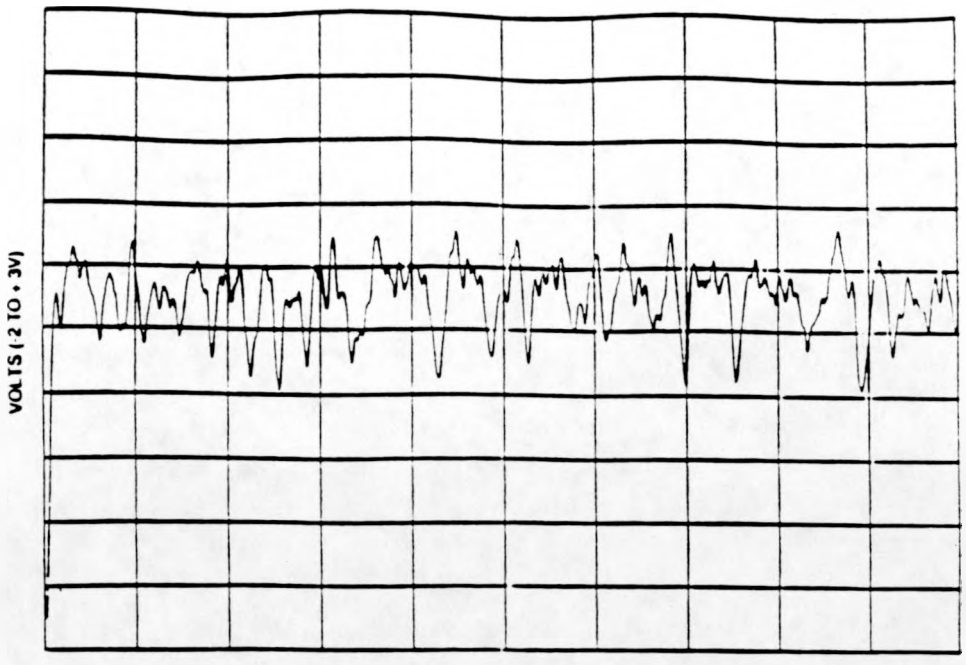
VOLTS (-2 TO +3V)
TIME (10 SECOND TRACE)

RUN NO [illegible]

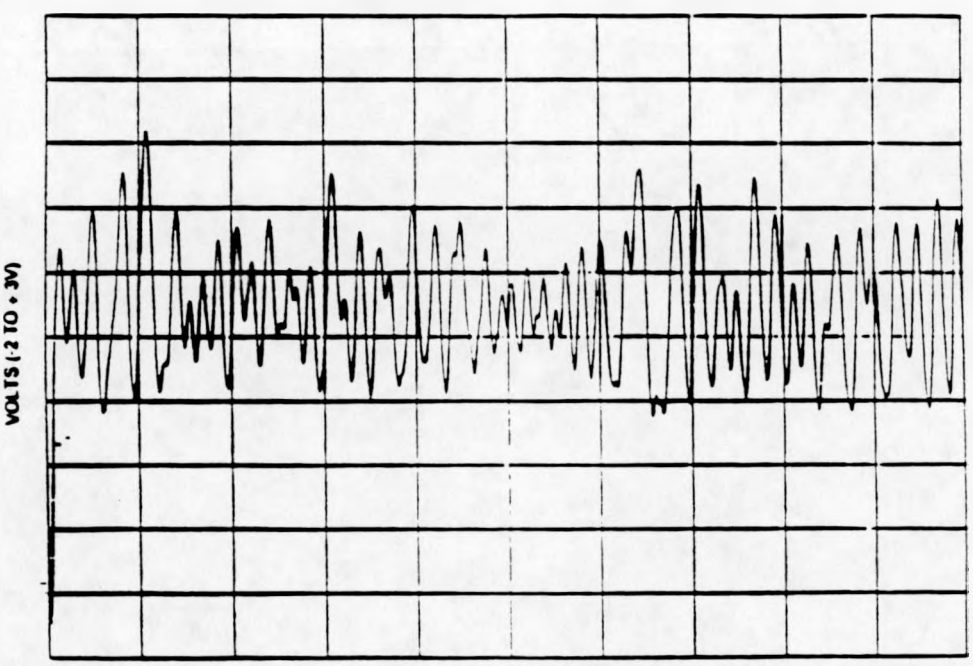
VOLTS (-2 TO +3V)
TIME (10 SECOND TRACE)

RUN NO [illegible]

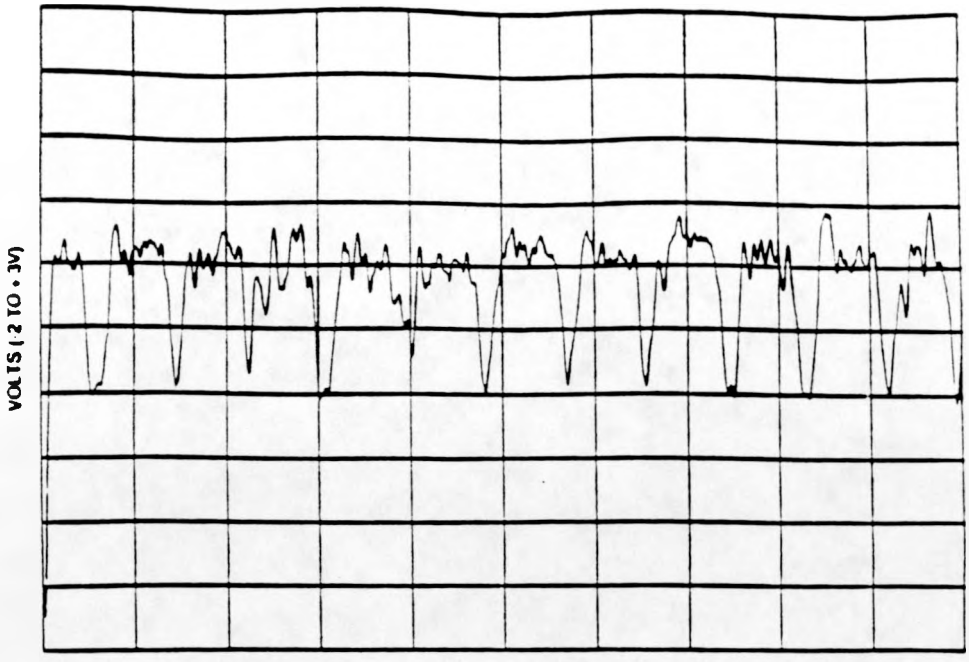

TIME (10 SECOND TRACE)

RUN NO. G21

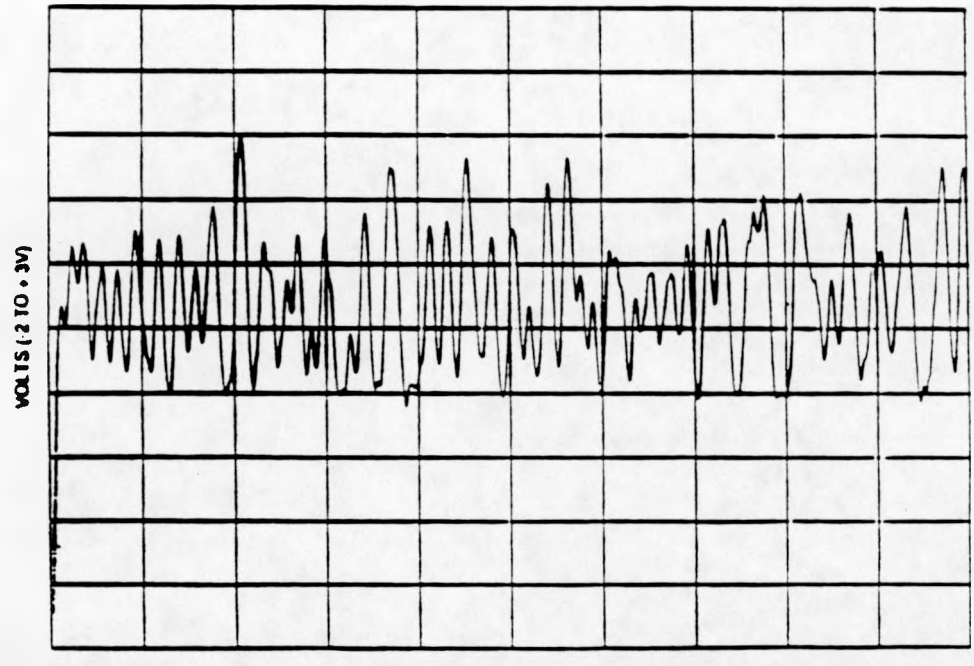

TIME (10 SECOND TRACE)

RUN NO. G22

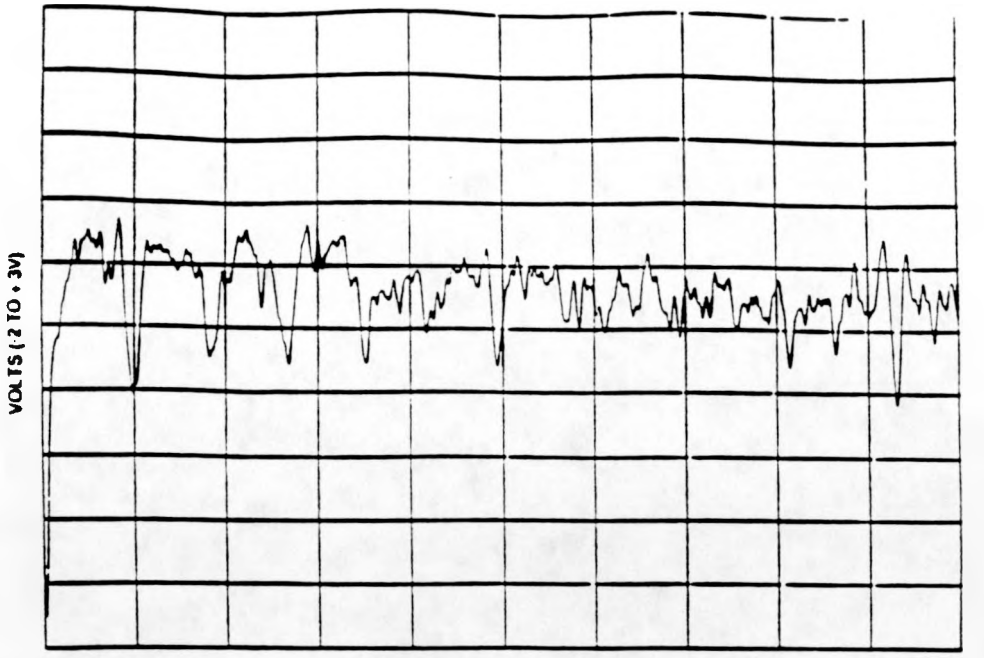

TIME (10 SECOND TRACE)

RUN NO [illegible]

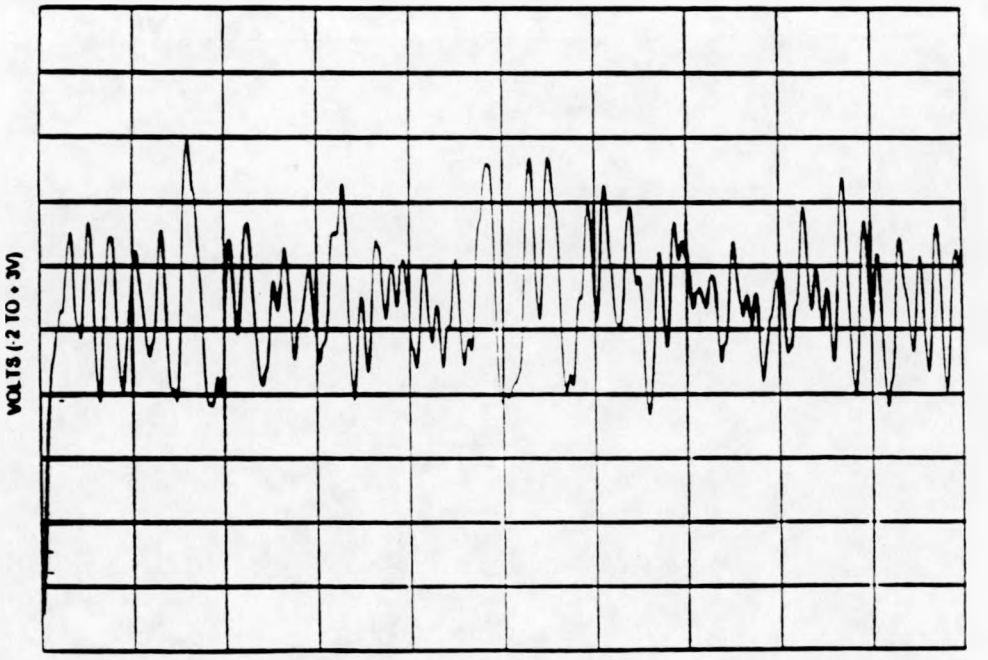

TIME (10 SECOND TRACE)

RUN NO [illegible]

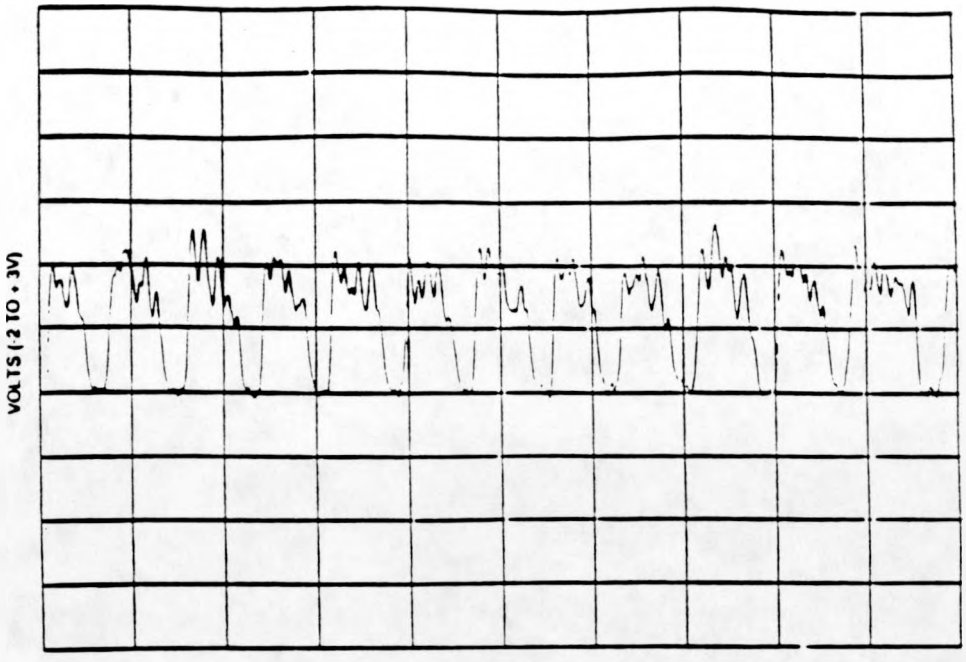

TIME (10 SECOND TRACE)

RUN NO. [illegible]

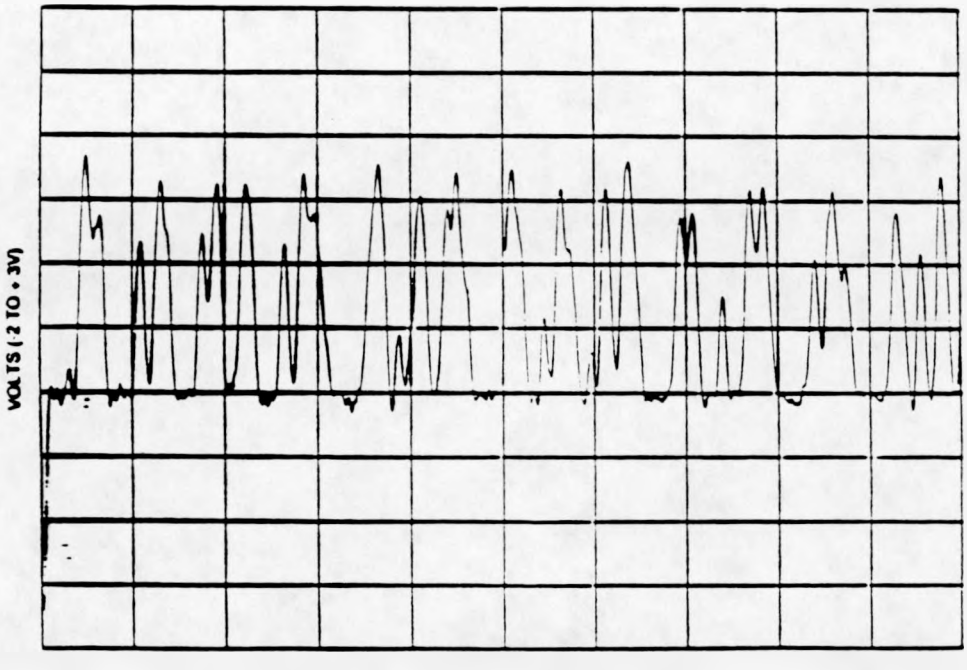

TIME (10 SECOND TRACE)

RUN NO. [illegible]

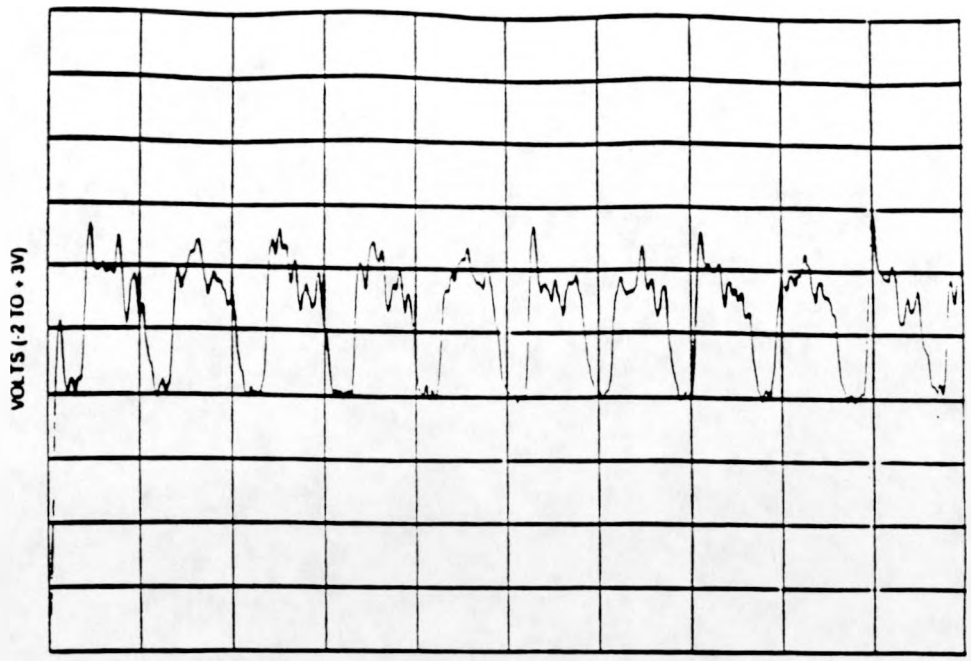

TIME (10 SECOND TRACE)

RUN NO 627

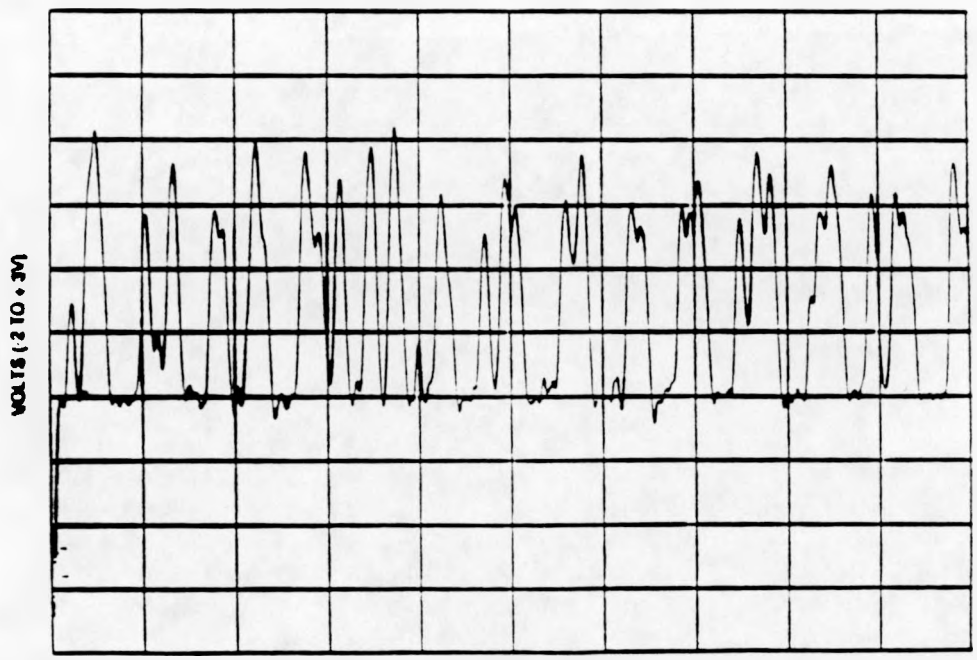

TIME (10 SECOND TRACE)

RUN NO 628

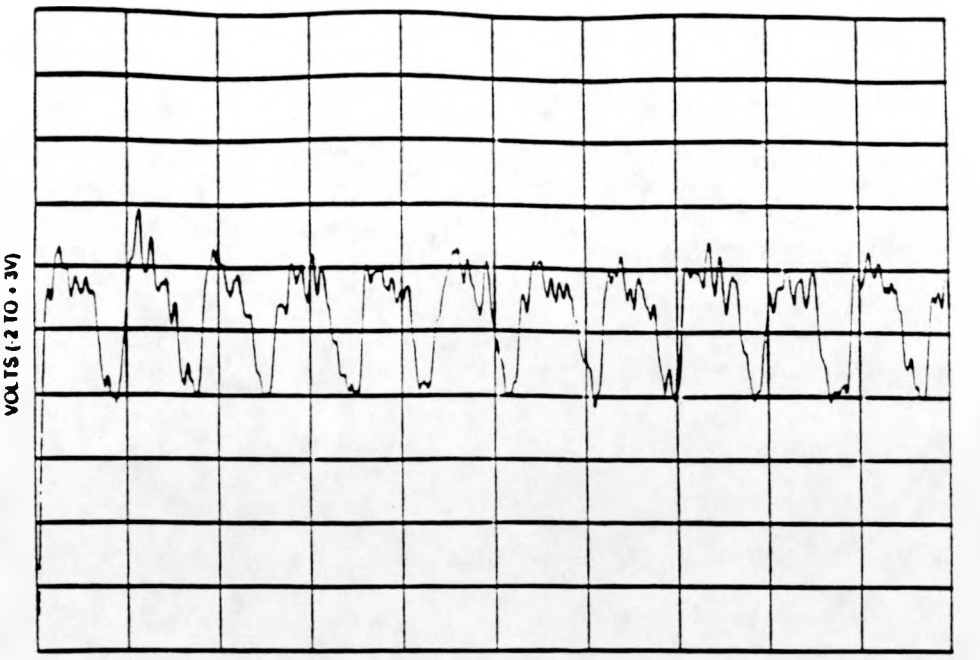
VOLTS (-2 TO +3V)
TIME (10 SECOND TRACE)
RUN NO 629

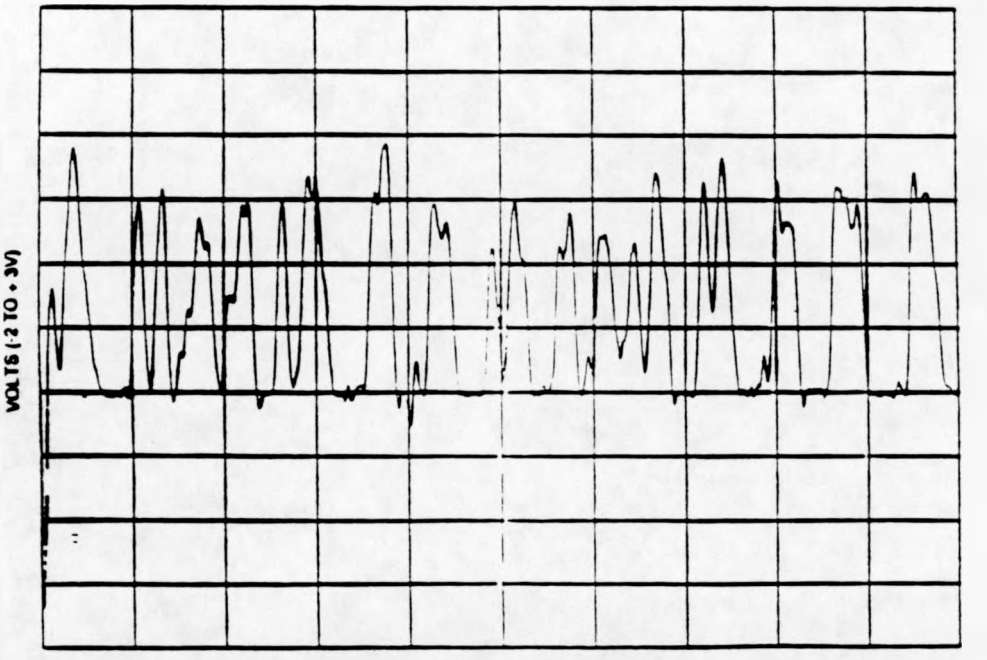
VOLTS (-2 TO +3V)
TIME (10 SECOND TRACE)
RUN NO

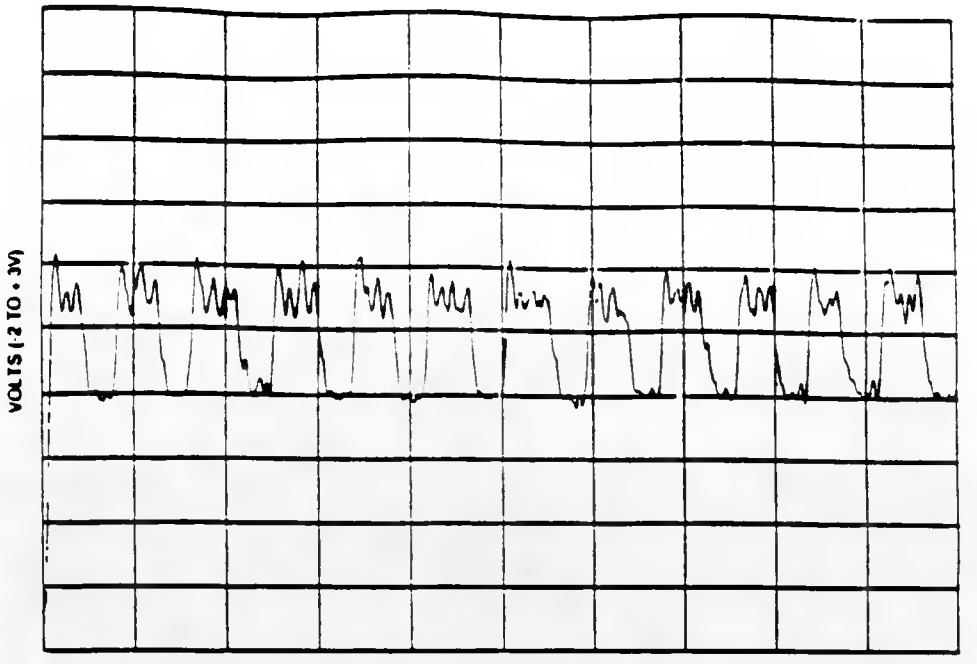

TIME (10 SECOND TRACE)

RUN NO. 031

TIME (10 SECOND TRACE)

RUN NO. 032

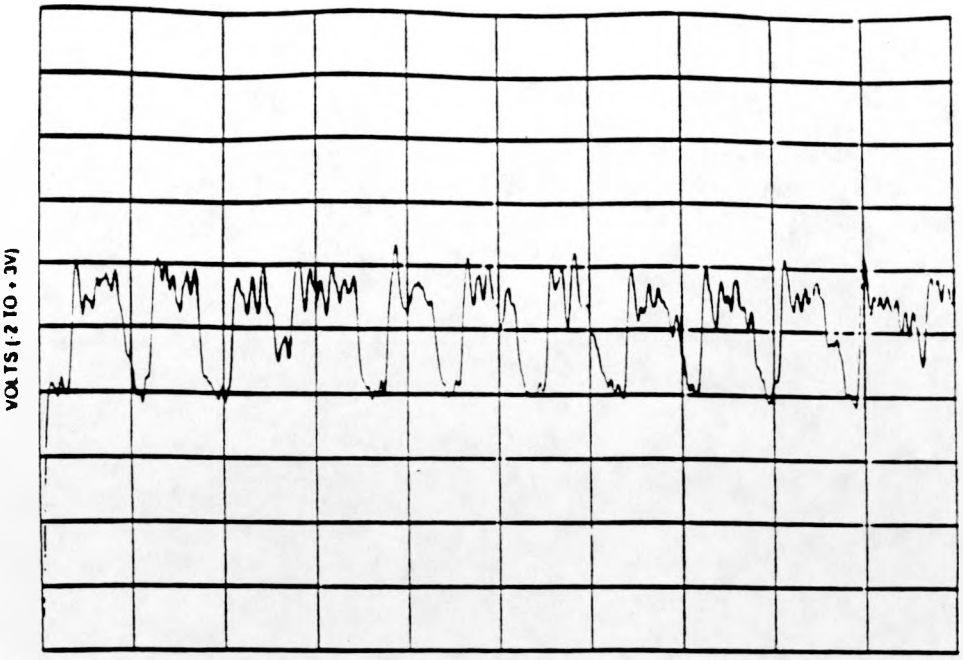
VOLTS (-2 TO +3V)
TIME (10 SECOND TRACE)
RUN NO. 011

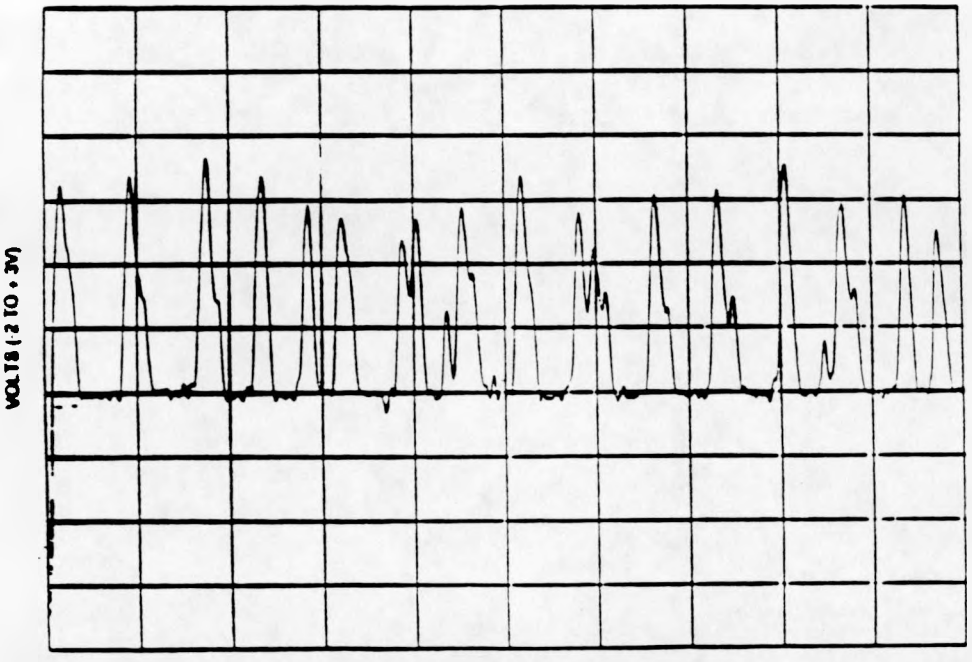
VOLTS (-2 TO +3V)
TIME (10 SECOND TRACE)
RUN NO

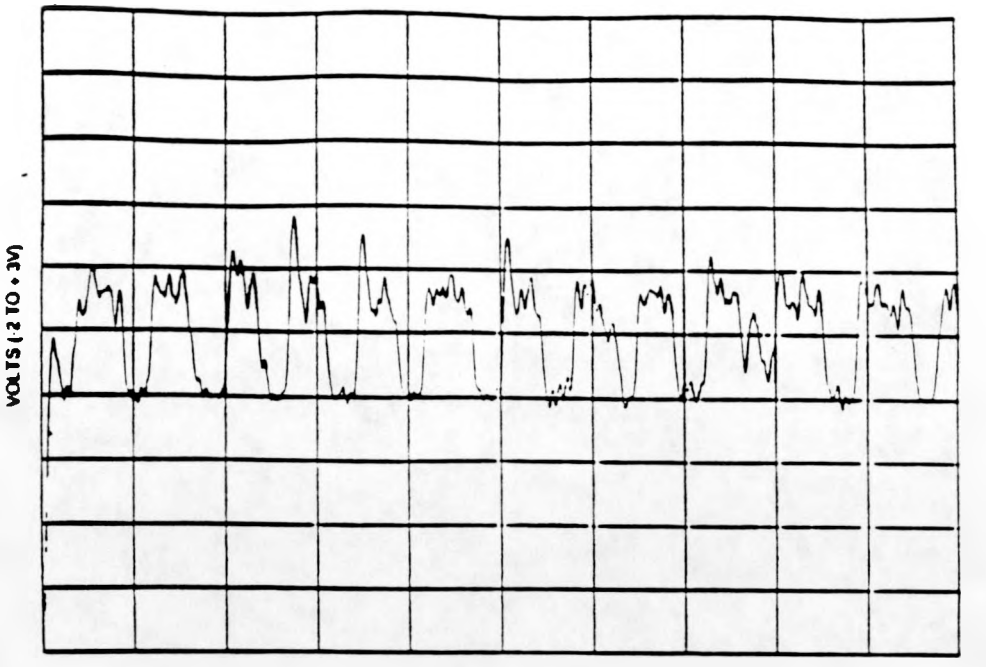

TIME (10 SECOND TRACE)

RUN NO [illegible]

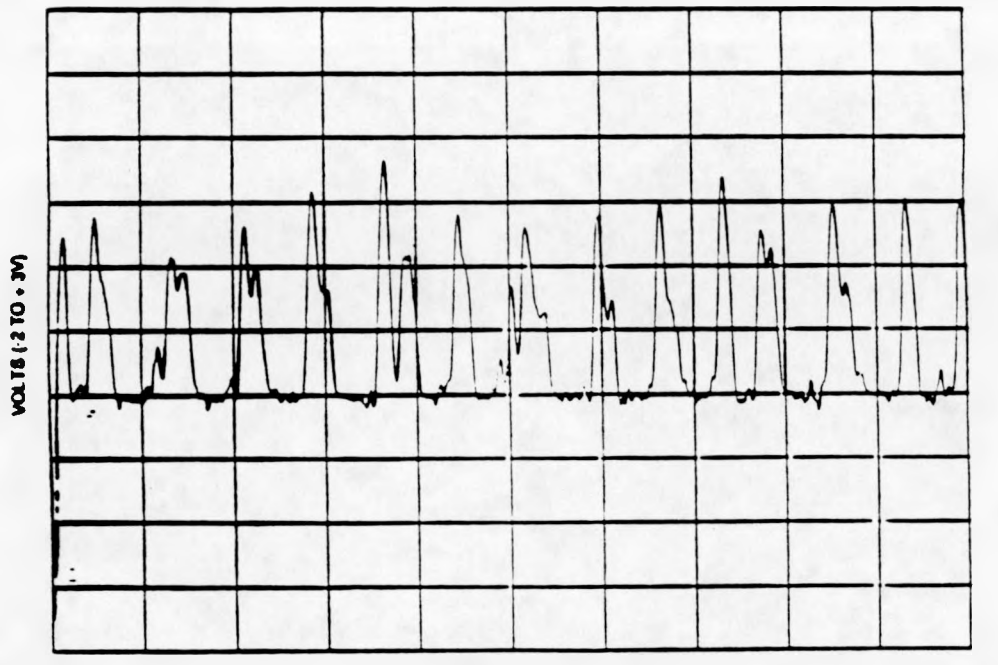

TIME (10 SECOND TRACE)

RUN NO [illegible]

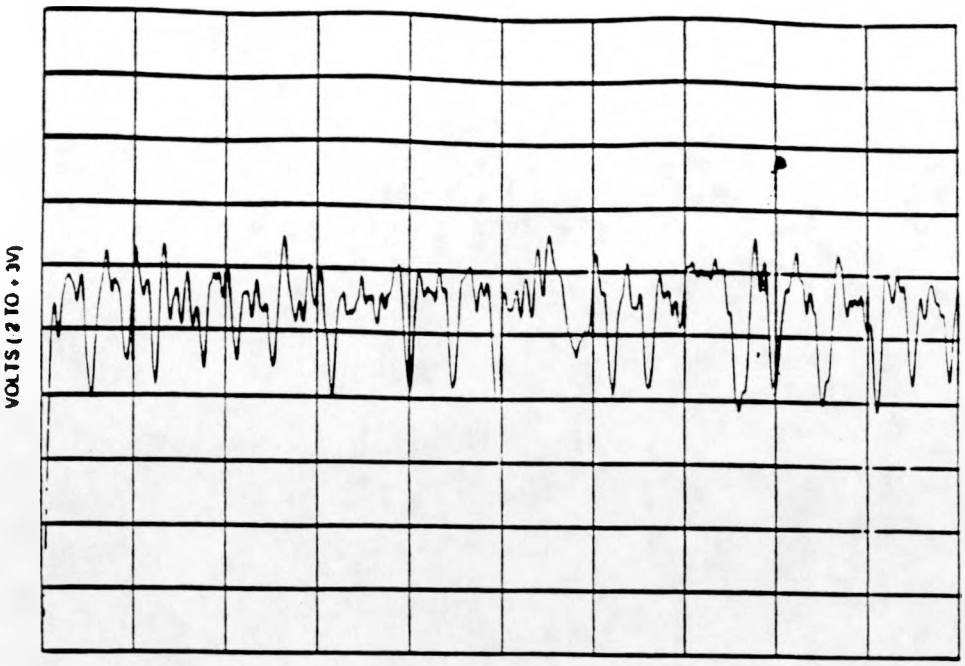

TIME (10 SECOND TRACE)

RUN NO 031

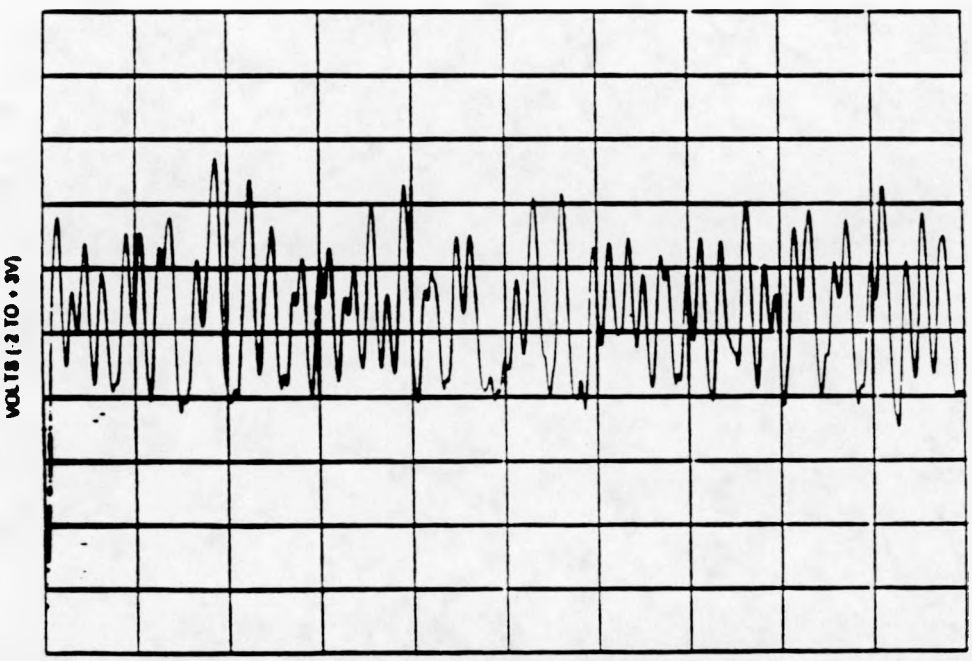

TIME (10 SECOND TRACE)

RUN NO 038

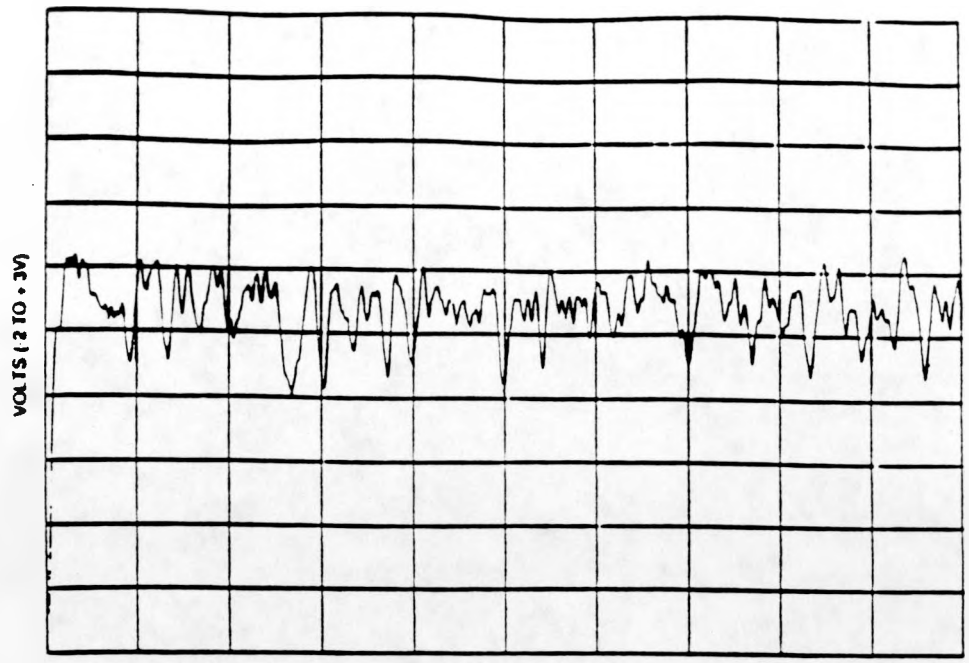
VOLTS (-2 TO +3V)
TIME (10 SECOND TRACE)
RUN NO

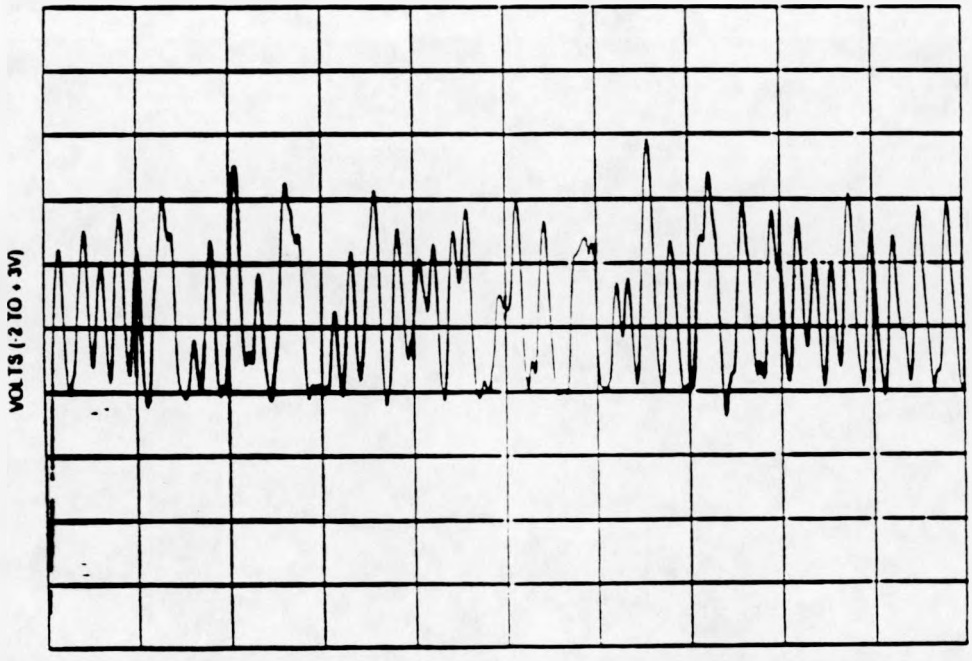
VOLTS (-2 TO +3V)
TIME (10 SECOND TRACE)
RUN NO

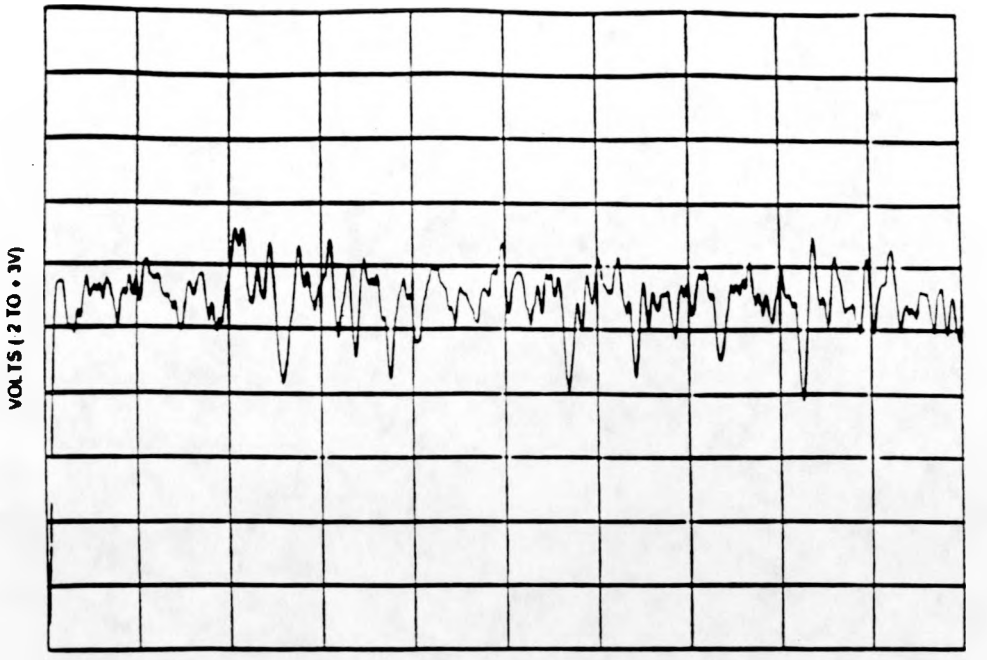

TIME (10 SECOND TRACE)

RUN NO CA1

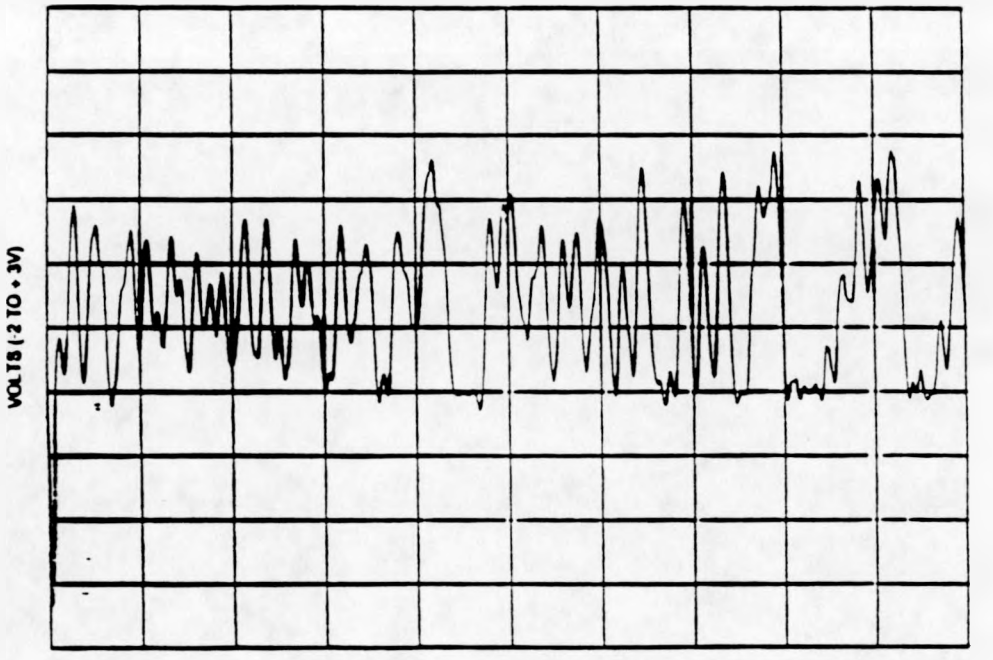

TIME (10 SECOND TRACE)

RUN NO. CA2

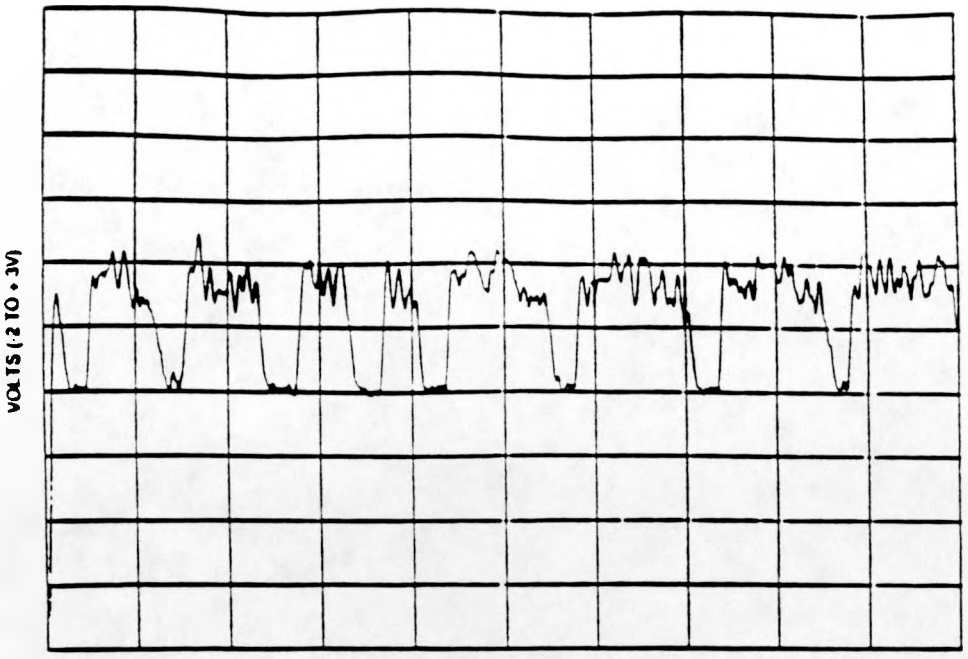
VOLTS (-2 TO +3V)
TIME (10 SECOND TRACE)
RUN NO. C41


VOLTS (-2 TO +3V)
TIME (10 SECOND TRACE)
RUN NO. C44

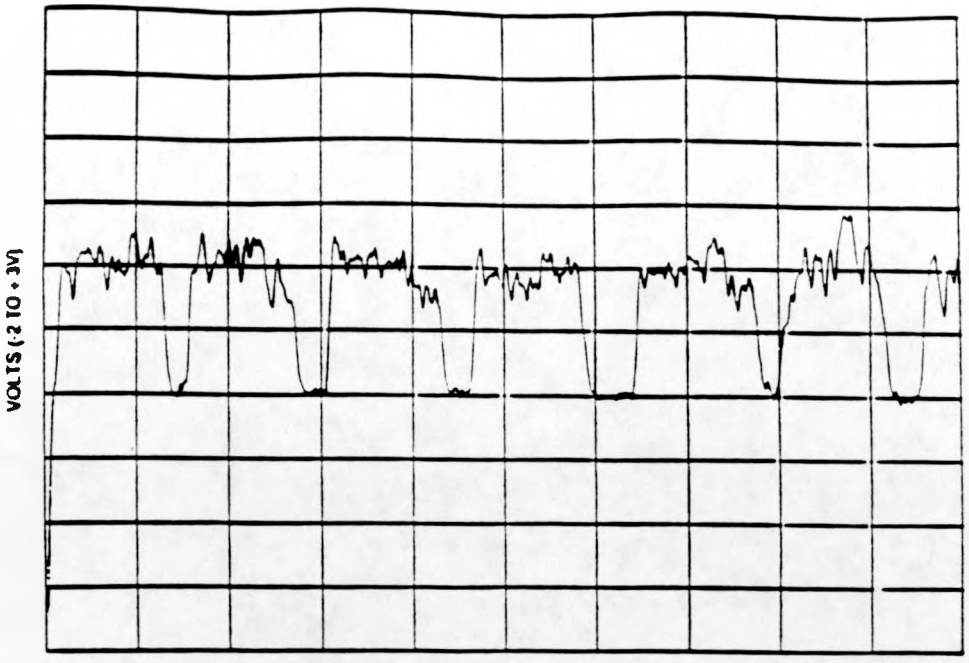

TIME (10 SECOND TRACE)

RUN NO. 084

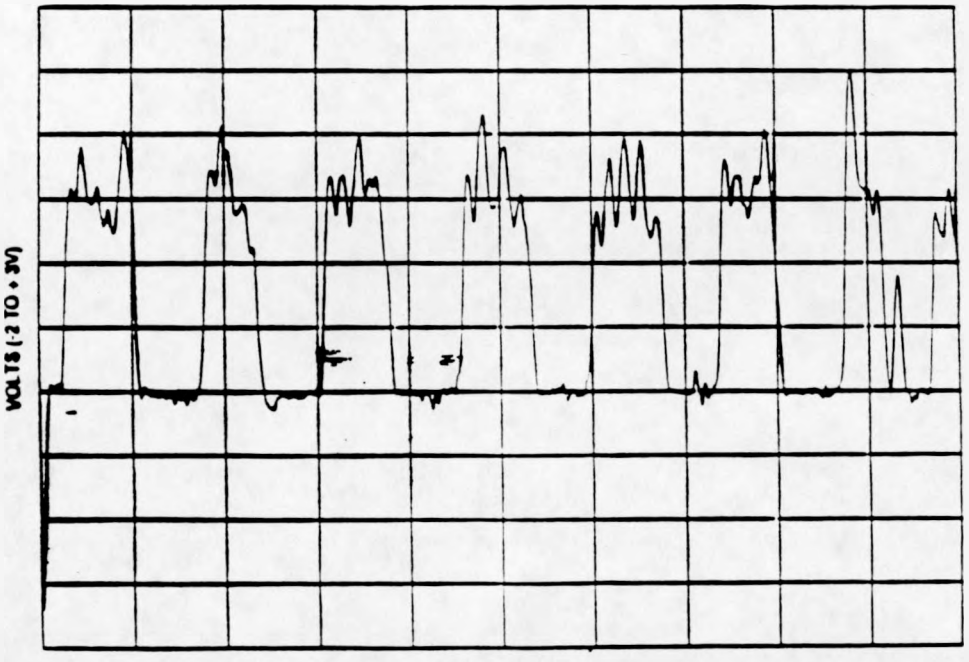

TIME (10 SECOND TRACE)

RUN NO. 086

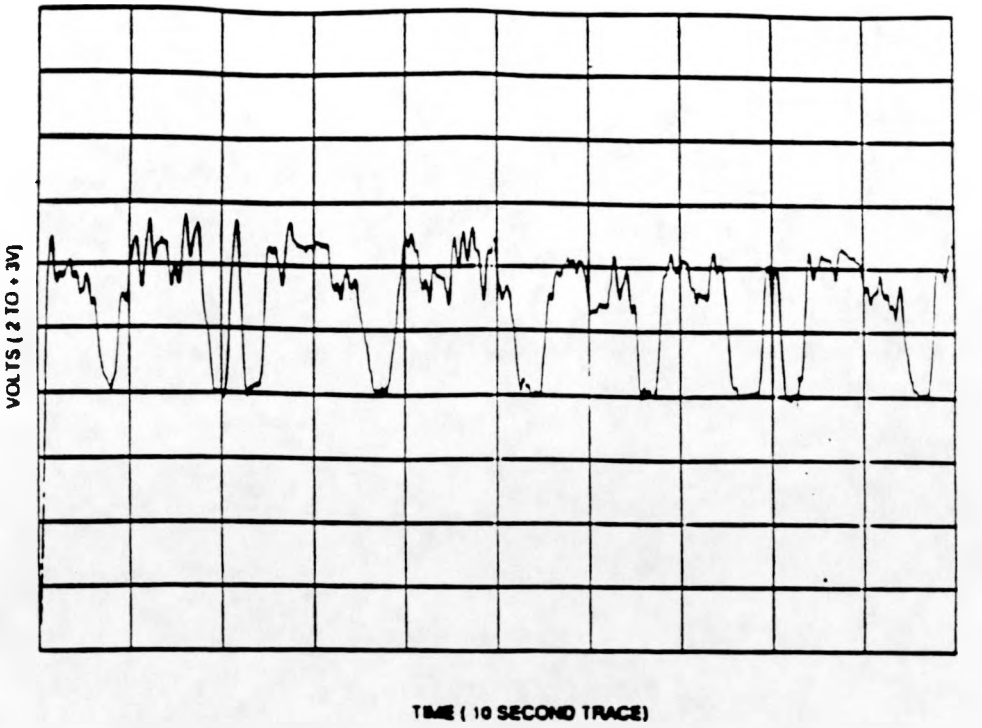
VOLTS (2 TO + 3V)
TIME (10 SECOND TRACE)
RUN NO. CA7

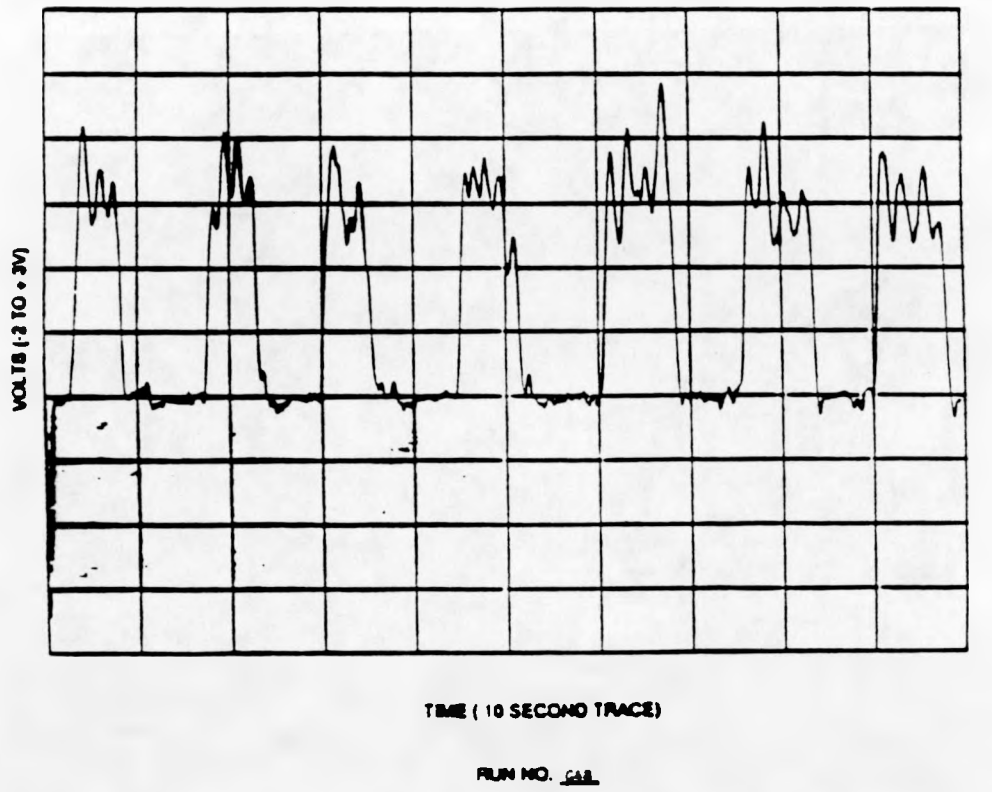
VOLTS (-2 TO + 3V)
TIME (10 SECOND TRACE)
RUN NO. CA8

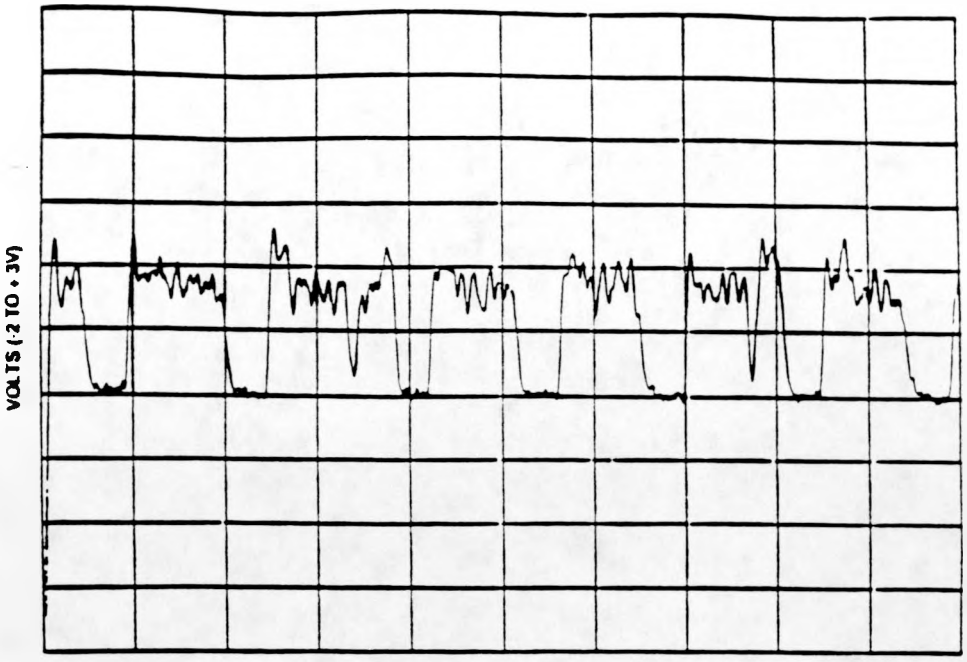
VOLTS (-2 TO +3V)
TIME (10 SECOND TRACE)
RUN NO. CA9


VOLTS (-2 TO +3V)
TIME (10 SECOND TRACE)
RUN NO. CX9

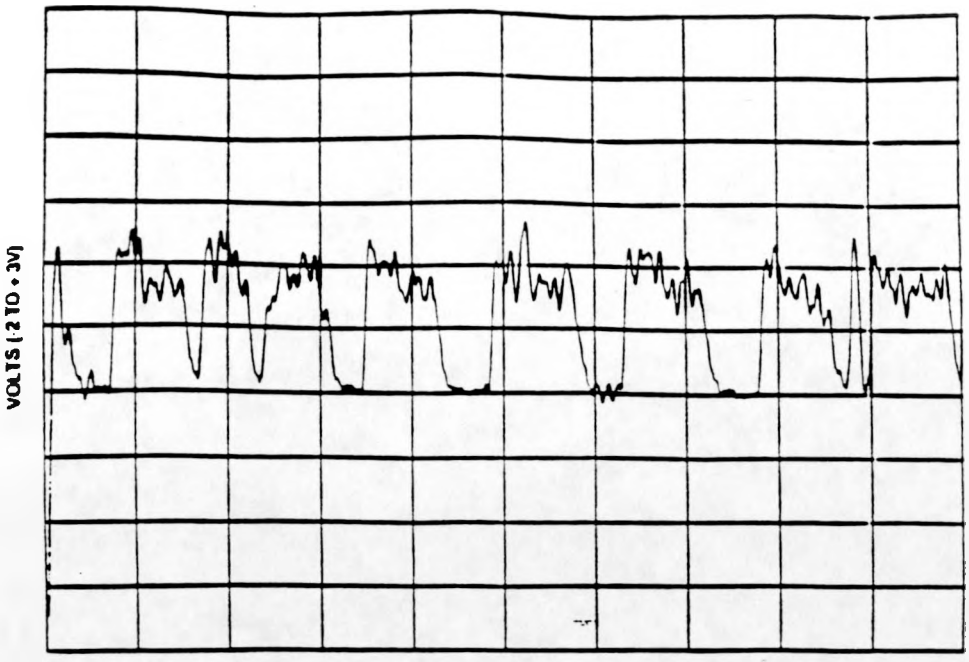

TIME (10 SECOND TRACE)

RUN NO. 531

TIME (10 SECOND TRACE)

RUN NO. 532

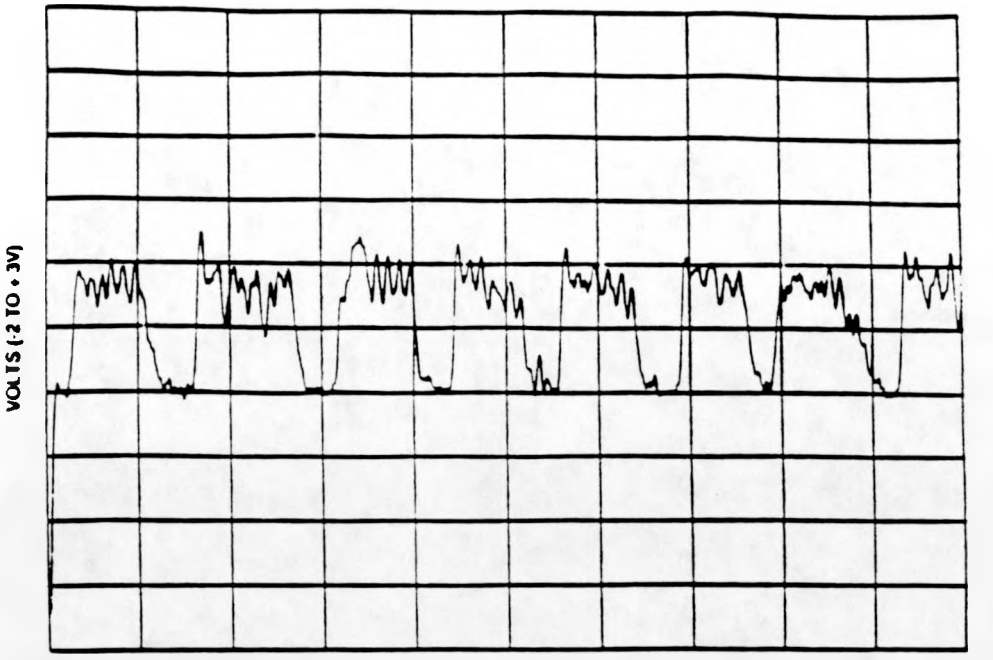
VOLTS (-2 TO + 3V)
TIME (10 SECOND TRACE)
RUN NO. C33

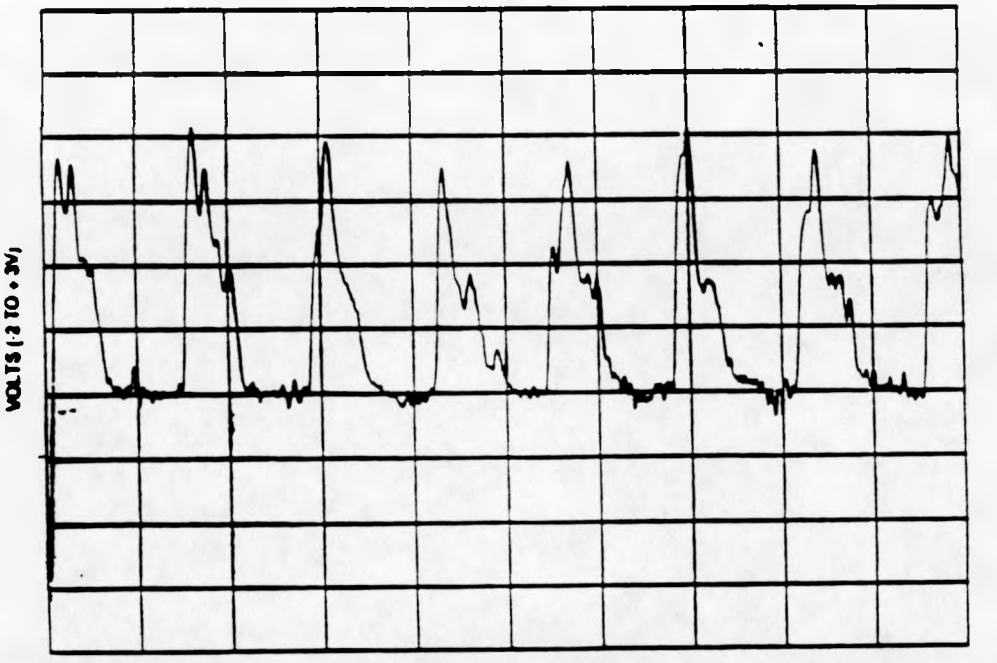
VOLTS (-2 TO + 3V)
TIME (10 SECOND TRACE)
RUN NO. C36

APPENDIX B

Quickbasic 4.5 Autocorrelation Function Program

```
Autocorrelation program to analyze data from a single dual
static pressure probe.
-----------------------------------------------------------------

DEFINT I-L, N, Q                          'Define values as integers
DIM Q(2000), R(2000)                      'Dimensions array for data
                                          'and.autocorrelation function

OPEN "C:\QB4\thesis\FILES.TXT" FOR INPUT AS #1
INPUT #1, NUM
FOR F = 1 TO NUM                          'Loop to retrieve each data
PRINT F
INPUT #1, FILE$                           'file from a text file
OPEN "c:\qb4\thesis\" + FILE$ FOR INPUT AS #2
SUM = 0
FOR J = 1 TO 2000                         'Loop to average data
INPUT #2, Q(J)
SUM = SUM + Q(J)
NEXT J
ave = SUM / 2000
CLOSE #2
rms = 0
FOR J = 1 TO 2000
rms = rms + (Q(J) - ave) * (Q(J) - ave)
NEXT J
QRMS = SQR(rms / 2000)
OPEN "c:\plot\thesis\" + FILE$ + ".DAT" FOR OUTPUT AS #2
                                          'Starting the autocorrelation
N = 2000                                  'Number of samples
M = N / 10      'M = I(max)               'Max lag number
FOR I = 1 TO M                            'Loop to autocorrelate
R(I) = 0
K = (N - I)     'K = J(max)
FOR J = 1 TO K
'Autocorrelation function

R(I) = R(I) + (Q(J) - ave) * (Q(J + I) - ave)

NEXT J
R(I) = R(I) / (N - I)
R(I) = R(I) / ((QRMS) ^ 2)
 PRINT I / 100, R(I)

NEXT I
FOR L = 1 TO M
WRITE #2, L / 100, R(L)                   'Writes to an output file
NEXT L
CLOSE #2
NEXT F
```

APPENDIX C

Quickbasic 4.5 Fast Fourier Transform Program via Quin-Curtis

```
'This program performs a Fast Fourier Transform (called FFT.BAS) on a
'set of data consisting of N equally spaced samples.
'The total number of data points (nd) must be a power of 2.
'In this case the total number was 2000 and the required number
'is 2048 so 48 0's were added to the end of the data set so
'as not to greatly effect the results.

'-------------------------------------------------------------------------
'This section declares the sub programs SUB FFTCalc,and SUB FFTSolve
'of the main module FFT.BAS for use.
'-------------------------------------------------------------------------
DECLARE SUB FFTCalc (xreal!(), yimag!(), numdat%)
DECLARE SUB FFTSolve (xreal!(), yimag!(), numdat%, flag%)
    DIM xreal(2048), yimag(2048)
    DIM nd AS INTEGER
    DIM i(2048)
    nd% = 2048
    SCREEN 9
    WINDOW (0, 0)-(2000, 1500)
'-------------------------------------------------------------------------
'This section inputs the data set of 2000 points from the data's home
'directory.
'-------------------------------------------------------------------------
        CLS
        PRINT "Input file name  (include path and directory)"
        INPUT ; "", a$

        OPEN a$ FOR INPUT AS #1
                FOR i = 0 TO 1999
                        INPUT #1, xreal(i)
                        LINE (i, 0)-(i, xreal(i))
                NEXT i
'-------------------------------------------------------------------------
'This section adds 48 0's to the end of the data set to bring the total to
'the required 2480 data points (2^11)
'-------------------------------------------------------------------------
        num = i
                    FOR i = num TO 2048
                            xreal(i) = 0
                            yimag(i) = xreal(i)
                            PRINT xreal(i), yimag(i), i
                    NEXT i
        CLOSE #1
'-------------------------------------------------------------------------
'This section calls the sub program FFTCalc, and uses the sub program
'FFTSolve to perform the actual Fourier Transform on the data set.
'-------------------------------------------------------------------------
    CALL FFTCalc(xreal(), yimag(), nd%)
        OPEN a$ + ".fft" FOR OUTPUT AS #1
                FOR i = 0 TO 2047
                        WRITE #1, i + 1, xreal(i)
                NEXT i
        CLOSE #1
```

```
'-------------------------------------------------------------------------------
'This section creats a quick plot of the Fourier Transform.
'-------------------------------------------------------------------------------
CLS
    max = 0
            FOR i = 1 TO 2047
                    xreal(i) = ABS(xreal(i))
                    IF xreal(i) > max THEN max = xreal(i)
            NEXT i
    FOR j = 1 TO 2047
            LINE (j, 0)-(j, xreal(j) / max * 500), 13
    NEXT j

    a1$ = ""
    WHILE a1$ = ""
        a1$ = INKEY$
    WEND
```

APPENDIX D

Quickbasic 4.5 Power Spectral Density Function via Quin-Curtis

```
'This program performs a  Power Spectral Desity function on a
'set of data consisting of N equally spaced samples.
'The total number of data points (nd) must be a power of 2.
'In this case the total number was 2000 and the required number
'is 2048 so 48 0's were added to the end of the data set so
'as not to greatly effect the results.
'-------------------------------------------------------------------------
DECLARE SUB PowerSpectrumCalc (xreal!(), yimag!(), numdat%, delta!)
    DIM xreal(2048), yimag(2048)
    DIM nd AS INTEGER
    DIM interval AS INTEGER

    DIM i(2048)
    nd% = 2048
    delta = .01
    SCREEN 9
    WINDOW (0, -1000)-(2000, 1000)
'-------------------------------------------------------------------------
'This section inputs the data set of 2000 points from the data's home
'directory.
'-------------------------------------------------------------------------
        CLS
        PRINT "Input file name  (include path and directory)"
        INPUT ; "", a$

        OPEN a$ FOR INPUT AS #1
                FOR i = 0 TO 2048
                        INPUT #1, xreal(i)
                        'PRINT i, xreal(i), yimag(i)
                        LINE (i, 0)-(i, xreal(i))
                NEXT i
'-------------------------------------------------------------------------
'This section adds 48 0's to the end of the data set to bring the total to
'the required 2480 data points (2^11)

'-------------------------------------------------------------------------
        num = i
                    FOR i = num TO 2048
                            xreal(i) = 0
                            yimag(i) = xreal(i)
                            PRINT xreal(i), yimag(i), i
                    NEXT i
        CLOSE #1
'-------------------------------------------------------------------------
'This section calls the sub program PowerSpectrumCalc, to calculate
'a power spectrum periodogram of the sampled data set.
'-------------------------------------------------------------------------
CALL PowerSpectrumCalc(xreal(), yimag(), nd%, delta!)
        OPEN a$ + ".spt" FOR OUTPUT AS #1
                FOR i = 0 TO 2048
                        WRITE #1, i + 1, xreal(i)
                NEXT i
        CLOSE #1
```

```
'-------------------------------------------------------------------------
'This section creats a quick plot of the Power Spectral Density function
'-------------------------------------------------------------------------
CLS
    max = 0
            FOR i = 0 TO 2048
                    xreal(i) = ABS(xreal(i))
                    IF xreal(i) > max THEN max = xreal(i)
            NEXT i
    FOR j = 0 TO 2048
            LINE (j, 0)-(j, xreal(j) / max * 500), 13
    NEXT j
    a1$ = ""
    WHILE a1$ = ""
        a1$ = INKEY$
    WEND
```

APPENDIX E

Quickbasic 4.5 Cross-correlation Function Program

```
    'Cross-correlation program to annalize data from two dual
    'static pressure probe.
    '-----------------------------------------------------------------

    DEFINT I-L, N, Q
    DIM Qb(2000), Qt(2000), R(2000)
CLS
PRINT "Input file name of bottom probe data "
INPUT ; "c:\rti\tony\", a$
    OPEN "c:\rti\tony\" + a$ FOR INPUT AS #1
    SUM = 0
            FOR J = 1 TO 2000
                INPUT #1, Qb(J)
                SUM = SUM + Qb(J)
            NEXT J
    aveb = SUM / 2000
    CLOSE #1
    rmsb = 0
        FOR J = 1 TO 2000
            rmsb = rmsb + (Qb(J) - aveb) * (Qb(J) - aveb)
        NEXT J
    QbRMS = SQR(rmsb / 2000)

CLS
PRINT "Input file name of top probe data"
INPUT ; "c:\rti\tony\", b$
    OPEN "c:\rti\tony\" + b$ FOR INPUT AS #1

    SUM = 0
            FOR J = 1 TO 2000
                INPUT #1, Qt(J)
                SUM = SUM + Qt(J)
            NEXT J
    avet = SUM / 2000
    CLOSE #1
    rmst = 0
        FOR J = 1 TO 2000
            rmst = rmst + (Qt(J) - avet) * (Qt(J) - avet)
        NEXT J
    QtRMS = SQR(rmst / 2000)
CLS
    PRINT "rmsb="; rmsb
    PRINT "rmst="; rmst
    PRINT "aveb="; aveb
    PRINT "avet="; avet
   ' a1$ = ""
   ' WHILE a1$ = ""
   '     a1$ = INKEY$
   ' WEND

    OPEN "c:\nlot\thesis\" + a$ + ".DAT" FOR OUTPUT AS #2

    N = 2000                                    'Number of samples
    M = N / 10      'M = I(max)                 'Max lag number
```

```
FOR i = 1 TO M
R(i) = 0
K = (N - i)      'K = J(max)
FOR J = 1 TO K

'Cross-correlation function

R(i) = R(i) + (Qb(J) - aveb) * (Qt(J + i) - avet)
NEXT J
R(i) = R(i) / (N - i)
R(i) = R(i) / ((QtRMS) ^ 2)
'PRINT I / 100, R(I)

NEXT i
FOR L = 1 TO M
WRITE #2, L / 100, R(L)                    'Writes to an output file
NEXT L
CLOSE #2
```

APPENDIX F

Intrusion Studies

As a preliminary measure of the degree to which an intrusive probe will disturb the fluidized bed, obstructions have been placed beneath a dual static pressure probe to see whether the resulting probe signal was visibly disrupted. This work was performed in the 6 inch diameter experimental fluidized bed, which operated in the slugging mode when 1/8 inch nylon beads were fluidized with air. the "disruption probes", consisting of threaded rods of two different diameters, protruded into the bed one inch below the dual static pressure probe. The distance the rod protruded into the bed could also be varied. Table 2.1 lists the details of these experimental runs and runs A1 to A10 show the traces obtained. One may conclude that these obstructions have little influence on the resulting signal, probably because of the one dimensional nature of slugging.

1 INCH PROBE SPACING WITH 12 INCH BED HEIGHT
WITH DISRUPTION PROBE DIAMETER = 0.1875 INCHS
1 INCH BELOW THE PROBE HEIGHT = 6.5 INCH

RUN NUMBER	FLOW RATE (SCFM)	PROBE HEIGHT (INCHES)	PROBE INTRUSION (INCHES)
A1	**34**	**7.5**	**0**
A2	**45**	**7.5**	**0**
A3	45	7.5	1
A4	45	7.5	2
A5	45	7.5	3
A6	45	7.5	4

1 INCH PROBE SPACING WITH 12 INCH BED HEIGHT
WITH DISRUPTION PROBE DIAMETER = 0.25 INCHS
1 INCH BELOW THE PROBE HEIGHT = 6.5 INCH

RUN NUMBER	FLOW RATE (SCFM)	PROBE HEIGHT (INCHES)	PROBE INTRUSION (INCHES)
A7	34	7.5	1
A8	45	7.5	1
A9	45	7.5	2
A10	45	7.5	3

TABLE 2.1: DETAILS OF RUNS A1 TO A10, PROBE INTRUSION STUDIES

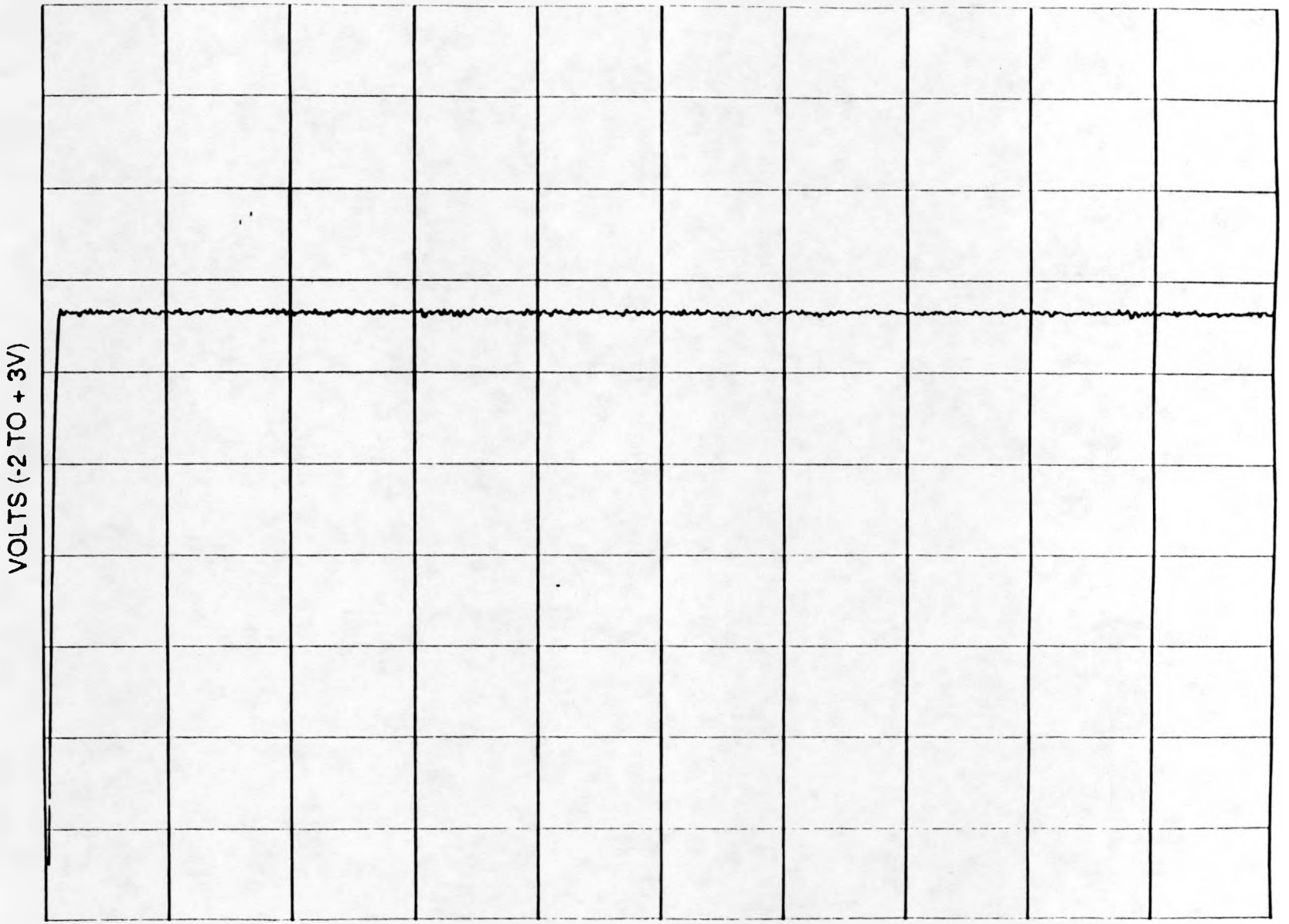

TIME (10 SECOND TRACE)

RUN NO. A1

RUN NO. A2

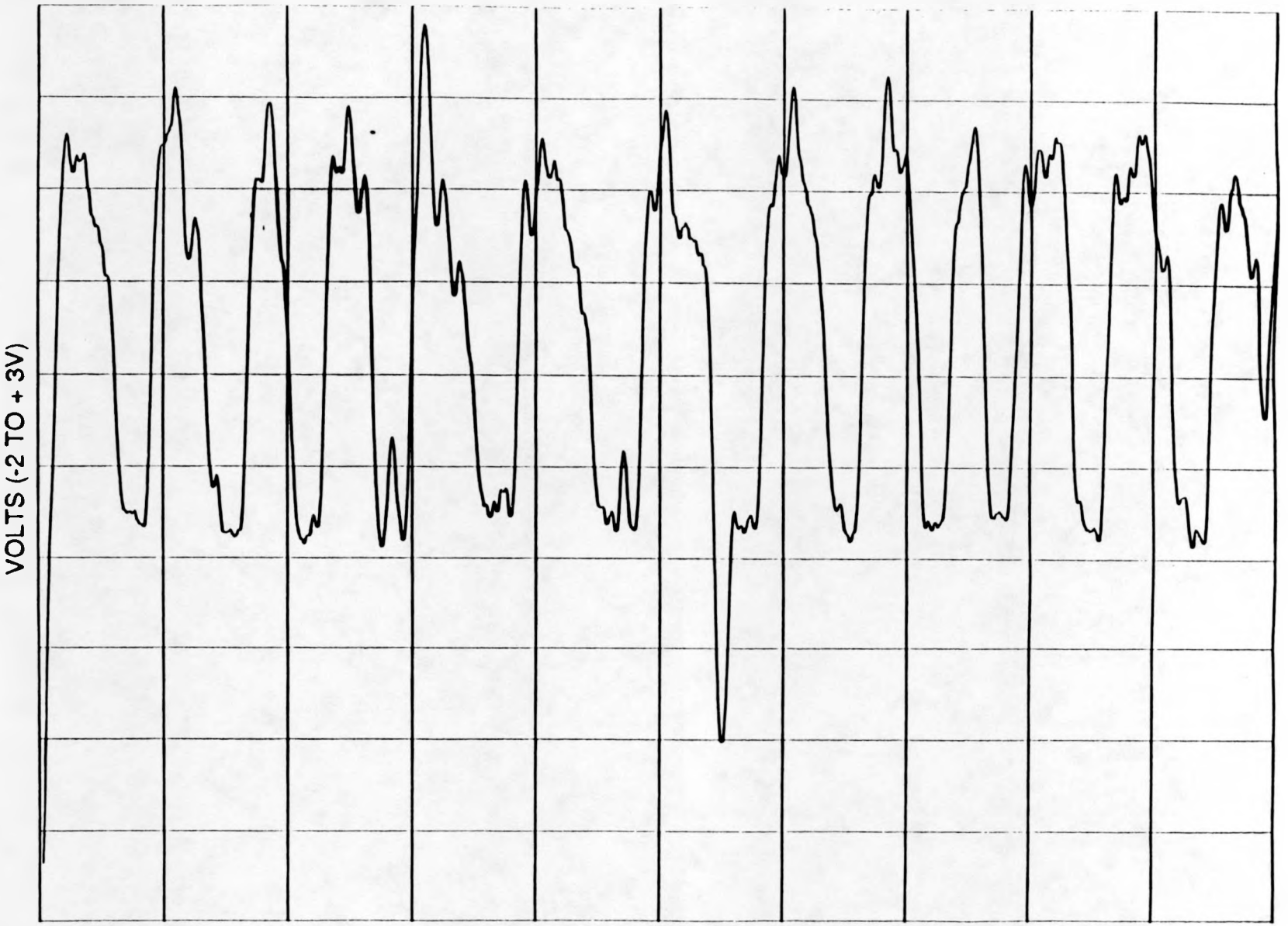

RUN NO. A3

RUN NO. A4

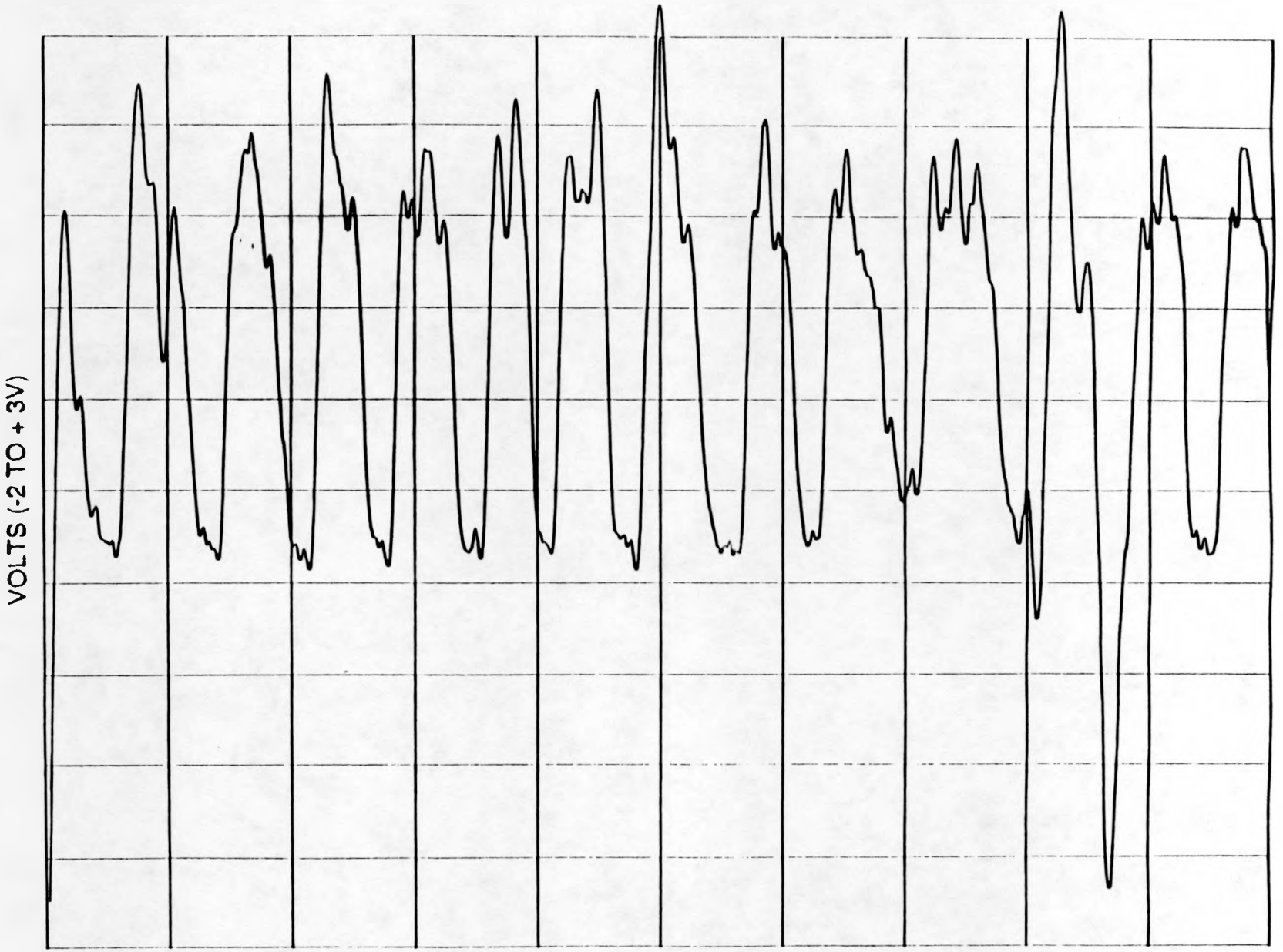

RUN NO. A5

RUN NO. A6

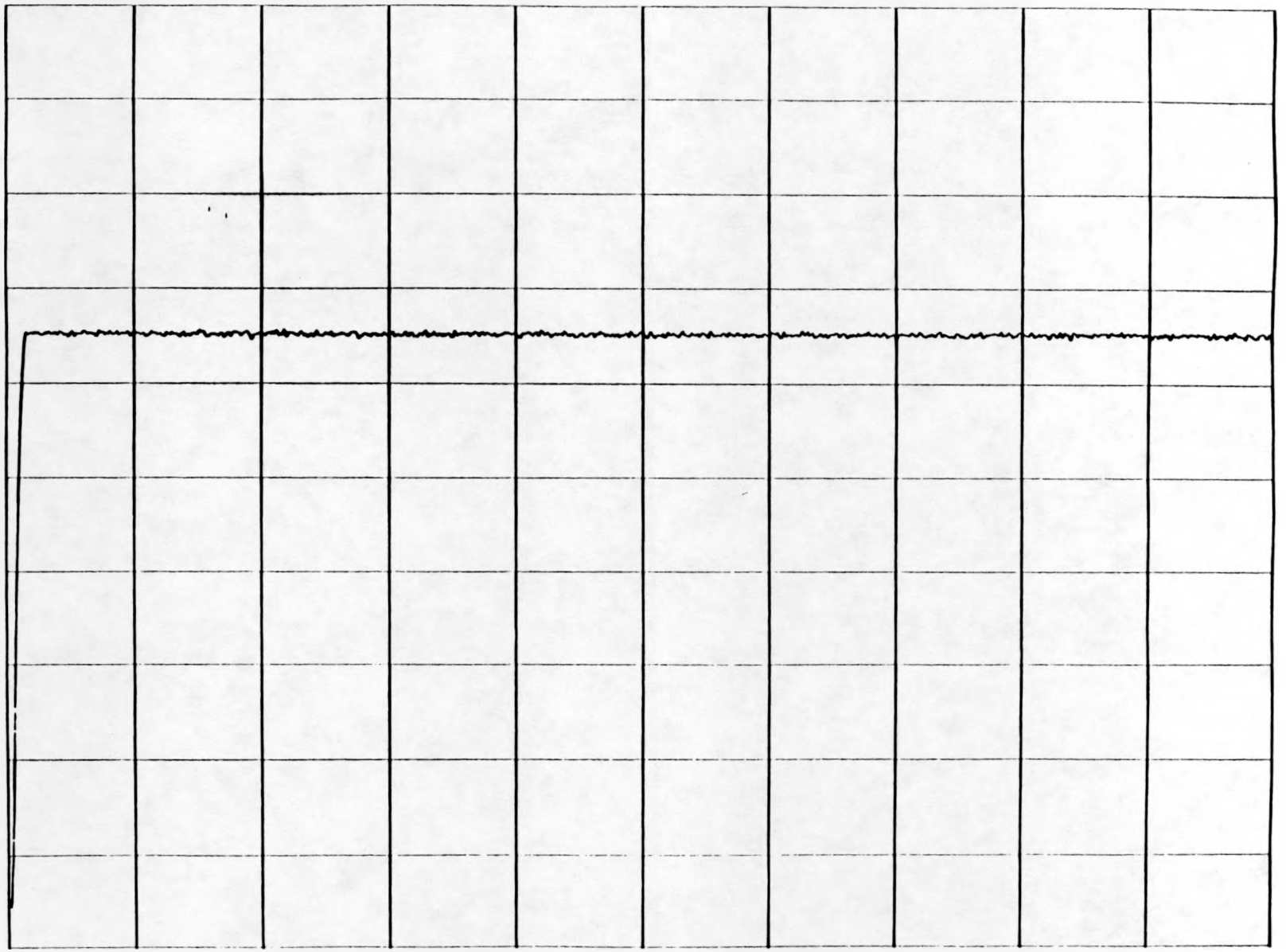

RUN NO. A7

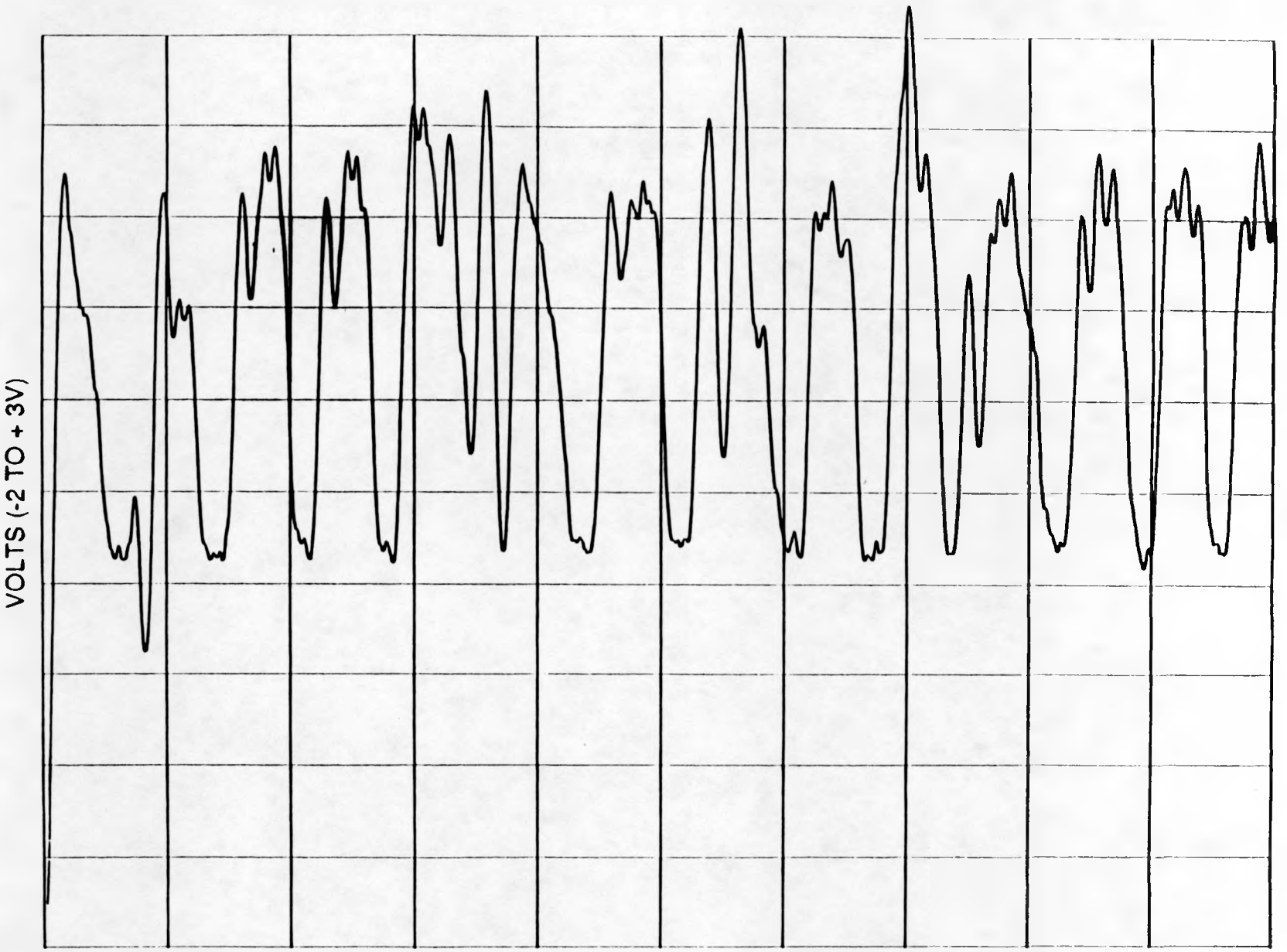

RUN NO. A8

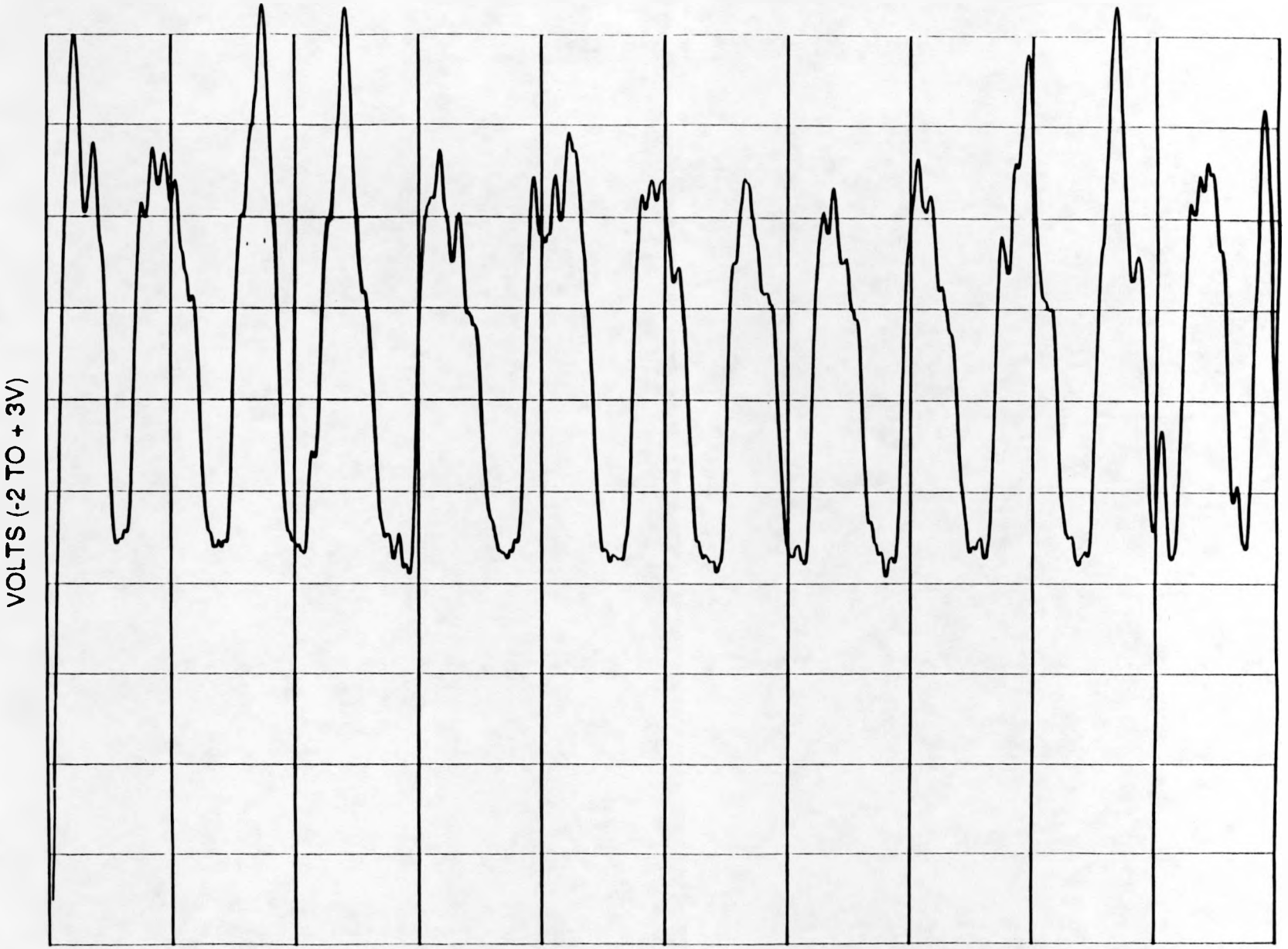

RUN NO. A9

RUN NO. A10